SLIP AND EDGE EFFECT IN COMPLETE CONTACTS

THESIS SUBMITTED TO THE DEPARTMENT OF ENGINEERING SCIENCE OF THE UNIVERSITY OF OXFORD IN PARTIAL FULFILMENT OF THE REQUIRMENTS FOR THE DEGREE OF DOCTOR IN PHILOSOPHY

by

HUI QIU

ORIEL COLLEGE

OXFORD

TRINITY TERM, 2008

Hui Qiu

Oriel College

D.Phil

Trinity Term, 2008

Edge and Slip Effect in Complete Contacts

Abstract

The general problem of an anticrack, present in a simple domain and subject to general remote loading is solved using distributed line forces, acting as strain nuclei, along the line of the anticrack. Subsequently, both dislocations and point forces are used as strain nuclei to achieve mixed boundary value conditions. The influence function for a pair of forces applied to the faces of a semi-infinite notch is found and finally this is used to find the true closure length and interfacial contact pressure.

When a sharp-edged indenter is pressed into a half plane material in the half-plane is displaced and 'laps around' the edges of the punch, possibly making contact with the side faces. This phenomenon is quantified within (coupled) half-plane theory, and applied first to an idealised indenter having the cross section of a trapezium, and then to a semi-infinite indenter. The latter allows an asymptotic form to be found which, through a generalised stress intensity factor may be collocated into the edge of any notionally sharp-edged indentation problem.

The effect of surface strains on the local slip angle, when an infinite cylinder is slid skew-wise across an elastically similar half-plane is found. It is shown that local frictional orthogonality is not completely consistent with global orthogonality.

The problems of a square-ended and an almost square-ended rigid punch sliding with both plane and anti-plane velocity components are studied. It is shown that, for a truly complete contact, if the contacting body is incompressible, convection effects are absent. Introducing either: (a) local rounding or (b) finite compressibility of the contacting body into

the problem introduces convection, giving rise to an inconsistency between the global and local requirement of the orthogonal friction law.

The state of stress in a three-quarter-plane undergoing antiplane shear deformation is studied, due to the presence of a screw dislocation along one of the projection lines extending from the free surfaces. A simple, accurate formula for the state of stress along the line is found, providing a useful kernel for the solution of crack and contact edge slip problems.

The state of stress induced in an axi-symmetric solid formed from a half-space and a bonded semi-infinite rod, by a family of ring dislocations of arbitrary Burgers vector is found. Particular care is given to the interaction between the Cauchy singularity near the dislocation core and the geometric singularity at the rod/half-space junction. Torsional contact between a semi-infinite elastic rod with square ends and an elastically similar half-space was then solved using the ring dislocations as influence functions. This provides an excellent illustration of the imposition of orthogonality condition for a complete contact.

Dedication

To my wife Hua Gao, my son Gaoyang Qiu, my parents and my parents in law, with love and gratitude.

Acknowledgements

I would like to thank my supervisor Professor David A. Hills for his excellent guidance and support. It was a great learning experience to work with Professor Hills which I enjoyed and will cherish. His knowledge, enthusiasm and insight have helped ensure that the project has been kept going towards the end. My thanks are also extended to Dr Daniele Dini, my co-supervisor, for his great help and fruitful discussions throughout my D.Phil.

I would also like to extend my appreciation to Professor Anthony Sackfield, Professor James R. Barber and Professor David Nowell who have helped me during my D.Phil.

I acknowledge the help from my colleagues: Mr. Robert Paynter, Dr. Saravanan Karuppanan, Dr. Chris Churchman, Dr. Gabriel Regino and Dr. Huaxiang Li. The discussions with them were very useful for my research. I would also like to acknowledge the support from Mrs. Amanda Bradbury (administrative assistant) and Mr. Guy Edwards (computing support officer).

I am very thankful to K C Wong Education Foundation and Overseas Research Students (ORS) awards system for financial support during my research.

Preface

This thesis is an account of work carried out by the author in Department of Engineering Science and the University of Oxford. The work was carried out under the supervision of Prof. David A. Hills and Dr. D. Dini. No part of this thesis has been submitted for a degree at any other university. The research described here is original, although the work of others has been drawn upon freely with due acknowledgements in the text.

Some of the work described in this thesis has been published in the following papers:

1. Qiu, H., Churchman, C.M., and Hills, D.A., 2008, The screw dislocation in a three-quarter plane, *European Journal of Mechanics A/Solids*, **27**, 730-736.

2. Qiu, H., Dini, D. and Hills, D.A., 2007, The influence function for self-equilibrating forces on a semi-infinite wedge, *The Journal of Strain Analysis for Engineering Design*, **42**, 351-360

3. Sackfield, A., Hills, D.A., and Qiu, H., 2007, Side-contact of sharp indenters, including the effects of friction, 2007, *International Journal of Mechanical Sciences,* **49,** 567–576

4. Qiu, H., Hills, D.A., Nowell, D. and Dini, D., 2008, Skew sliding of an elastic cylinder: An investigation of convection in contact, *International Journal of Mechanical Science,* **50**, 293-298.

5. Qiu, H., Paynter, R.J.H., Dini, D. and Hills, D.A., 2008, The state of stress induced by ring dislocations in a semi-infinite stepped shaft, *European Journal of Mechanics A/Solids*, **27,** 269–284

6. Qiu, H., Hills, D.A. and Dini, D., 2008a, An investigation of convection effects in complete and almost complete contact problems, *European Journal of Mechanics A/Solids*, under review

7. Qiu, H., Hills, D.A. and Dini, D., 2008b, Further consideration of closure at the root of a sharp notch, *The Journal of Strain Analysis for Engineering Design*, in press

8. Qiu, H., Dini, D., and Hills, D.A., 2008, Torsional contact of an elastic flat-ended cylinder. *Journal of the Mechanics and Physics of Solids*, under review.

Contents

Chapter 1

Introduction and Literature Review

1.1 Introduction

A mechanical device is assembled using several components and, in general, one component is made of many different parts. Under the action of external loads, the components or the parts will contact with each other at the interface, there will be stresses and displacements developed and some deformation will arise at the contact area. Contact mechanics is the study of the deformation of solids that touch each other at one or more points. Contact problems occur widely in industry and in nature and constitute a fundamental part of solid mechanics.

In contact mechanics, the state of stress adjacent to the contact area is very important and it should be carefully considered because that it often directly determines not only the life of components with contacting surfaces but also the normal running and service life of the device. In many cases, the failure of mechanical devices originates from the damage in the contact region such as at bolted lap joints, spline couplings, gears, cams, fan blade/disc couplings, rail-wheels and engineering bearings. Under action of the applied loads, a crack will first initiate at the contact area, and then it will propagate until, finally, it will increase to a critical length and failure occurs.

1.2 Literature Review

A milestone of contact mechanics is a paper published by Hertz (1882) in which the solution for the frictionless contact of two elastic bodies of ellipsoidal profile was discussed and provided. Nowadays Hertz's analysis is still the basis of some design procedures used in many industrial situations involving elastic contacts. Before the publication of Hertz's paper, contact mechanics was seldom considered in engineering solutions. Since then, the subject of contact mechanics has developed rapidly, with many valuable results achieved.

The subject of contact mechanics has been reviewed by many people, including Muskhelishvili (1953a, b), Gladwell (1980), Johnson (1985), Kikuchi and Oden (1988), Kalker (1990), Hills *et al.* (1993), Bhushan (1998), Barber and Ciavarella (2000), Adams and Nosonovsky (2000).

Muskhelishvili's research (1953a) was first published in Russia and the complex variable method was explained in his monograph -- this method has become one of the most important methods to solve contact problems. J.R.M. Radok introduced Muskhelishvili's work to the English speaking world, which greatly helped the development of contact mechanics in the West.

Gladwell (1980) summarised various contact geometries that had been solved in the previous decades and included an invaluable survey of the Russian literature on the subject. Johnson (1985) provided an overview of the range of contact problems including line loading of an elastic half-plane, point loading of an elastic half-space, normal contact of elastic solids -- Hertz theory, normal contact of inelastic solids, tangential loading and sliding contact, rolling contact of elastic bodies, rolling contact of inelastic bodies, calendering and lubrication, dynamic effects and impact, thermoelastic contact and rough surfaces contact.

Using variational formulations, Kikuchi and Oden (1988) dealt with the variational theory of frictionless and frictional contact, including classical problems and nonlinear problems involving large deflections, and buckling of thin plates with unilateral supports, dry friction with nonclassical laws, large elastic and elastoplastic deformations with frictional contact, dynamic contacts with dynamic frictional effects, and rolling contacts. The finite element method was extensively used in their monograph.

Kalker (1990) gave the algorithms for three-dimensional rolling contact problems, in particular for wheel/rail contact. Hills *et al.* (1993) provided comprehensive treatments of contact mechanics including classical mathematical and numerical methods to solve contact problems relating to engineering. In particular they present detailed solutions for the interior stress fields in elastic contact problems. Bhushan (1996, 1998) presented contact mechanics of rough surfaces for both single asperity and multi-asperity contacts.

Barber and Ciavarella (2000) reviewed the characteristics of contact mechanics within the mathematical framework of problems involving unilateral inequalities. They particularly focused on the additional features associated with the presence of friction at the interface. They also introduced the concept of self-similarity which provids a method for linear and nonlinear materials indentation problems and discussed other aspects of contact problems beyond classical elasticity theory. The specialised areas of anisotropic and elastodynamic contact were summarised. The characterisation of rough contacts and thermoelastic contacts were discussed.

Adams and Nosonovsky (2000) reviewed contact modelling with an emphasis on contact forces and their relationship with geometrical, material and mechanical properties of contacting bodies, and gave a general review of both single asperity and multi-asperity contact models. Simple Hertzian contact for spheres, cylinders, and ellipsoids were described first. Then the effect of friction, plasticity, adhesion, and higher-order terms were generalised. Different models of multi-asperity contacts which represent a rough surface contact were

included. Experimental investigations were also reviewed. Lastly, the dynamics and associated instabilities of sliding contact were presented and their applications were discussed.

During the development of contact mechanics, generally two main problems are considered. The first, and very common one, is the analysis of the stress state of a body that is subjected to specific loads and boundary conditions. The evaluation of both the stress distribution along the contact interface and the stress within the body is discussed in this problem. With the development of elastic mechanics, many approaches have become available to solve contact problems, described in the aforementioned books (Muskhelishvili, 1953a; Gladwell, 1980; Johnson, 1985; and Hills *et al.*, 1993).

Besides the stress state of the contacting bodies, the other main problem in contact mechanics concerns the formulation of damage or failure criteria in order to predict failure of the contacting components. This problem is directly related to crack initiation at the contact surface and crack propagation. Fenner *et al.* (1956), and Wright and O'Connor (1972) focused their attention on stress concentration effects along contacting surfaces. Collins and Tovey (1972) proposed an asperity-contact microcrack initiation mechanism based on stress concentration at the asperity level. Similar initiation models have also been attempted (Ballard *et al.*, 1995; Moobola, 1998). However, for asperity-based approaches, and generally for rough contact theories, the fundamental question of the resolution at which asperity features are measured remains yet to be solved. Nowell and Hills (1987, 1989) developed a distributed dislocation technique to calculate the stress intensity factor for cracks growing with different orientations with respect to the free surface, facilitating the investigation of the first stage of crack growth. The same group later discussed applications of this technique in their monograph (1996). A numerical method to solve integral equations was given which are helpful for developing solutions to analyse anticrack problems.

Generally, based on the geometrical and material properties of the indenter and contacting bodies, contact problems can be classified into the following three groups.

1). Incomplete contact. When two convex bodies are pressed together (Figure 1.1 (a)), contact first occurs at a point (or a line in the case of a plane problem). With the increase of the applied load, the contact patch grows gradually. The contacting bodies have the same tangent at the edge of contact region and the slope along the contact interface is continuous. This kind of contact problems is called incomplete contact. For example, gears, railway wheels and rolling element bearings all belong to this category. Incomplete contact is characterised by the fact that the contact pressure will decrease continuously to zero toward the edges of the contact.

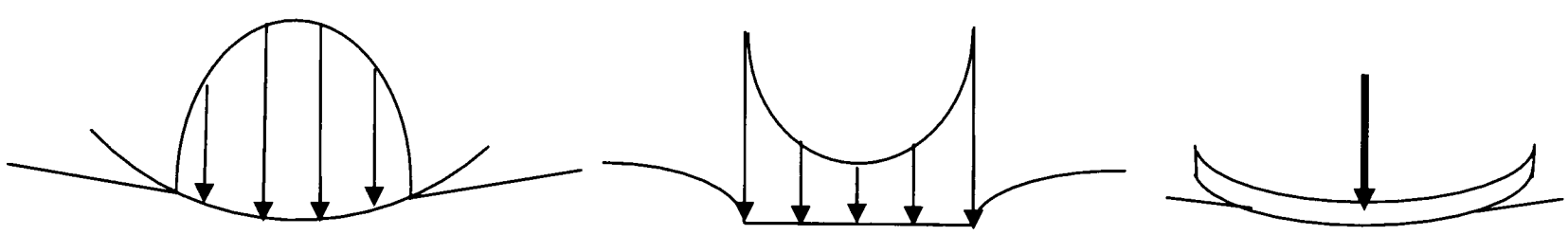

Figure 1.1: Various classes of contact (a) incomplete contact; (b) complete contact; (c) receding contact

2). Complete contact. When a flat-ended punch is pushed into a very large block of material, and the size of contact is independent of the contact force, and the second type of contact occurs. This is shown in Figure 1.1 (b) and it is referred to as complete contact. This differs from incomplete contact: the contact pressure is singular at each edge of the contact. A rigid flat-ended punch pressed onto an elastic half-plane is a common example of this kind of problem.

3) Receding contact. The third kind of contact is seldom met in practice. As shown in Figure 1.1 (c), a thin flat elastic plate is resting on an extended elastic block. In this case, when a concentrated normal force is applied, the contact dimension is decreased. So it is

called a receding contact. This category of contact has been discussed by Keer, Dundurs and Tsai (1972), Dundurs (1975) and Gladwell (1976).

1.2.1 Incomplete Contact

In contact mechanics, incomplete contacts comprise the most common case and a great number of practical contact problems belong to this category. A typical example of this kind of contact is the Hertzian contact. Contact problems which can be thought of as Hertizan should satisfy the following conditions: (1) the contact area is elliptical; (2) each body is approximated by an elastic half-space loaded over the plane elliptical contact area; (3) the dimension of the contact area must be small compared to the dimension of each body and to the radii of curvature of the surface; (4) strains are sufficiently small for linear elasticity to be valid; and (5) the contact is frictionless, so that only normal pressure is transmitted. Since 1882, a lot of effort has been put into removing these restrictions, and many incomplete contact problems such as two similar/dissimilar cylinders under different frictional situations have been studied. Because the contact size is small compared to the characteristic dimensions of the component, the bodies being loaded can be represented by half-planes or spaces. The formulation of elasticity problems appropriate to a semi-infinite body simplifies the calculation greatly. Detailed results such as contact traction, interior stresses and displacements for Hertzian contact area and interference vs. normal force are given by Cooper (1969) and Johnson (1985). Greenwood (1985) analysed a moderately elliptical Hertzian contact and showed that the contact pressure and approach could be approximated by using the circular contact formulas with an equivalent radius of curvature equal to $(AB)^{1/2}$, where A and B were the principal relative curvatures.

When there is friction at the contact interface, according to the 'Coulomb' friction law, any point in the contact area must be in one of two states – 'stuck' or 'slipping'. The contact state will change with the loading history. Mindlin and Deresiewicz (1953) investigated the phenomena occurring at the contact surfaces of elastic spheres subject to a variety of applied forces. They found that the changes in tractions and displacements depend not only upon the initial state of loading, but upon the entire past history of loading and the instantaneous relative change of the normal and tangential forces. They realised that for the plane strain contact of two cylinders, there is a central stick region surrounded by two slip zones. With an increase of tangential load, the size of the stick zone shrinks until eventually overall sliding happens. Comninou and Dundurs (1982) examined the case of unloading with strong friction, and also treated reloading of the unbounded solid with a semi-infinite cut to illustrate the complexity of history dependence. Jäger (1997) and Ciavarella (1998) separately discussed the shear traction distribution in the stick region. It was suggested that these results could be used to predict the size of the slip zone in conditions of fretting fatigue (Hills and Nowell, 1994).

The effect of friction without tangential loading was incorporated into a study of contacting spheres by Goodman (1962). Spence (1975) gave a complete solution of such a contact which included the effect of shear traction on normal pressure distribution. The details of the contact stresses for sliding of dissimilar materials were recorded by Johnson (1985) and Hills *et al.* (1993).

1.2.2 Complete Contact

Compared with incomplete contacts, complete contacts do not arise as often in engineering practice. The spline connection between split shafts in a gas turbine is an example

of this kind of contact. In the analysis of complete contact problems, the punch is often assumed to be rigid. However, in fact, the punch and the contact body are usually elastic. No real punch is perfectly rigid even when a solid of low elastic modulus such as polymer or rubber is indented by a metallic punch.

Khadem and O'Connor (1969) derived a solution for an elastic rectangle compressed by two identical elastic half-planes. Complete contact problems can be solved by using a formulation appropriate to an elastic strip.

Spence (1971) gave a solution for the two-dimensional indentation of an elastic half space by a rigid punch under a slowly applied normal load and there where friction is present between the surfaces. Sundelius (1981) considered an axisymmetric contact problem with given region of adhesion. Slip zones free of friction or with Coulomb friction were discussed. Traction distributions and the interior stress state for this category of problem are given by Hills *et al.* (1993).

Within the development of the solution of complete contact problems, the concept of almost complete contact problems emerged. Ciavarella *et al.* (1998) studied the contact problem and stress state for indentation by a flat punch with rounded edges, which may be called almost complete contact or nearly complete contact. Both surface pressure and interior stress field were given. They concluded that this solution was a realistic alternative to the rigid-flat punch idealization and has particular application to fretting fatigue tests. Navarro *et al.* (2003) gave a solution for the partial slip regime present under a square-ended punch and a punch having a flat plus rounded profile together with a Hertzian contact, when subjected to a monotonically increasing proportional shear force and bulk tension.

The asymptotic method has proved to be a very useful tool to analyse complete and almost complete contacts. An asymptotic method was first used for a sharp notch by Williams (1952). Based on the Bogy solution for an adhered interface between semi infinite wedges (Bogy, 1971), an asymptotic solution to slipping interfaces was developed by Gdoutos and

Theocaris (1975) and Comninou (1976). Mugadu *et al.* (2002) developed an asymptotic approach to crack initiation in fretting fatigue of complete contacts. Later, Mugadu and Hills (2002) applied this approach to the problem of a rigid, square-ended punch, pressed into an elastic half-plane of finite stiffness, and subject to a shearing force sufficient to cause sliding. Based on this theory, Mugadu *et al.* (2002) made modifications to a fretting-fatigue testing apparatus. Mugadu and Hills (2003) studied the case when a rigid, square-ended punch pressed against an incompressible half-plane by a constant normal load is subjected to both an oscillatory shearing force and bulk tension. An asymptotic approach was used to determine the order of singularity and spatial distribution of the local stress state. Churchman *et al.* (2003) provided asymptotic results for slipping complete frictional contact between elastically dissimilar bodies. Sackfield *et al.* (2003) developed the asymptotic method to characterising the process zone in almost complete frictionless contacts. Mugadu *et al.* (2004) gave the asymptotic solutions needed to characterise the process zone in almost complete frictional contacts. Lastly, Dini *et al.* (2004) discussed the correlation of the process zone properties in complete, incomplete and almost complete fretting contacts. They specified the conditions when a finite-sized flat and rounded contact might be replaced by a square-ended contact or a Hertzian contact.

1.3 Summary of Thesis

This dissertation is mainly concerned with slip and edge effect in complete contacts. A brief outline of the dissertation is as follows

In chapter 2, the general problem of thin, rigid 'flakes' or inclusions (anticracks), present in a simple domain and subject to general remote loading are considered. The problem is solved using distributed line forces, acting as strain nuclei, along the line of the anticrack

and strong parallels are drawn with the use of distributed dislocations in the solution of conventional cracks. This work was done principally as a prelude to the contact problem adhered in chapter 3 and 4.

Chapter 3 describes the application of both dislocations and point forces as strain nuclei to achieve mixed boundary value conditions.

When a remote compressive load is applied to a plate containing a sharp notch, closure will occur at the root. The true closure length and interfacial contact pressure are found in chapter 4.

In chapter 5, coupled half-plane theory is applied first to an idealised indenter having the cross section of a trapezium, and then to a semi-infinite indenter. The latter allows an asymptotic form to be found which, through a generalised stress intensity factor, may be collocated into the edge of any notionally sharp-edged indentation problem.

In chapter 6, the effect of surface strains on the local slip angle, when an infinite cylinder is slid skew-wise across an elastically similar half-plane is found. It is shown that local frictional orthogonality is not completely consistent with global orthogonality.

In chapter 7, the problems of a square-ended and an almost square-ended rigid punch sliding with both plane and anti-plane velocity components are studied. It is shown that for a truly complete contact, if the contacting body is incompressible, convection effects are absent.

In chapter 8, the state of stress in a three-quarter-plane undergoing anti-plane shear deformation is studied, due to the presence of a screw dislocation along one of the projection lines extending from the free surfaces. A simple, accurate formula for the state of stress along the line is found, providing a useful kernel for the solution of crack and contact edge slip problems.

In chapter 9, the state of stress induced in an axi-symmetric solid formed from a half-space and a bonded semi-infinite rod, by a family of ring dislocations of arbitrary Burgers

vector is found. Particular care is given to the interaction between the Cauchy singularity near the dislocation core and the geometric singularity at the rod/half-space junction.

Chapter 10 describes torsional contact between a semi-infinite elastic rod with square ends and an elastically similar half-space

Conclusions are made in chapter 11 and suggestions of the further work are given.

Chapter 2

Anticrack Problems

2.1. Introduction

Cracks arise widely in engineering components, and their properties are well-known. Much less well-known is the entity called an 'anticrack'. Up to a point this is an artificial contrivance, but it does have value in practical mechanics, and this will be described. In mechanical terms a crack may be thought of as a surface (or line in two dimensions), along which the traction components of stress are required to vanish, assuming that the crack is open, but the displacements may take any value. An anticrack is a surface or line within the material which has been painted with a perfectly rigid substance, so that no displacement gradients are permitted along its length: the anticrack is allowed to adopt whatever rigid body movements (both translational and rotational) the applied loading produces.

The primary projected use of anticracks, when they were first studied in the late 1960's, and early 1970's (Chang and Conway, 1968; Chu and Conway, 1970; Conway *et al.*, 1970; Conway and Chang, 1971; Burgel *et al.*, 1970; Brussat and Westmann, 1975), was to simulate the effects of relatively rigid fibres present in compliant matrices. They are very effective at describing the local stress field in such problems, but only when there are a relatively few fibres present, and the requirement that the fibre be so stiff in bending as to

inhibit all flexural deformation may also be quite hard to sustain, although at least one study used an anticrack with infinite extensional stiffness but zero bending stiffness (Erdogan and Gupta, 1972). More recent studies compared the characteristic crack and anti-crack tip fields (Wang *et al.*, 1985). A second reason for studying them, and the principal motivation in this thesis, is that they permit displacement boundary conditions to be imposed along fixed lines within solids of simple shapes, permitting more complex influence functions to be found; for example, it is possible to find the surface displacement of a semi-infinite wedge with opposed surface forces.

A general procedure for solving for the state of stress in the neighbourhood of cracks present in geometrically simple problems, and which has proved of great benefit in providing calibrations for stress intensity factors for cracks adjacent to contact problems, for example, is to use the distributed dislocation technique. Dislocations are ideal for generating perturbations on states of stress and readily permit traction boundary conditions to be imposed, but when displacement boundary conditions are needed, the use of a line-force solution (in two dimensional problems) is appropriate instead. Markenscoff, Ni and Dundurs (1994) comment that this is because a crack can 'absorb' a dislocation, but not a line force, whereas an anticrack can 'absorb' a line force, but not a dislocation. The first step in any anticrack problem is therefore to determine the solution for a line-force present in the required domain. The correspondence between line force solutions and edge dislocation solutions has been studied extensively by Dundurs (1968). It follows that, if a solution for an edge dislocation is available for the domain under consideration, a line-force solution will be available, too.

The problem studied here is that of an anticrack in a half-plane, Figure 2-1, because this is amenable to closed form analysis, and has direct application to the subsequent problem which is the state of stress and displacement in a semi-infinite wedge with surface forces. Before considering a half-plane, it may be appropriate, first, to look at the solution for a line

force in an infinite plane, as this enables the characteristics of the solution to be found without the complication of free boundaries.

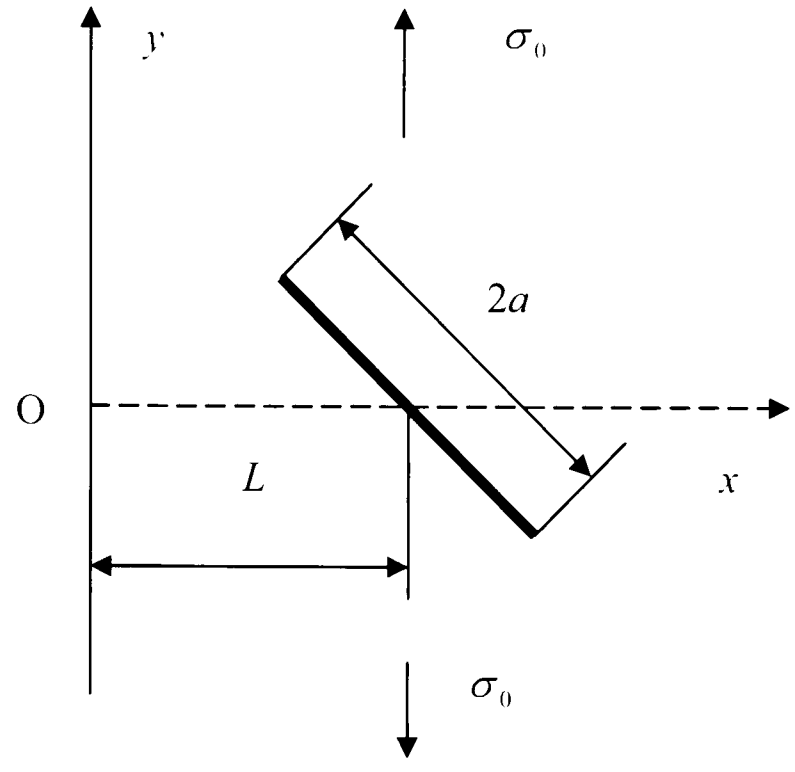

Figure 2-1: An anticrack in a half plane.

2.2. Formulation: Line Force Influence Function

Figure 2-2 shows an infinite plane with a line force P_x applied at the origin. Timoshenko and Goodier (1970) gives the displacement field (u_x, u_y), and state of stress (σ_{xx}, σ_{yy}, σ_{xy}) at (x, y) as

$$2\mu u_x(x,y) = \frac{P_x}{\pi(\kappa+1)}\{-\kappa \ln r + \frac{x^2}{r^2}\} + \mathrm{C} \tag{2-1a}$$

$$2\mu u_y(x,y) = \frac{P_x}{\pi(\kappa+1)}\frac{xy}{r^2} + \mathrm{C} \tag{2-1b}$$

$$\sigma_{xx}(x,y) = \frac{P_x}{2\pi(\kappa+1)}\{-(\kappa-1)\frac{x}{r^2} - 4\frac{x^3}{r^4}\} \tag{2-2a}$$

$$\sigma_{xy}(x,y) = \frac{P_x}{2\pi(\kappa+1)}\{-(\kappa-1)\frac{y}{r^2} - 4\frac{x^2 y}{r^4}\} \tag{2-2b}$$

$$\sigma_{yy}(x,y)=\frac{P_x}{2\pi(\kappa+1)}\{(\kappa-1)\frac{x}{r^2}-4\frac{xy^2}{r^4}\} \tag{2-2c}$$

where $r=\sqrt{x^2+y^2}$, $\kappa=3-4\nu$ for plane strain, $\kappa=(3-\nu)/(1+\nu)$ for plane stress, ν is Poisson's ratio, and μ is the shear modulus. Suppose that the anticrack lies along the line $y=0$ and spans the interval $-a\le x\le a$. By taking the limit $y\to 0$, the state of stress along this line can be found from (2-2) as

$$2\mu\frac{\partial u_x(x,0)}{\partial x}=-\frac{P_x\kappa}{\pi(\kappa+1)}\frac{1}{x} \tag{2-3a}$$

$$2\mu\frac{\partial u_y(x,0)}{\partial x}=0 \tag{2-3b}$$

$$\sigma_{xx}(x,0)=-\frac{P_x(3+\kappa)}{2\pi(\kappa+1)}\frac{1}{x} \tag{2-4a}$$

$$\sigma_{xy}(x,0\pm)=\mp\frac{P_x}{2}\delta(x) \tag{2-4b}$$

$$\sigma_{yy}(x,0)=\frac{P_x(\kappa-1)}{2\pi(\kappa+1)}\frac{1}{x} \tag{2-4c}$$

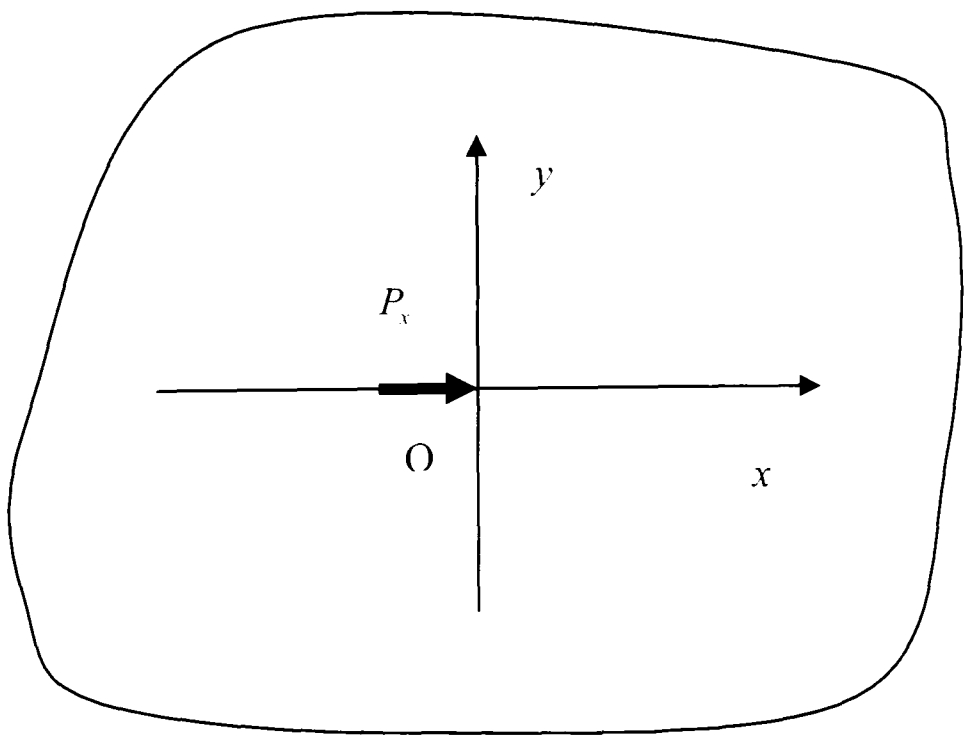

Figure 2-2: A point force P_x acting at the origin of the coordinate system in an infinite plane.

In fact, we will choose to specify the displacement gradients, because this removes the unknown rigid body term. There are Cauchy type singularities in both direct components of stress, and in the gradient of the x-direction displacement component, whilst the shear stress exhibits a Dirac function behaviour to 'support' the line force. A point force applied in the x-direction tends to stretch material lying on the plane $y=0$, and is therefore appropriate for imposing prescribed extensional behaviour. A transverse force (acting in the y-direction) is imposed in order to control flexural deformation. The corresponding stresses and displacement gradients, again along the line $y=0$, for a line force at the origin, are given by

$$2\mu\frac{\partial u_x(x,0)}{\partial x}=0 \tag{2-5a}$$

$$2\mu\frac{\partial u_y(x,0)}{\partial x}=-\frac{P_y\kappa}{\pi(\kappa+1)}\frac{1}{x} \tag{2-5b}$$

$$\sigma_{xx}(x,0\pm)=\mp\frac{P_y(3-\kappa)}{2(\kappa+1)}\delta(x) \tag{2-6a}$$

$$\sigma_{xy}(x,0)=-\frac{P_y(\kappa-1)}{2\pi(\kappa+1)}\frac{1}{x} \tag{2-6b}$$

$$\sigma_{yy}(x,0\pm)=\mp\frac{P_y}{2}\delta(x)\,. \tag{2-6c}$$

The main solutions needed when formulating the problem are the displacement gradients induced by the line forces. These solutions (equations 2-3a, 2-5b) are, of course, for line forces applied at the origin, in an infinite plane. If the anticrack problem to be solved lies in another domain, bounded terms will be added to these solutions. Also, the problem will, in general, no longer be uncoupled; that is, forces applied in the x-direction will induce displacement in the y-direction, and vice versa.

Reverting to the infinite plane solution, if the applied force is applied at point (ξ, 0) the displacements at point (x, 0) may be found by a simple change of coordinates, and if we

replace the line forces by distributed forces $p_x(\xi)$ ($= dP_x / dx$), $p_y(\xi)$ ($= dP_y / dx$), the displacement gradients induced are given by

$$2\mu \frac{\partial u_x(x,0)}{\partial x} = \frac{\kappa}{\pi(\kappa+1)} \int_a^a \frac{p_x(\xi)}{\xi - x} d\xi \tag{2-7}$$

$$2\mu \frac{\partial u_y(x,0)}{\partial x} = \frac{\kappa}{\pi(\kappa+1)} \int_a^a \frac{p_y(\xi)}{\xi - x} d\xi \tag{2-8},$$

where the integrals are taken along the line of the anticrack.

If the anticrack experiences a rigid body displacement α in the x-direction, and β in the y-direction, together with a rotation ω, the displacements of particles along the line of the anticrack are given by

$$\tilde{u}_x(x,y) = \alpha - \omega y \,, \tilde{u}_y(x,y) = \beta + \omega x \tag{2-9}$$

so that, if the anticrack occupies the interval $|x| \le a$, $y = 0$,

$$\frac{\partial \tilde{u}_x(x,0)}{\partial x} = 0 \,, \quad \frac{\partial \tilde{u}_y(x,0)}{\partial x} = \omega \,, \; |x| \le a. \tag{2-10}$$

Assume that, in the absence of the anticrack, the external loads induce in the body displacements $\bar{u}_x$ and $\bar{u}_y$, so that the boundary conditions can be written as

$$\frac{\partial \tilde{u}_x(x,0)}{\partial x} = \frac{\partial u_x(x,0)}{\partial x} + \frac{\partial \bar{u}_x(x,0)}{\partial x} = 0 \,, |x| \le a \tag{2-11a}$$

$$\frac{\partial \tilde{u}_y(x,0)}{\partial x} = \frac{\partial u_y(x,0)}{\partial x} + \frac{\partial \bar{u}_y(x,0)}{\partial x} = \omega \,, |x| \le a \tag{2-11b}$$

and the following two simultaneous integral equations for the unknown line force densities can be written down

$$\frac{\kappa}{2\mu\pi(\kappa+1)} \int_{-a}^{a} \frac{p_x(\xi)d\xi}{\xi - x} + \frac{\partial \bar{u}_x(x,0)}{\partial x} = 0 \,, \; |x| \le a \tag{2-12a}$$

$$\frac{\kappa}{2\mu\pi(\kappa+1)} \int_{-a}^{a} \frac{p_y(\xi)d\xi}{\xi - x} + \frac{\partial \bar{u}_y(x,0)}{\partial x} = \omega \,, \; |x| \le a \,. \tag{2-12b}$$

Three further equations express equilibrium between any external forces and the moment on the anticrack, (F_x, F_y, M), and the line force densities

$$\int_a^a p_x(x)dx = F_x \tag{2-13a}$$

$$\int_a^a p_y(x)dx = F_y \tag{2-13b}$$

$$\int_{-a}^{a} xp_y(x)dx = M\,. \tag{2-13c}$$

Of course if the anticrack simply 'floats' in the matrix, these three integrals must all vanish.

The integral equations formed have exactly the same properties as those arising in distributing dislocations to solve crack problems: the kernels are Cauchy in character (with a bounded term if there are free boundaries present) and may be inverted using either the Riemann-Hilbert procedure (Muskhelishvili, 1963) or a numerical inversion procedure, based on special quadratures adapted to the Cauchy nature of the kernel (Hills *et al.*, 1995). For brevity an example problem of an anticrack present in a half-plane will be considered.

2.3. AntiCrack in a Half-Plane

The first step in the solution is to determine the state of stress due to line forces in the domain of interest and this is done by using a combination of the stress state induced in a half-plane by a dislocation (Nowell and Hills, 1987), and the Dundurs dislocation/line force analogy (Dundurs, 1968). The axis set employed is shown in Figure 2-3, with the y-axis along the surface and x-axis perpendicular to it, with a point force located at (c, d). The general results for the stress and displacement fields are complicated, and are included, for reference, in Appendix A. These results are needed primarily for an anticrack inclined at an angle to the

free surface, and a special case is when the anticrack lies perpendicular to the free surface, so that d is set to zero, and the y coordinate of the observation point is also set to zero, giving

$$2\mu\frac{\partial u_x(x,0)}{\partial x}=\frac{P_x}{2\pi(\kappa+1)}\{\frac{-2\kappa}{x-c}-\frac{(\kappa^2+1)}{x+c}-\frac{4c}{(x+c)^2}+\frac{8c^2}{(x+c)^3}\} \tag{2-14a}$$

$$2\mu\frac{\partial u_y(x,0)}{\partial x}=0 \tag{2-14b}$$

$$\sigma_{xx}(x,0)=\frac{P_x}{2\pi(\kappa+1)}\{\frac{-3-\kappa}{x-c}-\frac{3\kappa+1}{x+c}+\frac{2\kappa c-10c}{(x+c)^2}+\frac{8c^2}{(x+c)^3}\} \tag{2-15a}$$

$$\sigma_{yy}(x,0)=\frac{P_x}{2\pi(\kappa+1)}(\frac{\kappa-1}{x-c}+\frac{1-\kappa}{x+c}+\frac{2c-2\kappa c}{(x+c)^2}-\frac{8c^2}{(x+c)^3}) \tag{2-15b}$$

$$\sigma_{xy}(x,0\pm)=\mp\frac{P_x}{2}\delta(x)\,. \tag{2-15c}$$

The corresponding results for a line force, P_y, are as follows, with the complete expressions, needed for a generally oriented anticrack, relegated to Appendix A.

$$2\mu\frac{\partial u_x(x,0)}{\partial x}=0 \tag{2-16a}$$

$$2\mu\frac{\partial u_y(x,0)}{\partial x}=\frac{P_y}{2\pi(\kappa+1)}\{\frac{-2\kappa}{x-c}-\frac{(\kappa^2+1)}{x+c}-\frac{4c}{(x+c)^2}+\frac{8c^2}{(x+c)^3}\} \tag{2-16b}$$

$$\sigma_{xx}(x,0\pm)=\mp\frac{(3-\kappa)P_y}{2(\kappa+1)}\delta(x) \tag{2-17a}$$

$$\sigma_{yy}(x,0\pm)=\mp\frac{P_y}{2}\delta(x) \tag{2-17b}$$

$$\sigma_{xy}(x,0)=\frac{P_y}{2\pi(\kappa+1)}(\frac{1-\kappa}{x-c}+\frac{\kappa-1}{x+c}-\frac{2\kappa c+6c}{(x+c)^2}+\frac{8c^2}{(x+c)^3})\,. \tag{2-17c}$$

From these expressions, for line loads with local densities $p_x(x)$ and $p_y(x)$ acting on the x-axis within the interval [a, b] in the x- and y- direction, the following results apply

$$2\mu\frac{\partial u_x(x,0)}{\partial x}=\frac{1}{2\pi(\kappa+1)}\int_a^b\{\frac{-2\kappa}{x-\xi}-\frac{(\kappa^2+1)}{x+\xi}-\frac{4\xi}{(x+\xi)^2}+\frac{8\xi^2}{(x+\xi)^3}\}p_x(\xi)d\xi \tag{2-18}$$

$$\sigma_{xx}(x,0)=\frac{1}{2\pi(\kappa+1)}\int_a^b\{\frac{-3-\kappa}{x-\xi}-\frac{3\kappa+1}{x+\xi}+\frac{2\kappa\xi-10\xi}{(x+\xi)^2}+\frac{8\xi^2}{(x+\xi)^3}\}p_x(\xi)d\xi \tag{2-19a}$$

$$\sigma_{yy}(x,0)=\frac{1}{2\pi(\kappa+1)}\int_a^b(\frac{\kappa-1}{x-\xi}+\frac{1-\kappa}{x+\xi}+\frac{2\xi-2\kappa\xi}{(x+\xi)^2}-\frac{8\xi^2}{(x+\xi)^3})p_x(\xi)d\xi \tag{2-19b}$$

$$\sigma_{xy}(x,0\pm)=\mp\frac{1}{2}p_x(x) \tag{2-19c}$$

$$2\mu\frac{\partial u_y(x,0)}{\partial x}=\frac{1}{2\pi(\kappa+1)}\int_a^b\{\frac{-2\kappa}{x-\xi}-\frac{(\kappa^2+1)}{x+\xi}-\frac{4\xi}{(x+\xi)^2}+\frac{8\xi^2}{(x+\xi)^3}\}p_y(\xi)d\xi \tag{2-20}$$

$$\sigma_{xx}(x,0\pm)=\mp\frac{(3-\kappa)}{2(\kappa+1)}p_y(x) \tag{2-21a}$$

$$\sigma_{yy}(x,0\pm)=\mp\frac{1}{2}p_y(x) \tag{2-21b}$$

$$\sigma_{xy}(x,0)=\frac{P_y}{2\pi(\kappa+1)}\int_a^b(\frac{1-\kappa}{x-\xi}+\frac{\kappa-1}{x+\xi}-\frac{2\kappa\xi+6\xi}{(x+\xi)^2}+\frac{8\xi^2}{(x+\xi)^3})p_y(\xi)d\xi\,. \tag{2-21c}$$

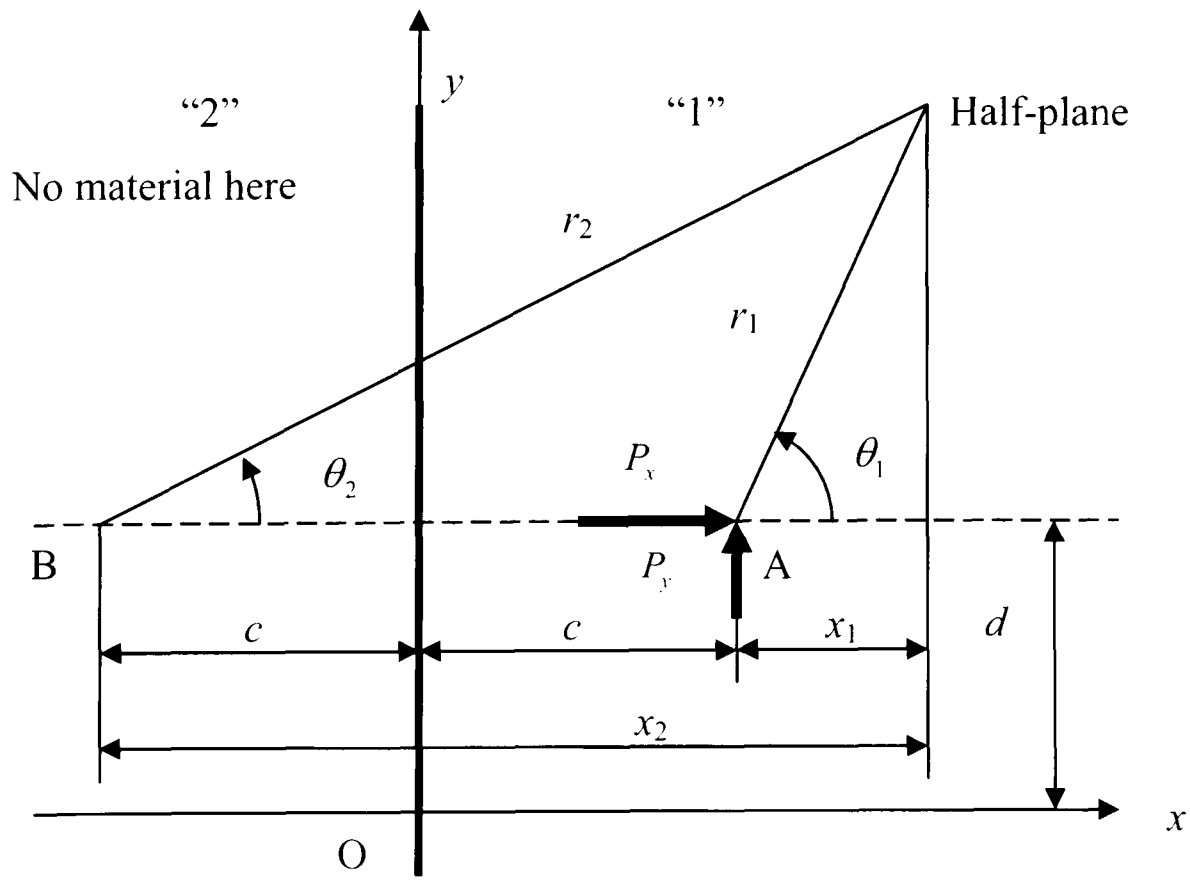

Figure 2-3: Two half planes with point forces P_x, P_y.

2.4. Solution

The problem of an anticrack in a half plane lying perpendicular to the free surface, having the simplified influence functions are appropriate is treated first. Thus the effects of x- and y- direction line forces are uncoupled, so that an x-direction force produces no y-direction displacement, and a y-direction force produces no x-direction displacement. Figure 2-4 displays the geometry, and the applied loading is simply uniform tension parallel with the free surface, so that

$$2\mu\frac{\partial\overline{u}_x(x,0)}{\partial x}=2\mu\varepsilon_{xx}=2\mu\frac{1}{8\mu}[(1+\kappa)\sigma_{xx}+(\kappa-3)\sigma_{yy}]=\frac{(\kappa-3)\sigma_0}{4} \tag{2-22a}$$

$$2\mu\frac{\partial\overline{u}_y(x,0)}{\partial x}=0. \tag{2-22b}$$

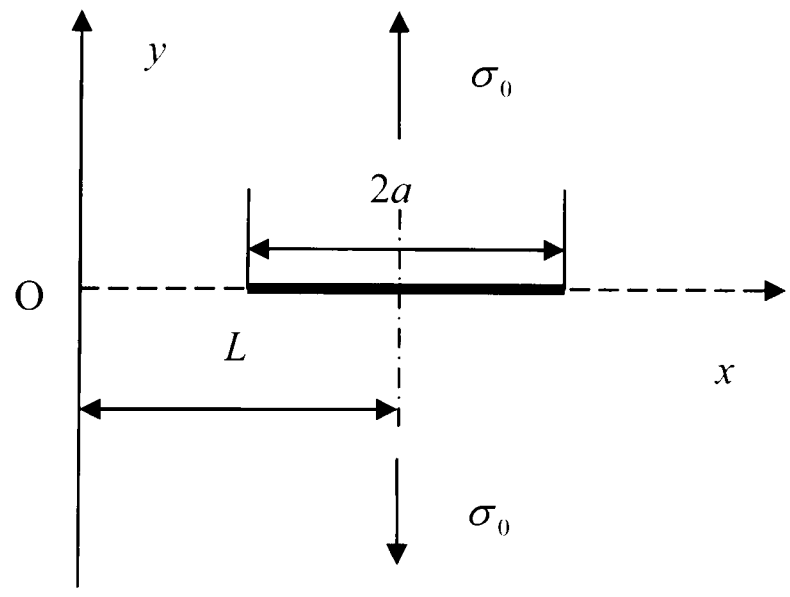

Figure 2-4: A perpendicular anticrack in a half plane in a uniform stress field.

Because both the total extensional strain and the change of curvature, due to the applied remote loading and the body forces, must vanish, the following integral equation holds

$$\frac{1}{2\pi(\kappa+1)}\int_{L-a}^{L+a}\{\frac{-2\kappa}{x-\xi}-\frac{(\kappa^2+1)}{x+\xi}-\frac{4\xi}{(x+\xi)^2}+\frac{8\xi^2}{(x+\xi)^3}\}p_x(\xi)d\xi=-\frac{(\kappa-3)\sigma_0}{4} \tag{2-23}$$

and a side condition, expressing the requirement that there be no net force on the anticrack, is

$$\int_{L-a}^{L+a} p_x(\xi)d\xi = 0\,. \tag{2-24}$$

The integral equation now has a generalised Cauchy kernel (in the case of a line force in an infinite plane the kernel is, of course, strictly Cauchy), and analytical inversion is impossible, but the use of standard Gauss-Chebyshev quadaratures works well, and convergence is quickly achieved.

In order to solve the integral equation (2-23) it was written in normalised form through the substitutions

$$s = \frac{\xi - L}{a}, \qquad t = \frac{x - L}{a}. \tag{2-25}$$

The equation then becomes

$$\frac{a}{2\pi(\kappa+1)}\int_{-1}^{1}\left\{\begin{array}{l}\dfrac{-2\kappa}{at-as} - \dfrac{(\kappa^2+1)}{(as+at+2L)} \\ -\dfrac{4(L+as)}{(as+at+2L)^2} + \dfrac{8(L+as)^2}{(as+at+2L)^3}\end{array}\right\} p_x(s)ds = -\frac{(\kappa-3)\sigma_0}{4}\,. \tag{2-26}$$

The side condition becomes

$$\int_{-1}^{1} p_x(s)ds = 0\,. \tag{2-27}$$

It is known that the state of displacement derivative is singular at both ends of the anticrack. Hence we write

$$p_x(s) = \phi_x(s)(1-s^2)^{-1/2} \tag{2-28}$$

and the discretised forms of the integral equations are

$$\sum_{i=1}^{n} W_i\phi_x(s_i)\left\{\begin{array}{l}\dfrac{-2\kappa}{at_k - as_i} - \dfrac{(\kappa^2+1)}{(as_i+at_k+2L)} \\ -\dfrac{4(L+as_i)}{(as_i+at_k+2L)^2} + \dfrac{8(L+as_i)^2}{(as_i+at_k+2L)^3}\end{array}\right\} = -\frac{\pi(\kappa+1)(\kappa-3)\sigma_0}{2a} \quad k = 1,\ldots,n-1 \tag{2-29}$$

$$\sum_{i=1}^{n} W_i\phi_x(s_i) = 0 \tag{2-30}$$

where

$$s_i = \cos\left(\frac{2i-1}{2n}\pi\right), \qquad i = 1,\ldots,n \tag{2-31a}$$

$$t_k = \cos\left(\frac{k}{n}\pi\right), \qquad k = 1,\ldots,n-1 \tag{2-31b}$$

$$W_i = \frac{\pi}{n}. \tag{2-31c}$$

These represent a system of n simultaneous equations for the n unknowns $\phi_x(s_i)$. When these values have been found, the stresses and displacements at an arbitrary point can be determined.

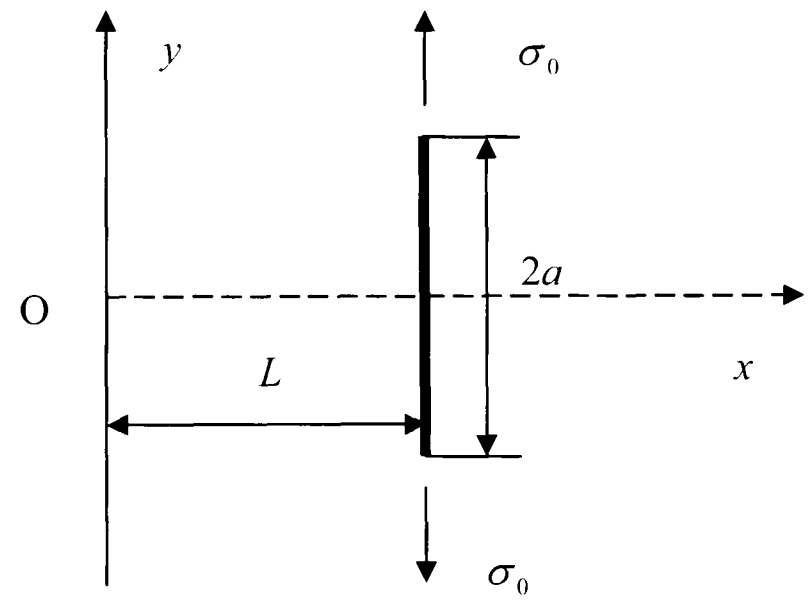

Figure 2-5: A parallel anticrack in a half plane in a uniform stress field.

The next step in increasing complexity is to consider an anticrack parallel with the free surface, Figure 2-5. This retains the simplification that the axis set employed can be used without transformation, but it is no longer true to say that the problem is uncoupled, as x-direction forces induce both x- and y- direction displacements, and vice versa. The example loading chosen is again uniform tension parallel with the free surface. The displacements induced by the *remote loading* are

$$2\mu\frac{\partial\overline{u}_x(L;y)}{\partial y} = 0 \tag{2-32a}$$

$$2\mu\frac{\partial\overline{u}_y(L;y)}{\partial y}=2\mu\varepsilon_{yy}=2\mu\frac{1}{8\mu}[(1+\kappa)\sigma_{yy}+(\kappa-3)\sigma_{xx}]=\frac{(1+\kappa)\sigma_0}{4} \tag{2-32b}$$

whilst the boundary conditions are

$$2\mu\frac{\partial u_x(L;y)\big|p_x}{\partial y}+2\mu\frac{\partial u_x(L;y)\big|p_y}{\partial y}=0 \tag{2-33a}$$

$$2\mu\frac{\partial u_y(L;y)\big|p_x}{\partial y}+2\mu\frac{\partial u_y(L;y)\big|p_y}{\partial y}+2\mu\frac{\partial\overline{u}_y(L;y)\big|\sigma_0}{\partial y}=0\,. \tag{2-33b}$$

The following integral equations therefore ensure that the anticrack remains straight and of the same length:

$$\begin{aligned}&\frac{1}{2\pi(\kappa+1)}\int_{-a}^{a}(y-\eta)\{\frac{-2\kappa}{(y-\eta)^2}-\frac{1+\kappa^2}{(4L^2+(y-\eta)^2)}-\frac{16L^2\kappa-8L^2}{(4L^2+(y-\eta)^2)^2}-\frac{128L^4}{(4L^2+(y-\eta)^2)^3}\}p_x(\eta)d\eta+\\&\frac{1}{2\pi(\kappa+1)}\int_{-a}^{a}\{\frac{(-1+\kappa^2)2L}{(4L^2+(y-\eta)^2)}-\frac{16L^3}{(4L^2+(y-\eta)^2)^2}+\frac{64L^3(y-d)^2}{(4L^2+(y-\eta)^2)^3}\}p_y(\eta)d\eta=0\end{aligned} \tag{2-34a}$$

$$\begin{aligned}&\frac{1}{2\pi(\kappa+1)}\int_{-a}^{a}\{-\frac{(-1+\kappa^2)2L}{(4L^2+(y-\eta)^2)}+\frac{16L^3}{(4L^2+(y-\eta)^2)^2}-\frac{64L^3(y-\eta)^2}{(4L^2+(y-\eta)^2)^3}\}p_x(\eta)d\eta+\\&\frac{1}{2\pi(\kappa+1)}\int_{-a}^{a}(y-\eta)\{\frac{-2\kappa}{(y-\eta)^2}-\frac{1+\kappa^2}{(4L^2+(y-\eta)^2)}-\frac{128L^4}{(4L^2+(y-\eta)^2)^3}\}p_y(\eta)d\eta\\&=-\frac{(1+\kappa)\sigma_0}{4}.\end{aligned} \tag{2-34b}$$

The side conditions ensuring that there is no nett force on the anticrack are

$$\int_{-a}^{a}p_x(\eta)d\eta=0 \tag{2-35a}$$

$$\int_{-a}^{a}p_y(\eta)d\eta=0 \tag{2-35b}$$

Integral Equations (2-34, 2-35) comprise the solution to the problem. As with the solution for a crack in an infinite plane the integral equations (2-34) include dominant Cauchy terms but now also bounded terms representing the free surfaces. These are solved using numerical quadratures as described in the previous section.

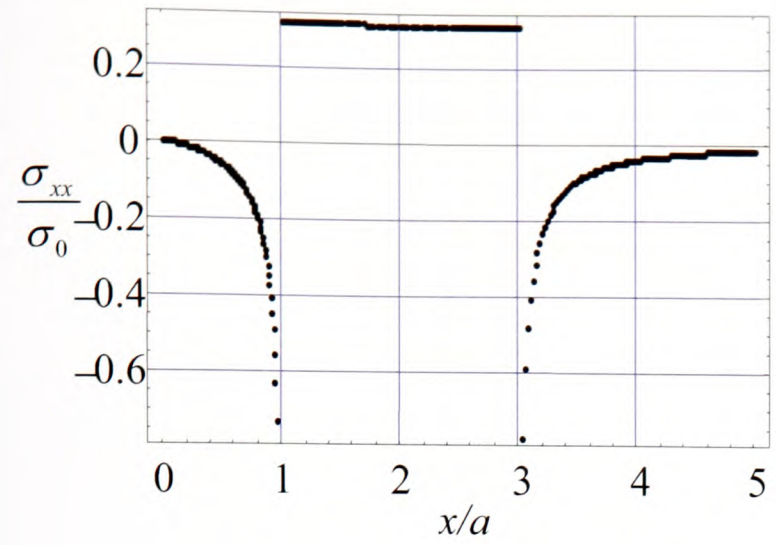

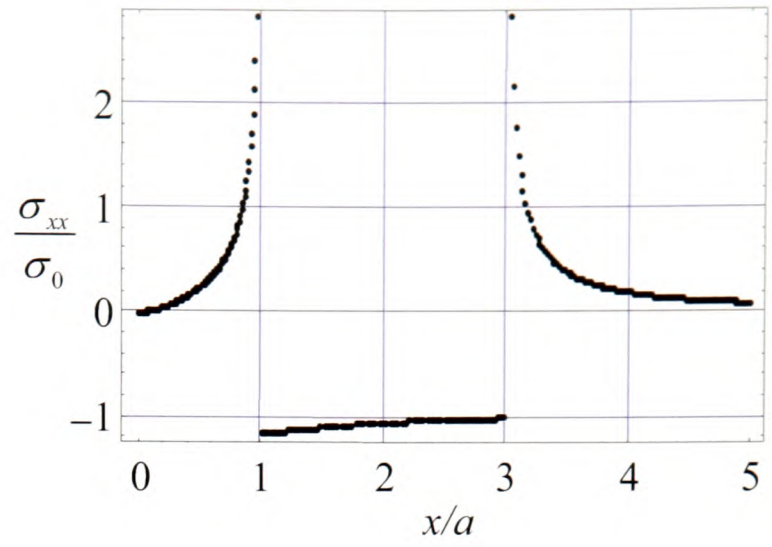

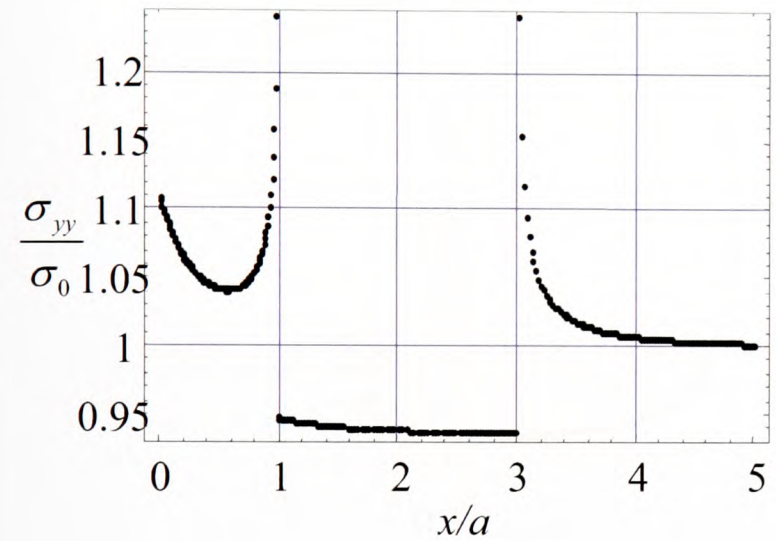

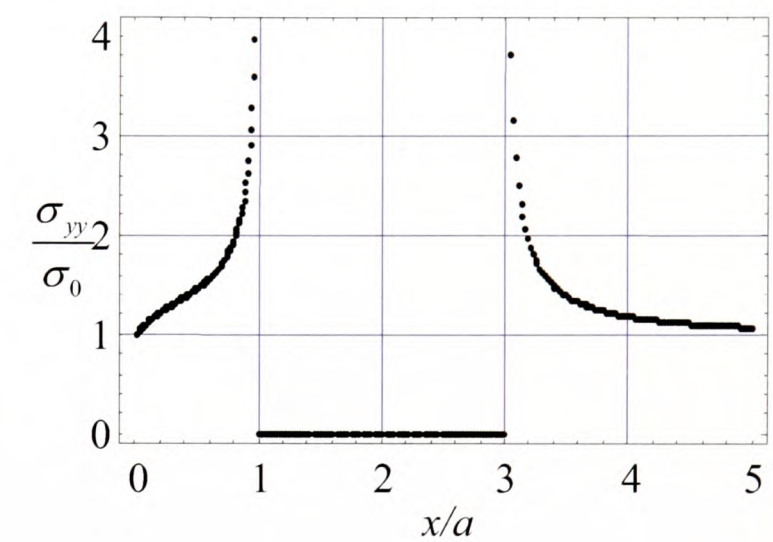

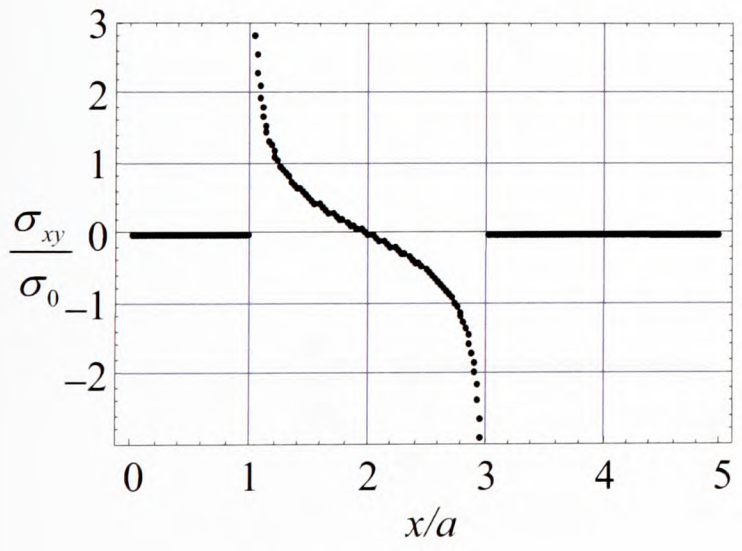

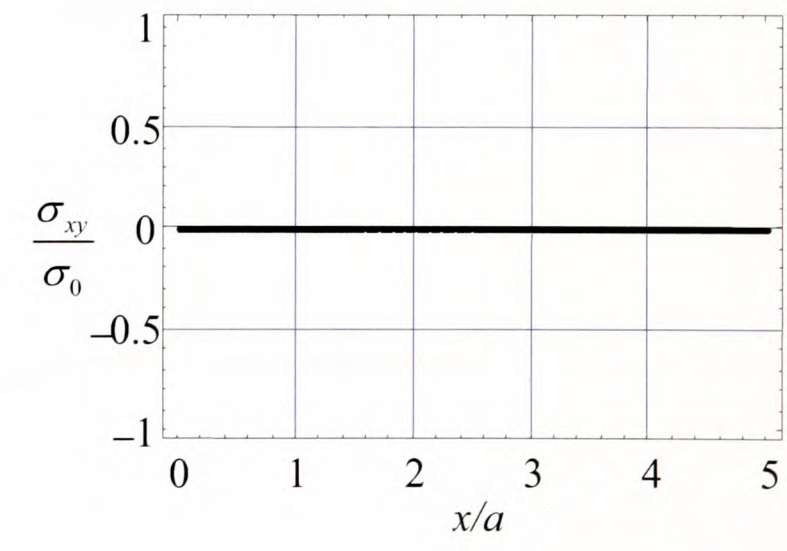

(a) Stresses along the line of an anticrack ($\nu = 0.25$) (b) Stresses along the line of a crack

Figure 2-6: Stresses ($\sigma_{xx}, \sigma_{yy}, \sigma_{xy}$ respectively) comparison of a crack and an anticrack in a half-plane, for a crack/anticrack perpendicular to the free surface, geometry shown in Figure 2-4, where $\nu = 0.25$, $L/a = 2$.

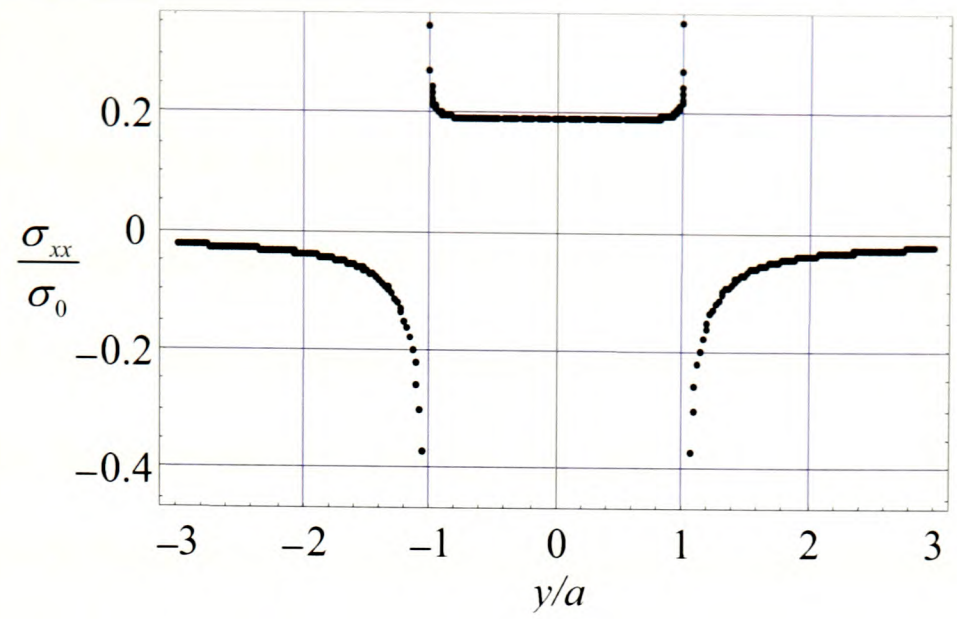

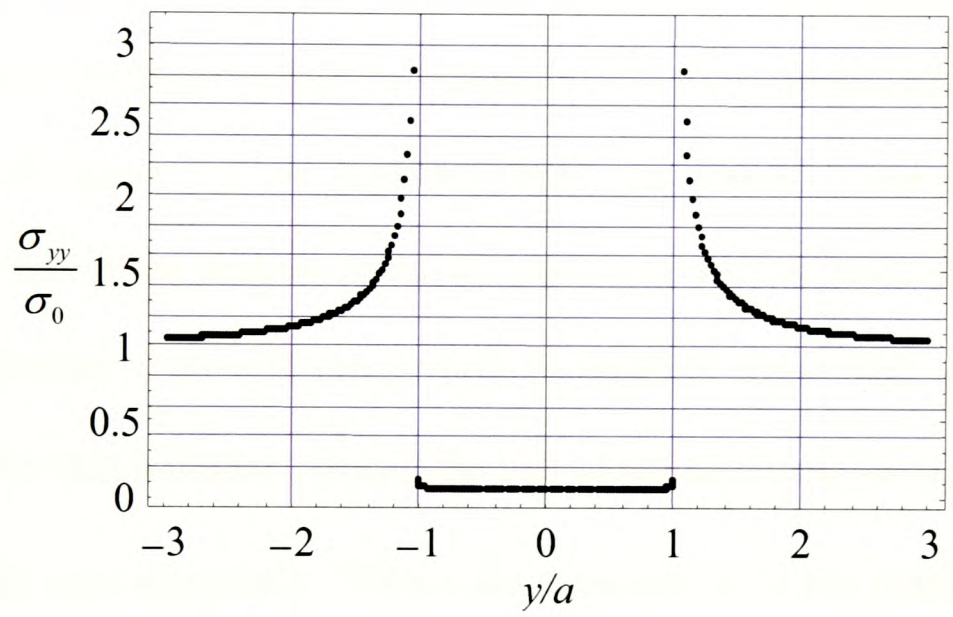

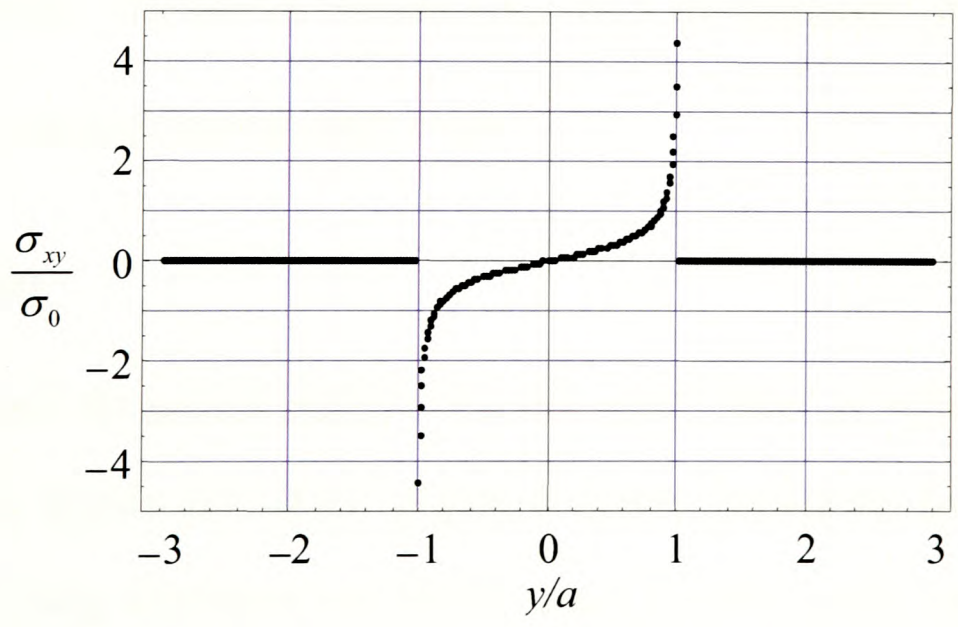

Figure 2-7: Stresses (σ_{xx}, σ_{yy}, σ_{xy} respectively) of an anticrack in a half-plane, for an anticrack parallel to the free surface, geometry shown in Figure 2-5, where $\nu = 0.25$, $L/a = 2$.

2.5. Results

Referring to Figure 2-4, an anticrack perpendicular to the free surface, the resultant stresses along the line of the anticrack and a similarly positioned crack are compared and shown in Figure 2-6. For a crack problem the state of stress induced is independent of elastic constants whilst for the anticrack the solution depends on Possion's ratio. There are clear parallels to be drawn between the two columns of figures, but also differences. It is quite clear that the traction boundary conditions are reflected in the crack problem, whilst it is, effectively, strain boundary conditions which are imposed along the anticrack. Thus, the latter inevitably involves a coupling through the Poisson effect when stresses are displayed.

Referring to Figure 2-5, an anticrack under the depth, L, and parallel to the free surface, this gives rise to the stresses along the line of the anticrack are shown in Figure 2-7. Of course an equivalent crack will not perturb the applied stress field at all, and hence no results are shown for this problem. Around the tips of the anticrack, the normal stresses (σ_{xx}, σ_{yy}) show a square root singularity. Within the anticrack, it is the shear stress, σ_{xy}, which displays the sigularity. The normal stresses (σ_{xx}, σ_{yy}) are symmetric about x-axis, but the shear stress, σ_{xy}, is anti-symmetric about x-axis.

2.6 Conclusion

In this chapter the general problem of a thin, rigid 'flake' or inclusion (an anticrack), present in a simple domain and subject to general remote loading has been considered. The problem is solved using distributed line forces, acting as strain nuclei, along the line of the anticrack and strong parallels are drawn with the use of distributed dislocations in the solution of conventional cracks: the integral equations derived have similar properties and may be solved using similar methods, but of course the anticrack-end general stress field is rather different in character, and corresponds to a different asymptotic problem.

Chapter 3

The Influence Function for Self-Equilibrating Forces on a Semi-Infinite Wedge

3.1 Introduction

This chapter is concerned with the determination of the normal surface displacement for a pair of opposed forces applied to the surfaces of a semi-infinite wedge, Figure 3-1. The reason for studying this problem is to provide an influence function permitting the effect of notch closure under remote compression to be studied (Churchman, Dini and Hills, 2006), although it also has application to other notch-contact problems. One possible technique for examining the problem at hand would be to use the Mellin transform (Barber, 1992). However, the principal feature required in the solution is the surface displacement, and it seems natural to ensure that, if the observation point is close to the force itself, the half-plane solution be recovered. It was also noted that, along the notch bisector $\theta = 0$, Figure 3-1, the shearing stress must vanish, together with the θ-direction displacement. Thus, by imposing, along this line, the hybrid traction/ displacement boundary conditions described, the correct boundary conditions along the notch bisector can be achieved, and the half-plane solution automatically recovered when the observation point moves from the 'notch' apex toward the

point of application of the force (and this observation applies *a fortiori* if the observation point is exterior to the line force).

The accepted way of achieving a traction boundary condition along an internal line is to employ a distribution of dislocations as strain nuclei (Hills, Kelly, Dai and Korsunsky, 1996). This has been done many times and does not merit a detailed description here. On the other hand, point forces are more suited to the imposition of internal displacement boundary conditions, as described in Chapter 2. Although a combination of the crack and anticrack techniques should work in principle, it remained to be seen if the Cauchy nature of the two kernels, when expressing the state of stress, would be complementary or produce a conflict in the ensuing quadrature. The subject of this chapter is therefore two-fold. First, it permits the imposition of mixed boundary conditions along an internal line in a plane problem. In this case the line exists within a half-plane, but the problem could equally be applied to other domains in which the solution for nuclei is known. Secondly, the specific application analyzed permits useful influence functions for the problem shown in Figure 3-1 to be found.

3.2 Formulation

The problem to be addressed is shown in detail in Figure 3-1 (a). Symmetry conditions show that, along the notch bisector, $u_\theta = \tau_{r\theta} = 0 \quad \forall r$. It follows that the state of stress in the sector $0 \le \theta \le \alpha$ can be found from the half-plane problem depicted in Figure 3-1 (b). In order to do this, it is required to find the state of stress induced in the half plane by a normal load, P, with a correction to establish the condition $u_{\hat{y}} = \tau_{\hat{x}\hat{y}} = 0$ on the line $\hat{y} = 0$, $\hat{x} \ge 0$. It is assumed that the influence functions giving the state of stress and displacement within a half-plane, due to both a line force and a dislocation are known. Thus, it is known the four influence functions

connecting a dislocation b_k and a line force P_k with displacement $u_i(x,y)$ and the state of stress $\sigma_{ij}(x,y)$ (i.e. the functions G_{kij}, U_{ki} (Hills, Kelly, Dai and Korsunsky, 1996), S_{kij}, D_{ki} see Appendix A) are defined in the following four equations, where (c, d) are the coordinates of the strain nucleus, and (x, y) the observation point:

$$\sigma_{bij}(x,y)=\frac{2\mu}{\pi(\kappa+1)}b_k(c,d)G_{kij}(x,y,c,d) \qquad k,i,j=x,y \tag{3-1}$$

$$u_{bi}(x,y)=\frac{1}{2\pi(\kappa+1)}b_k(c,d)U_{ki}(x,y,c,d) \qquad k,i=x,y \tag{3-2}$$

$$\sigma_{Pij}=\frac{1}{2\pi(\kappa+1)}P_k(c,d)S_{kij}(x,y,c,d) \qquad k,i,j=x,y \tag{3-3}$$

$$u_{Pi}(x,y)=\frac{1}{2\mu 2\pi(\kappa+1)}P_k(c,d)D_{ki}(x,y,c,d) \quad k,i=x,y. \tag{3-4}$$

Here, μ is the modulus of rigidity and κ is Kolosov's constant.

The intention is to write down two (coupled) singular integral equations to establish the following boundary conditions along the line of crack/anticrack,

$$0=\sigma_{\hat{y}\hat{y}}(\hat{x},0)\equiv\overline{\sigma}_{\hat{y}\hat{y}}(\hat{x},0)+\widetilde{\sigma}_{b\hat{y}\hat{y}}(\hat{x},0)+\widetilde{\sigma}_{P\hat{y}\hat{y}}(\hat{x},0), \qquad \hat{y}=0,\hat{x}\geq 0. \tag{3-5}$$

$$0=u_{\hat{y}}(\hat{x},0)\equiv\overline{u}_{\hat{y}}(\hat{x},0)+\widetilde{u}_{b\hat{y}}(\hat{x},0)+\widetilde{u}_{P\hat{y}}(\hat{x},0), \qquad \hat{y}=0,\hat{x}\geq 0. \tag{3-6}$$

where, in each equation, the first term on the right hand side is associated with the surface normal load, P, whilst the second is the corrective term associated with dislocations and the third the corrective term associated with point forces, the last two distributed along the line segment $\hat{y}=0$, $\hat{x}\geq 0$. In fact, we will choose to specify the displacement gradients, because this removes the unknown rigid body term. The boundary conditions become

$$0=\sigma_{\hat{y}\hat{y}}(\hat{x},0)\equiv\overline{\sigma}_{\hat{y}\hat{y}}(\hat{x},0)+\widetilde{\sigma}_{b\hat{y}\hat{y}}(\hat{x},0)+\widetilde{\sigma}_{P\hat{y}\hat{y}}(\hat{x},0), \qquad \hat{y}=0,\hat{x}\geq 0. \tag{3-7}$$

$$0=\frac{\partial u_{\hat{y}}(\hat{x},0)}{\partial\hat{x}}\equiv\frac{\partial\overline{u}_{\hat{y}}(\hat{x},0)}{\partial\hat{x}}+\frac{\partial\widetilde{u}_{b\hat{y}}(\hat{x},0)}{\partial\hat{x}}+\frac{\partial\widetilde{u}_{P\hat{y}}(\hat{x},0)}{\partial\hat{x}}, \qquad \hat{y}=0,\hat{x}\geq 0. \tag{3-8}$$

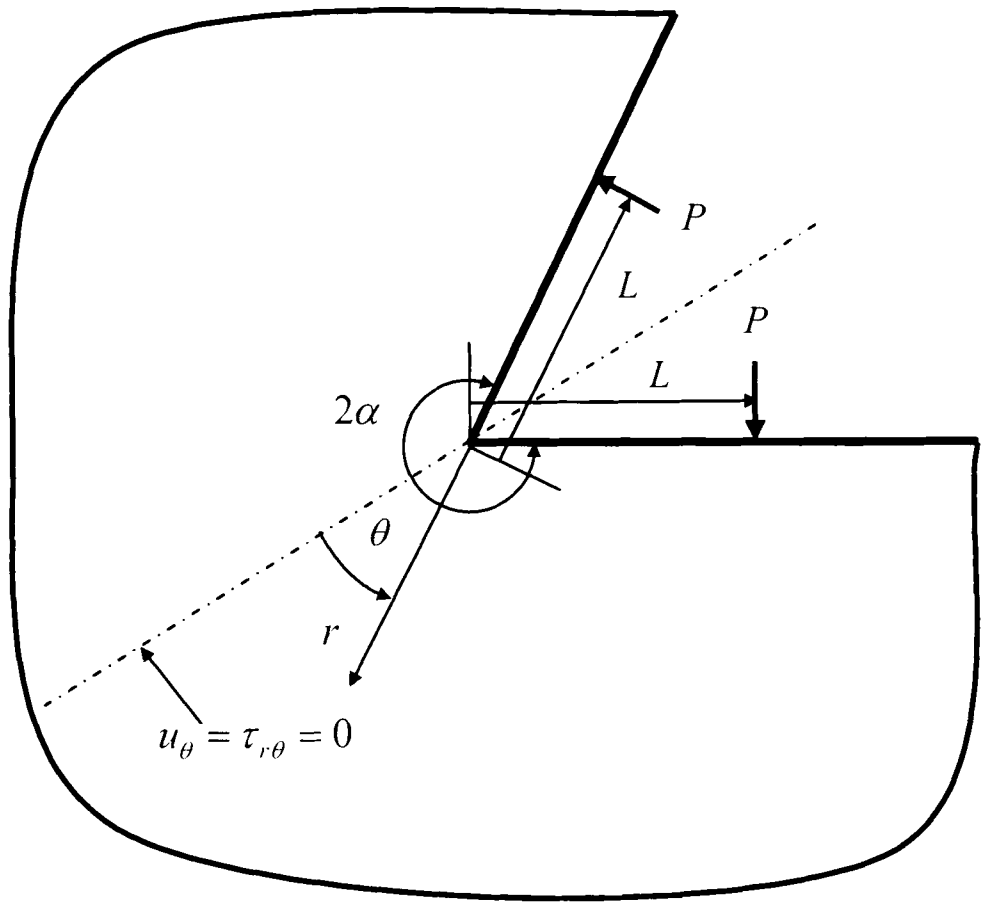

(a)

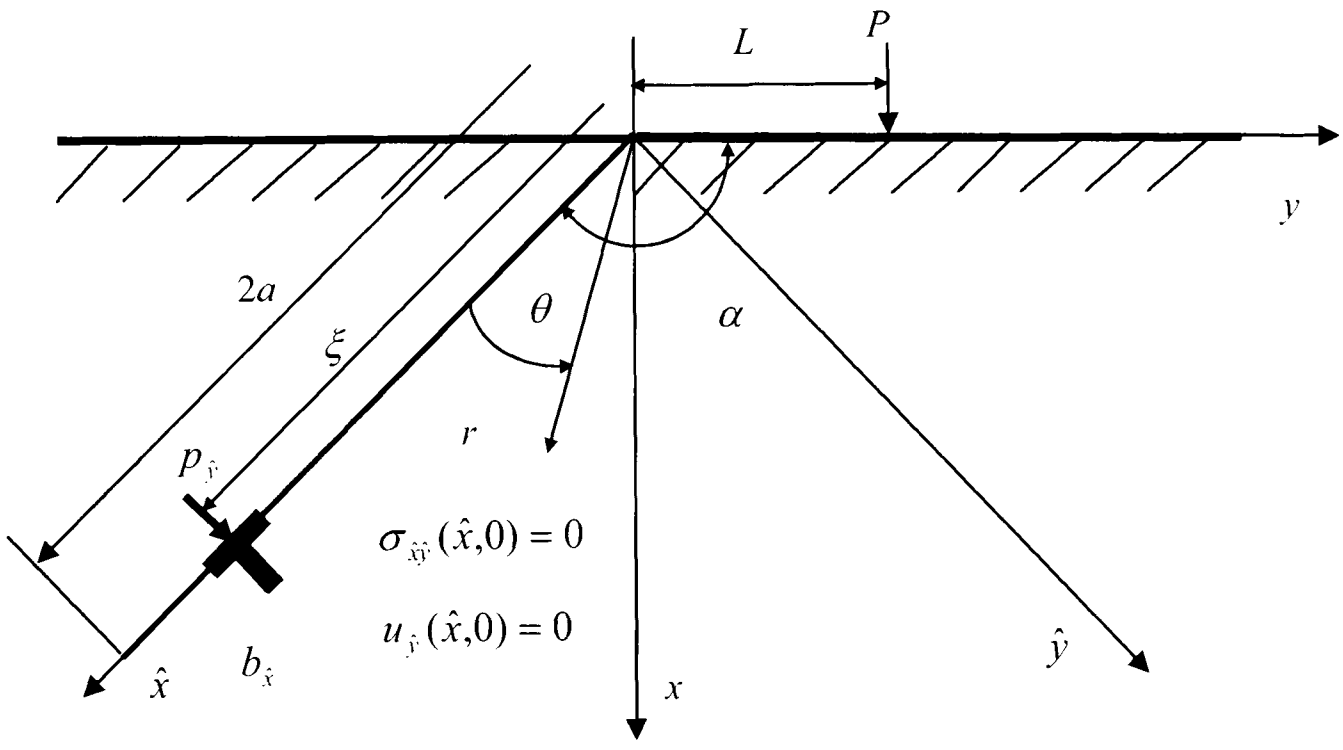

(b)

Figure 3-1: (a) A semi-infinite notch under the action of normal forces *P*. (b) A half plane subject to displacement and traction boundary conditions along the line $\theta = 0$, to represent conditions along the notch bisector.

Before this is possible two steps are needed. First, we must establish which of the terms in the four influence functions are singular and which are not, so that there are no conflicting requirements in the quadratures employed. Secondly, the axis set in which the solutions are expressed must be re-oriented along the local axis set fixed to crack/anticrack, so that the boundary conditions can be properly established. The latter will be considered first.

Two steps in the operation are needed: first, the Burgers vector of the dislocation is, of course, a vector quantity, and the standard vector rotation matrix may be employed in order to express the Burgers' components in the local axis set, i.e.

$$\begin{Bmatrix} b_x \\ b_y \end{Bmatrix} = \begin{bmatrix} \cos(\pi/2-\alpha) & -\sin(\pi/2-\alpha) \\ \sin(\pi/2-\alpha) & \cos(\pi/2-\alpha) \end{bmatrix} \begin{Bmatrix} b_{\hat{x}} \\ b_{\hat{y}} \end{Bmatrix}. \tag{3-9}$$

Secondly, in order to transform the state of stress induced the standard second order transformation, which must be employed and is written as

$$\begin{Bmatrix} \sigma_{\hat{x}\hat{x}} \\ \sigma_{\hat{y}\hat{y}} \\ \sigma_{\hat{x}\hat{y}} \end{Bmatrix} = \begin{bmatrix} \cos^2(\pi/2-\alpha) & \sin^2(\pi/2-\alpha) & \sin(\pi-2\alpha) \\ \sin^2(\pi/2-\alpha) & \cos^2(\pi/2-\alpha) & -\sin(\pi-2\alpha) \\ -\frac{1}{2}\sin(\pi-2\alpha) & \frac{1}{2}\sin(\pi-2\alpha) & \cos(\pi-2\alpha) \end{bmatrix} \begin{Bmatrix} \sigma_{xx} \\ \sigma_{yy} \\ \sigma_{xy} \end{Bmatrix}, \tag{3-10}$$

whilst the displacement state transforms also as a vector, i.e.

$$\begin{Bmatrix} u_{\hat{x}} \\ u_{\hat{y}} \end{Bmatrix} = \begin{bmatrix} \cos(\pi/2-\alpha) & \sin(\pi/2-\alpha) \\ -\sin(\pi/2-\alpha) & \cos(\pi/2-\alpha) \end{bmatrix} \begin{Bmatrix} u_x \\ u_y \end{Bmatrix}. \tag{3-11}$$

When the transformation equations are applied to the influence functions and the boundary conditions along the line imposed (equations 3-7, 3-8) the integral equations are

$$\begin{aligned} 0 = \overline{\sigma}_{\hat{x}\hat{y}}(\hat{x},0) &+ \frac{2\mu}{\pi(\kappa+1)} \int_0^{2a} B_{\hat{x}}(\xi,0) G_{\hat{x}\hat{x}\hat{y}}(\hat{x},0,\xi,0)\, d\xi \\ &+ \frac{1}{2\pi(\kappa+1)} \int_0^{2a} p_{\hat{y}}(\xi,0) S_{\hat{y}\hat{x}\hat{y}}(\hat{x},0,\xi,0)\, d\xi \qquad \hat{y}=0, \quad 0 \le \hat{x} \le 2a \end{aligned} \tag{3-12}$$

$$\begin{aligned} 0 = \frac{\partial \overline{u}_{\hat{y}}(\hat{x},0)}{\partial \hat{x}} &+ \frac{1}{2\pi(\kappa+1)} \int_0^{2a} B_{\hat{x}}(\xi,0) \frac{\partial U_{\hat{x}\hat{y}}(\hat{x},0,\xi,0)}{\partial \hat{x}}\, d\xi \\ &+ \frac{1}{2\mu 2\pi(\kappa+1)} \int_0^{2a} p_{\hat{y}}(\xi,0) \frac{\partial D_{\hat{y}\hat{y}}(\hat{x},0,\xi,0)}{\partial \hat{x}}\, d\xi \quad \hat{y}=0, \quad 0 \le \hat{x} \le 2a \end{aligned} \tag{3-13}$$

where $B_{\hat{x}}(\xi,0) = db_{\hat{x}}/d\xi$ and $p_{\hat{y}}(\xi,0) = dP_{\hat{y}}/d\xi$.

The kernels arising in equation (3-12) can be split into bounded parts, where a prime is added below, together with a Cauchy singular term

$$G_{\hat{x}\hat{x}\hat{y}}(\hat{x},0,\xi,0) = \frac{1}{\hat{x}-\xi} + G'_{\hat{x}\hat{x}\hat{y}}(\hat{x},0,\xi,0) \tag{3-14}$$

$$S_{\hat{y}\hat{x}\hat{y}}(\hat{x},0,\xi,0) = \frac{1-\kappa}{\hat{x}-\xi} + S'_{\hat{y}\hat{x}\hat{y}}(\hat{x},0,\xi,0). \tag{3-15}$$

Similarly, the kernels arising in equation (3-13) can be split into a bounded part, where a prime is added, together with a Cauchy singular term

$$\frac{\partial U_{\hat{x}\hat{y}}(\hat{x},0,\xi,0)}{\partial\hat{x}} = \frac{(1-\kappa)}{(\hat{x}-\xi)} + \frac{\partial U'_{\hat{x}\hat{y}}(\hat{x},0,\xi,0)}{\partial\hat{x}} \tag{3-16}$$

$$\frac{\partial D_{\hat{y}\hat{y}}(\hat{x},0,\xi,0)}{\partial\hat{x}} = \frac{-2\kappa}{(\hat{x}-\xi)} + \frac{\partial D'_{\hat{y}\hat{y}}(\hat{x},0,\xi,0)}{\partial\hat{x}}. \tag{3-17}$$

Equations (3-12) and (3-13) can therefore be written in the following form, when the singular terms are explicitly separated

$$\begin{aligned} -\overline{\sigma}_{\hat{x}\hat{y}}(\hat{x},0) = {} & \frac{2\mu}{\pi(\kappa+1)}\int_0^{2a} B_{\hat{x}}(\xi,0)\left[\frac{1}{\hat{x}-\xi} + G'_{\hat{x}\hat{x}\hat{y}}(\hat{x},0,\xi,0)\right]d\xi \\ & + \frac{1}{2\pi(\kappa+1)}\int_0^{2a} p_{\hat{y}}(\xi,0)\left[\frac{1-\kappa}{\hat{x}-\xi} + S'_{\hat{y}\hat{x}\hat{y}}(\hat{x},0,\xi,0)\right]d\xi \qquad \hat{y}=0,\ \ 0\le\hat{x}\le 2a \end{aligned} \tag{3-18}$$

$$\begin{aligned} -2\mu\frac{\partial\overline{u}_{\hat{y}}(\hat{x},0)}{\partial\hat{x}} = {} & \frac{2\mu}{2\pi(\kappa+1)}\int_0^{2a} B_{\hat{x}}(\xi,0)\left[\frac{(1-\kappa)}{(\hat{x}-\xi)} + \frac{\partial U'_{\hat{x}\hat{y}}(\hat{x},0,\xi,0)}{\partial\hat{x}}\right]d\xi \\ & + \frac{1}{2\pi(\kappa+1)}\int_0^{2a} p_{\hat{y}}(\xi,0)\left[-\frac{2\kappa}{(\hat{x}-\xi)} + \frac{\partial D'_{\hat{y}\hat{y}}(\hat{x},0,\xi,0)}{\partial\hat{x}}\right]d\xi \qquad \hat{y}=0,\ \ 0\le\hat{x}\le 2a \end{aligned} \tag{3-19}$$

In order to solve the integral equations they must be written in normalised form through the substitutions

$$s = \frac{\xi}{a} - 1, \qquad t = \frac{\hat{x}}{a} - 1. \tag{3-20}$$

The equations then become

$$-\overline{\sigma}_{\hat{x}\hat{y}}(t,0)=\frac{2\mu}{\pi(\kappa+1)}\int_{-1}^{1}B_{\hat{x}}(s,0)\left[\frac{1}{t-s}+aG'_{\hat{x}\hat{x}\hat{y}}(t,0,s,0)\right]ds$$
$$+\frac{1}{2\pi(\kappa+1)}\int_{-1}^{1}p_{\hat{y}}(\xi,0)\left[\frac{1-\kappa}{t-s}+aS'_{\hat{x}\hat{x}\hat{y}}(t,0,s,0)\right]ds \qquad -1\le t\le 1 \tag{3-21}$$

$$-2\mu\frac{\partial\overline{u}_{\hat{y}}}{\partial\hat{x}}(t,0)=\frac{2\mu}{2\pi(\kappa+1)}\int_{-1}^{1}B_{\hat{x}}(s,0)\left[\frac{(1-\kappa)}{(t-s)}+a\frac{\partial U'_{\hat{x}\hat{y}}}{\partial\hat{x}}(t,0,s,0)\right]ds$$
$$+\frac{1}{2\pi(\kappa+1)}\int_{-1}^{1}p_{\hat{y}}(s,0)\left[-\frac{2\kappa}{(t-s)}+a\frac{\partial D'_{\hat{y}\hat{y}}}{\partial\hat{x}}(t,0,s,0)\right]ds \quad -1\le t\le 1 \tag{3-22}$$

It is known that, at the corner of the notch, the stress state varies as $r^{\lambda-1}$, where r is a radial coordinate from the 'notch' apex, and $-0.5\le\lambda-1\le-0.45555$ for a notch $270°\le 2\alpha\le 360°$, by using Williams' asymptotic approach (Williams, 1952). This behaviour is approximated by one which is square-root singular in our choice of fundamental function, and hence we write

$$B_{\hat{x}}(s)=\phi_{\hat{x}}(s)(1-s^2)^{1/2} \tag{3-23a}$$

$$p_{\hat{y}}(s)=\phi_{\hat{y}}(s)(1-s^2)^{-1/2}. \tag{3-23b}$$

The side conditions are

$$\int_0^{2a}B_{\hat{x}}(\xi)d\xi=\int_{-1}^{1}B_{\hat{x}}(s)ds=0 \tag{3-24}$$

$$\int_0^{2a}p_{\hat{y}}(\xi)d\xi=\int_{-1}^{1}p_{\hat{y}}(s)ds=0\,, \tag{3-25}$$

and the discretised forms of the integral equations are

$$-\overline{\sigma}_{\hat{x}\hat{y}}(t_k)=\sum_{i=1}^{n}W_i\left\{\begin{array}{l}\dfrac{2\mu}{(\kappa+1)}\phi_{\hat{x}}(s_i)\left[\dfrac{1}{t_k-s_i}+aG'_{\hat{x}\hat{x}\hat{y}}(t_k,s_i)\right]\\ +\dfrac{1}{2(\kappa+1)}\phi_{\hat{y}}(s_i)\left[\dfrac{1-\kappa}{t_k-s_i}+aS'_{\hat{y}\hat{x}\hat{y}}(t_k,s_i)\right]\end{array}\right\}\quad k=1,\ldots,n-1 \tag{3-26}$$

$$-2\mu\frac{\partial\overline{u}_{\hat{y}}}{\partial\hat{x}}(t_k)=\sum_{i=1}^{n}W_i\left\{\begin{array}{l}\dfrac{\mu}{(\kappa+1)}\phi_{\hat{x}}(s_i)\left[\dfrac{(1-\kappa)}{(t_k-s_i)}+a\dfrac{\partial U'_{\hat{x}\hat{y}}}{\partial\hat{x}}(t_k,s_i)\right]\\ +\dfrac{1}{2(\kappa+1)}\phi_{\hat{y}}(s_i)\left[-\dfrac{2\kappa}{(t_k-s_i)}+a\dfrac{\partial D'_{\hat{y}\hat{y}}}{\partial\hat{x}}(t_k,s_i)\right]\end{array}\right\}\quad k=1,\ldots,n-1 \tag{3-27}$$

$$\sum_{i=1}^{n} W_i \phi_{\hat{x}}(s_i) = 0 \tag{3-28}$$

$$\sum_{i=1}^{n} W_i \phi_{\hat{y}}(s_i) = 0 \tag{3-29}$$

where

$$s_i = \cos\left(\frac{2i-1}{2n}\pi\right), \qquad i = 1, \ldots, n \tag{3-30a}$$

$$t_k = \cos\left(\frac{k}{n}\pi\right), \qquad k = 1, \ldots, n-1 \tag{3-30b}$$

$$W_i = \frac{\pi}{n}. \tag{3-30c}$$

These represent a system of $2n$ simultaneous equations for the $2n$ unknowns $\phi_{\hat{x}}(s_i)$ and $\phi_{\hat{y}}(s_i)$. When these values have been found, the stresses and displacements at an arbitrary point can be determined.

Lastly, the left hand side of equations (3-26) and (3-27) represent the stresses and displacements gradients resulting from a point force acting on the surface of a half plane and are given by Timoshenko and Goodier (Timoshenko and Goodier, 1970)

$$\bar{\sigma}_{xx} = -\frac{2Px^3}{\pi[x^2 + (y-L)^2]^2} \tag{3-31a}$$

$$\bar{\sigma}_{yy} = -\frac{2Pxy^2}{\pi[x^2 + (y-L)^2]^2} \tag{3-31b}$$

$$\bar{\sigma}_{xy} = -\frac{2Px^2 y}{\pi[x^2 + (y-L)^2]^2} \tag{3-31c}$$

$$\bar{u}_x = -\frac{4P(y-L)^2 + P[x^2 + (y-L)^2]^2(1+\kappa)\ln[x^2 + (y-L)^2]}{8\pi\mu[x^2 + (y-L)^2]} - B \tag{3-32}$$

$$\bar{u}_y = \frac{P\left[2x(y-L) - [x^2 + (y-L)^2](\kappa-1)\arcsin\left(\frac{(y-L)}{\sqrt{x^2 + (y-L)^2}}\right)\right]}{4\pi\mu[x^2 + (y-L)^2]} \tag{3-33}$$

where the constant B is determined by setting $\overline{u}_\lambda$ to zero at a point on the surface. In this case, because at the apex of the notch, the displacements are chosen equal to zero, $\overline{u}_\lambda(0) = 0$.

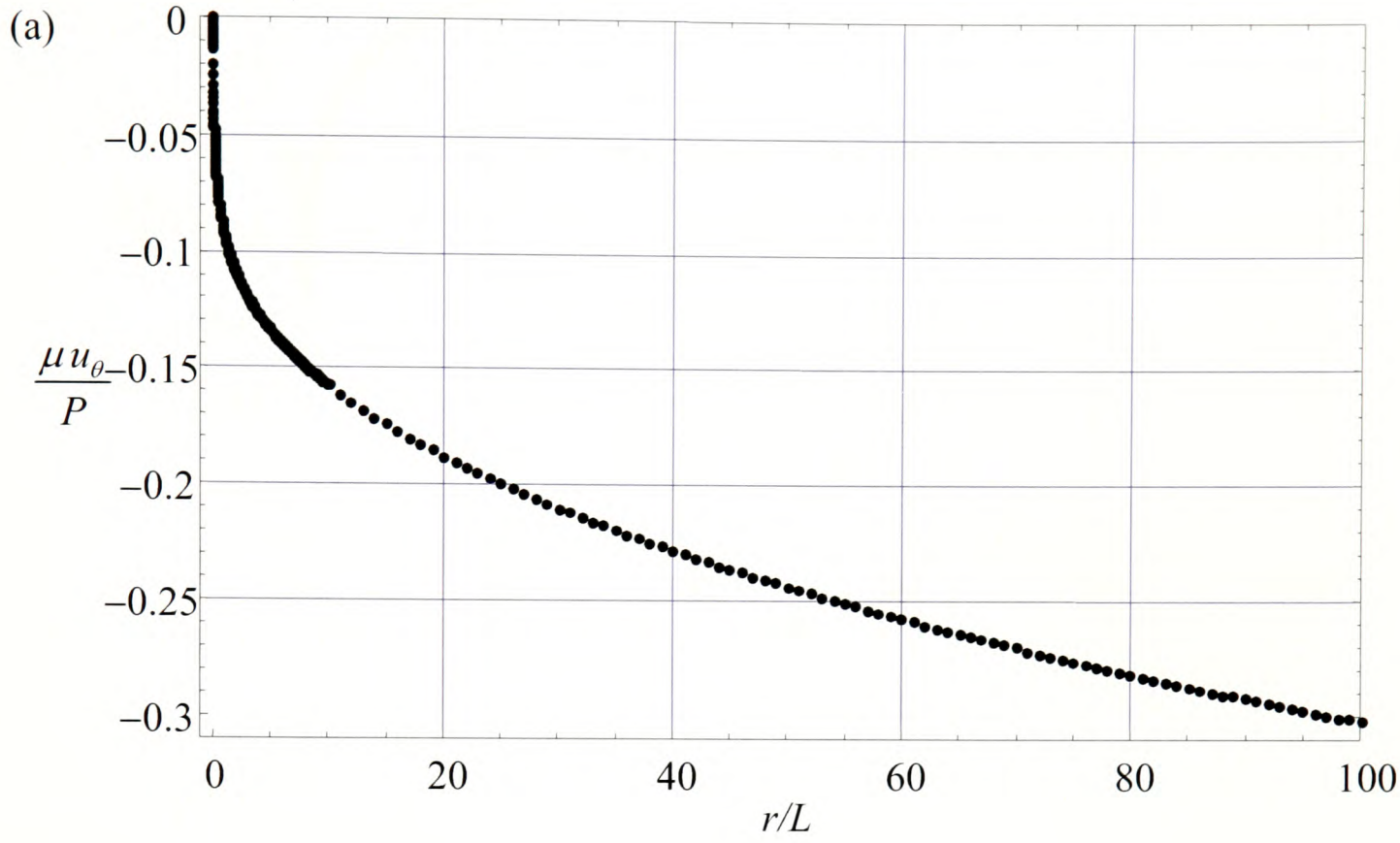

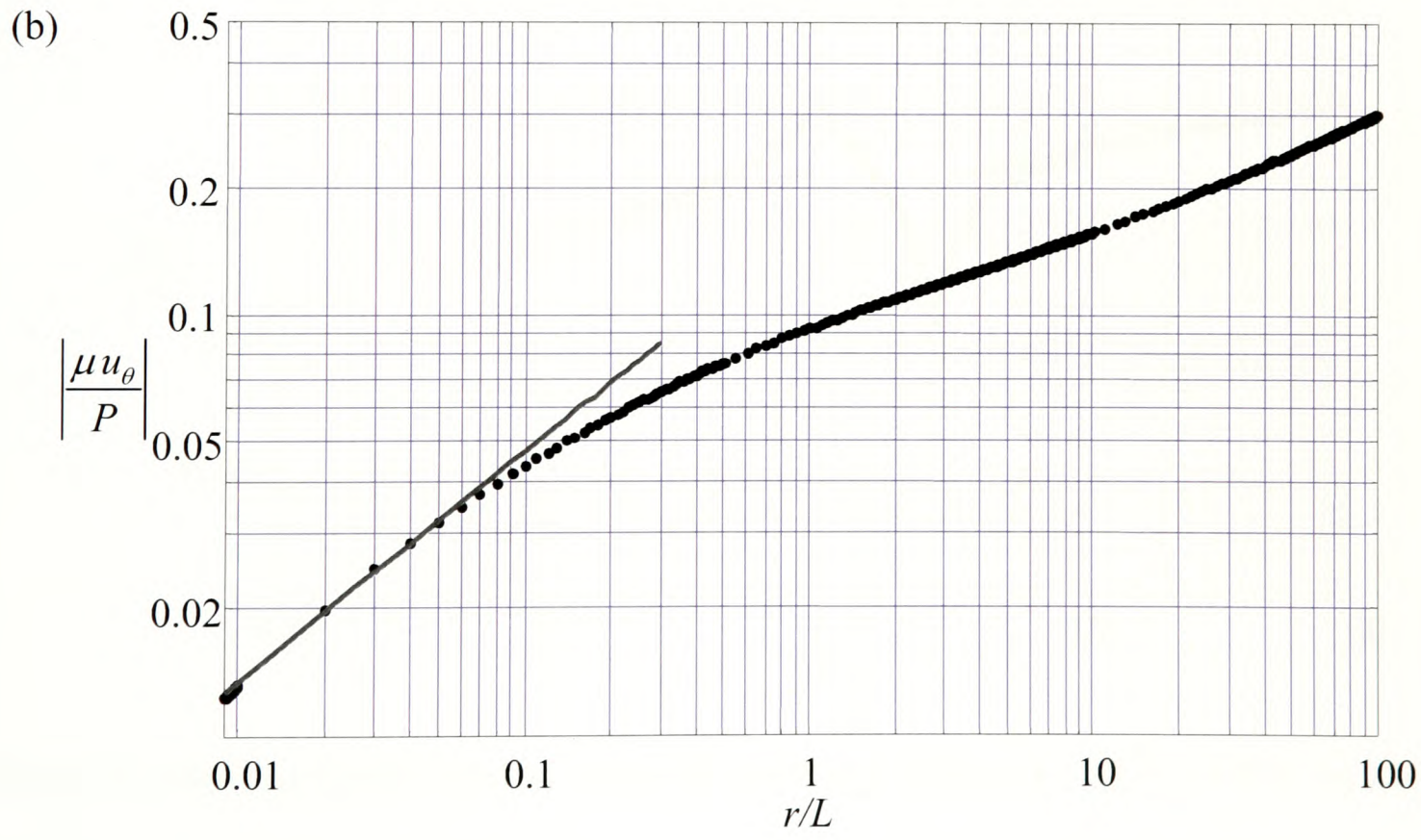

Figure 3-2: The connection displacement generated by the strain nuclei. (a) Linear plot (b) Log-Log plot of displacement μ_θ (black points) together with the asymptote (grey line)

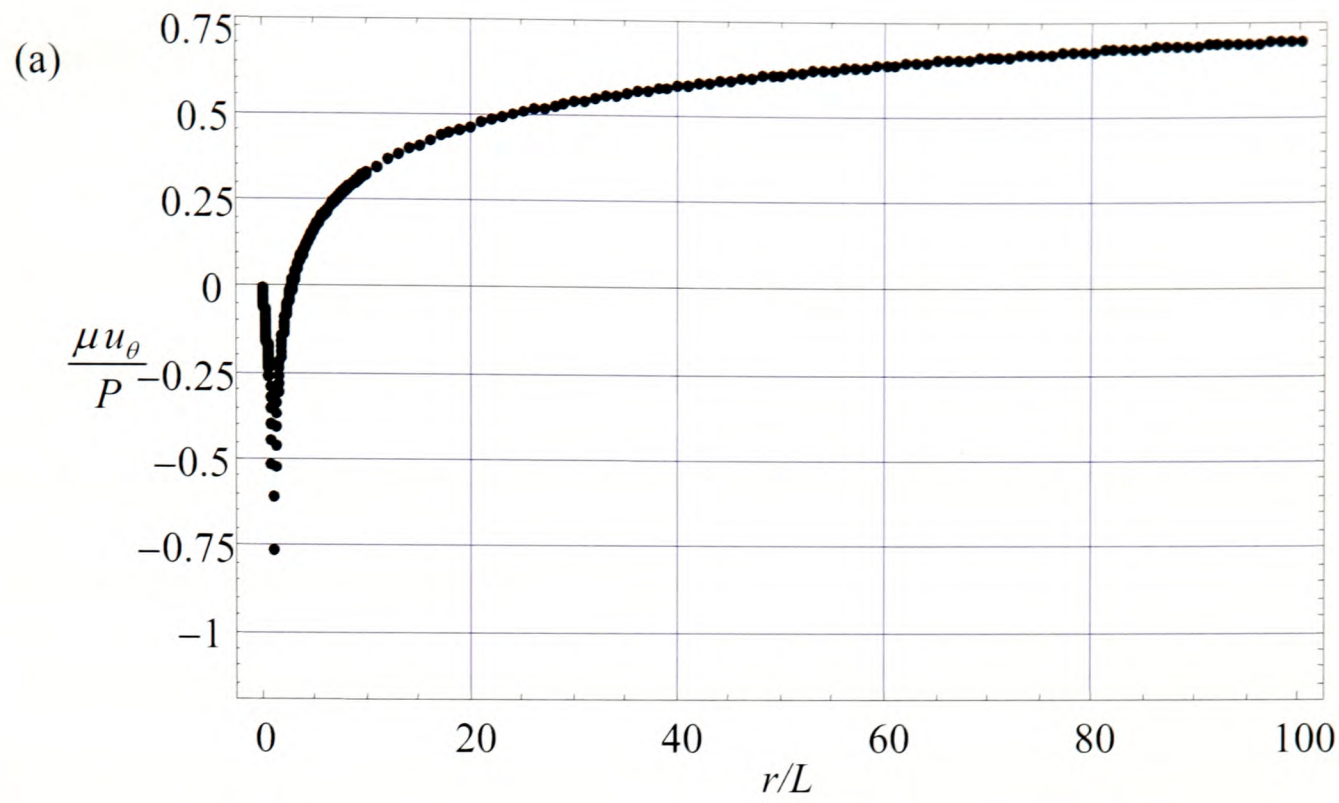

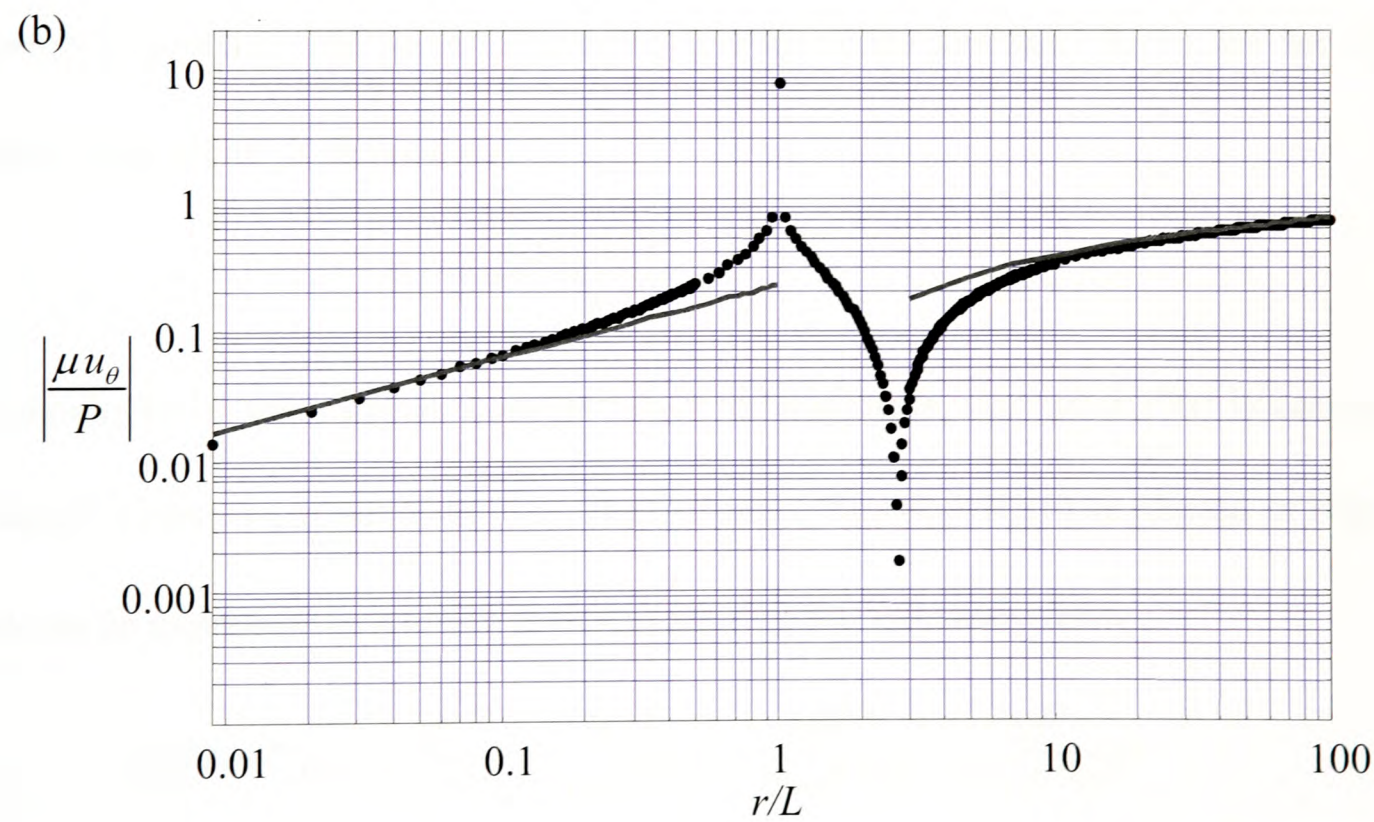

Figure 3-3: State of displacement u_θ along the notch side surface $\alpha = 135°, \nu = 0.3$. (a) Linear plot (b) Log-Log plot of displacement μ_θ (black points) together with the asymptotes (grey lines)

3.3 Results

We wish to find the effect of the mixed boundary conditions imposed within the half-plane on the normal displacement induced along the line $x=0$ for $y>0$ (Figure 3-1 (b)) by the normal point force. Because there is only a single length dimension in the problem (L) this can be used to non-dimensionalise the coordinates.

The total normal displacement along the notch surface is found by taking the effect of the applied point force on a half plane and adding a corrective solution and writing

$$u_\theta(0,\hat{r}) = \widetilde{u}_\theta(0,\hat{r}) + \overline{u}_\theta(0,\hat{r}), \tag{3-34}$$

where $\hat{r} = y/L$, $\overline{u}_\theta$ is the displacement caused by the point force on a half-plane and $\widetilde{u}_\theta$ is the displacement caused by the nuclei. The corrective influence function, $F_\theta(\hat{r})$, for the effect of the strain nuclei alone, is defined by

$$F_\theta(\hat{r}) = \frac{\mu \widetilde{u}_\theta(0,\hat{r})}{P}. \tag{3-35}$$

In the remainder of this chapter a single angle for the notch, viz. $2\alpha = 270°$ is concentrated and Poisson's ratio, ν, is set to be 0.3. The influence function $F_\theta(\hat{r})$ is plotted in Figure 3-2 (a), and can be expressed as a series representation of the following form:

$$F_\theta(\hat{r}) = \hat{r}^\lambda (c_0 + \frac{c_1 \hat{r}^{1/2}}{1+\hat{r}^{1/2}} + \frac{c_2 \hat{r}}{(1+\hat{r}^{1/2})^2} + \frac{c_3 \hat{r}^{3/2}}{(1+\hat{r}^{1/2})^3} + \frac{c_4 \hat{r}^2}{(1+\hat{r}^{1/2})^4}) \tag{3-36}$$

where λ is determined using Williams' asymptotic solution (Williams, 1952) and this gives $\lambda = 0.5445$. Figure 3-2 (b) displays the solution in log-log form, highlighting the characteristic gradients at each end of the range of the solution. When the coefficients have been collected we find that

$$F_\theta(\hat{r}) = \hat{r}^{0.5445}(-0.208 - \frac{0.073\hat{r}^{1/2}}{1+\hat{r}^{1/2}} + \frac{0.977\hat{r}}{(1+\hat{r}^{1/2})^2} - \frac{1.245\hat{r}^{3/2}}{(1+\hat{r}^{1/2})^3} + \frac{0.534\hat{r}^2}{(1+\hat{r}^{1/2})^4}) \quad (3\text{-}37)$$

while the displacement caused by the point force is given by

$$\overline{u}_\theta(0,\hat{r}) = \frac{P(1-\nu)}{\mu\pi}\log|\hat{r}-1|. \quad (3\text{-}38)$$

Thus the *total* normal displacement can be written as

$$u_\theta(0,\hat{r}) = \frac{P}{\mu}\left[\begin{array}{l}\hat{r}^{0.5445}(-0.208 - \frac{0.073\hat{r}^{1/2}}{1+\hat{r}^{1/2}} + \frac{0.977\hat{r}}{(1+\hat{r}^{1/2})^2} - \frac{1.245\hat{r}^{3/2}}{(1+\hat{r}^{1/2})^3} + \frac{0.534\hat{r}^2}{(1+\hat{r}^{1/2})^4}) \\ + \frac{(1-\nu)}{\pi}\ln|\hat{r}-1|\end{array}\right]. \quad (3\text{-}39)$$

It can be seen that $\hat{r}^\lambda$ dominates the $\ln|\hat{r}-1|$ term close to the corner of the notch, and $\ln|\hat{r}-1|$ dominates the $\hat{r}^\lambda$ term in the far field ($\hat{r}/L >> 1$). The total displacement is plotted in Figure 3-3 (a) and the value in log-log form is displayed in Figure 3-3 (b).

In this solution, there are two numerical approximations. One is the truncation of the semi-infinite interval to a finite one along the inclined line within the half-plane, and the second is the order of discretisation (n) used in the numerical quadrature. In order to achieve convergence of the solution, setting a/L to 100 was found to be appropriate, and for numerical convergence of the quadrature, it was found that $n = 200$ was appropriate.

3.4 Conclusion

This chapter describes the application of both dislocations and point forces as strain nuclei to achieve mixed boundary value conditions. These have been imposed successfully, and the technique has been used to derive the influence function for a pair of forces applied to the faces of a semi-infinite notch which permits the dominant behaviour adjacent to the notch root, adjacent to the point of application of the force, and remotely, to be found.

Chapter 4

Further Consideration of Closure at the Root of a Sharp Notch

4.1 Introduction

The problem we wish to address in this chapter is the quantification of the closure region when a notch having a sharp root is subjected to a compressive force, tending to close it. This is of practical importance in estimating the fatigue life of a sharp notch, and the possibility of nucleating a crack, because the local state of stress which the nucleating crack experiences will depend on the degree of closure, and whether or not it encompasses the 'process zone'. It is not necessary to examine the problem of a finite notch within whatever geometry it exists, because the closure zone will, for practical purposes, nearly always be small compared with the crack length. It is therefore appropriate to consider the behaviour of a semi-infinite notch, and then to use the generalised stress intensity factor scaling the notch solution to fit it into whatever finite problem is being examined. We have already looked at this problem once, using merely the Williams notch solution itself, and checking for violations in the surface displacements, i.e. finding the point at which the surface displacements of the notch faces suggest that there will be interpenetration (Churchman, Dini,

and Hills, 2006). This is clearly a useful first step in estimating the amount of closure, but it is approximate, and will be rather poor when the external notch half-angle, α (Figure 4-1) approaches π radians, or becomes crack-like. In order to solve the problem the general method of attack will be initially to permit interpenetration, as indicated by the dashed lines in Figure 4-1 (a), and then to apply a distributed contact pressure along the notch flanks so as to push the surfaces back to a common boundary. This solution has become feasible because the influence function for a pair of equal, opposed forces applied to the surfaces of a notch has been solved (Qiu, Dini and Hills, 2007), and this will form the kernel of an integral equation formulation for this problem.

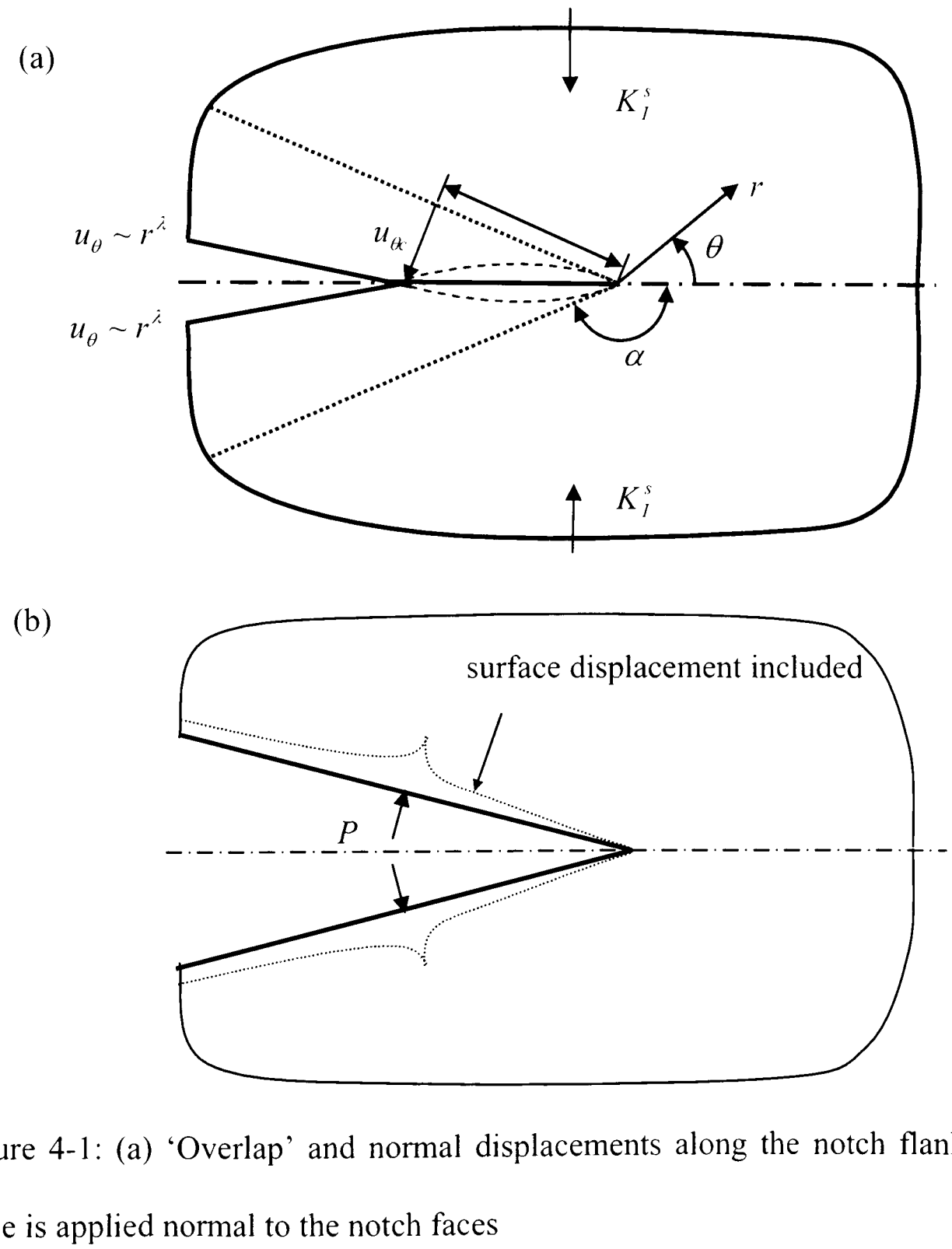

Figure 4-1: (a) 'Overlap' and normal displacements along the notch flanks (b) A point force is applied normal to the notch faces

4.2 Formulation

The first step is to deduce the form of the surface normal displacement of the notch itself, due to a remote applied load. Note that, in general, we might expect a remote load to induce both a mode I (symmetric) and a mode II (antisymmetric) field, but the latter will only cause a local rotation of the notch, and will not affect the separation of the notch faces. The surface normal displacement may be found directly from the Williams asymptotic form (Williams, 1952), and is given by

$$2\mu u_\theta^I(r,\theta) = -K_I^s r^{\lambda_I}\left[\frac{(\lambda_I - 1)\dfrac{\sin[(\lambda_I - 1)\alpha]}{\sin[(\lambda_I + 1)\alpha]}\sin[(\lambda_I + 1)\theta] - (\kappa + \lambda_I)\sin[(\lambda_I - 1)\theta]}{\lambda_I(\lambda_I + 1)\dfrac{1 - \cos[(\lambda_I - 1)\alpha]}{\cos[(\lambda_I + 1)\alpha]}}\right], \qquad (4\text{-}1)$$

$$-\alpha \le \theta \le \alpha$$

where the generalised stress intensity factor, K_I^s, is given by

$$K_I^s = \lim_{r\to 0}\frac{\sigma_{\theta\theta}(r,0)}{r^{\lambda_I - 1}}. \qquad (4\text{-}2)$$

It follows that the relative normal displacement between the two notch surfaces may be found by specialising equation (4-1), by setting $\theta = \pm\alpha$, to give

$$u_\theta^I(r,\theta) = \frac{K_I^s r^{\lambda_I}}{E^*}\Lambda \qquad (4\text{-}3)$$

where

$$\Lambda = \frac{\sin 2\alpha}{\lambda_I \sin\alpha \sin\lambda_I\alpha} = \frac{2\cos\alpha}{\lambda_I \sin\lambda_I\alpha}. \qquad (4\text{-}4)$$

In order to establish the true closure length, r_c, an integral equation in terms of the contact pressure will be set up. This could be expressed in terms of the surface displacement itself, but, in practice, it is preferable to work in terms of the surface displacement gradient, $\partial u_\theta^I / \partial r$,

as this means that the kernel will be Cauchy rather than logarithmic in nature, and hence become easier to handle. With this in mind, we write down the boundary condition along the closure line as

$$\frac{\partial u_\theta^l(r,\alpha)}{\partial r} - \frac{\partial u_\theta^p(r,\alpha)}{\partial r} = \tan(\pi-\alpha), \tag{4-5}$$

where $u_\theta^p(r,\alpha)$ is the displacement due to a continuous distribution of line forces along the edge-contact, and is given by

$$\frac{\partial u_\theta^p(r,\alpha)}{\partial r} = \int_0^{r_c} p(\xi) D_\theta^m[r,\alpha,\xi]d\xi \qquad 0 \le r \le r_c. \tag{4-6}$$

Here $D_\theta^m[r,\alpha,\xi]$ is the displacement derivative influence function for opposed line forces applied to a semi-infinite wedge. By setting

$$s = \frac{2\xi}{r_c} - 1, \tag{4-7a}$$

$$t = \frac{2r}{r_c} - 1, \tag{4-7b}$$

the normalized interval of the integral equation becomes

$$\frac{\partial u_\theta^l(r,\alpha)}{\partial r} - \tan(\pi-\alpha) = \frac{r_c}{2}\int_{-1}^{1} p(s) D_\theta^m[t,\alpha,s]ds \qquad -1 \le s \le 1. \tag{4-8}$$

We know that, at the corner of the notch, the stress is singular and at the contact edge, it is bounded, and we write

$$p(s) = p_\alpha(s)(1-s)^{1/2}(1+s)^{1/2}. \tag{4-9}$$

The discretised form of the integral equation is

$$\frac{\partial u_\theta^l(t_k,\alpha)}{\partial r} - \tan(\pi-\alpha) = \frac{r_c}{2}\sum_{i=1}^{n} W_i p_\alpha(s_i) D_\theta^m[t_k,\alpha,s_i] \quad k = 1, \ldots, n \tag{4-10}$$

where

$$s_i = \cos\left(\frac{2i}{2n+1}\pi\right), \qquad i = 1, \ldots, n \tag{4-11a}$$

$$t_k = \cos\left(\frac{2k-1}{2n+1}\pi\right), \qquad k = 1,\ldots, n \tag{4-11b}$$

$$W_i = \frac{2\pi(1-s_i)}{2n+1}. \tag{4-11c}$$

These represent a system of n simultaneous equations for n unknown $p_\alpha(s_i)$, together with the closure length, r_c.

A first estimate of the closure distance, r_c^o, is found from the point of overlap of the Williams solution, and is given by

$$r_c^o = \left[\frac{K_I^s}{E^*}\frac{\Lambda}{\tan(\pi-\alpha)}\right]^{\frac{1}{1-\lambda_I}} = \left[\frac{K_I^s}{\mu}\frac{(1-\nu)\cos\alpha}{\lambda_I \sin(\lambda_I\alpha)\tan(\pi-\alpha)}\right]^{\frac{1}{1-\lambda_I}}. \tag{4-12}$$

The true closure length, r_c, is found iteratively: the contact pressure must be negative value along the contact interface, and the notch must be open external to the contact distance. Improved values of r_c are chosen until there two inequalities are satisfied.

Because of the limitation of linear elastic theory, which explicitly exclude rotation effects, the solution will apply only if 2α is large. Notches of 300° 330° and 350° were chosen as detailed examples. The influence functions for these cases are as follows:

1. 350° notch

$$D_\theta^m[r,\alpha,\xi] = \frac{1}{\mu}\left[\begin{array}{l} -\dfrac{4.628r^2}{\left(1+\sqrt{\frac{r}{\xi}}\right)^5\xi} + \dfrac{8.0655r^2}{\left(1+\sqrt{\frac{r}{\xi}}\right)^4\sqrt{\frac{r}{\xi}}\xi^3} - \dfrac{15.606r}{\left(1+\sqrt{\frac{r}{\xi}}\right)^3\xi^2} + \dfrac{0.8205r}{\left(1+\sqrt{\frac{r}{\xi}}\right)^2\sqrt{\frac{r}{\xi}}\xi^2} \\ -\dfrac{1.641}{\left(1+\sqrt{\frac{r}{\xi}}\right)\xi} - \dfrac{0.0805}{\sqrt{\frac{r}{\xi}}\xi} + \dfrac{7.278\sqrt{\frac{r}{\xi}}}{\left(1+\sqrt{\frac{r}{\xi}}\right)^2\xi} + \dfrac{5.785\left(\frac{r}{\xi}\right)^{3/2}}{\left(1+\sqrt{\frac{r}{\xi}}\right)^4\xi} + \dfrac{(1-\nu)}{\pi\xi}\dfrac{1}{\left(\frac{r}{\xi}-1\right)} \end{array}\right] \tag{4-13}$$

2. 330° notch

$$D_\theta^m[r,\alpha,\xi]=\frac{1}{\mu}\left[\begin{array}{l}-\dfrac{2.946r^2}{\left(1+\sqrt{\dfrac{r}{\xi}}\right)^5\xi}+\dfrac{5.0235r^2}{\left(1+\sqrt{\dfrac{r}{\xi}}\right)^4\sqrt{\dfrac{r}{\xi}}\xi^3}-\dfrac{9.754r}{\left(1+\sqrt{\dfrac{r}{\xi}}\right)^3\xi^2}+\dfrac{0.4855r}{\left(1+\sqrt{\dfrac{r}{\xi}}\right)^2\sqrt{\dfrac{r}{\xi}}\xi^2}\\ -\dfrac{0.971}{\left(1+\sqrt{\dfrac{r}{\xi}}\right)\xi}-\dfrac{0.106}{\sqrt{\dfrac{r}{\xi}}\xi}+\dfrac{4.584\sqrt{\dfrac{r}{\xi}}}{\left(1+\sqrt{\dfrac{r}{\xi}}\right)^2\xi}+\dfrac{3.6825\left(\dfrac{r}{\xi}\right)^{3/2}}{\left(1+\sqrt{\dfrac{r}{\xi}}\right)^4\xi}+\dfrac{(1-\nu)}{\pi\xi}\dfrac{1}{\left(\dfrac{r}{\xi}-1\right)}\end{array}\right] \tag{4-14}$$

3. 300° notch

$$D_\theta^m[r,\alpha,\xi]=\frac{1}{\mu}\left[\begin{array}{l}-\dfrac{2.864r^2}{\left(1+\sqrt{\dfrac{r}{\xi}}\right)^5\xi}+\dfrac{5.0505r^2}{\left(1+\sqrt{\dfrac{r}{\xi}}\right)^4\sqrt{\dfrac{r}{\xi}}\xi^3}-\dfrac{9.773r}{\left(1+\sqrt{\dfrac{r}{\xi}}\right)^3\xi^2}+\dfrac{0.4805r}{\left(1+\sqrt{\dfrac{r}{\xi}}\right)^2\sqrt{\dfrac{r}{\xi}}\xi^2}\\ -\dfrac{0.961}{\left(1+\sqrt{\dfrac{r}{\xi}}\right)\xi}-\dfrac{0.0755}{\sqrt{\dfrac{r}{\xi}}\xi}+\dfrac{4.5585\sqrt{\dfrac{r}{\xi}}}{\left(1+\sqrt{\dfrac{r}{\xi}}\right)^2\xi}+\dfrac{3.58\left(\dfrac{r}{\xi}\right)^{3/2}}{\left(1+\sqrt{\dfrac{r}{\xi}}\right)^4\xi}+\dfrac{(1-\nu)}{\pi\xi}\dfrac{1}{\left(\dfrac{r}{\xi}-1\right)}\end{array}\right] \tag{4-15}$$

4.3 Results

Figure 4-2 shows the interfacial contact pressure predicted for the three example cases. The coordinate axis has been normalised with respect to the distance to the violation point, r_c^o, and it may be seen that the actual closure length is shorter than the value implied by the bilateral solution. The difference increases with increasing value of α. When the observation point is very close to the contact edge, we can see that the interfacial contact pressure is bounded and we may find a connexion between its value and the unilateral (open notch) stress distribution. If t is a coordinate measured inwards from the contact edge, the local contact pressure has the form

$$p(t)=K_I^B t^{1/2}, \tag{4-16}$$

and the value of the multiplier may be found by interpolation of the form of the contact pressure (equation (4-9)) to the edges of the contact interval. Thus, we may write

$$K_I^B = C\frac{K_I^s}{(r_c^o)^{3/2-\lambda_I}}, \tag{4-17}$$

and the values of λ_I and C for the three cases studied, together with a further intermediate angle, are given in Table 4-1. Figure 4-3 provides a close-up view of the true contact pressure adjacent to the edge of the contact region, and the contact pressure distribution implied by the asymptote.

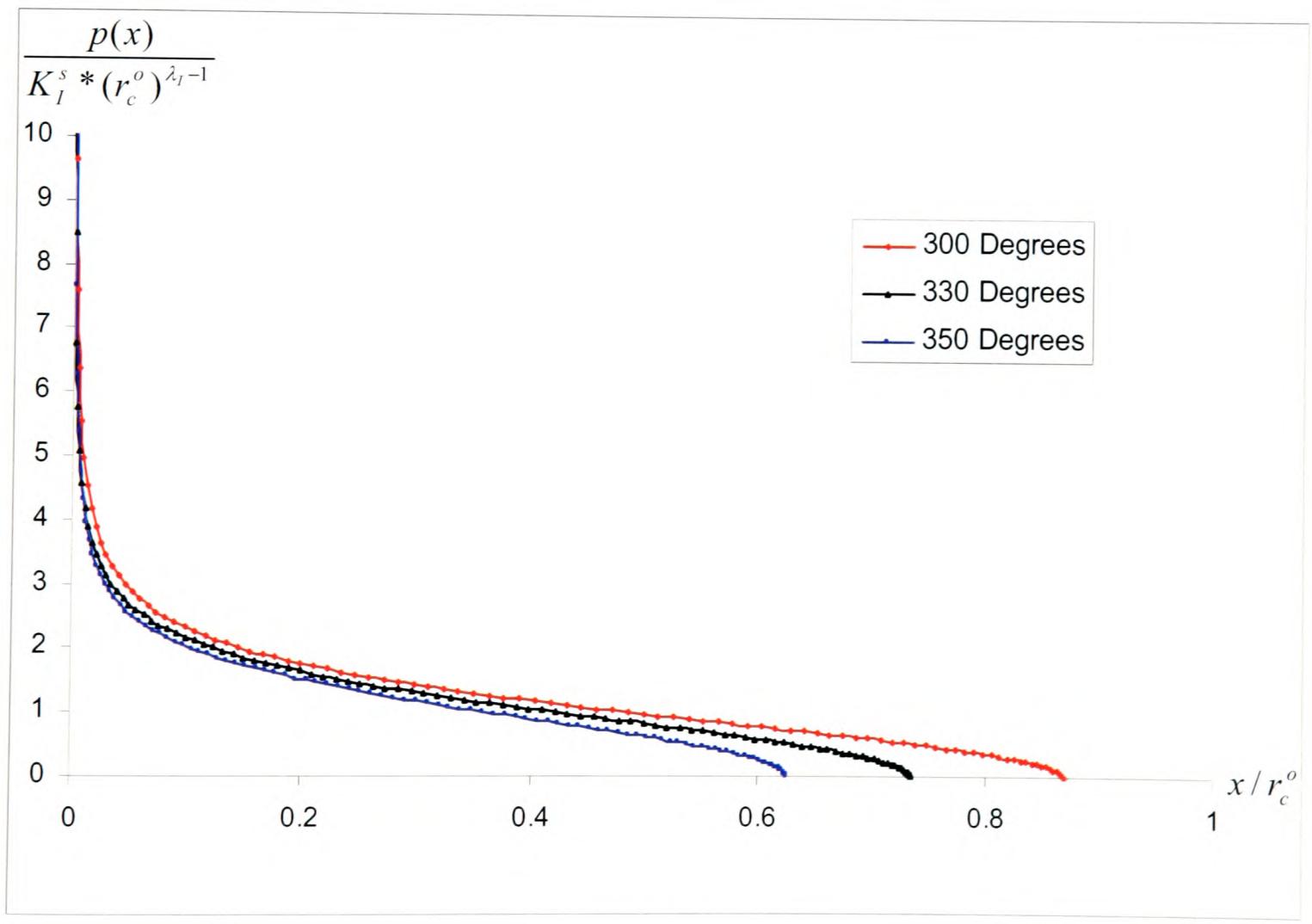

Figure 4-2: Predicted interfacial contact pressure and true closure length.

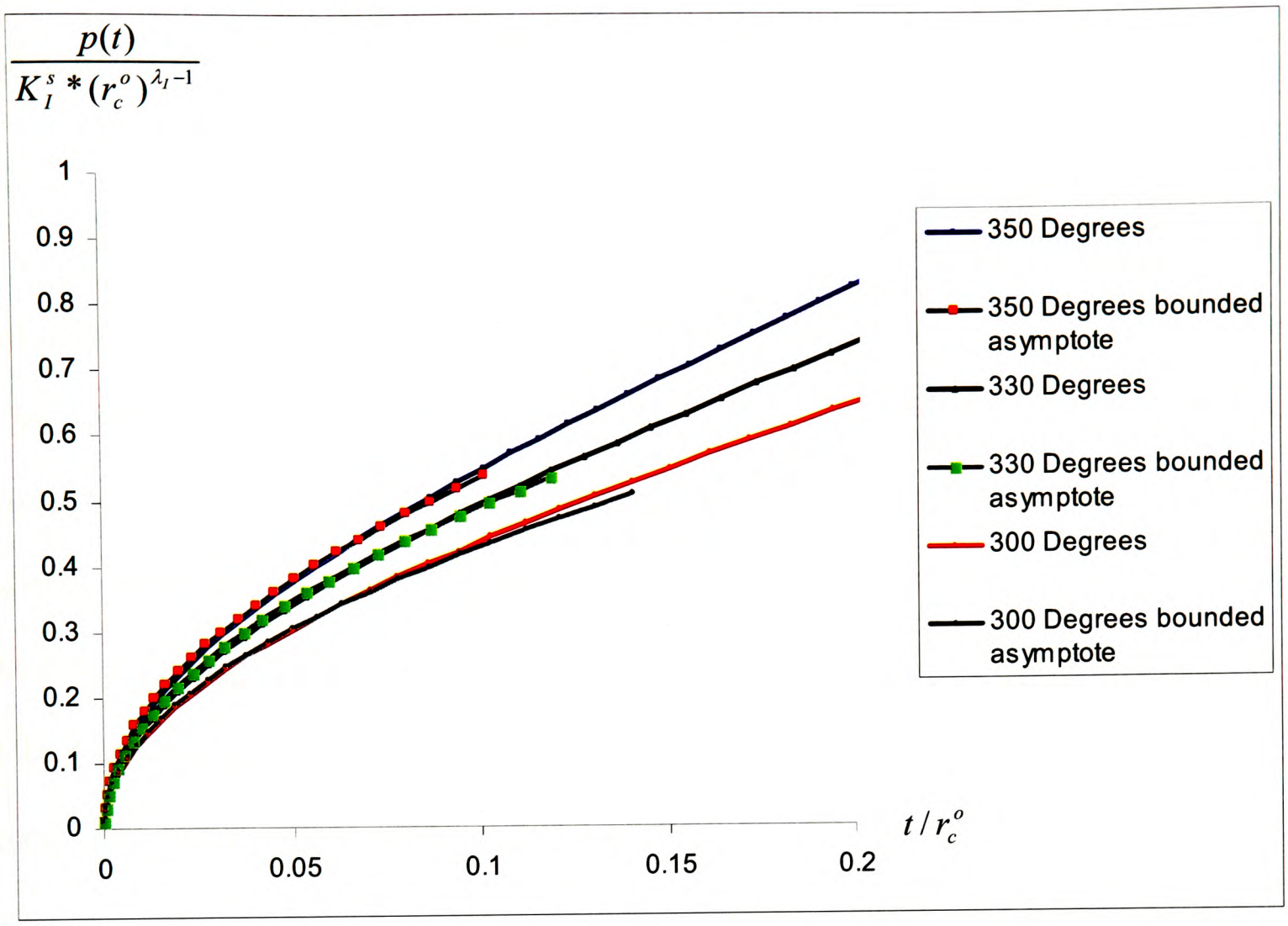

Figure 4-3: A comparison of the true contact pressure near the point of separation and that implied by the bounded asymptote.

Table 4-1

	350°	340°	330°	300°
λ_I	0.50005	0.50043	0.50145	0.51222
C	1.692	1.559	1.553	1.362

4.4 Conclusion

When a remote compressive load is applied to a plate containing a sharp notch closure will occur at the root. This phenomenon is normally neglected, because the solution is taken to be 'bilateral'. The implications of this assumption were examined in an earlier paper, simply by looking for violations in the displacement field which implied interpenetration of material when the notch is compressed. The true closure length and interfacial contact pressure are found in this chapter. The contact pressure between the notch faces is very large at the root, but falls smoothly to zero in a square root fashion at the point of separation. The relationship between the bounded stress intensity factor K_I^B (which characterises the contact edge solution) and the generalised stress intensity factor, K_I^s which relates to the crack root, is found. The true contact length is very close to that implied by interpenetration when the internal notch angle is not 'very large' (< 300°), but the difference becomes much more marked when the notch becomes crack-like in character.

Chapter 5

Side-Contact of Sharp Indenters, Including the Effects of Friction

5.1 Introduction

This chapter is concerned with the characteristics of a complete contact, subjected to a normal force and sliding along a second, large body, Figure 5-1(a). Although the principles involved may be applied to problems with a range of values of elastic constants, here, the case when the body defining the size of the contact (the upper body in Figure 5-1(a)), is rigid, and the lower body has a finite compressibility, with Poisson's ratio ν and modulus of rigidity μ is addressed. The problem is to be analysed using a conventional linear, small strain approach with small displacements. The degree of side contact and indentation is shown greatly exaggerated in Figure 5-1 in order to display the phenomenon clearly. A typical value of the ratio a/b occurring in practice is, as will be shown, about 1.001. This analysis was prompted by recent work done on the design of complete 'spline' couplings in split gas turbine shafts, and where the phenomenon to be investigated proved important in explaining the fretting damage which occurs in such joints.

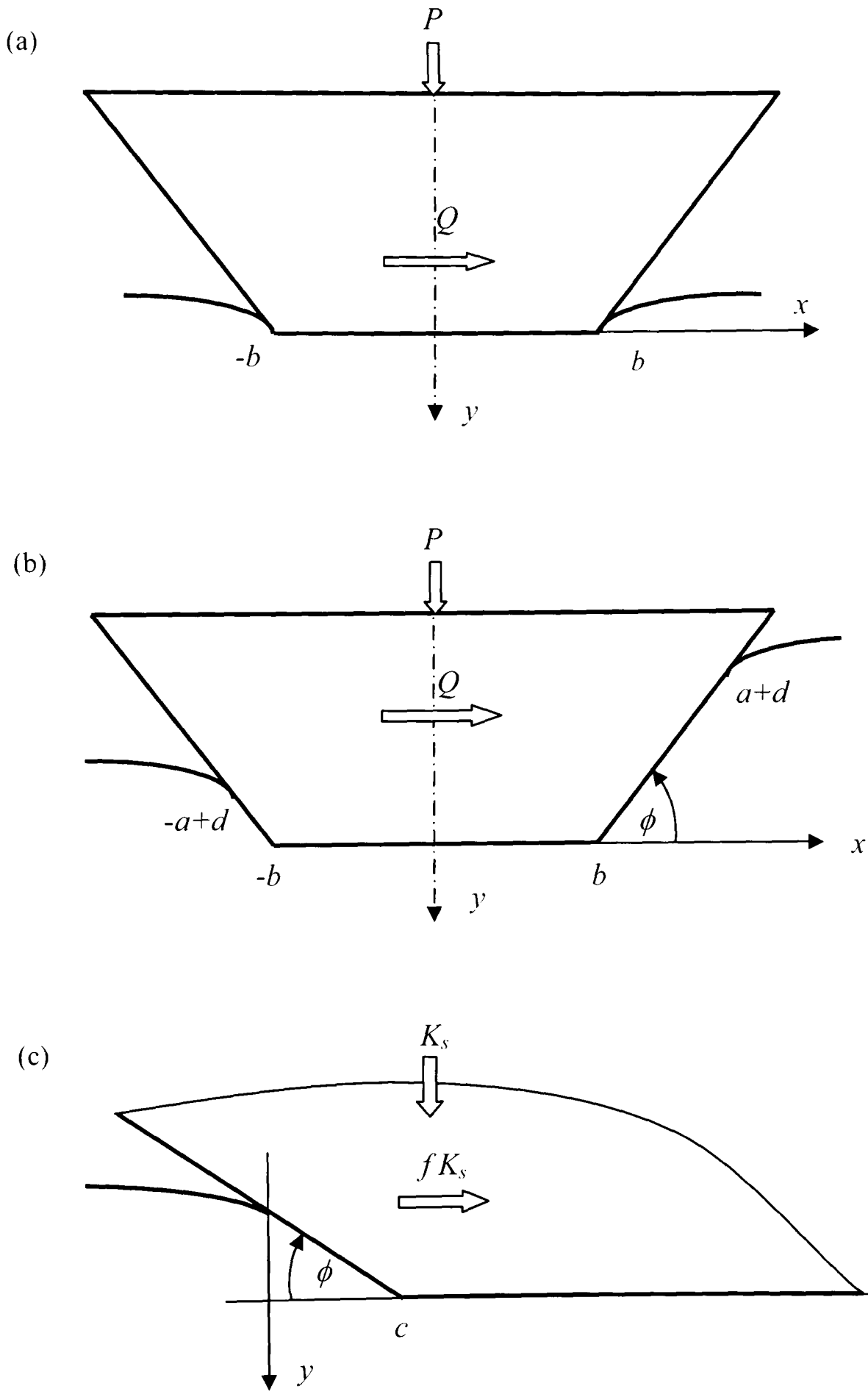

Figure 5-1: Geometry of the problem (a) Apparent extent of contact for a sharp-edged indenter (b) True extent of contact allowing for 'lapping around' of material onto side flanks (c) Asymptotic form of solution when the indenter is semi-infinite in extent

The flat face of the rigid punch is of width $2b$, and, in a straightforward application of half-plane contact theory (Hills *et al.*, 1993), it is that dimension which defines the size of the contact. If the coefficient of friction between the two bodies is f, and this is, for consistency with an asymptotic solution to be derived as part of the solution, given a sign, such that a positive value of f corresponds to the punch sliding to the left, standard results show that the contact pressure is

$$p(x) = \frac{P}{\pi} \sin \lambda\pi (b-x)^{\lambda-1} (b+x)^{-\lambda}, \tag{5-1}$$

where λ is given by

$$\tan \lambda\pi = \frac{1}{f\beta}, \quad 0 < \lambda < 1, \tag{5-2}$$

P is the normal force and β, Dundurs' second constant, is

$$\beta = \frac{(1-2\nu)}{2(1-\nu)}. \tag{5-3}$$

It is clear that, at each end of the contact, the pressure becomes singular, and, by making the simple transformation of coordinates $r = x + b$, the precise form of the contact pressure at the edge $x = -b$ is of the form

$$p(r) \sim r^{-\lambda} \tag{5-4}$$

which shows explicitly that it is power-order in form. From now on the left hand side of the contact will mainly be considered, and this may be changed from the leading to the trailing edge simply by changing the sign of f.

Prima facie this represents a full, exact solution for the contact pressure, but it is intuitively clear (and may be shown analytically), that if the sides of the punch slope outwards, as shown in Figure 5-1(a), the punch will indent the half plane so that contact is also made on the side flanks, Figure 5-1(b), where, for clarity, the lengths $c_L = a - d - b$, $c_R = a + d - b$ are shown greatly exaggerated. The object, here, is to define explicitly the true extent of the

contact, i.e. to find a, d, and the corresponding interfacial pressure distribution for this problem, both for this specific finite problem and, through an asymptotic solution, for *any* sharp-edged elastic contact. The solution will be found using coupled half-plane theory, so that the interaction between the direct and shear components of traction is accounted for properly, but the external angle of the side flank, ϕ, Figure 5-1(b), must be relatively small in order for element rotations to be within acceptable levels for small strain elasticity theory, and the results to be derived cannot be expected to be reliable unless this condition holds. Qualitatively, the modified solution, which allows for side-contact, was expected to display bounded behaviour as the contact edges are approached and, as the discontinuities in surface profile (at $x = \pm b$) become internal to the contact, for a weak (logarithmic) singularity to replace the power order one. Problems of this class have been studied before under conditions of adhesion (Adams, G.G., 1979), but not for sliding.

A further form of the solution to the problem will be found, which extends the repertoire of geometries to which this approach maybe applied. The second form of the problem is displayed in Figure 5-1(c). Again an indenter is pressed into a half-plane, but this time the punch is semi-infinite in extent. It follows that, remote from the corner ($x >> c$) the contact pressure will display the same characteristic power order behaviour as that exhibited by the finite punch of Figure 5-1(a), when $r << b$, and this property may be used to define a generalised stress intensity factor to scale the semi-infinite punch solution, and so deduce the effect of chamfering for any shape of sharp-cornered punch. As an example, the semi-infinite solution will be re-applied to the square ended plane punch problem.

5.2 Formulation: Finite Punch

The integral equation to be solved, relating the surface displacement, $h(x)$, of the half-plane to the contact pressure, $p(x)$, is (Hills *et al.*, 1993)

$$\beta\!\!f p(x)+\frac{1}{\pi}\int_{-a-d}^{a-d}\frac{p(\xi)}{\xi-x}d\xi=-\frac{h'(x)}{A}, \tag{5-5}$$

where

$$\frac{1}{A}=\frac{\mu}{1-\nu}, \qquad h'(x)=\begin{cases}-m, & -a+d<x<-b\\ 0, & -b<x<b\\ m, & b<x<a+d.\end{cases} \tag{5-6}$$

and $m=\tan\phi$. Make the substitutions

$$\xi=at+d, \qquad x=as+d, \tag{5-7}$$

so that in terms of s the contact range is $-1<s<1$, and write

$$p(x)=r(s), \qquad -\frac{h'(x)}{A}=g(s) \tag{5-8}$$

so that

$$\beta\!\!f r(s)+\frac{1}{\pi}\int_{-1}^{1}\frac{r(t)}{t-s}dt=g(s) \tag{5-9}$$

With

$$g(s)=\begin{cases}m/A, & -1<s<-c_0,\\ 0, & -c_0<s<c_1,\\ -m/A, & c_1<s<1,\end{cases} \quad c_0=\frac{b+d}{a},\ c_1=\frac{b-d}{a}. \tag{5-10}$$

A solution for the contact pressure which is 'bounded both ends' is required, and hence the Riemann-Hilbert inversion procedure gives (5-9)

$$r(s)=\frac{1}{1+\beta^2 f^2}\left[\beta\!\!f g(s)-\frac{w(s)}{\pi}\int_{1}\frac{g(t)dt}{w(t)(t-s)}\right] \tag{5-11}$$

subject to the consistency condition

$$\int_{-1}^{1} \frac{g(t)dt}{w(t)} = 0\,, \tag{5-12}$$

where

$$w(s) = (1-s)^{1-\lambda}(1+s)^{\lambda} \tag{5-13}$$

and λ is defined by equation(5-2).

5.3 Solution

Consider, first, the consistency condition, which, on substituting for $g(s)$ becomes

$$\int_{-1}^{-c_0} \frac{(m/A)}{w(t)}dt + \int_{c_1}^{1} \frac{(-m/A)}{w(t)}dt = 0 \tag{5-14}$$

and hence

$$\int_{-1}^{-c_0} \frac{1}{w(t)}dt = \int_{c_1}^{1} \frac{1}{w(t)}dt\,. \tag{5-15}$$

After some manipulation the consistency condition becomes

$$\frac{k_0^{1-\lambda}(1-k_0)^{\lambda}}{1-\lambda}\,{}_2F_1(1,\,1,\,2-\lambda,\,k_0) = \frac{k_1^{\lambda}(1-k_1)^{1-\lambda}}{\lambda}\,{}_2F_1(1,\,1,\,1+\lambda,\,k_1) \tag{5-16}$$

where

$$k_0 = \frac{1-c_0}{2}, \qquad k_1 = \frac{1-c_1}{2} \tag{5-17}$$

and in addition

$$\frac{b}{a} = 1 - \frac{k_0+k_1}{2}, \qquad \frac{d}{a} = \frac{k_1-k_0}{2}. \tag{5-18}$$

Attention is now turned to the main equation for the contact pressure, i.e.

$$r(s) = \frac{1}{1+\beta^2 f^2}\left[\beta f g(s) - \frac{w(s)}{\pi}\frac{m}{A}(I_1 - I_2)\right], \tag{5-19}$$

where

$$I_1 \equiv \int_{-1}^{c_0} \frac{dt}{w(t)(t-s)}, \qquad I_2 \equiv \int_{c_0}^{1} \frac{dt}{w(t)(t-s)}). \tag{5-20}$$

These integrals are evaluated in the Appendix B, where four functions J_1, J_2, K_1, K_2 appear, which reflect whether the integrals in question are Cauchy or regular in a particular interval, and

$$I_1 - I_2 = \begin{cases} J_1 - K_2, & -1 < s < -c_0, \\ J_2 - K_2, & -c_0 < s < c_1, \\ J_2 - K_1, & c_1 < s < 1, \end{cases} \tag{5-21}$$

where the various definitions of the right hand side have also been noted. With these results, the final solution is given

$$\frac{A\pi r(s)}{mw(s)\sin^2 \pi\lambda} = \begin{cases} \dfrac{1}{\lambda(1-s)}\left[\alpha_0^{\lambda} F(1, \lambda, 1+\lambda, \alpha_0 \dfrac{1+s}{1-s}) + \dfrac{1}{\alpha_1^{\lambda}} F(1, \lambda, 1+\lambda, \dfrac{1}{\alpha_1}\dfrac{1+s}{1-s})\right] & -1 < s < -c_0, \\ \dfrac{\alpha_0^{\lambda-1}}{(1-\lambda)(1+s)} F(1, 1-\lambda, 2-\lambda, \dfrac{1}{\alpha_0}\dfrac{1-s}{1+s}) + \dfrac{\alpha_1^{-\lambda}}{\lambda(1-s)} F(1, \lambda, 1+\lambda, \dfrac{1}{\alpha_1}\dfrac{1+s}{1-s}) & -c_0 < s < c_1, \\ \dfrac{1}{(1-\lambda)(1+s)}\left[\alpha_0^{\lambda-1} F(1, 1-\lambda, 2-\lambda, \dfrac{1}{\alpha_0}\dfrac{1-s}{1+s}) + \alpha_1^{1-\lambda} F(1, 1-\lambda, 2-\lambda, \alpha_1 \dfrac{1-s}{1+s})\right] & c_1 < s < 1, \end{cases} \tag{5-22}$$

as

$$\sin^2 \pi\lambda = \frac{1}{1+\beta^2 f^2}. \tag{5-23}$$

5.4 Characteristics of the Pressure Distribution

First, note that in all three regions the pressure distribution takes the form

$$r(s) = w(s) \times G_n(s) \tag{5-24}$$

where

$$w(s) = (1-s)^{1/2}(1+s)^{\lambda} \tag{5-25}$$

and $G_n(s)$ ($n = 1,2,3$) represents the collection of hypergeometric functions in the three regions: 1. $-1 < s < -c_0$, 2. $-c_0 < s < c_1$ and 3. $c_1 < s < 1$ respectively. Both $G_1(-1)$ and $G_3(1)$ are finite and non-zero so that $r(\pm 1) = 0$, i.e. the pressure falls continuously to zero at the end points of the contact. The form of the contact pressure distribution adjacent to the end points may be abstracted, together with that at the points of discontinuity in surface gradient.

5.4.1 At the left hand end, near $s = -1$

Write $\varepsilon = s + 1$. Then, in the interval $-1 < s < -c_0$

$$\frac{A\pi r(s)}{m\sin^2 \pi\lambda} = \frac{\varepsilon^{\lambda}}{\lambda(2-\varepsilon)^{\lambda}}\left[\alpha_0^{\lambda} F(1,\lambda,1+\lambda,\alpha_0\frac{\varepsilon}{2-\varepsilon}) + \frac{1}{\alpha_1^{\lambda}} F(1,\lambda,1+\lambda,\frac{1}{\alpha_1}\frac{\varepsilon}{2-\varepsilon})\right]. \tag{5-26}$$

Expanding in powers of ε and retaining only the terms in ε below the power of 1 we have

$$\frac{A\pi r(s)}{m\sin^2 \pi\lambda} = \frac{\varepsilon^{\lambda}}{\lambda 2^{\lambda}}[\alpha_0^{\lambda} + \frac{1}{\alpha_1^{\lambda}}] + \cdots. \tag{5-27}$$

5.4.2 At the right hand end, near $s = +1$

Write $\varepsilon = 1 - s$. Then in the interval $c_1 < s < 1$,

$$\frac{A\pi r(s)}{m\sin^2 \pi\lambda} = \frac{\varepsilon^{1-\lambda}}{(1-\lambda)(2-\varepsilon)^{1-\lambda}} \left[\alpha_0^{\lambda-1} F(1,1-\lambda,2-\lambda,\frac{1}{\alpha_0}\frac{\varepsilon}{2-\varepsilon}) + \alpha_1^{1-\lambda} F(1,1-\lambda,2-\lambda,\alpha_1\frac{\varepsilon}{2-\varepsilon})\right]. \tag{5-28}$$

and again expanding in powers of ε we have

$$\frac{A\pi r(s)}{m\sin^2\pi\lambda} = \frac{\varepsilon^{1-\lambda}}{(1-\lambda)2^{1-\lambda}}[\alpha_0^{\lambda-1} + \alpha_1^{1-\lambda}] + \cdots . \tag{5-29}$$

5.4.3 At the points of discontinuity in surface gradient, near $s = c_1, c_0$

The property of the hypergeometric function $F(a, b; c; z)$ is, when $c = a + b$,

$$F(a, b; c; z) / \{\frac{\Gamma(c)}{\Gamma(b)\Gamma(c-b)} \ln(\frac{1}{1-z})\} \to 1 \qquad as\, z \to 1_{(-)}. \tag{5-30}$$

The "buried corners" are at $x = \pm b$, i.e. $s = c_1$ (corresponding to $x = b$) and $s = -c_0$ (corresponding to $x = -b$), so, remembering that

$$\alpha_0 = \frac{1 + c_0}{1 - c_0} \tag{5-31}$$

then

$$F(1, \lambda, 1+\lambda, \alpha_0 \frac{1+s}{1-s}) = -\lambda \ln(1 - \alpha_0 \frac{1+s}{1-s}) \tag{5-32}$$

which proves the existence of the logarithmic behaviour anticipated.

5.5 Contact Law

The contact law, i.e. equations specifying the overall size of the contact, $2a$, and the offset of the contact patch, d, in terms of the applied load and its line of action are found from the following two equations expressing overall equilibrium:

$$P = \int_{-a+d}^{a+d} p(x)dx, \tag{5-33}$$

$$M = \int_{-a+d}^{a+d} p(x)x dx. \tag{5-34}$$

After a great deal of manipulation, the following results are achieved

$$\frac{AP}{ma\sin\pi\lambda} = 2k_0^{-\lambda}(1-k_0)^{1+\lambda}[F(1,\,1,\,1-\lambda,\,k_0)-1]-2k_1^{\lambda}(1-k_1)^{1-\lambda}[F(1,\,1,\,1+\lambda,\,k_1)-1]. \quad (5\text{-}35)$$

$$M=[d+a(2\lambda-1)]P+\frac{4ma^2\sin\lambda\pi}{A} \times\left[\frac{k_0^{2-\lambda}(1-k_0)^{1+\lambda}}{2-\lambda}F(1,\,3,\,3-\lambda,\,k_0)-\frac{k_1^{1-\lambda}(1-k_1)^{2-\lambda}}{1+\lambda}F(1,\,3,\,2+\lambda,\,k_1)\right]. \quad (5\text{-}36)$$

5.6 Semi-Infinite Punch

This solution will prove useful in judging the amount of 'lapping around' on the contact onto the side face of a general plane contact (or one of arbitrary planform in the absence of friction). The same form of second order integral equation relating the profile of the punch to the contact pressure (equation (5-5)) may be used here, but the surface profile is now (Figure 5-1(c))

$$h'(x)=\begin{cases} -m, & 0<x<c \\ 0, & c<x<\infty \end{cases} \quad (5\text{-}37)$$

and the limits of both the integral and range of imposition of the right hand side now change to [0, ∞], so that

$$\frac{1}{\pi}\int_0^{\infty}\frac{p(\xi)d\xi}{\xi-x}+f\beta p(x)=-\frac{1}{A}h'(x) \qquad 0\le x<\infty \quad (5\text{-}38)$$

A solution for $p(x)$ which bounded at both $x=0$ and $x\to\infty$ is sought and it is noted that there is a buried sharp discontinuity in the displacement at $x=c$. The pressure is given by

$$p(x)=\begin{cases} \dfrac{m(x/c)^{\lambda}\sin^2\pi\lambda}{A\pi\lambda}F(1,\,\lambda,\,1+\lambda,\,\dfrac{x}{c}), & x<c, \\ \dfrac{m(x/c)^{\lambda-1}\sin^2\pi\lambda}{A\pi(1-\lambda)}F(1,\,1-\lambda,\,2-\lambda,\,\dfrac{c}{x}). & x>c. \end{cases} \quad (5\text{-}39)$$

These hypergeometric functions (in which the third parameter is the sum of the first two parameters) are logarithmically singular at $x = c$, and give the result

$$p(x) = \begin{cases} -\dfrac{m(x/c)^{\lambda}\sin^2\pi\lambda}{A\pi}\ln(1-\dfrac{x}{c}), & x/c \to 1_{(+)}, \\ -\dfrac{m(x/c)^{\lambda-1}\sin^2\pi\lambda}{A\pi}\ln(1-\dfrac{c}{x}), & x/c \to 1_{(-)}. \end{cases} \tag{5-40}$$

The asymptotic behaviour of the contact pressure is as follows:

(1) Singular asymptote $x >> c$

Because $F(1, 1-\lambda, 2-\lambda, c/x) \to 1$ when $x/c \to \infty$, and it is required that

$$p(x) = K_S(x)^{\lambda-1}, \qquad x >> c \tag{5-41}$$

the calibration for K_S is given by

$$K_S = \frac{m\sin^2\lambda\pi}{\pi A(1-\lambda)c^{\lambda-1}}, \tag{5-42}$$

so that

$$p(x) = K_S(x)^{\lambda-1}F(1, 1-\lambda, 2-\lambda, \frac{c}{x}), \tag{5-43}$$

where the length of the contact on the contact side is given by

$$c = \left(\frac{\pi A(1-\lambda)K_S}{m\sin^2\pi\lambda}\right)^{1/1-\lambda}. \tag{5-44}$$

(2) Logarithmic asymptote $|x-c| << c$

In terms of the stress intensity factor defined, the magnitude of the contact pressure in the neighbourhood of the corner is given by

$$p(x) = \begin{cases} -K_S\dfrac{1-\lambda}{c}(x)^{\lambda}\ln(1-\dfrac{x}{c}), & x/c \to 1_{(-)}, \\ -K_S(1-\lambda)(x)^{\lambda-1}\ln(1-\dfrac{c}{x}), & x/c \to 1_{(-)}. \end{cases} \tag{5-45}$$

or, if we make the transformation of coordinates, $c - x = s$, where $s << c$

$$p(s)=\begin{cases} K_L \ln(\dfrac{s}{c}), & s \to 0, \\ K_L \ln(\dfrac{s}{c+s}), & s^- \to 0. \end{cases}$$

where

$$K_L = -(1-\lambda)c^{\lambda-1}K_S = -\frac{m\sin^2\pi\lambda}{A\pi}. \tag{5-46}$$

(c) Bounded asymptote $x << c$

At the outer edge of the contact, $F(1, \lambda, 1+\lambda, x/c) \to 1$ as $x/c \to 0$. Therefore

$$p(x) = K_B(x)^{\lambda}, \qquad x << c, \tag{5-47}$$

where

$$K_B = \frac{(1-\lambda)}{\lambda c}K_S = \frac{m\sin^2\pi\lambda}{\pi A\lambda c^{\lambda}}. \tag{5-48}$$

5.7 Results

Consider, first, the problem of the finite punch. There are obviously a large number of possible independent variables present, and so $f = \pm 0.5$ and $\nu = 0.3$ are set, which means that $\lambda = 0.4548,\ 0.5452$, where the first value corresponds to a positive value of f and the second to a negative value. Figure 5-2 shows the relationship between normalised contact load, $PA/b\tan\phi$, and the contact geometry parameters a/b and d/b for sample coefficients of friction f and with the Possion's ratio of half-plane, ν, set to a representative value, 0.3. From Figure 5-2(a), it can be seen that the contact size, a/b, increases with an increase of the normalised total load, but is very insensitive to the value of the coefficient of friction f. On the other hand, it is clear from Figure 5-2 (b) that the offset of the contact patch, d/b, is quite strongly dependent on the coefficient of friction and, as expected, the sign of d depends on the

sign of f, i.e. the direction of sliding. Figure 5-2(c) summarises the connection between d/b and a/b.

In order to help decide representative pressures when plotting the dimensionless loads, it is useful to collect data for the relative strength/stiffness ratios of common engineering materials. Table 5-1 is a list of material properties for common metallic alloys, where σ_y is the yield stress in simple tension. A representative mean pressure in a practical contact might be about half the yield stress, i.e. $P/2b \approx \sigma_y/2$ and this means that, for titanium, $AP/2b = 0.007$ might be chosen. The difference between the approximate 'complete contact' solution and the 'side contact' solution is obviously very small when ϕ is large, and this is also the regime where the half-plane idealisation is called into question, so, in the next example, ϕ will be set to 10°. In Figure 5-3 the normalised contact pressure distribution is shown using both forms of the solution (front face contact only and allowing for side face contact), for the case when the force is applied centrally through the punch face, and with a dimensionless load $AP/b = 0.014$, ($\lambda = 0.5452$) which corresponds to $f = -0.5$ and $\nu = 0.3$. The values of a/b and d/b are 1.00105 and 0.00075 respectively. At the leading edge the contact pressure distributions near the contact corner are virtually indistinguishable, whilst at the trailing edge the two do show some separation and, of course, the 'flared out' pressure on the side flank does show up when magnified (Fig 5-3(b,c). In Figure 5-4 the change in contact geometry, a/b, d/b as a function of ϕ, is shown again using the same dimensionless applied load and the same values of f, ν. It is clear that the contact length will increase rather less with an increase in the angle ϕ, whilst the dimensionless offset, d/b also decreases with increasing ϕ.

Now consider the properties of the asymptote. In order to be able to use the solution effectively the dominant behaviour is abstracted and used as a scaling factor. First, though, it is instructive to plot example pressure distributions out, and this is done in Figure 5-5. The

full asymptotic solution itself is displayed by chain lines, and three plots are given, corresponding to $\lambda = 0.4$, 0.5, 0.6. Also shown as 'asymptotes to the asymptote' are the bounded, logarithmic and inner (power order) asymptotic formed abstracted at the end of the last section. As an example in its use we will apply it to the finite problem already studied, as the closed-form full solution is available for comparison. The first step is to abstract the stress intensity factors from the 'front face only' contact, equation (5-1), and this is readily done by applying the binomial theorem, giving

$$K_L^S = \frac{P}{\pi} \sin \lambda\pi (2b)^{-\lambda}, \tag{5-49}$$

$$K_R^S = \frac{P}{\pi} \sin \lambda\pi (2b)^{1-\lambda}. \tag{5-50}$$

If these are substituted into equation (5-44) the following emerge immediately as the estimated extent of the left and right side contact regions.

$$c_L^S / b = 2\left[\frac{A(1-\lambda)P}{m \sin \lambda\pi 2b}\right]^{\frac{1}{1-\lambda}}, \tag{5-51}$$

$$c_R^S / b = 2\left[\frac{A\lambda P}{m \sin(1-\lambda)\pi 2b}\right]^{\frac{1}{\lambda}}, \tag{5-52}$$

whereas the exact values are

$$c_L^F = (a - d - b) = \frac{k_0 b}{(1-(k_0+k_1)/2)}, \tag{5-53}$$

$$c_R^F = (a + d - b) = \frac{k_1 b}{(1-(k_0+k_1)/2)}. \tag{5-54}$$

Clearly the values of *a/b*, *d/b* must be replaced by those calculated, but it is not possible to do this in closed form. Instead, in Figure 5-6 they are plotted out; but they have proved indistinguishable. It is concluded that the asymptotic form is an extremely accurate representation of the true effect, and may confidently be applied to a wide range of problems.

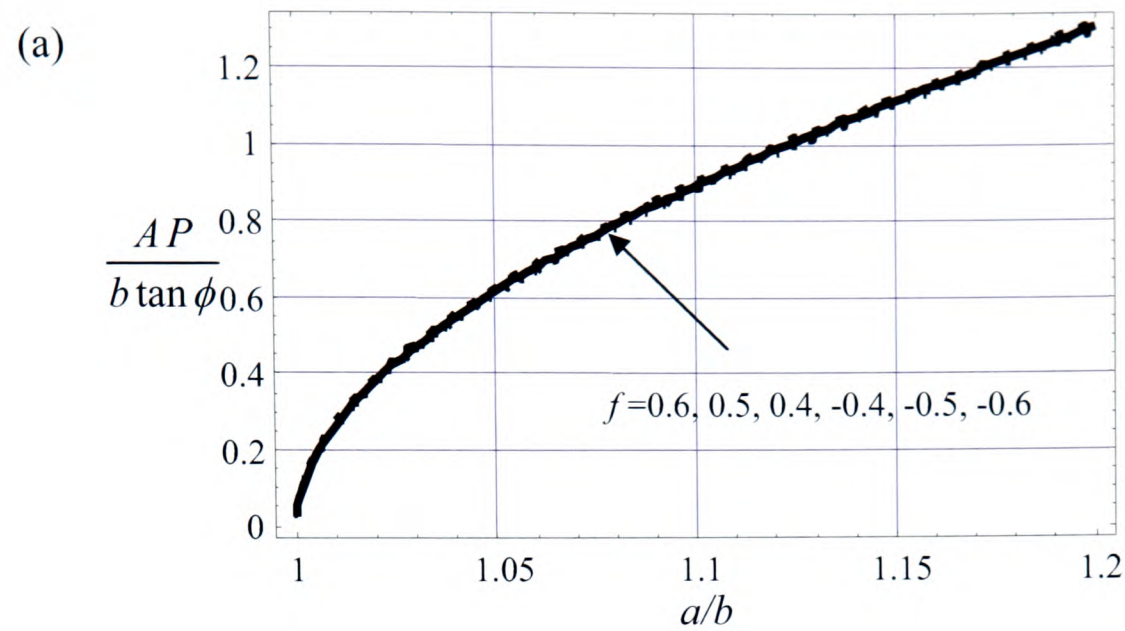

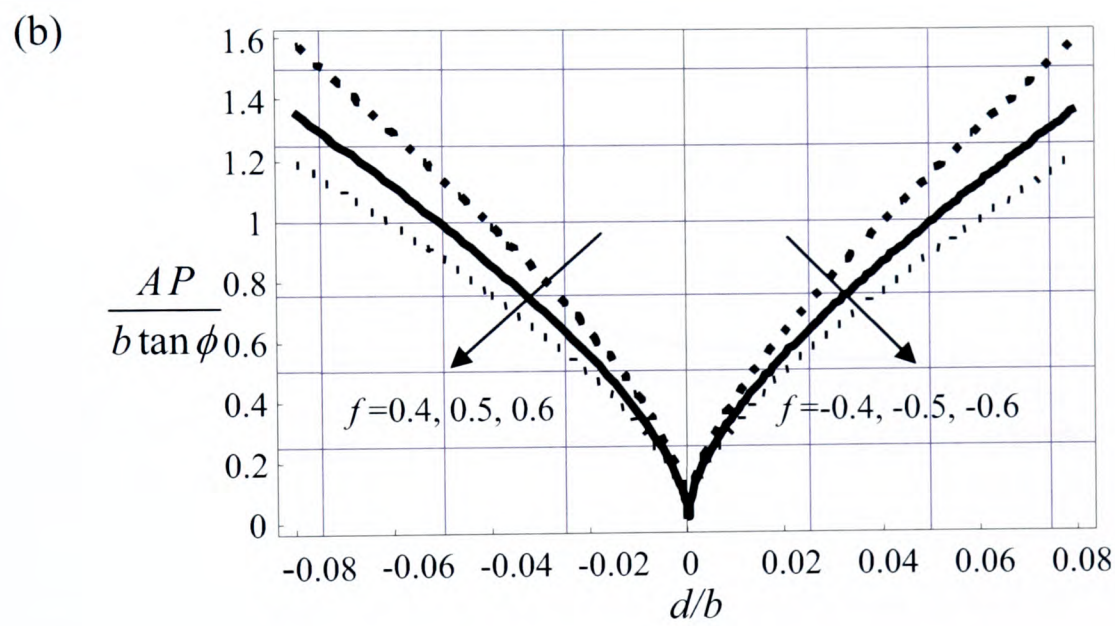

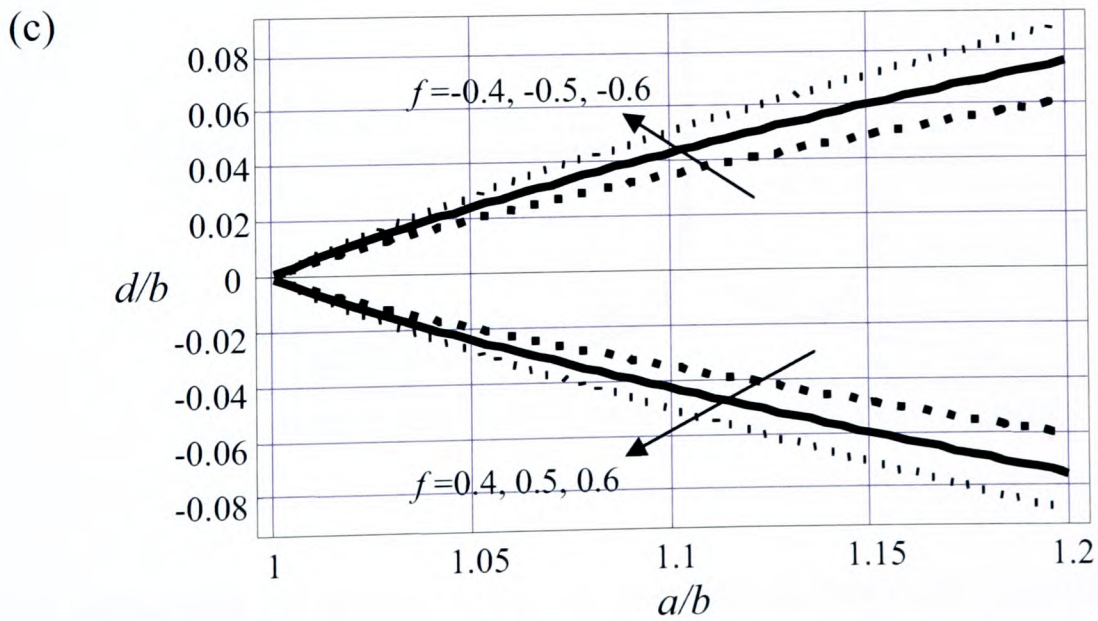

Figure 5-2: Contact law. Poisson's ratio $\nu = 0.3$ (a) Relationship between normalised contact load and contact size, *a/b* (b) Relationship between normalised contact load and contact offset, *d/b* (c) Relationship between *a/b* and *d/b*

(a)

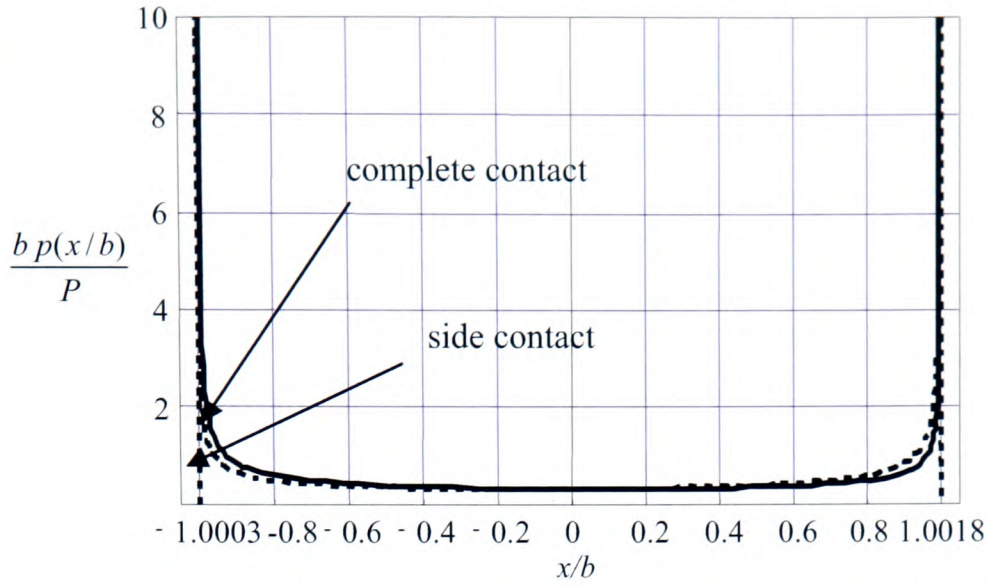

(b)

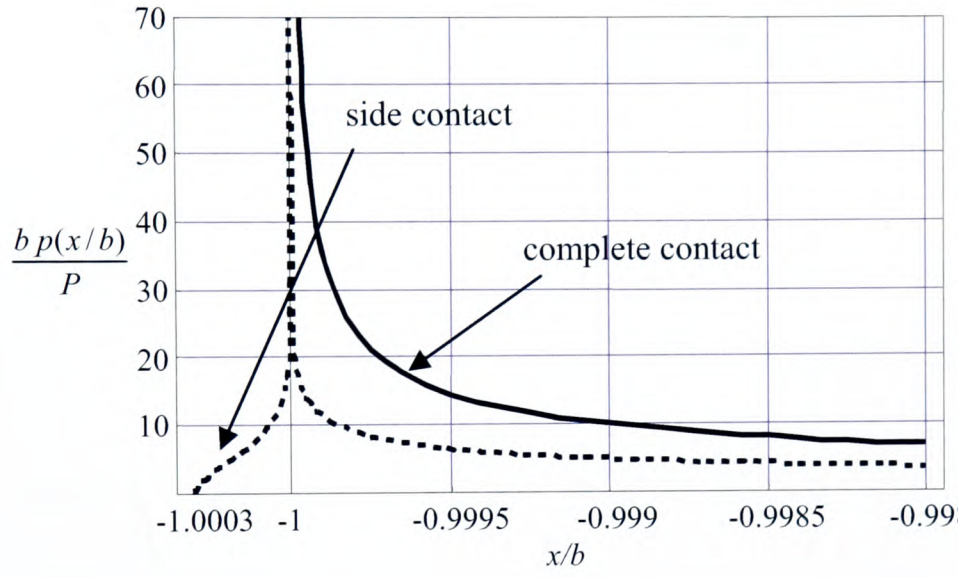

(c)

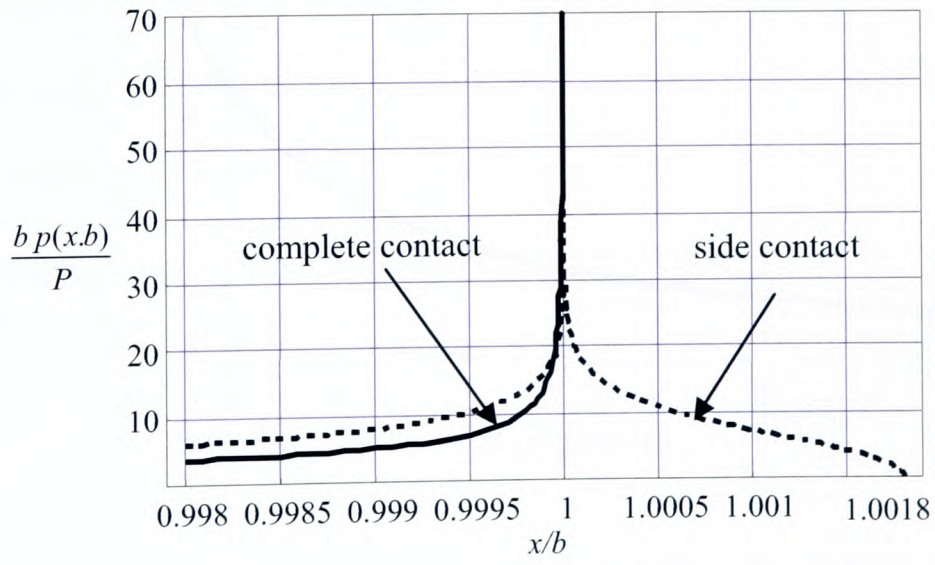

Figure 5-3: Comparison of contact pressure distributions between 'complete contact' and 'side contact' when the dimensionless load $\frac{AP}{b} = 0.014$, $\phi = 10°$ and $\lambda = 0.5452$, which is corresponds to $f = -0.5$ and $\nu = 0.3$ (a) Overall normalised contact pressure distribution along the contact interface (b) Normalised contact pressure distribution detailed comparison at the left hand side (c) Normalised contact pressure distribution detailed comparison at the right hand side

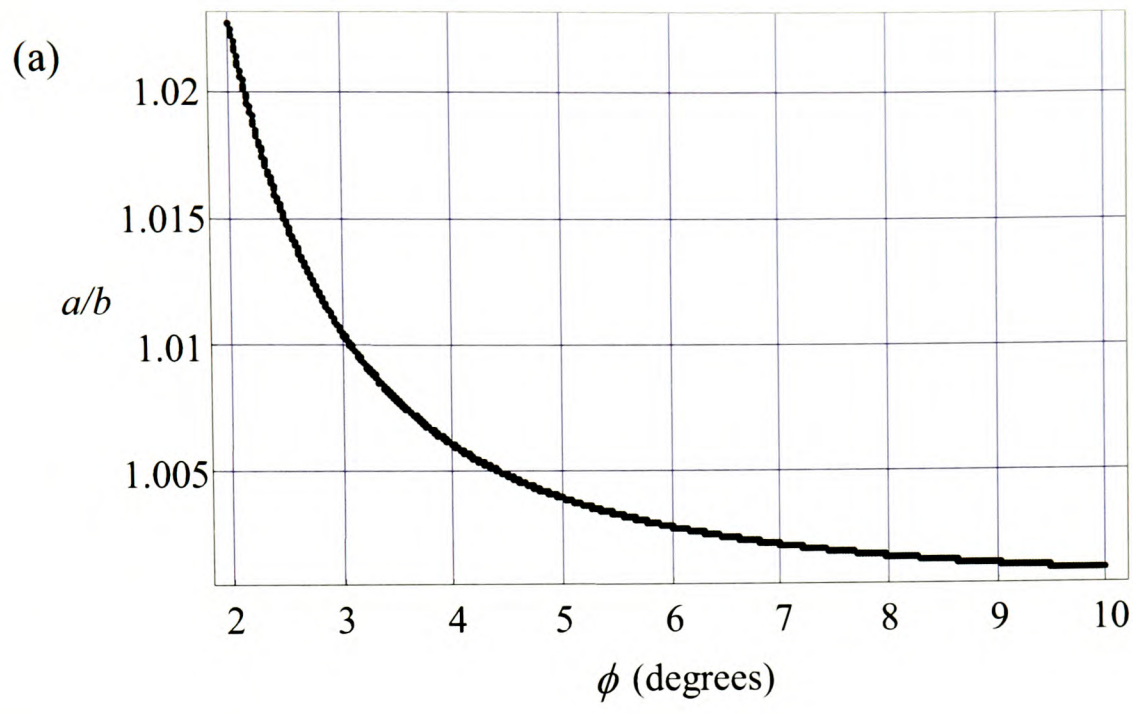

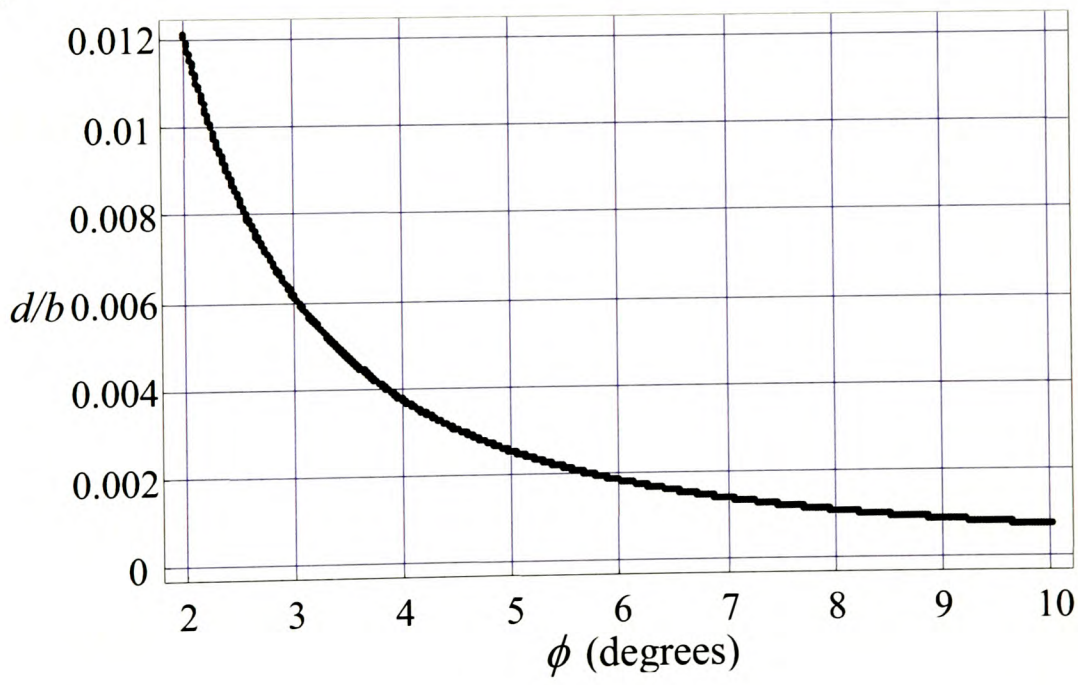

Figure 5-4: Plot of relationship between (a) a/b and ϕ (b) d/b and ϕ, when $\frac{AP}{b} = 0.014$ and $\lambda = 0.5452$ ($f = -0.5$ and $\nu = 0.3$)

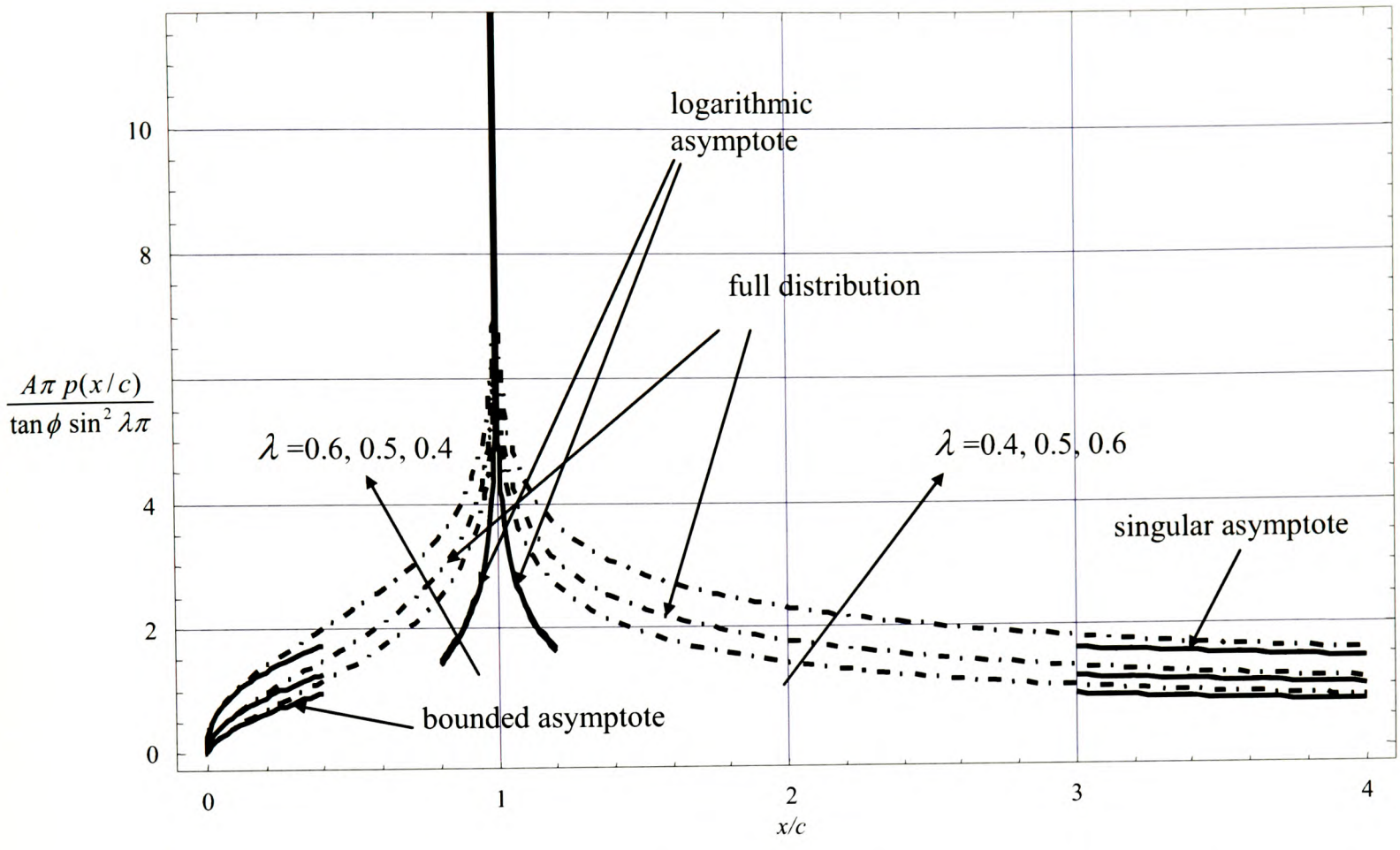

Figure 5-5: Normalised contact pressure distribution and asymptotes for sample eigenvalues λ .

Table 5-1

Material	E(GPa)	ν	μ(GPa)	1/A(GPa)	σ_Y (MPa)	$A\sigma_Y$
Mild Steel	210	0.3	80.77	115.5	240	0.002
Aluminium 2024	72	0.33	27.07	40.4	395	0.01
Titanium-6Al-4V	115	0.3	44.23	63	900	0.014

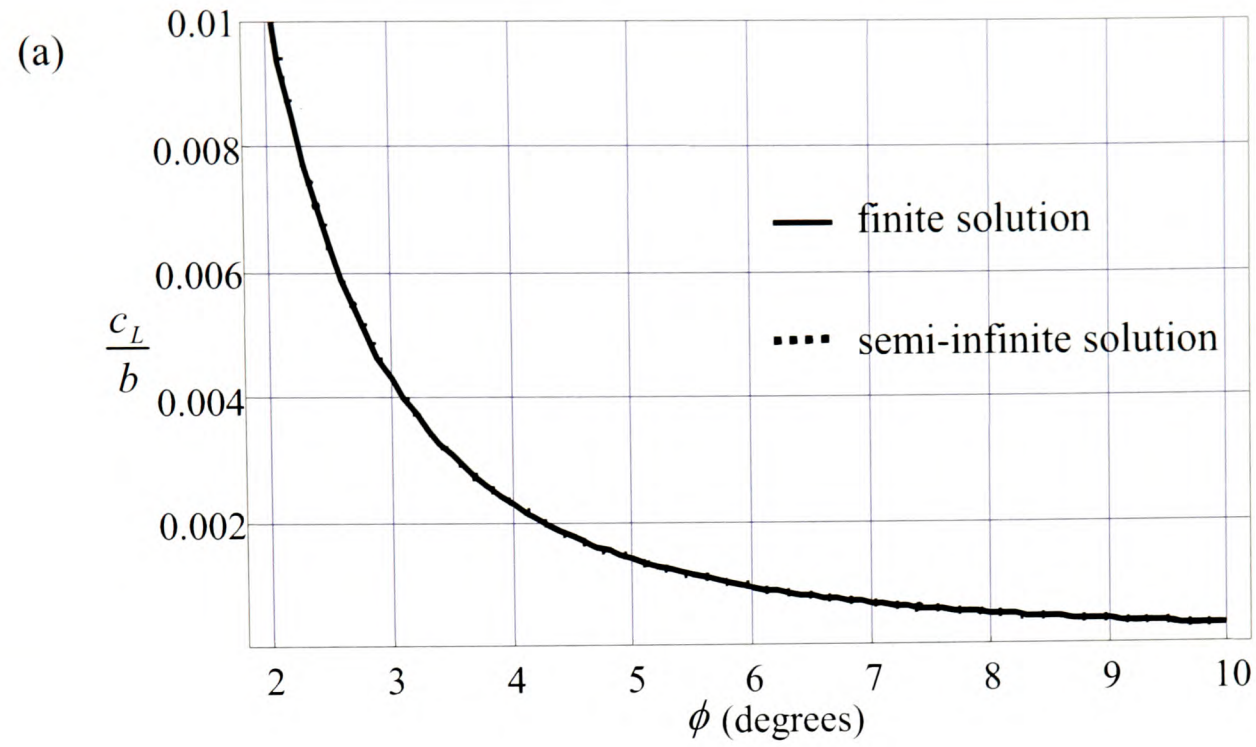

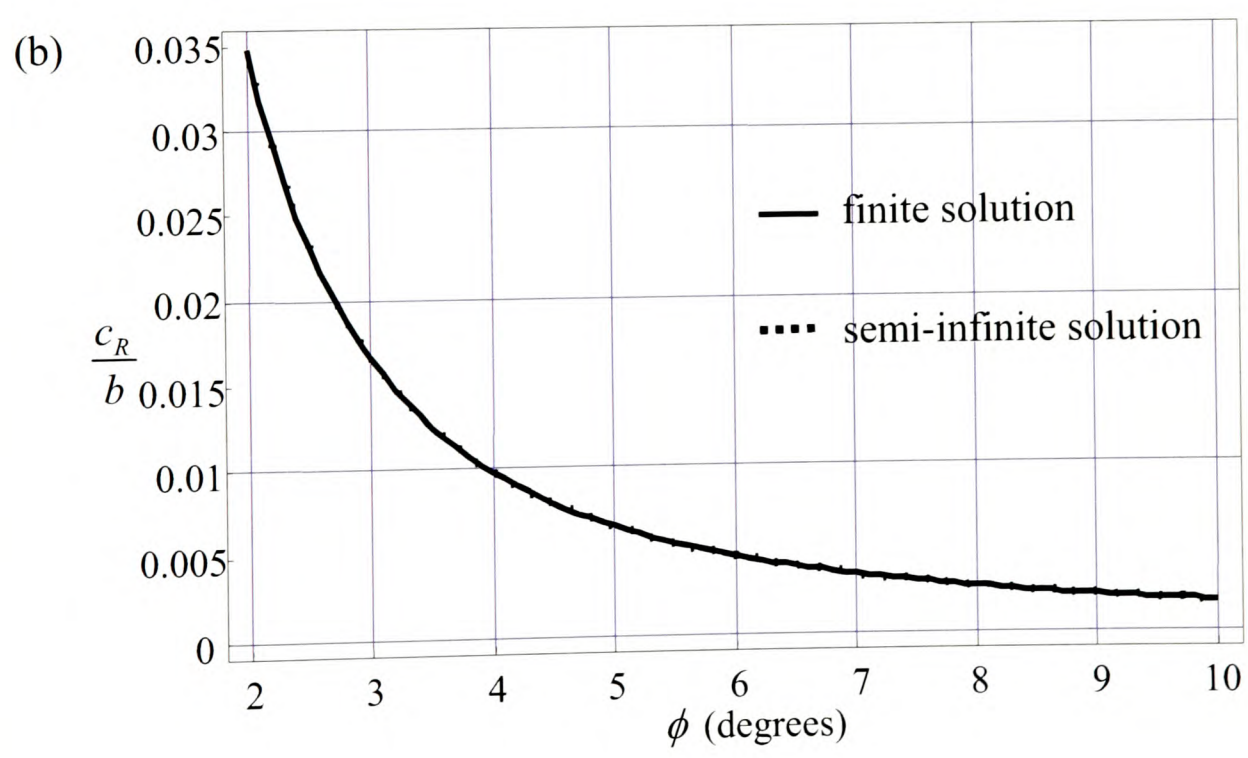

Figure 5-6: Comparison of the side contact lengths of finite trapezium punch (Figure 5-1 (b)) and it approximation using semi-infinite solution (Figure 5-1 (c)) when $\frac{AP}{b} = 0.014$ and $\lambda = 0.5452$ ($f = -0.5$ and $\nu = 0.3$). (a) Left hand side (b) Right hand side

5.8 Conclusion

First, it is noted that, when a sharp indenter is pressed into an elastic half-space, there will be implied side contact, according to linear elasticity theory, if $\phi < \pi/2$. In fact linear elasticity theory cannot treat side contact properly at anything approaching this value, but the theory does hold well at smaller values of ϕ. As an example, the problem of a plane punch sliding along a compressible half-plane has been treated in full. This provides a vehicle for comparison with a different form of the solution to problems of this class, using a semi-infinite asymptote. The asymptotic form has also been derived explicitly, and applied first to the trapezium shaped indenter, to display its accuracy. The important feature of the application of the asymptotic form is that it is necessary to solve the initial contact problem only under conditions of front-face contact, which is very much easier to do, and then to abstract the generalised stress intensity factor characterising the solution at the contact edge. When once this has been found the collocation of the asymptotic form into the edge of the simplified contact solution is extremely straightforward, and very accurate. The procedure as a whole is important because it demonstrates, quantitatively, that in many problems of the class considered the power order singularity present at a contact edge is, in fact, replaced by a logarithmic singularity, which is in close juxtaposition to a power-order bounded contact pressure. Thus, in many practical problems, even without plasticity, the contact edge pressure distribution may be ameliorated from its singular form.

Chapter 6

Skew Sliding of an Elastic Cylinder: an Investigation of Convection in Contact

6.1 Introduction

When a sphere is pressed into and slid along an elastically similar half-space, it is tacitly assumed that particles pass through the contact patch along a straight line parallel with the direction of sliding. Similarly, when spherical Hertzian contact is subject to partial slip, the application of Cattaneo's method (Cattaneo, 1938) ignores the transverse displacement of surface particles, and the solution is only strictly valid when the contacting bodies exhibit no Poisson effect; in other cases the true stick-slip pattern is more complex (Munisamy, 1994). Ciavarella recognises this same limitation in his generalisation of the Cattaneo principle (Ciavarella, 1998). In this chapter we aim to investigate this phenomenon, but in the geometrically very much simpler context of an infinitely long cylinder, pressed onto a half-plane to form a plane Hertzian contact, but sliding along a general skew direction, Figure 6-1, with plane and anti-plane velocity components. We wish, specifically, to consider the detailed effects of convection on slip and the concomitant change in relative curvature will be ignored.

The latter will, of course, very slightly change the contact pressure distribution, but this will have a second order influence on the slip response.

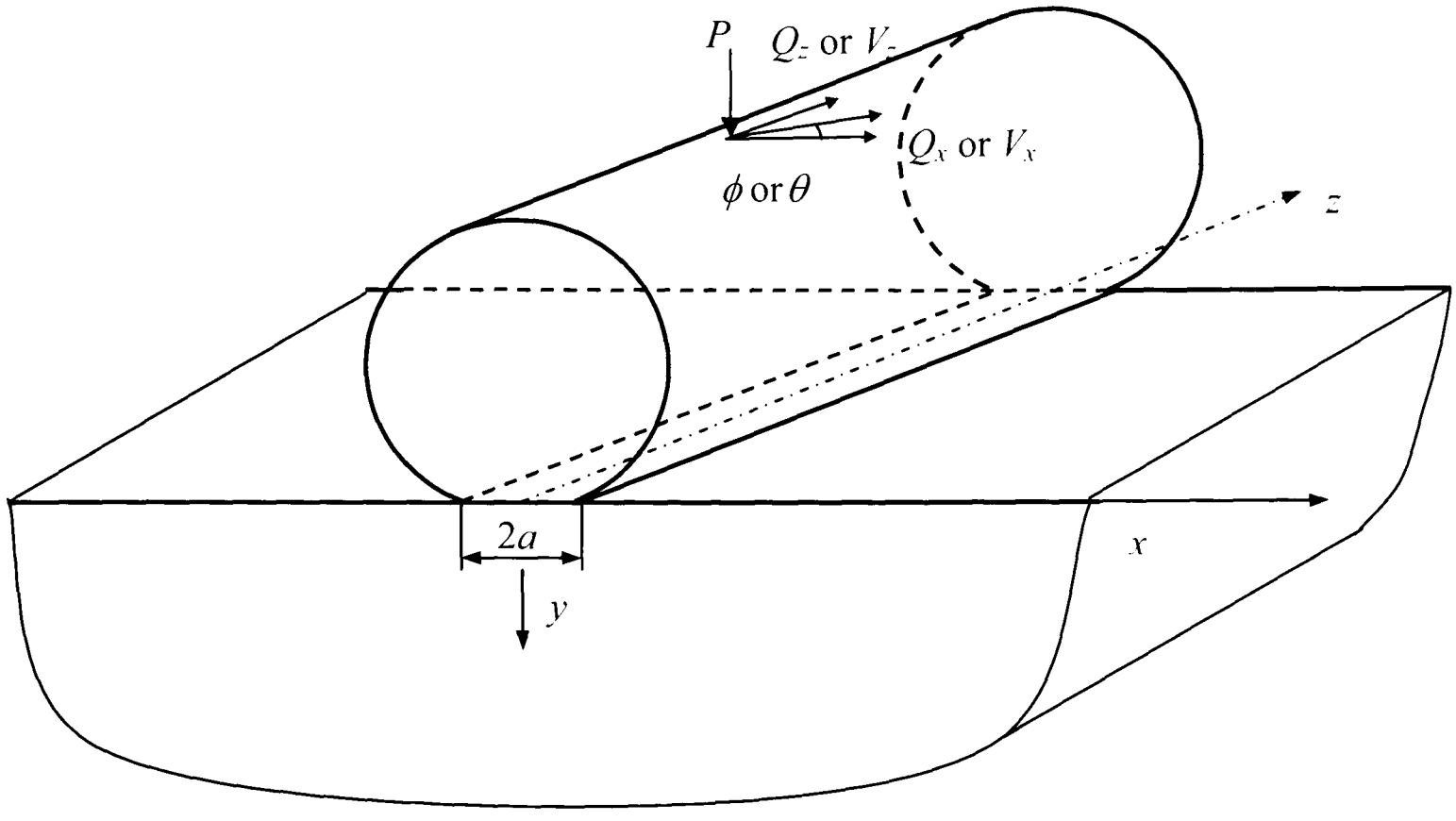

Figure 6-1: A long cylinder pressed onto a half-plane and sliding along a skew direction, ϕ.

The simplest way to view the problem is as a cylinder of finite radius, and pressed onto a half-plane, by a normal load P (per unit length), so as to form a Hertzian contact, which extends from $(-a \le x \le a)$. The contacting bodies are elastically similar, so that the contact pressure distribution (ignoring convection) is unaffected by the presence of shearing tractions, and is equal to

$$p(x) = p_0 \sqrt{1-(x/a)^2} \tag{6-1}$$

where p_0 is the peak pressure. The cylinder is now displaced, at a constant velocity, V, in a direction which makes an angle ϕ with the x direction. At first sight it might be thought that this would require a shearing force, Q, given by fP, where f is the coefficient of interfacial friction, applied in the same direction: certainly this is approximately true, but we aim to look in detail at the nature of the trajectory of particles as they flow through the contact patch, in a

frame of reference fixed in the cylinder, and hence to find the precise distribution of shearing traction components, q_x, q_z, present along the interface. We shall assume that the cylinder has been sliding for a significant distance ($>> a$) so that a steady state has been established and, of course, even though the problem is three dimensional in nature, there are no gradients in the z direction. When particles in the half space approach the contact they will move from their unstrained positions. In order to remove the unknown rigid body component of displacement we will work in terms of displacement gradients, and therefore, if the shear traction distributions in the x, z directions are $q_x(x), q_z(x)$ the surface displacements in either body are given by

$$\frac{\partial u_x^i}{\partial x} = -\frac{2(1-\nu^2)}{\pi E}\int_a^b \frac{q_x(\xi)}{x-\xi}d\xi - \frac{(1-2\nu)(1+\nu)}{\pi E}p(x) \tag{6-2}$$

$$\frac{\partial u_z^i}{\partial x} = -\frac{2(1+\nu)}{\pi E}\int_a^b \frac{q_z(\xi)}{x-\xi}d\xi, \qquad i=1,2 \tag{6-3}$$

where superscript $i=1$ refers to the cylinder and $i=2$ to the half-space, ν, E are Poisson's ratio and Young's modulus, and the shearing tractions are related to the contact pressure by

$$f^2 p^2(x) = q_x^2(x) + q_z^2(x). \tag{6-4}$$

The axis set is fixed to the cylinder and hence the components of relative local slip velocity at each point within the contact are given by a rigid body term and a convection term, so that

$$V_x = V\cos\phi + \frac{\partial u_x^1}{\partial x}\frac{\partial x}{\partial t} - \frac{\partial u_x^2}{\partial x}\frac{\partial x}{\partial t} = V\cos\phi\left(1-\frac{\partial u_x}{\partial x}\right) \tag{6-5}$$

$$V_z = V\sin\phi + \frac{\partial u_z^1}{\partial x}\frac{\partial x}{\partial t} - \frac{\partial u_z^2}{\partial x}\frac{\partial x}{\partial t} = V\sin\phi\left(1-\cot\phi\frac{\partial u_z}{\partial x}\right). \tag{6-6}$$

As the displacements in the cylinder (body 1) do not vary with time, we may now drop the superscript 2 without introducing any ambiguity. Next, we seek to impose the normality condition of friction in a pointwise sense, within the contact. If the local slip direction is $\varphi(x)$, and φ is not necessarily equal to ϕ, we have

$$\cot\varphi = \frac{q_x}{q_z} = \frac{V_x}{V_z} = \frac{\cos\phi(1-\frac{\partial u_x}{\partial x})}{\sin\phi(1-\cot\phi\frac{\partial u_z}{\partial x})}. \tag{6-7}$$

It is clear that the deviation of the local slip direction form the local sliding direction is of order of the strain. The entire formulation here is based on linear theory, employing an infinitesimal (first order) definition of strain. The calculation is therefore implicitly restricted to cases where the strains induced are adequately described and this must be borne in mind when the results are considered. Equations (6-2), (6-3) and (6-7) are sufficient to solve, in principle, this family of equations, and the primary output is the variation of local shearing traction with position across the contact. When this has been found it is straightforward to determine the components of shearing force

$$Q_z = \int_{-a}^{a} q_z(x)dx \tag{6-8}$$

$$Q_x = \int_{-a}^{a} q_x(x)dx, \tag{6-9}$$

and therefore the direction in which it must be applied, θ, in order to achieve sliding at an angle ϕ, is given by

$$\tan\theta = \frac{Q_z}{Q_x}. \tag{6-10}$$

6.2 Formulation

The practical difficulty in carrying out this calculation is that if integral equations (6-2) and (6-3) are inverted, and their solutions substituted into equations (6-4) and (6-7) the resulting non-linear equations cannot easily be solved. Therefore, instead, we replace the continuous traction distribution by a piecewise linear representation, following the pioneering technique developed by Bentall and Johnson (Benthall and Johnson, 1968), and adapted for

anti-plane partial slip problems in (Kim, Hills and Nowell, 2000). In this method the true traction distribution is replaced by a set of overlapping triangles, Figure 6-2, and the starting point for the solution is to write down their influence functions. If the width of the base of the element of traction is $2d$, and the element is placed at the origin, the surface tangential displacements are given by

$$\left.\frac{\partial u_x}{\partial x}\right|_q = -\frac{q_x}{d}\frac{(1-\nu^2)}{\pi E}[(x+d)\ln(\frac{x+d}{x})^2 + (x-d)\ln(\frac{x-d}{x})^2] \qquad (6\text{-}11)$$

$$\left.\frac{\partial u_x}{\partial x}\right|_p = -\frac{(1-2\nu)(1+\nu)}{\pi E}p(x) \qquad (6\text{-}12)$$

$$\left.\frac{\partial u_z}{\partial x}\right|_q = -\frac{q_z}{d}\frac{(1+\nu)}{\pi E}[(x+d)\ln(\frac{x+d}{x})^2 + (x-d)\ln(\frac{x-d}{x})^2]. \qquad (6\text{-}13)$$

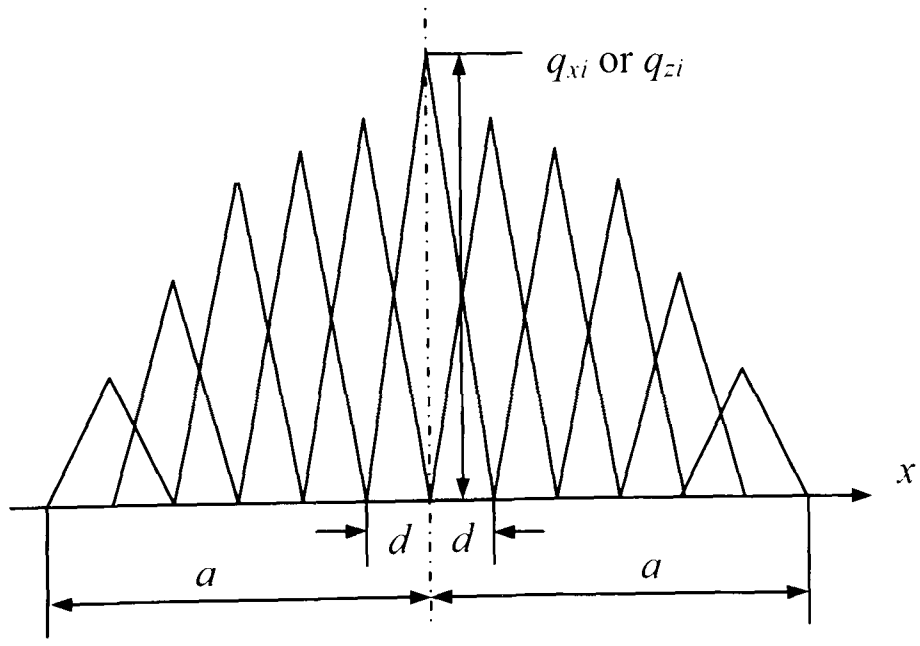

Figure 6-2: Piecewise linear representation of the shear traction distribution

We now discretise the contact patch into $2s$ elements, and use the results just cited, together with a shift of origin, so that we may develop a connexion between the distribution of

shearing traction elements, q_{xj}, q_{zj} and the slip displacements $\partial u_x/\partial x$, $\partial u_z/\partial x$ at point j. These are

$$\frac{\partial u_x}{\partial x}(i) = -\frac{1}{\pi E^*}\sum_{j=-s+1}^{s-1} q_{xj}[(i-j+1)\ln(\frac{i-j+1}{i-j})^2 + (i-j-1)\ln(\frac{i-j-1}{i-j})^2] - \frac{1-2\nu}{E^{**}}p(i) \quad (6\text{-}14)$$

$$\frac{\partial u_z}{\partial x}(i) = -\frac{1}{\pi E^{**}}\sum_{j=-s+1}^{s-1} q_{zj}[(i-j+1)\ln(\frac{i-j+1}{i-j})^2 + (i-j-1)\ln(\frac{i-j-1}{i-j})^2] \quad (6\text{-}15)$$

where E^* is the plane strain stiffness $= E/(1-\nu^2)$, and E^{**} is the antiplane stiffness $= E/(1+\nu)$ (which is, of course, twice the modulus of rigidity). Note that a third form of the material stiffness appears in the relation to the effect of normal pressure. The contact pressure distribution is given by (6-1), and the shear tractions may be written as

$$q_{xj} = fp_j\cos\varphi = fp_0(1-(\frac{j}{s})^2)^{1/2}\cos\varphi \quad (6\text{-}16)$$

$$q_{zj} = fp_j\sin\varphi = fp_0(1-(\frac{j}{s})^2)^{1/2}\sin\varphi, \quad (6\text{-}17)$$

so that

$$\frac{V_x}{V_z} = \frac{\cos\phi(1+\frac{1}{\pi E^*}\sum_{j=-s+1}^{s-1} q_{xj}c(i,j) + \frac{1-2\nu}{E^{**}}p(i))}{\sin\phi(1+\cot\phi\frac{1}{\pi E^{**}}\sum_{j=-s+1}^{s-1} q_{zj}c(i,j)}. \quad (6\text{-}18)$$

This equation must be solved by sequential iteration, although the contact pressure is, of course, uncoupled, and therefore always equal to the Hertzian distribution. Before starting the iteration, it is helpful to note the characteristic dimensionless quantities which determine the magnitude of the solution. The displacements are proportional to the loads (via p_0), and inversely proportional to the stiffnesses of the materials, E^*, E^{**}. We therefore need to choose an appropriate dimensionless ratio for p_0/E^*, p_0/E^{**}, and the best way to do this is to introduce the yield strength of the material, σ_Y. We can then choose a representative normal load, and here we have set $p_0/\sigma_Y = 1$ in the numerical calculations, as this is typical

of a moderately heavily loaded contact. The remaining dimensionless material parameters, $\sigma_Y / E^*, \sigma_Y / E^{**}$ are given for typical materials in table 6-1, where it is clear that, for metals these numbers are of order 10^{-3}, whilst for rubber they are of order 0.3, and we therefore expect the convection effect we are investigating to be much more pronounced for rubber. It was noted in the Introduction that, as this is a linear analysis, it applies rigorously only when small strain theory applies. In the case of rubber very much larger strains are clearly present: their approximation by a first order term should be viewed guardedly. In order to solve the set of equations we start by assuming that the direction of the shearing traction is everywhere defined by the rigid body motion, and determine the local slip direction everywhere, $\varphi(x)$, from equation (6-7). We then use this to re-apportion the shearing traction at each point, and repeat the process until convergence occurs. In practice convergence is extremely rapid and, within eight cycles, the solution is always within 1% of the final value.

6.3 Results

The most extreme set of conditions was initially chosen to display the maximum effect: rubber material with a normalised load, as stated, of $p_0 / \sigma_Y = 1$ with the coefficient of friction set to 0.5. Figure 6-3 shows the slip displacement variation across the section for various sliding angles: there is no effect, of course, at $\phi = 0$, $\pi/2$, and it is the rotation of the lines from a constant value of φ which is the biggest indication of the effects of the surface strain effect, i.e. convection. The difference between the angle at which sliding occurs, ϕ and the angle at which the shearing force must be applied, θ, is just apparent under these load conditions, and is shown in Figure 6-4. The magnitude of the applied force, Q, needed to come sliding is no longer precisely equal to fP. As Q_x, Q_z are easily found from equations (6-

8, 6-9) the total shear force is known. Figure 6-5 displays the ratio Q/fP where $Q^2 = Q_x^2 + Q_y^2$ as a function of ϕ. The shearing force is slightly less than that implied by the same fraction. A further portrayal of the results is provided in Figure 6-6: parts (a, b) relate to rubber and show, first, the deviation between the angle of sliding and the angle of pushing, and secondly, the moment which must also be applied if the shearing force is exerted through the centre of the contact. It is assumed that motion is imparted by the application of a line force, extending indefinitely in the $\pm z$ direction. If there is to be no resultant motion about the y-axis, it is argued that the line of action must be displaced from the $x = 0$ plane, or alternatively a distributed moment applied, given by a $M = \int_{-a}^{a} fp(x)dx$ along the line $x = 0$. The remainder of the plots show the rather less pronounced effects seen when the components are made from aluminium. First Figure 6-6 (c, d) shows the mismatch between the sliding angle and direction of applied shearing force, together with the applied moment needed to maintain rotational equilibrium, and lastly, Figure 6-7 shows the variation of local slip angle with position, for $\phi = 30°, f = 0.5$; the effect is small, as expected, with a variation of about $0.1°$ over the contact width, which is about 1/40th of the magnitude of the effect in rubber. Further, when rubber is considered the variation of the slip angle with position across the contact is monotonic, Figure 6-3, whereas here it has a different form. The reason is that rubber is almost incompressible, and so the effect of the shear traction term, q_x, dominates the solution, from equation (6-2). With aluminium the two terms are more nearly equal in importance, and the effect of the pressure is to produce the local internal turning point.

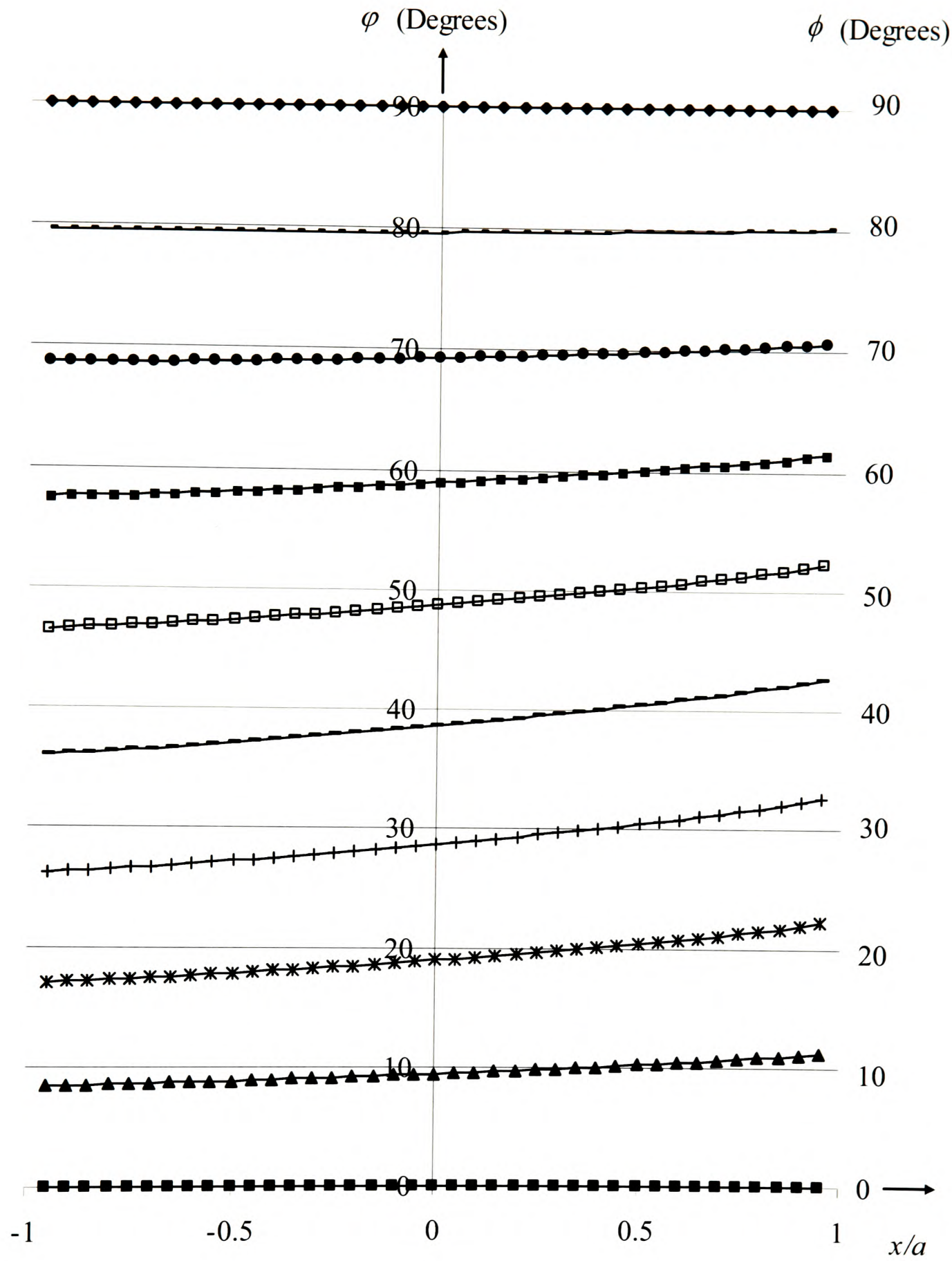

Figure 6-3: Variation of local slip direction, $\varphi(x)$, across the contact for rubber, $p_0/\sigma_y = 1$, $f = 0.5$ and sliding at various angle ϕ.

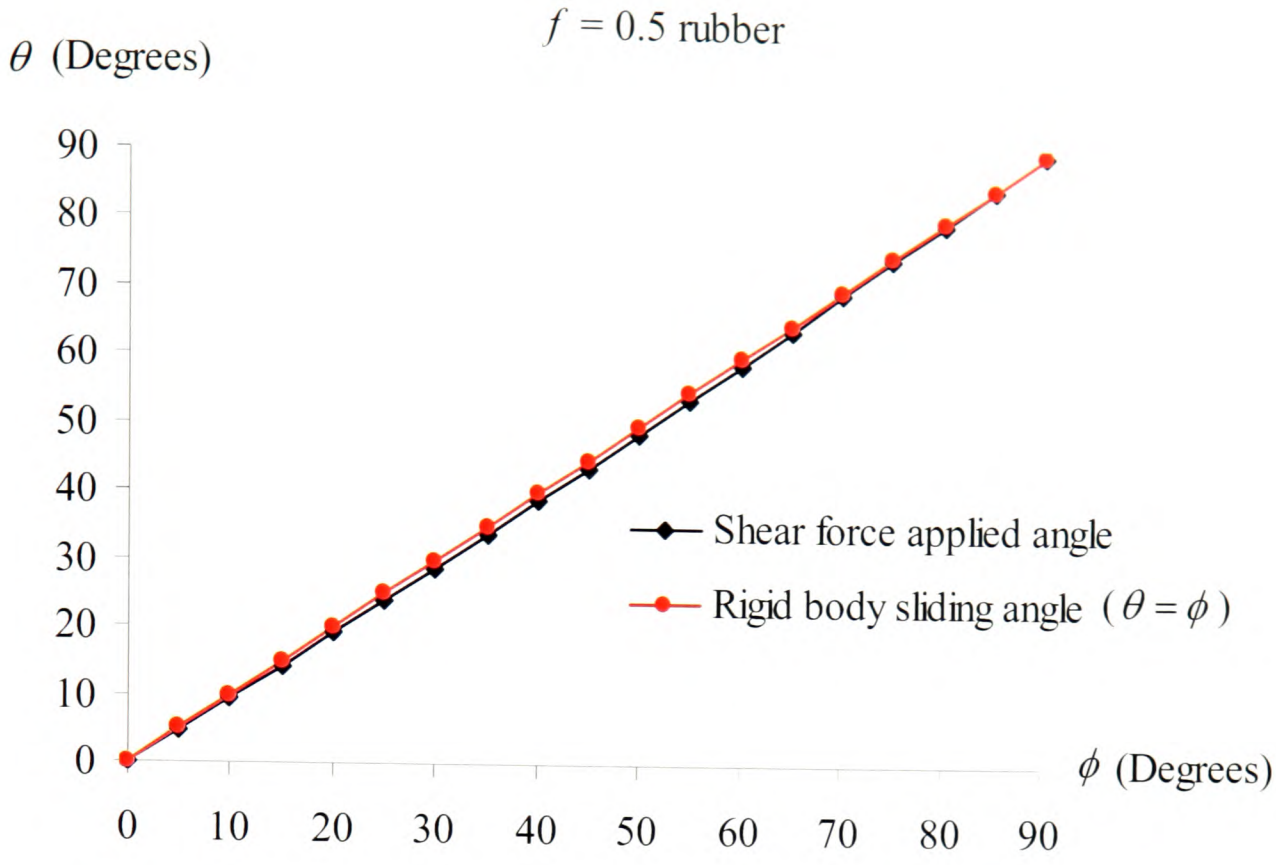

Figure 6-4: Angle of sliding, ϕ, versus angle at which the shear force is exerted, θ. . (Rubber, $p_0 / \sigma_y = 1$, $f = 0.5$)

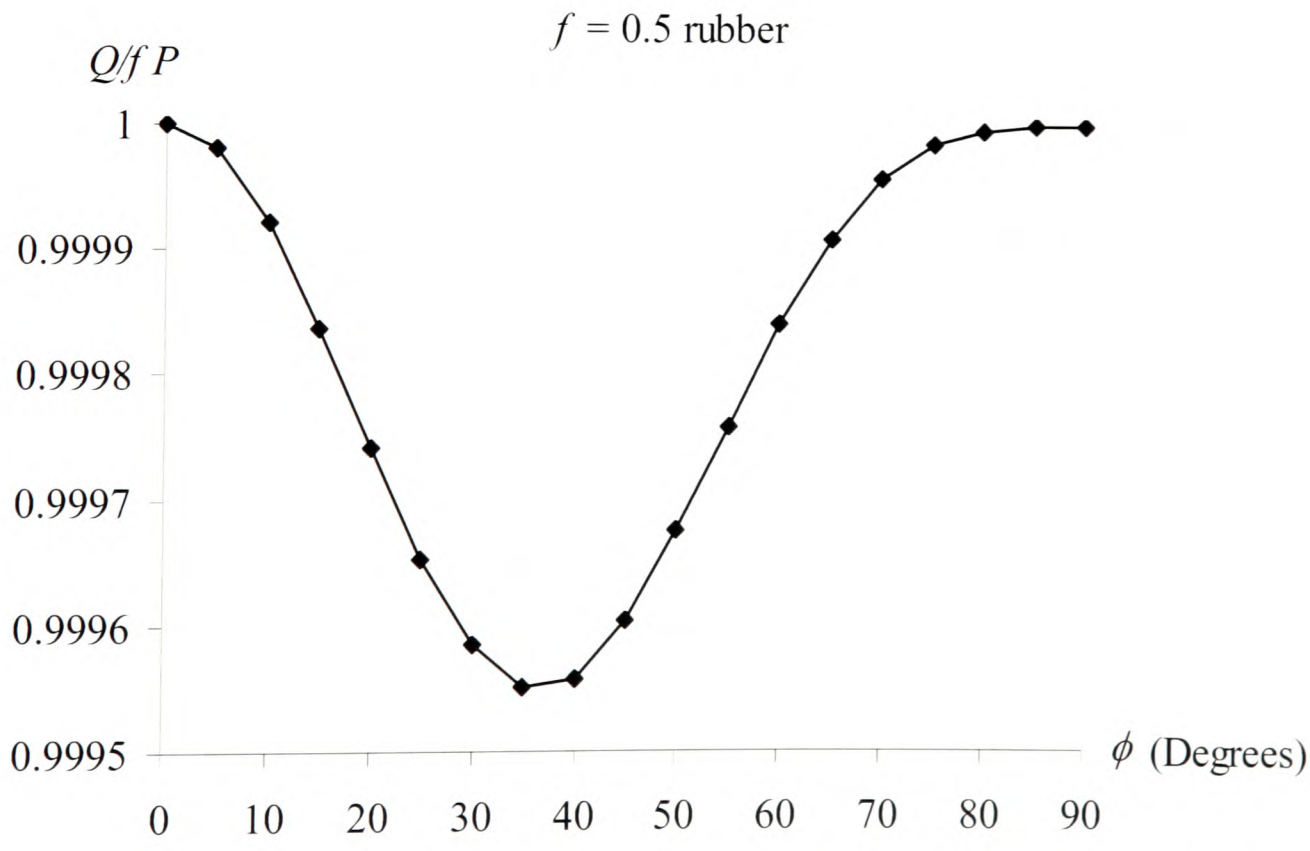

Figure 6-5: $Q/f\,P$ versus angle of sliding, ϕ. (Rubber, $p_0 / \sigma_y = 1$, $f = 0.5$)

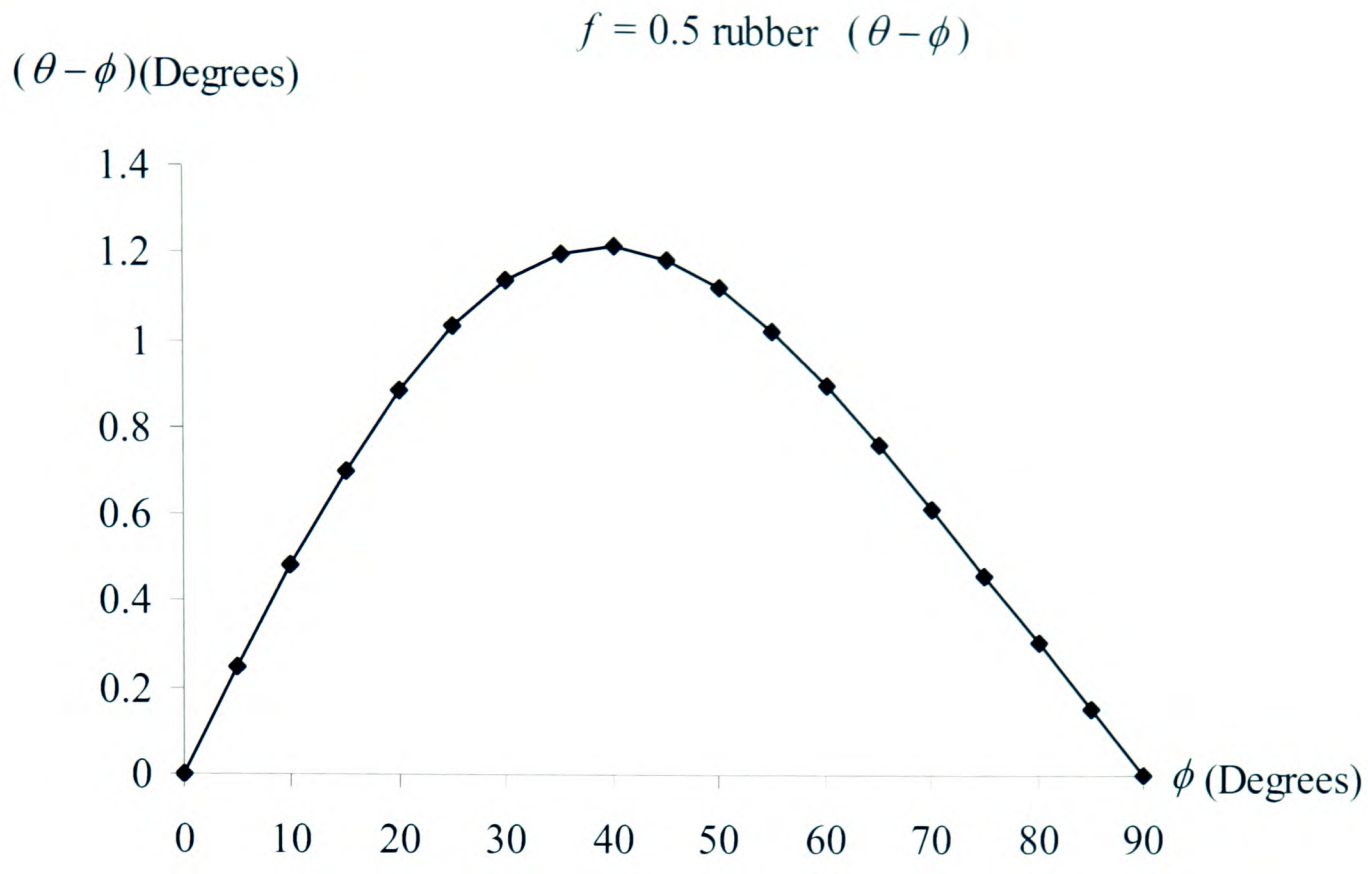
f = 0.5 rubber $(\theta-\phi)$
$(\theta-\phi)$(Degrees)
1.4
1.2
1
0.8
0.6
0.4
0.2
0
0
10
20
30
40
50
60
70
80
90
ϕ (Degrees)

(a)

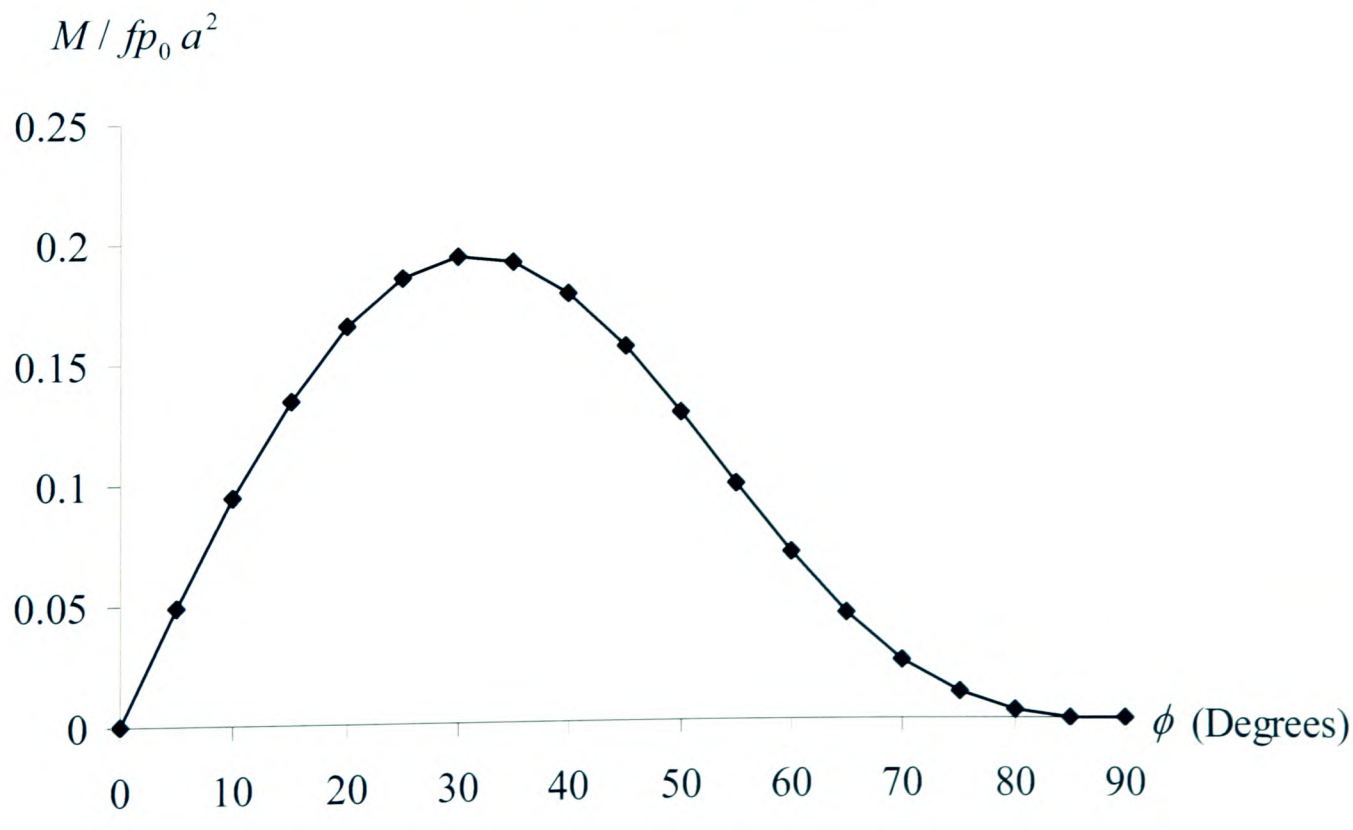
f = 0.5 rubber Moment
$M / fp_0 a^2$
0.25
0.2
0.15
0.1
0.05
0
0
10
20
30
40
50
60
70
80
90
ϕ (Degrees)

(b)

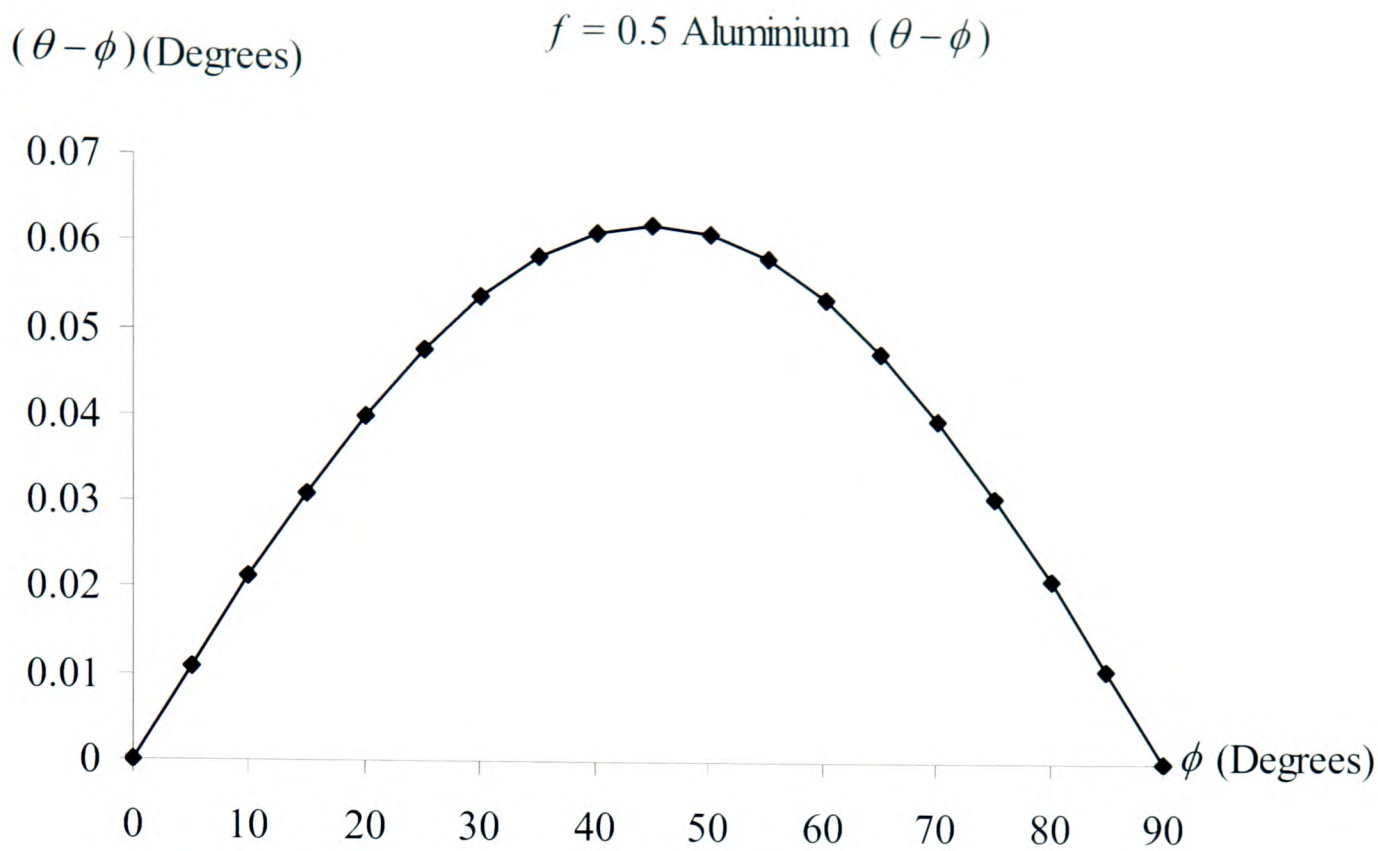

(c)

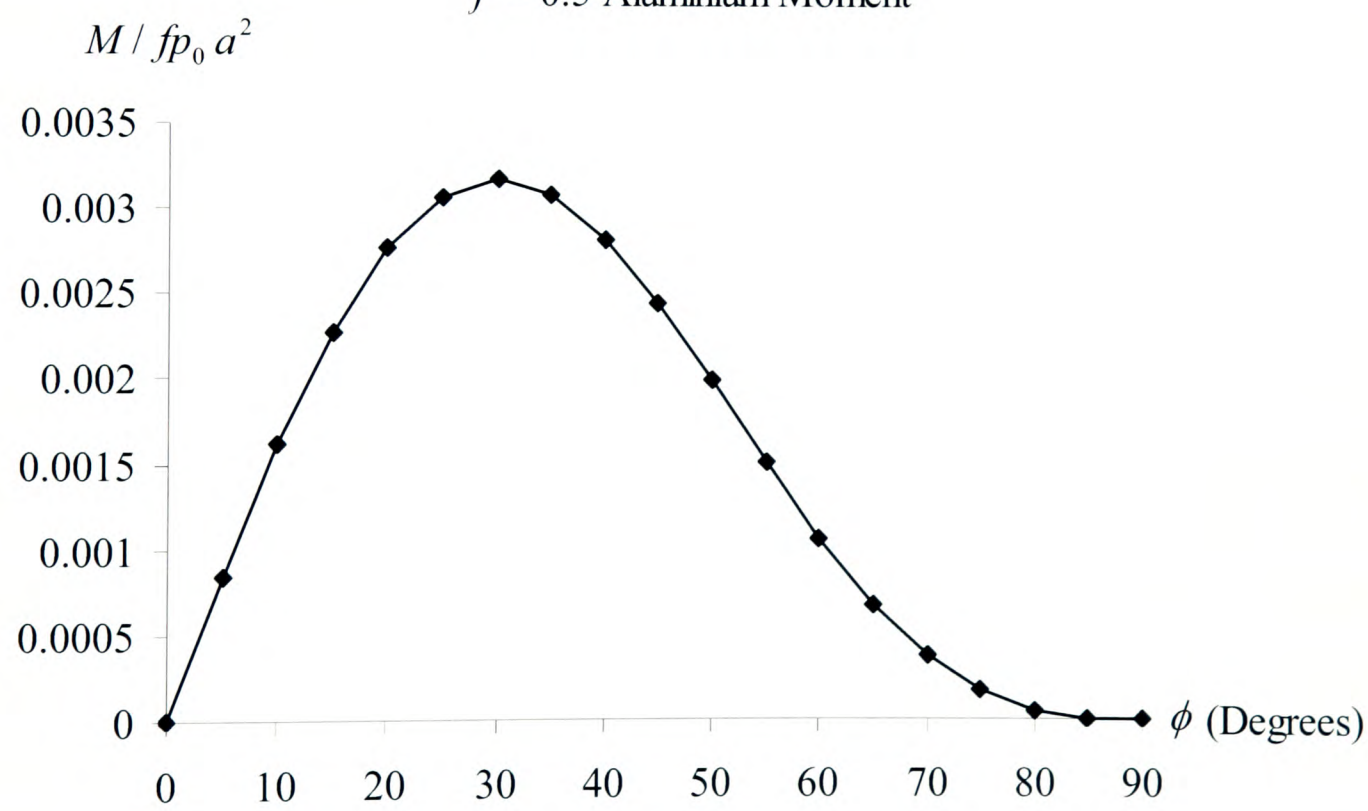

(d)

Figure 6-6: Plots (a, b) are for rubber and (c, d) for aluminium. They show in plots (a, c) the deviation between the angle of sliding and the angle at which the cylinder must be pushed, and in (b, d) the moment which must also be applied if the shearing force is applied at $x = 0$. ($p_0 / \sigma_y = 1$, $f = 0.5$).

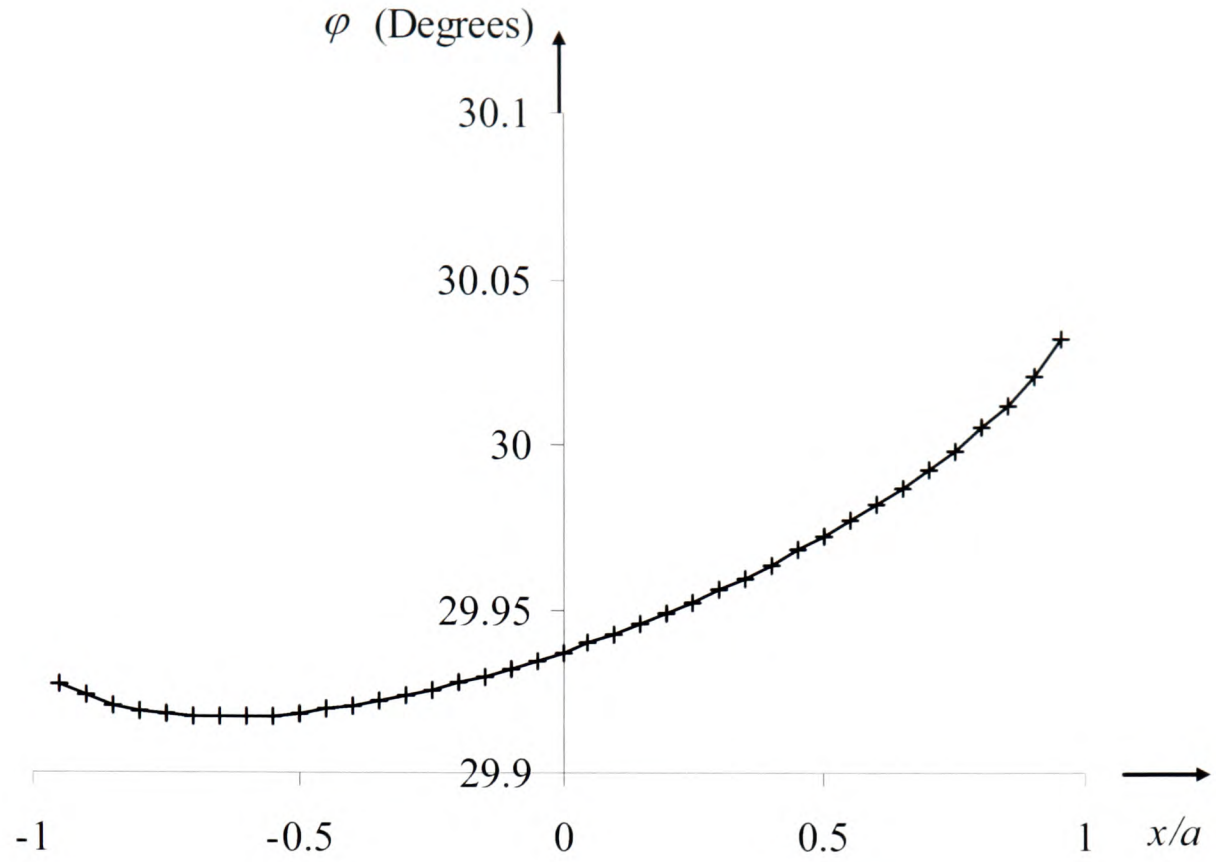

Figure 6-7: The variation of slip angle $\varphi(x)$ with position for aluminium, $p_0/\sigma_Y = 1$, $f = 0.5$, and $\phi = 30$ degrees.

Table 6-1

Material	E (GPa)	ν	E^* (GPa)	E^{**} (G Pa)	σ_Y (MPa)	σ_Y / E^*	σ_Y / E^{**}
Mild steel	210	0.3	231	161.7	240	0.001	0.0014
Aluminium	72	0.33	80.8	54.1	395	0.005	0.0075
Titanium-6Al-4V	115	0.3	126	88.2	900	0.007	0.010
Rubber	0.02	0.45	0.025	0.01375	5	0.200	0.364

6.4 Conclusion

The convection effect for frictional sliding contact between elastically similar bodies has been explored for the simplest possible configuration - skew sliding of a Hertzian contact. This has permitted a very straightforward analysis of an effect known to be present in more complex geometries, for example, a sliding sphere, under similar conditions. For practical engineering materials the effect is very small indeed, but the analysis is important because its magnitude is revealed. It is usually assumed that macroscopic frictional orthogonality and a pointwise application of the same principle are completely consistent. It is shown, here, that this is not precisely correct. Although it has a negligible effect in sliding its presence is also felt in static contacts, where it will materially affect the interfacial slip zones present.

Chapter 7

An Investigation of Convection Effects in Complete and Almost Complete Contact Problems

7.1 Introduction

If two bodies are pressed together and subject to a shear force sufficient to cause sliding, the frictional orthogonality requirement is normally taken to mean that the sliding direction is collinear with the direction of the applied shearing force. The same principle may be applied in a pointwise sense within the contact patch, i.e. the local slip direction must, at every point, be parallel with the direction of the local shearing traction. It is usually assumed that all particles within the contact will suffer relative slip in the same direction, and this will, in addition, be the same as the direction of sliding. But, this assumption neglects the effects of local deformation of the bodies. It is tempting to assume that, in a frame of reference fixed within the contact, particles in the contacting body flow through along straight lines parallel with the direction of sliding; but this is not so, precisely because of the effects of elastic distortion, or 'convection'.

We have already examined convection for an incomplete contact, by studying a cylinder, pressed onto a half-plane and sliding with both an in-plane and anti-plane velocity

component in the before chapter. This is a very convenient geometry to consider because there are no gradients in the direction perpendicular to the plane of the analysis, which is therefore 'plane' whilst retaining the essential 3-D element. In this chapter, we shall carry out an equivalent analysis for the case of a complete or sharp-edged contact, which shows some extra features. Recently, Adams and others noted a paradox common to all complete frictional sliding contacts (Adams *et al.*, 2005); this is that, regardless of the elasticity of the contacting bodies, there are extremely narrow zones attached to the edges of the contact where the singularity in the direct strain parallel with the free surface means that, relative to the punch, material actually flows in completely the opposite direction to that required by the rigid body motion. Thus, there are, inevitably, two thin bands, having a width of order 10^{-7} times the contact length (readily swamped either by local plasticity or by the presence of rounding, (Hills *et al.*, 2006), where orthogonality of friction and local slip simply cannot be satisfied: this phenomenon is quite separate from the one currently being studied. In what follows, the component defining the size of the contact is either perfectly sharp edged, or has only slight edge rounding, and so must be assumed rigid for half-plane theory to apply. We shall first develop a general formulation for the resulting contact problem and then address, as a special case, the form of the solution when the contacting half-plane is incompressible.

7.2 General Formulation

Figure 7-1 shows the general arrangement of the geometry of the problem, and the axis-set adopted. Axis set 1 is fixed to the rigid punch, whilst body 2 is an elastic half-plane having a Young's modulus E and Poisson's ratio ν. The deformation of the half-plane, subject to a pressure distribution $p(x)$ and shearing tractions $q_x(x)$, $q_z(x)$ is given by

$$\frac{\partial u_x}{\partial x} = \frac{2(1-\nu^2)}{\pi E}\int_{-a}^{a} \frac{p(\xi)}{x-\xi} d\xi + \frac{(1-2\nu)(1+\nu)}{E} q_x(x) \tag{7-1}$$

$$\frac{\partial u_x}{\partial x} = -\frac{2(1-\nu^2)}{\pi E}\int_{-a}^{a} \frac{q_x(\xi)}{x-\xi} d\xi - \frac{(1-2\nu)(1+\nu)}{E} p(x) \tag{7-2}$$

$$\frac{\partial u_z}{\partial x} = -\frac{2(1+\nu)}{\pi E}\int_{-a}^{a} \frac{q_z(\xi)}{x-\xi} d\xi, \tag{7-3}$$

where the contact extends over the interval [$-a$ a]. If the coefficient of friction is f, the local slipping condition means that the total shear traction is everywhere related to the contact pressure by

$$f^2 p^2(x) = q_x^2(x) + q_z^2(x). \tag{7-4}$$

Suppose, now, that the punch is sliding with a velocity V, and that the sliding direction makes an angle ϕ with the x direction. It follows that, relative to particles on the bottom face of the punch, particles on the surface of the half-plane have velocity components

$$V_x = V\cos(\phi) + \frac{\partial u_x}{\partial x}\frac{dx}{dt} = V\cos(\phi)(1 - \frac{\partial u_x}{\partial x}) \tag{7-5}$$

$$V_z = V\sin(\phi) + \frac{\partial u_z}{\partial x}\frac{dx}{dt} = V\sin(\phi)(1 - \cot(\phi)\frac{\partial u_z}{\partial x}), \tag{7-6}$$

where the first term is the rigid-body contribution and the second term represents the effect of convection. If we apply the concept of orthogonality pointwise we obtain the following relationship between the sliding direction, ϕ, and the local slip direction, $\varphi(x)$ (which is indeed very close to but not necessarily equal to ϕ):

$$\begin{aligned}\cot(\varphi) = \frac{q_x}{q_z} = \frac{V_x}{V_z} &= \frac{\cos(\phi)(1 - \frac{\partial u_x}{\partial x})}{\sin(\phi)\left[1 - \cot(\phi)\frac{\partial u_z}{\partial x}\right]} \\ &= \frac{\cos(\phi)\left[1 + \frac{2(1-\nu^2)}{\pi E}\int_{-a}^{a}\frac{q_x(\xi)}{x-\xi}d\xi + \frac{(1-2\nu)(1+\nu)}{E}p(x)\right]}{\sin(\phi)\left[1 + \cot(\phi)\frac{2(1+\nu)}{\pi E}\int_{-a}^{a}\frac{q_z(\xi)}{x-\xi}d\xi\right]}\end{aligned} \tag{7-7}$$

Finally, overall equilibrium in the x, z directions demands that

$$Q_z = \int_a^a q_z(x)dx \tag{7-8}$$

$$Q_x = \int_a^a q_x(x)dx \tag{7-9}$$

where Q_x, Q_z are the components of applied shearing force. Its resultant direction, θ, and magnitude are given by

$$\tan\theta = \frac{Q_z}{Q_x}, \qquad Q^2 = Q_x^2 + Q_z^2 \tag{7-10}$$

where we shall assume that θ is not necessarily equal to ϕ, and, furthermore, Q is not necessarily equal to fP.

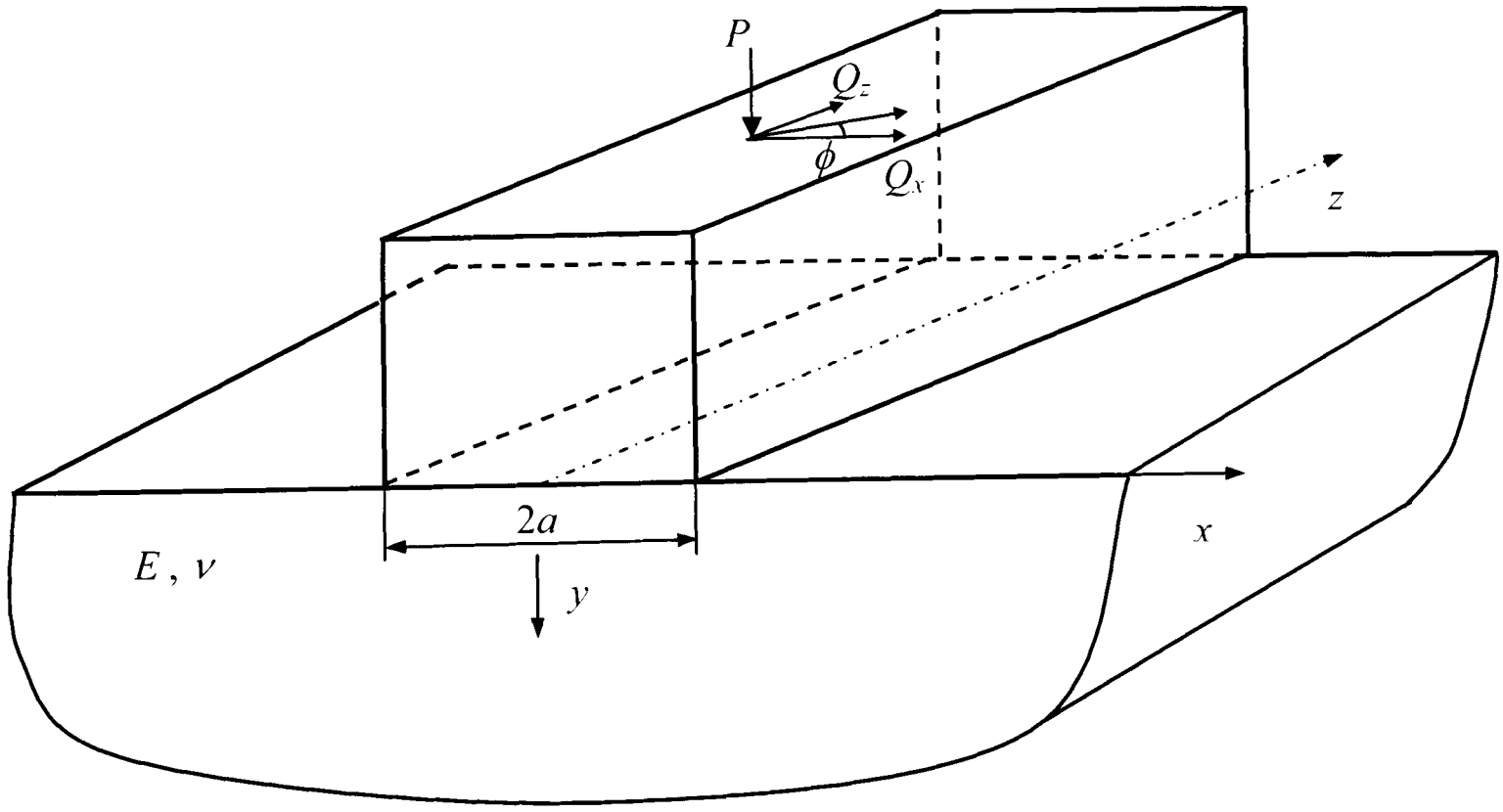

Figure 7-1: A long square punch pressed onto a half-space and sliding along a skew direction, ϕ.

7.2.1 Incompressible Half Space

Equation (7-7), which governs the pointwise orthogonality requirement, may be seen to contain two elements which contribute to convection; one is the contact pressure, where the associated elastic constant is seen to vanish when the material is incompressible ($\nu = 1/2$), whilst the other is concerned with the effects of shear. In the latter case, although the associated elastic constants depend on Poisson's ratio, no practical choice of ν can make it vanish. In the case of an incompressible half-space, the reduced version of the pointwise orthogonality requirement is

$$\cot(\varphi(x)) = \frac{\cos(\phi)\left[1+\dfrac{2(1-\nu^2)f}{\pi E}\displaystyle\int_{-a}^{a}\frac{p(\xi)\cos(\varphi(\xi))}{x-\xi}d\xi\right]}{\sin(\phi)\left[1+\cot(\phi)\dfrac{2(1+\nu)f}{\pi E}\displaystyle\int_{-a}^{a}\frac{p(\xi)\sin(\varphi(\xi))}{x-\xi}d\xi\right]} \tag{7-11}$$

For the particular case of square-ended contact the pressure becomes

$$p(x) = p_0(a^2 - x^2)^{1/2} \tag{7-12}$$

where $p_0 = \dfrac{P}{\pi}$. If this function is substituted into equation (7-11) and the interval of integration normalised to [-1 1], the following integral emerges

$$\int_{-1}^{1}\frac{1}{(x-\xi)\sqrt{1-\xi^2}}d\xi = 0, \tag{7-13}$$

so that, in this case, $\varphi(x) = \phi = \theta$, and there are no convection effects: pointwise and global orthogonality requirements are consistent.

7.2.2 Compressible Half-Plane

When a rigid, square-ended, punch is pressed and slid on an elastic half-plane, we see that the pressure distribution is

$$p(x) = p_0 \sin(\lambda\pi)(a-x)^{\lambda-1}(a+x)^{\lambda} \tag{7-14}$$

where[1]

$$\tan(\lambda\pi) = \frac{1}{\beta f \cos(\phi)}, 0 < \lambda < 1 \tag{7-15}$$

$$\beta = \frac{1-2\nu}{2(1-\nu)}. \tag{7-16}$$

The pointwise orthogonality requirement then becomes, when the interval of integration is normalised,

$$\cot(\varphi(x)) = \frac{\cos(\phi)\left[1 + \frac{2(1-\nu^2)f}{\pi E}\int_{-1}^{1}\frac{p_0 \sin(\lambda\pi)(1-\xi)^{\lambda-1}(1+\xi)^{\lambda}\cos(\varphi(\xi))}{x-\xi}d\xi + \frac{(1-2\nu)(1+\nu)}{E}p(x)\right]}{\sin(\phi)\left[1 + \cot(\phi)\frac{2(1+\nu)f}{\pi E}\int_{-1}^{1}\frac{p_0 \sin(\lambda\pi)(1-\xi)^{\lambda-1}(1+\xi)^{\lambda}\sin(\varphi(\xi))}{x-\xi}d\xi\right]}. \tag{7-17}$$

7.2.3 Numerical Procedure

It does not seem possible to solve integral equation (7-17) analytically. Instead, the shearing traction distribution is represented as a series of elements, Figure 7-2. Away from the edges, overlapping triangles of shearing traction, as developed by Benthall and Johnson

[1] Although, strictly speaking, we should use the locally resolved shearing traction, $\varphi(x)$, in practice the difference from ϕ is very small, and this will not materially affect the solution.

(Benthall and Johnson, 1968) are used, to give a piecewise linear representation of the tractions. Details of the influence functions needed are given in the original reference, and here we merely record the surface displacements induced. If the width of the base of the triangle element of traction is $2s$, the surface tangential displacements are given by

$$\frac{\partial u_x}{\partial x}\Big|_q^t = -\frac{q_x}{s}\frac{(1-\nu^2)}{\pi E}\left[(x+s)\ln(\frac{x+s}{x})^2 + (x-s)\ln(\frac{x-s}{x})^2\right] \tag{7-18}$$

$$\frac{\partial u_z}{\partial x}\Big|_q^t = -\frac{q_z}{s}\frac{(1+\nu)}{\pi E}\left[(x+s)\ln(\frac{x+s}{x})^2 + (x-s)\ln(\frac{x-s}{x})^2\right], \tag{7-19}$$

where the element is here centred at the origin, and the subscript t refers to the contribution of one triangular element to the surface displacements. At the ends of the punch the form of the traction distribution is known - it is power order singular, and very close to the left edge, the pressure can be written as

$$p(r) = \frac{\sin(\lambda\pi)}{2^{1-\lambda} r^{\lambda}}, \tag{7-20}$$

where r is the distance from the edge. A special singular element is used here to represent the effect of the corresponding shear traction. If the width of the element is c, the surface displacements are

$$\frac{\partial u_x}{\partial x}\Big|_q^s = -q_x\frac{(1-\nu^2)}{\pi E}\frac{2cF[1-\lambda,1,2-\lambda,\frac{c}{r}]}{r(1-\lambda)} \tag{7-21}$$

$$\frac{\partial u_z}{\partial x}\Big|_q^t = -q_z\frac{(1+\nu)}{\pi E}\frac{2cF[1-\lambda,1,2-\lambda,\frac{c}{r}]}{r(1-\lambda)}, \tag{7-22}$$

where F is the hypergeometric function, and the subscript s refers to the contribution of the special singular element to the surface displacements. Similarly, at the right hand side of the contact, the pressure varies as

$$p(r) = p_0\frac{\sin(\lambda\pi)}{2^{\lambda} r^{1-\lambda}}, \tag{7-23}$$

and again a special element can be used to represent the effects of shear with the required characteristic. If the width of this singular element is c, the surface displacements are

$$\frac{\partial u_x}{\partial x}|_q^s = -q_x \frac{(1-\nu^2)}{\pi E} \frac{2c(r + r\lambda + c\lambda F[1+\lambda, 1, 2+\lambda, \frac{c}{r}]}{r^2 \lambda(1+\lambda)} \tag{7-24}$$

$$\frac{\partial u_z}{\partial x}|_q^s = -q_z \frac{(1+\nu)}{\pi E} \frac{2c(r + r\lambda + c\lambda F[1+\lambda, 1, 2+\lambda, \frac{c}{r}]}{r^2 \lambda(1+\lambda)}. \tag{7-25}$$

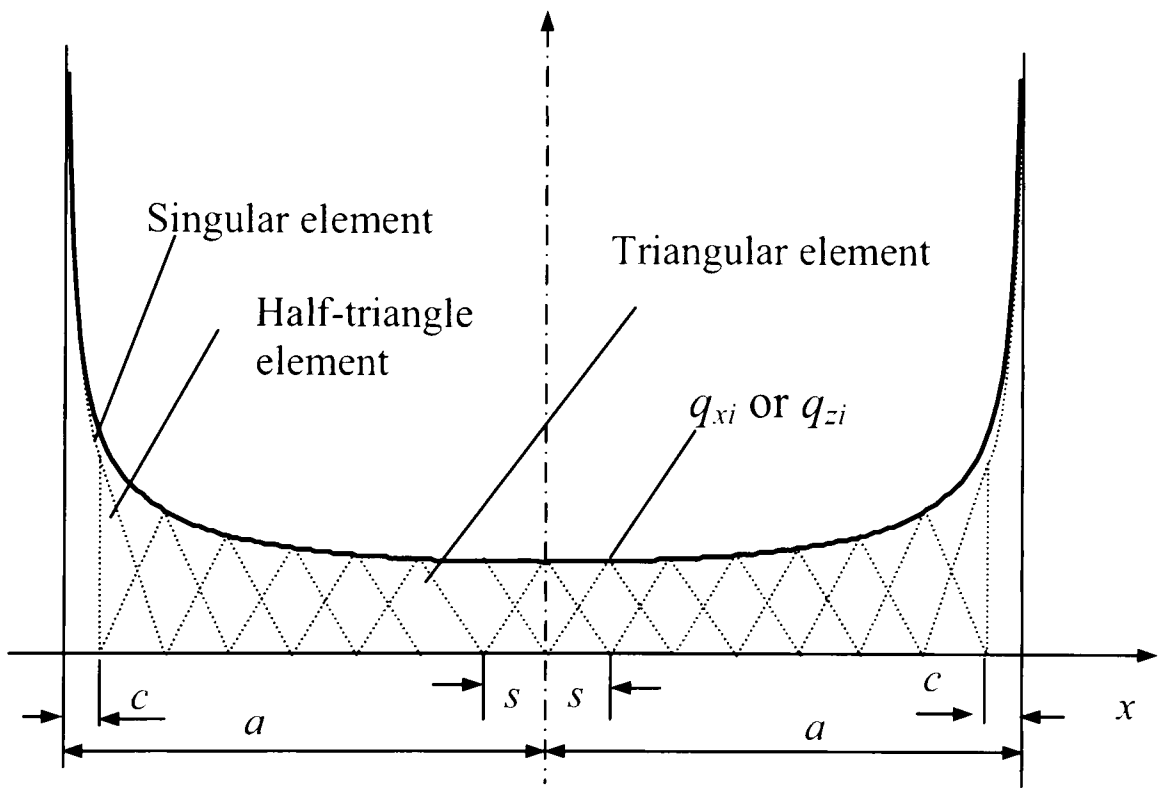

Figure 7-2: Piecewise linear representation of the shear traction distribution of a complete contact

In addition, in order to make a smooth transition to the piecewise linear representation, a special half-triangular element is needed, in general of width s, and the corresponding surface tangential displacements are given by

$$\frac{\partial u_x}{\partial x}|_q^{ht} = -\frac{q_x}{s} \frac{(1-\nu^2)}{\pi E} \left[2s + (x-s) \ln(\frac{x-s}{x})^2 \right] \tag{7-26}$$

$$\frac{\partial u_z}{\partial x}|_q^{ht} = -\frac{q_z}{s} \frac{(1+\nu)}{\pi E} \left[2s + (x-s) \ln(\frac{x-s}{x})^2 \right], \tag{7-27}$$

where the subscript *ht* refers to the contribution of half-triangular element to the surface displacements. The magnitude of the special singular elements may be chosen so as precisely to match the traction state when $r \to 0$. The middle part of the contact patch $[-a+c\ \ a-c]$ is discretised into *2n* elements and, using the results just cited, together with a shift of origin, we may develop a piecewise linear representation of the integral equation (7-17), connecting the distribution of shearing traction with the slip displacements. Equation for the displacement gradients, expressed in terms of the magnitude of the elements, are lengthy, and are explicitly given in Appendix D, in which the stiffness E^*, E^{**} are introduced. The contact pressure distribution is given by (7-14), and the shear tractions may be written as

$$q_{xj} = fp_j \cos\phi = fp_0 \sin(\lambda\pi)(1-\frac{j}{n})^{\lambda-1}(1+\frac{j}{n})^{\lambda} \cos\phi \tag{7-28}$$

$$q_{zj} = fp_j \sin\phi = fp_0 \sin(\lambda\pi)(1-\frac{j}{n})^{\lambda-1}(1+\frac{j}{n})^{\lambda} \sin\phi, \tag{7-29}$$

so that, finally, orthogonality requires

$$\frac{V_x}{V_z} = \frac{\cos\phi(1-\frac{\partial u_x}{\partial x}(i))}{\sin\phi(1-\frac{\partial u_z}{\partial x}(i))}. \tag{7-30}$$

This equation must be solved by sequential iteration. Before starting the iteration, it is helpful to note the characteristic dimensionless quantities which determine the magnitude of the solution. The displacements are proportional to the loads but inversely proportional to the stiffnesses of the materials, E^*, E^{**}, $E^{**}/(1-2\nu)$. It is not easy to see how we should choose values for p_0/E^*, p_0/E^{**} directly, and so we introduce the yield strength of the material, σ_Y. We can then choose a representative normal load, and here we have set $p_0/\sigma_Y = 1$ in the numerical calculations, as this is typical of a moderately heavily loaded contact. The remaining dimensionless material parameters, σ_Y/E^*, σ_Y/E^{**} are given for typical materials in Table 7-1. To solve the set of equations we start by assuming that the direction of the

shearing traction is everywhere defined by the rigid body motion, and determine the local slip direction, $\varphi(x)$, from equation (7-7). We then use this to re-apportion the shearing traction at each point, and repeat the process until convergence occurs.

7.3 Finite Rounded and Semi-Infinite Rounded Punches

At this point we introduce two further geometries of punch which we have used in the study. The principal reason for doing so is that we know from (Adams *et al.*, 2005) that there is a paradox at the edge of complete sliding contact problems with friction, so that formally the orthogonality requirement can certainly never be imposed right up to the contact edge. In order to circumvent this, two further problems are introduced. The first is the slightly rounded punch displayed in Figure 7-3(a), which can actually be adapted to have a geometry anywhere between the sharp edged punch and a Hertzian contact (Ciavarella *et al.*, 1998), and hence provides a connexion with our earlier study. The second, shown in Figure 7-3(b), is a semi-infinite version of the same punch. The principal reason for studying this is that the solution found may be collocated into that for any notionally sharp edged contact of arbitrary planform, whilst it may also be conveniently compared with the slightly rounded finite punch just described.

The contact pressure distribution for the slightly rounded punch sliding in the presence of friction is known when the contacting component is incompressible, and is given by:

$$p(x)=\left(\frac{E^*}{2\pi R}\right)\left\{\left[2\sin^{-1}\left(\frac{a}{b}\right)-\pi\right]\sqrt{1-\left(\frac{x}{b}\right)^2}-\ln\left(\left|\frac{\frac{x}{b}\sqrt{1-\left(\frac{a}{b}\right)^2}+\frac{a}{b}\sqrt{1-\left(\frac{x}{b}\right)^2}}{\frac{x}{b}\sqrt{1-\left(\frac{a}{b}\right)^2}-\frac{a}{b}\sqrt{1-\left(\frac{x}{b}\right)^2}}\right|^{\frac{x}{b}}\left|\frac{\sqrt{1-\left(\frac{x}{b}\right)^2}-\sqrt{1-\left(\frac{a}{b}\right)^2}}{\sqrt{1-\left(\frac{x}{b}\right)^2}-\sqrt{1-\left(\frac{a}{b}\right)^2}}\right|^{\frac{a}{b}}\right)\right\} \tag{7-31}$$

When this punch is slid skew-wise over an incompressible half-plane the shearing traction distribution may be satisfactorily described by the family of overlapping triangles of traction described above, but without the need for special elements at the edges.

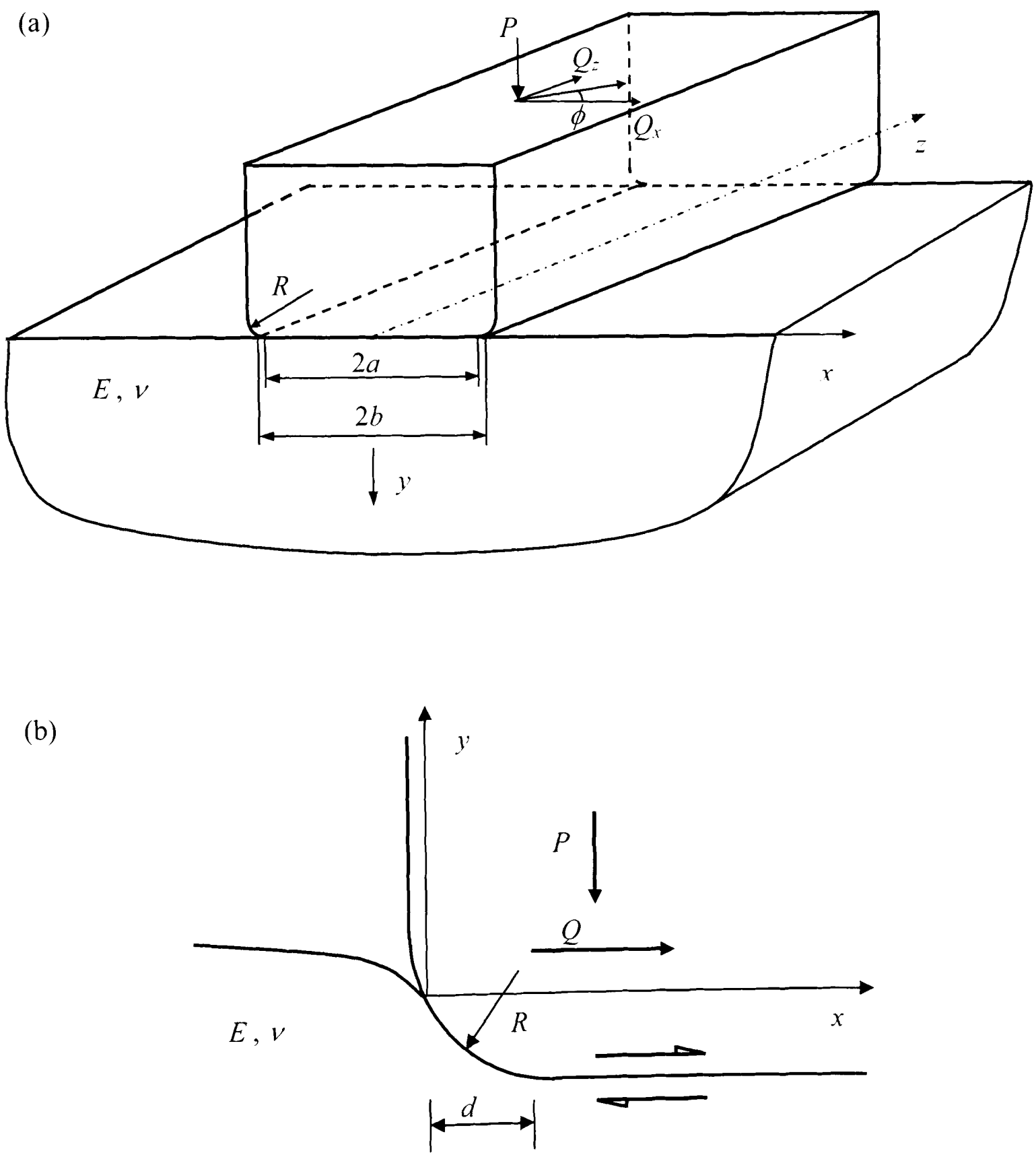

Figure 7-3: Slightly rounded rigid punches (a) three-dimensional schematic of the finite punch, and (b) two-dimensional view of the semi-infinite flat and rounded punch.

The last geometry of punch to be studied is the semi-infinite form of the flat and rounded punch, Figure 7-3(b). When this is in contact with an incompressible half-plane the contact pressure distribution (Sackfield *et al.*, 2003) is

$$\begin{aligned} p(x) &= \frac{3K^*}{4\sqrt{d^3}}\left[2\sqrt{xd} + (x-d)\ln\left|\frac{\sqrt{d}-\sqrt{x}}{\sqrt{d}+\sqrt{x}}\right|\right], \quad x>0 \\ &= \frac{3K^*\sqrt{x}}{d}, \qquad 0<x<d \\ &= \frac{K^*}{\sqrt{x}}, \qquad d<<x. \end{aligned} \tag{7-32}$$

where, x is now measured from the edge of the contact (Figure 7-3(b), K^* is the generalised stress intensity factor, d is the length scale ($=b-a$.), which is also the part of the contact length present in the radius of the punch. It is noteworthy that the form of the contact pressure remote from the punch edge implies square root 'singular' decay, so that it is clear that, when the punch was made infinitely long, the solution evolved became suitable only for the case when the punch is rigid and the contacting half-plane incompressible, and this limitation should be borne in mind. Returning to the details of the solution, the length d is given by the following relationship, which serves as a contact law

$$d = \sqrt[3]{\frac{9\pi^2 R^2 K^{*2}}{4E^{*2}}}, \tag{7-33}$$

where R is the radius of the punch.

The shear traction distribution may again be represented by a family of overlapping triangles, as described earlier, and no special elements are required at the contact edge. However, the punch is semi-infinite in extent, and so a special element describing the square root singular form of traction decay, remote from the contact edge, is needed. To do this, we take a singular element of width c, and placed at ($x=a$). The surface tangential displacements are given by

$$\frac{\partial u_x}{\partial x}\Big|_q^s = -q_x \frac{(1-\nu^2)}{\pi E}\frac{\sqrt{a}}{\sqrt{x}}\left[\ln\left(\frac{\sqrt{a+c}+\sqrt{x}}{\sqrt{a+c}-\sqrt{x}}\right)^2 - \ln\left(\frac{\sqrt{a}+\sqrt{x}}{\sqrt{a}-\sqrt{x}}\right)^2\right] \tag{7-34}$$

$$\frac{\partial u_z}{\partial x}\Big|_q^s = -q_z \frac{(1+\nu)}{\pi E}\frac{\sqrt{a}}{\sqrt{x}}\left[\ln\left(\frac{\sqrt{a+c}+\sqrt{x}}{\sqrt{a+c}-\sqrt{x}}\right)^2 - \ln\left(\frac{\sqrt{a}+\sqrt{x}}{\sqrt{a}-\sqrt{x}}\right)^2\right]. \tag{7-35}$$

When c tends to infinity, equations (7-34), (7-35) become

$$\frac{\partial u_x}{\partial x}\Big|_q^s = q_x \frac{(1-\nu^2)}{\pi E}\frac{\sqrt{a}}{\sqrt{x}}\ln\left(\frac{\sqrt{a}+\sqrt{x}}{\sqrt{a}-\sqrt{x}}\right)^2 \tag{7-36}$$

$$\frac{\partial u_z}{\partial x}\Big|_q^s = q_z \frac{(1+\nu)}{\pi E}\frac{\sqrt{a}}{\sqrt{x}}\ln\left(\frac{\sqrt{a}+\sqrt{x}}{\sqrt{a}-\sqrt{x}}\right)^2, \tag{7-37}$$

and this provides the correct properties.

The next step is to express the surface displacement gradients in terms of the magnitude of the elements (hence obtaining a discretised form equivalent to the one used for the complete contact formulation above), and the shear tractions as a function of the pressure distribution and the sliding direction angle, ϕ. The problem is then solved by sequential iteration and the local slip direction, $\varphi(x)$, is calculated everywhere within the contact, as before.

7.4 Results

First, we look at the case of a perfectly sharp (complete) punch sliding across a compressible half plane. Figure 7-4 depicts the variation of local slip direction, $\varphi(x)$, across the face of the punch, moving across an aluminium half-plane (see Table 7-1), $p_0/\sigma_Y = 1$, $f = 0.5$ and sliding at various angles ϕ. The slip displacement variation across the section shows no convection effect at $\phi = 0$; $\phi = \pi/2$, and a modest effect at intermediate values of

ϕ between these two limits, apart from a very tiny region attached to each edge. This edge phenomenon is displayed in more detail for the example case of a punch sliding at about $\phi = 40°$, in Figure 7-5. Here the presence of the singularity at the edge of the contact greatly influences the mismatch between the sliding and the local slip directions ($\phi - \varphi(x)$), resulting in a maximum discrepancy of about 6° right at the leading edge of the sliding punch.

The very abrupt change in behaviour near to the contact edge looks suspicious, as if it were caused by a numerical problem, and called for further investigation. This was done by appealing to the solution for the finite flat and rounded punch, and determining the trend. Note, though, that the solution being employed does not properly allow for coupling effects and, as stated, is strictly applicable only to the case of a rigid punch sliding on an incompressible material. Figure 7-6(a) shows the result of the investigation, for the same material, same normalised load, and same sliding angle, but with a range of ratios of flat to rounded portion of the contact face. The figure displays slip angle variations for the Hertzian contact, and for *a/b* values from 0.1 to 0.95. The trend is consistent, and shows a developing cusp which moves ever nearer to the leading edge of the contact. It disappears only when the punch becomes perfectly sharp, and seems consistent with the findings for the perfectly sharp case, bearing in mind that the latter relate to the problem of a punch sliding on compressible material.

We now turn to the solution of the plane semi-infinite flat and rounded punch problem, again sliding on incompressible material. Here the contact law (7-33) links the generalised stress intensity factor, K^*, the radiused portion of the punch in contact, d, and the elastic properties of the material under investigation. Therefore, the appropriate dimensionless ratio for $\frac{K^*}{E^*\sqrt{d}}$, $\frac{K^*}{E^{**}\sqrt{d}}$ should be chosen to describe the problem instead of the normalised value

of the average pressure used for the finite complete contact discussed above[2]. For the case of $a/b = 0.95$, a value of $\frac{K^*}{E^*\sqrt{d}} = 0.00063$ is typical. Figure 7-6(b) shows a 'zoomed in' part of Figure 7-6(a), for the particular case of $a/b = 0.95$, and includes also the solution for the semi-infinite punch. The two correlate well in the region of interest, and bolster our confidence in the nature of the solution for a slightly rounded contact for the rigid/incompressible material combination case.

One other feature of the nature of the solution for a truly sharp punch on a compressible half-plane, Figures 7-4/7-5, calls for comment. This is that, in contrast to the Hertzian convection investigation (Qiu *et al.*, 2007), the discrepancy between $\phi(x)$ and θ is *not* always of the same sign. As with the incomplete contacts, there is a small difference between rigid body sliding direction and the orientation of the applied force, Figure 7-7(a), but, in addition here, there is small difference between the magnitude of the pointwise defined coefficient of friction and a macroscopically defined value, Figure 7-7(b).

Table 7-1

Material	E (GPa)	ν	E^* (GPa)	E^{**} (G Pa)	σ_Y (MPa)	σ_Y / E^*	σ_Y / E^{**}
Mild steel	210	0.3	231	161.7	240	0.001	0.0014
Aluminium	72	0.33	80.8	54.1	395	0.005	0.0075
Titanium-6Al-4V	115	0.3	126	88.2	900	0.007	0.010
Rubber	0.02	0.45	0.025	0.01375	5	0.200	0.364

[2] It should be noted here that a calibration of the value of K^* needs to be performed in order for the asymptotic solution presented here to be applied to *any* finite problem in the presence of local rounding.

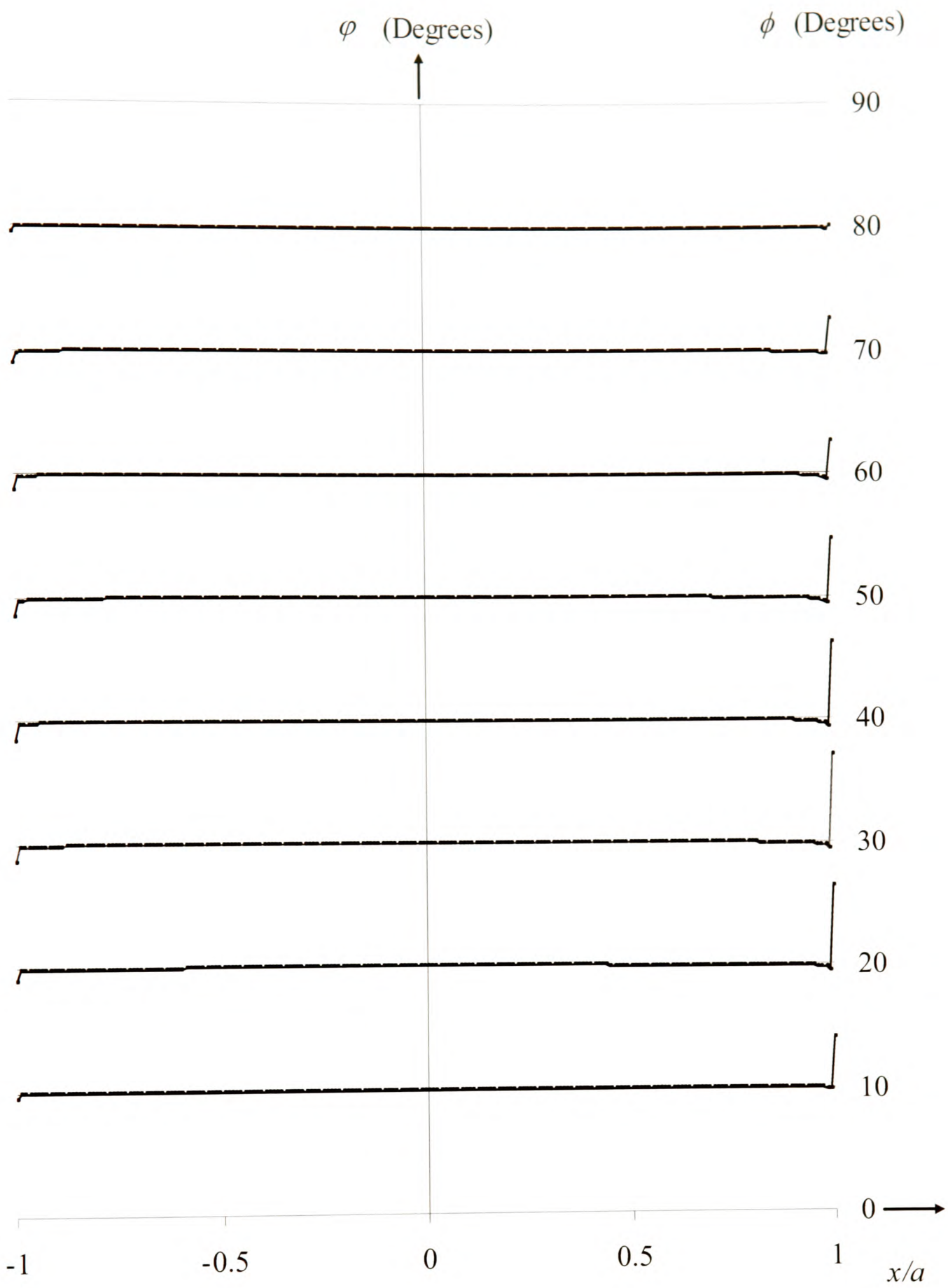

Figure 7-4: Variation of local slip direction, $\varphi(x)$, across the complete contact for aluminium, $p_0/\sigma_y = 1$, $f = 0.5$ and sliding at various angle ϕ.

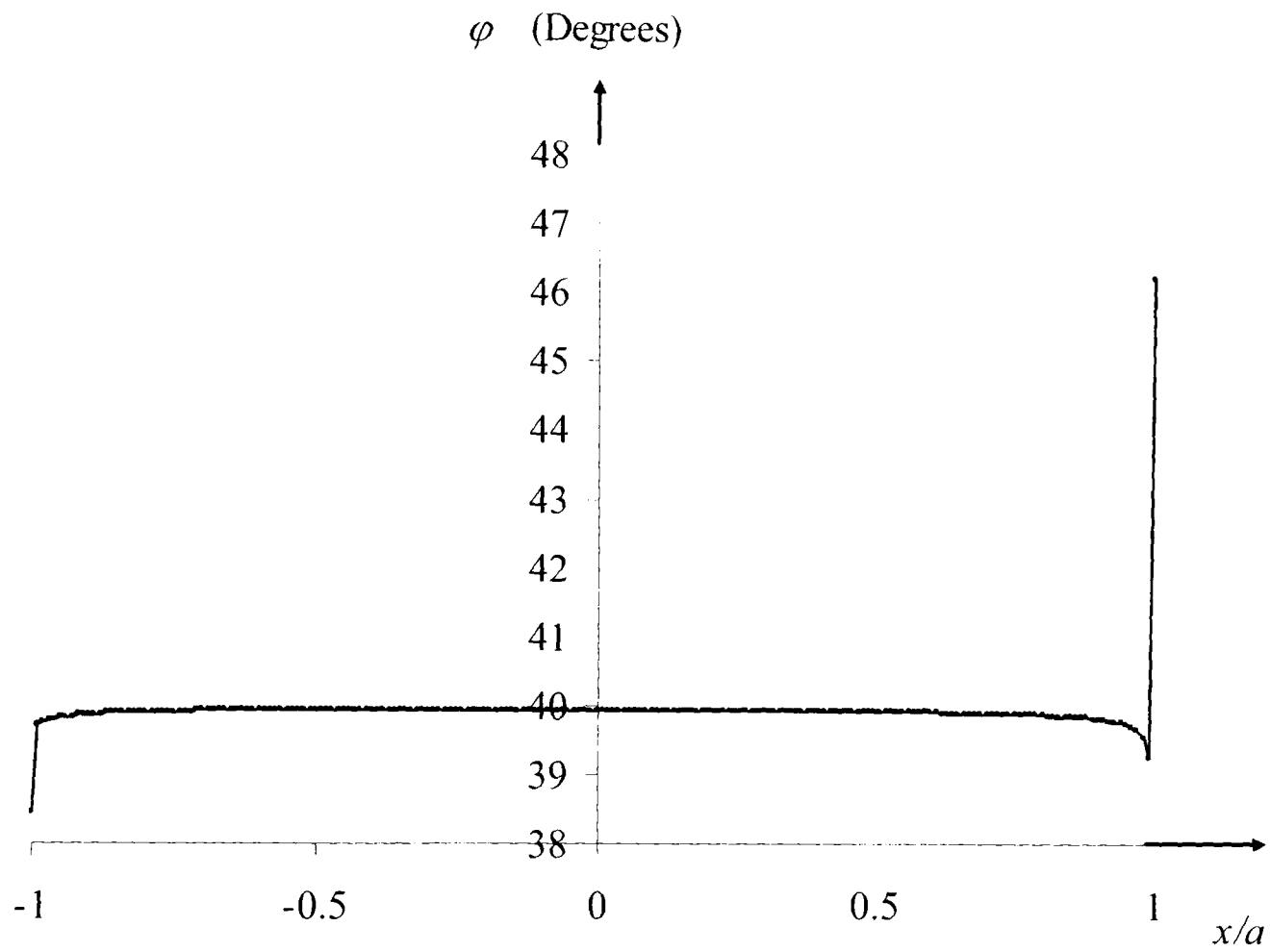

Figure 7-5: The variation of slip angle $\varphi(x)$ with position for aluminium, $p_0/\sigma_y = 1$, $f = 0.5$, and $\phi = 40$ degrees for the complete contact.

(a)

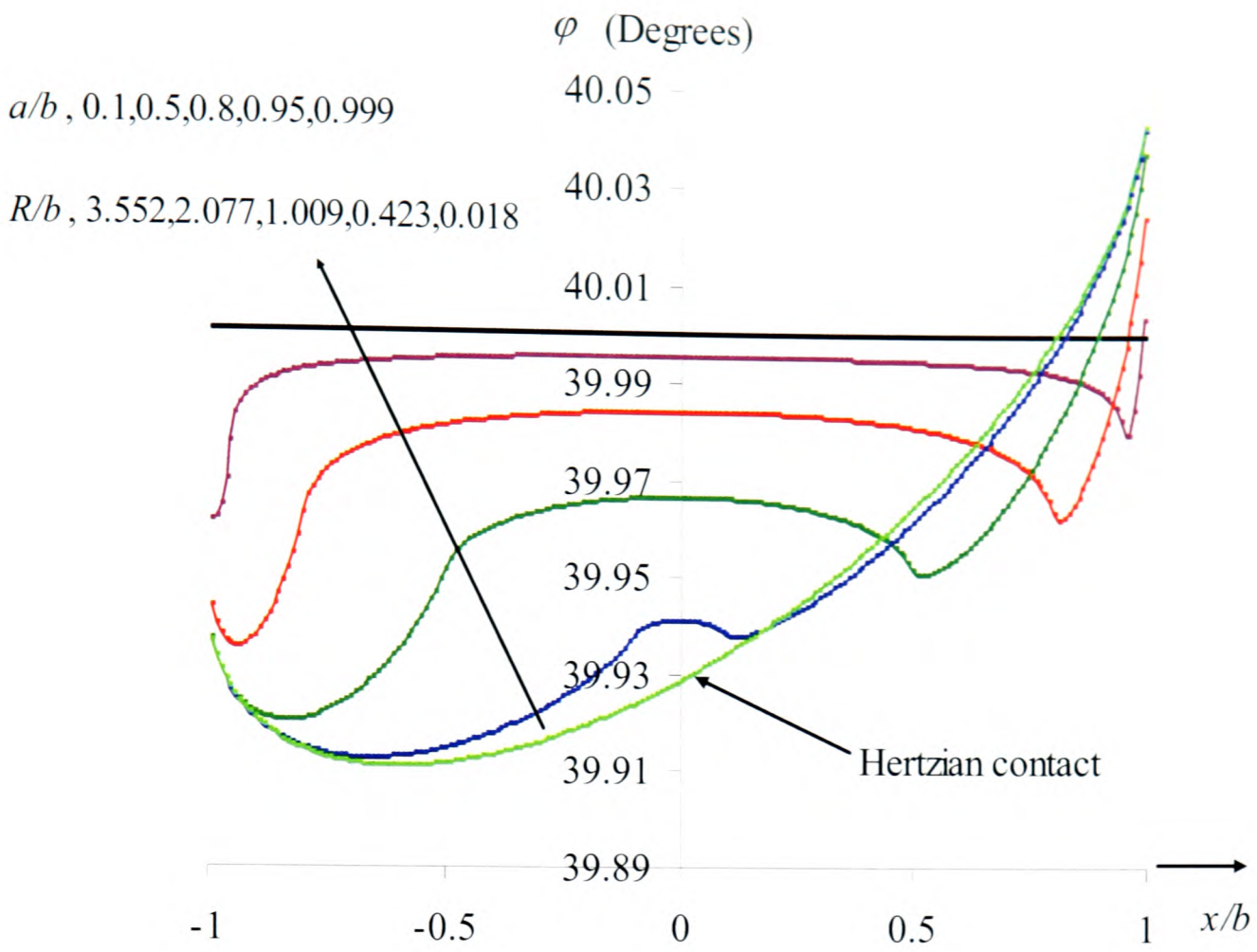

(b)

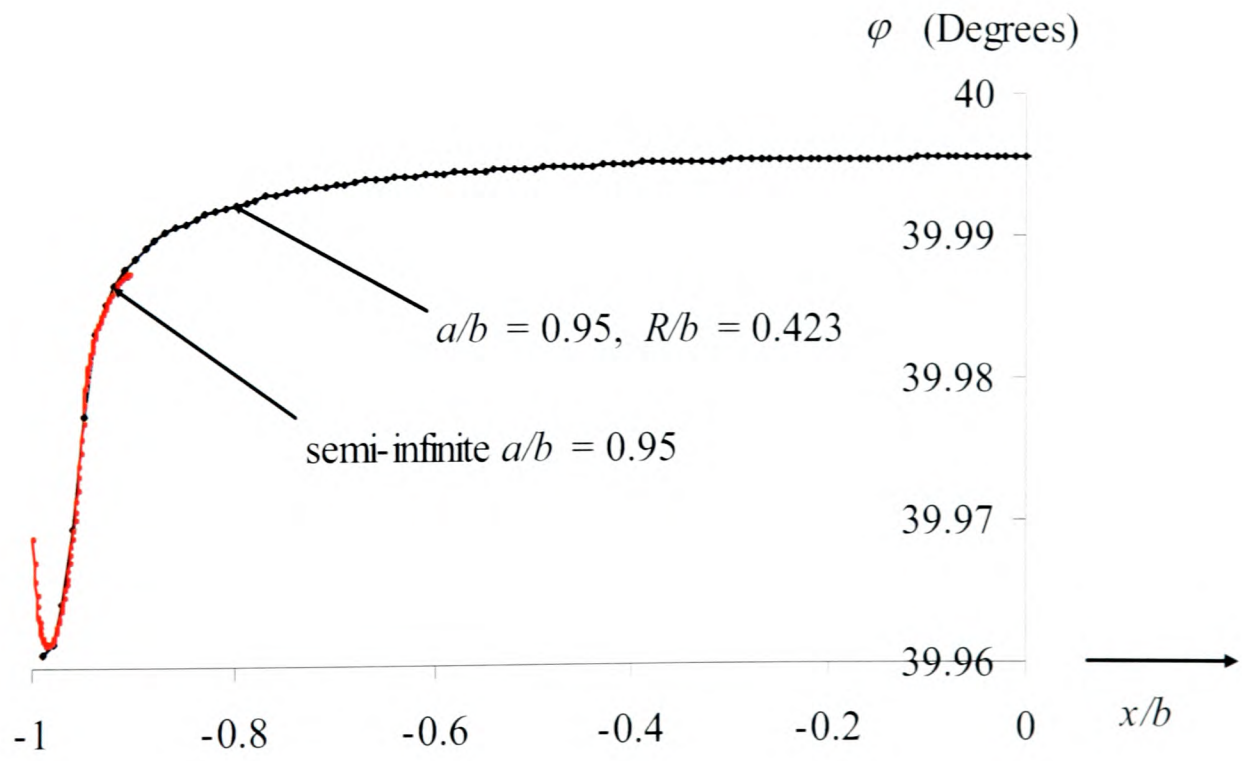

Figure 7-6: Rigid punch sliding on an incompressible half plane. The contact pressure has been chosen to be able to compare these results with those for aluminium in Figure 7-4, *i.e.* $\frac{\sigma_Y}{E^*} = 0.005$, $p_0/\sigma_y = 1$, $f = 0.5$ and sliding angle $\phi = 40$ degrees.

(a)

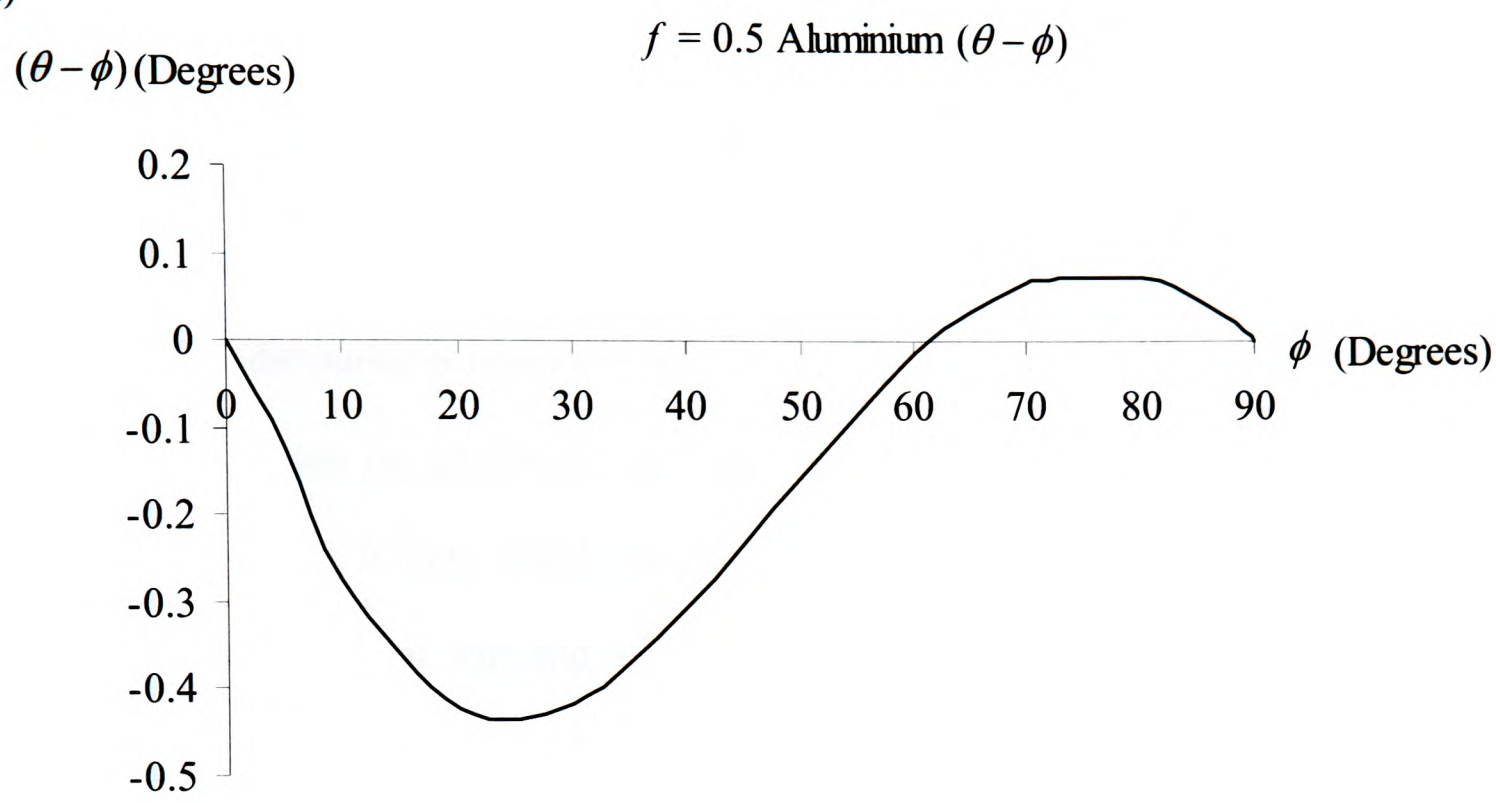

(b)

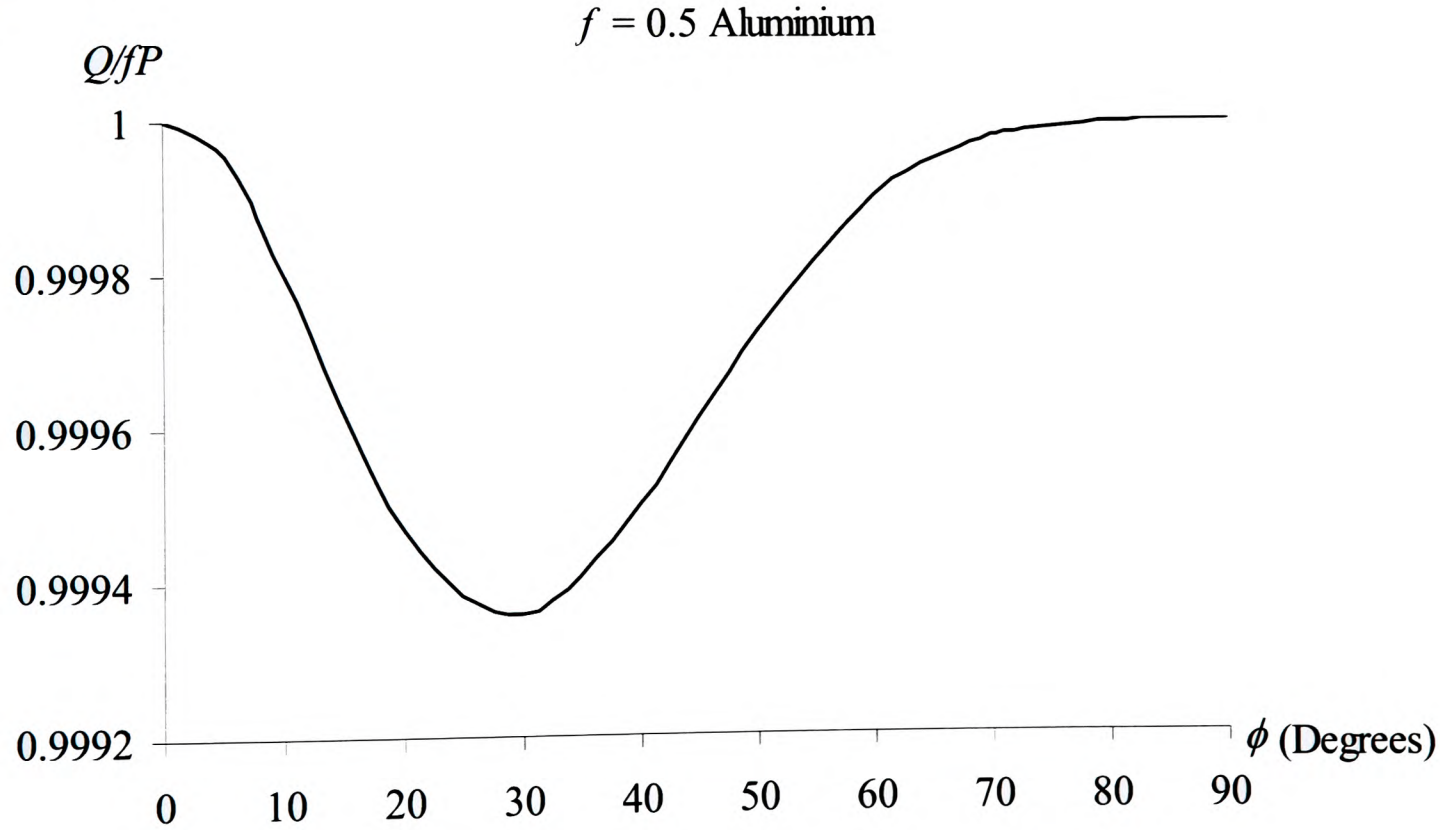

Figure 7-7: Example results for aluminium. They show: (a) the mismatch between the sliding angle, ϕ, and the angle defining the direction of application of the tangential load, θ, as a function of the sliding angle and (b) Q/fP versus the sliding angle, ϕ ($p_0/\sigma_1 = 1$, $f = 0.5$).

7.5 Conclusion

The convection effect for frictional sliding complete and almost complete contacts, for the case when the punch is rigid, has been explored in this article. First, the skew sliding of a square-ended punch on an elastic half-space has been studied. For practical engineering materials the effect is very small, but the analysis is important because the magnitude of mismatch between local slip and sliding direction is revealed. It is usually assumed that macroscopic frictional orthogonality and a pointwise application of the same principle are completely consistent. It is shown, here, that this is not precisely correct, and that this is manifested in several ways. If the contacting half-plane is incompressible, there is no convection effect whatsoever, and the classical assumptions apply without modification.

Secondly, it is shown that, even if the half-plane is incompressible, the presence of any degree of local edge rounding does introduce convection effects, and that these become progressively greater as the edge radii become more important in describing a bigger fraction of the contact profile, Figure 7-6(a). This effect is also accurately represented by a semi-infinite punch when the edge radius is small.

Chapter 8

The Screw Dislocation in a Three-Quarter Plane

8.1 Introduction

This chapter presents the solution for the state of stress arising in a three-quarter plane due to a screw dislocation present on the projection line from one of the free surfaces, Figure 8-1. The corresponding solution for a similarly positioned edge dislocation (Churchman, Korsunsky and Hills, 2006) is used as a "model". The motivation for studying this particular pair of problems is that frequently slip or separation occur adjacent to the edge of a contact; this could be because two components have been bonded together, and the interface forms a line of weakness, along which a crack may start. Or, it could be because the upper component and lower 'half-plane' are merely pressed together, and slip or separation may initiate at a similar position (Churchman and Hills, 2006a). In either event, the solution required to form an integral equation to describe the slip or separation, and, if appropriate, to find the corresponding stress intensity factor (Churchman and Hills, 2006b), is a knowledge of state of stress induced by a dislocation. In particular, the tractions induced along a projection line from the free surface are required. The edge dislocation is appropriate to represent separation if the Burgers vector is perpendicular to the line of the interface, or in-plane slip if it lies parallel with it. Thus, the edge dislocation restricts the type of analysis which may be

performed to an 'in-plane' one. The addition of the screw dislocation to the repertoire means that out-of-plane slip (with corresponding out-of-plane traction) may be catered for, and hence a general state of edge slip and separation may be handled. Further, as we are interested only in a solution very local to the edge of the contact, the general solution found may be applied to any geometry of complete contact. For example, for the sliding cylinder problem shown in Figure 8-1 (b), on the plane of symmetry an edge dislocation may be used to represent separation (if the Burgers vector is normal to the interface) and slip (if it is parallel to the interface). On a transverse plane the edge dislocation may still be used to present separation, but now a screw dislocation is needed to model slip. This pair of solutions is ideal for tracking out local slipping edge behaviour, and ensuring that the frictional orthogonality condition is obeyed.

The approach to be pursued mirrors that employed in the edge dislocation solution (Churchman, Korsunsky and Hills, 2006), where dislocations are distributed along the semi-infinite trace lines ($x > 0,\ y \geq 0,\ y = 0,\ x \leq 0$) which become the free edges of the three-quarter plane Figure 8-1 (a). Here the dislocations will be distributed over semi-infinite intervals and a simple transformation will be applied to preserve the fidelity of the Gaussian quadrature. Also, because the solution is conveniently carried out using a Cartesian axis set, Figure 8-1, no transformation or rotation of axes will be required.

8.2 Solution

The starting point for the solution is the state of stress induced in an infinite plane, at a general point (x, y), by a screw dislocation, having Burgers vector b_z (Weertman, 1996), located at (x_d, y_d). This is

$$\overline{\sigma}_{iz}(x,y,x_d,y_d) = \frac{\mu}{2\pi} b_z(x_d,y_d) G_{iz}(x,y,x_d,y_d), \qquad i = x,y, \tag{8-1}$$

where μ is the modulus of rigidity, and

$$G_{xz}(x,y,x_d,y_d) = -\frac{(y-y_d)}{(x-x_d)^2+(y-y_d)^2} \tag{8-2a}$$

$$G_{yz}(x,y,x_d,y_d) = \frac{(x-x_d)}{(x-x_d)^2+(y-y_d)^2}. \tag{8-2b}$$

We choose to deploy distributions of dislocations along the two half-lines forming the free surfaces to render them traction-free, i.e. to achieve the conditions

$$\sigma_{xz} = 0 \qquad 0 < y < \infty, x = 0 \tag{8-3a}$$

$$\sigma_{yz} = 0 \qquad -\infty < x < 0, y = 0. \tag{8-3b}$$

First, in order to determine, and ultimately cancel, the traction $\sigma_{xz}(0,y)$ (equation 8-3a), we need to consider the influence of an individual object screw dislocation, the one whose effect we ultimately require, located at (ξ , 0), and which is given by

$$\overline{\sigma}_{xz}(0,y) = \frac{\mu b_z(\xi,0)}{2\pi} G_{xz}(0,y,\xi,0). \tag{8-4}$$

Also, an array of screw dislocations, present along the half-line $0 < y < \infty$, $x = 0$, induces a shear stress $\widetilde{\sigma}^1_{xz}(0,y)$ given by

$$\widetilde{\sigma}^1_{xz}(0,y) = \int_0^\infty \frac{\mu B_z(y_d)}{2\pi} G_{xz}(0,y,0,y_d)\,dy_d, \tag{8-5}$$

where

$$B_z(y_d) = \frac{db_z}{dy_d} \tag{8-6}$$

is the dislocation density.

Similarly, an array of screw dislocations, present along the half-line $-\infty < x < 0$, $y = 0$, induces a shear stress $\widetilde{\sigma}^2_{xz}(0,y)$ given by

$$\tilde{\sigma}^{2}_{xz}(0,y) = \int_{0}^{\infty} \frac{\mu B_z(x_d)}{2\pi} G_{12}(0,y,x_d,0)dx_d. \tag{8-7}$$

where

$$B_z(x_d) = \frac{db_z}{dx_d}. \tag{8-8}$$

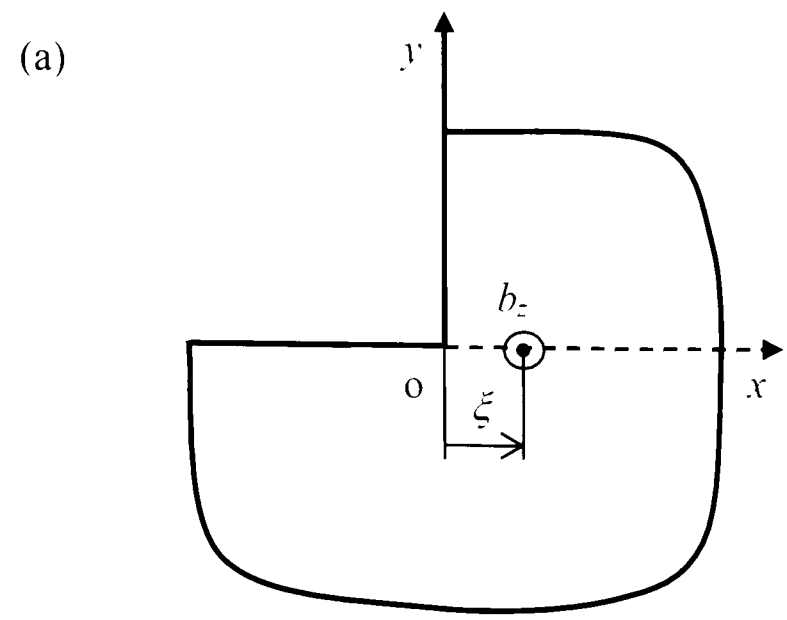

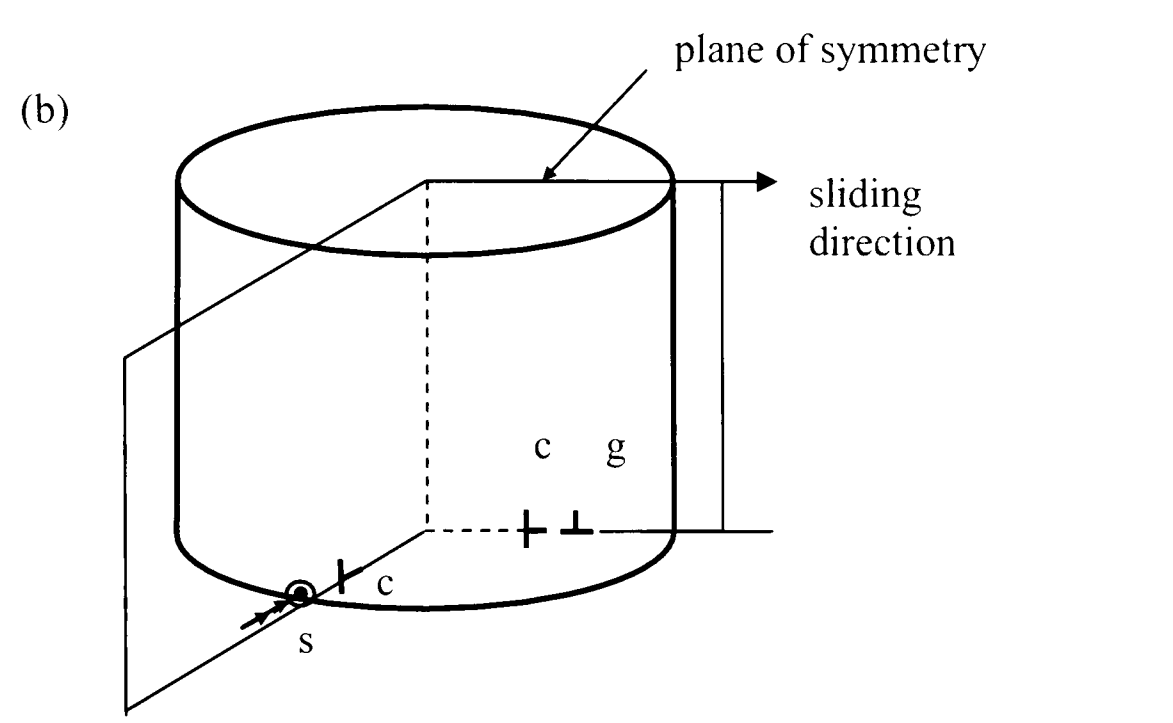

c – edge climb dislocation (separation)

g – edge glide dislocation (local in-plane slip)

s – screw dislocation (local out-plane slip)

Figure 8-1: (a) A screw dislocation b_z located at (ξ, 0) in a three-quarter plane. (b) A sliding cylinder

Secondly, in order to determine, and ultimately cancel, the traction $\sigma_{yz}(x,0)$ (equation 8-3b), the effects of the object dislocation at $(\xi, 0)$ and the screw dislocation distributions along $-\infty < x < 0, y = 0$ and $0 < y < \infty$, $x = 0$ must be considered. The contribution from the object screw dislocation is

$$\bar{\sigma}_{yz}(x,0) = \frac{\mu b_z(\xi,0)}{2\pi} G_{yz}(x,0,\xi,0). \tag{8-9}$$

whilst that due to the screw dislocation distribution along $0 < y < \infty$, $x = 0$ is

$$\tilde{\sigma}^1_{yz}(x,0) = \int_0^{\infty} \frac{\mu B_z(y_d)}{2\pi} G_{yz}(x,0,0,y_d)dy_d, \tag{8-10}$$

and lastly, that due to the screw dislocation distribution along $-\infty < x < 0, y = 0$ is

$$\tilde{\sigma}^2_{yz}(x,0) = \int_{-\infty}^{0} \frac{\mu B_z(x_d)}{2\pi} G_{xz}(x,0,x_d,0)dx_d. \tag{8-11}$$

If the boundary conditions, equations (8-3), are imposed we arrive at the following two simultaneous Cauchy singular equations

$$\begin{aligned} &b_z G_{xz}(0,y,\xi,0) + \int_0^{\infty} B_z(y_d) G_{xz}(0,y,0,y_d)dy_d \\ &+ \int_{-\infty}^{0} B_z(x_d) G_{xz}(0,y,x_d,0)dx_d = 0, \qquad 0 < y < \infty, x = 0 \end{aligned} \tag{8-12a}$$

$$\begin{aligned} &b_z G_{yz}(x,0,\xi,0) + \int_0^{\infty} B_z(y_d) G_{yz}(x,0,0,y_d)dy_d \\ &+ \int_{-\infty}^{0} B_z(x_d) G_{yz}(x,0,x_d,0)dx_d = 0, \qquad -\infty < x < 0, y = 0. \end{aligned} \tag{8-12b}$$

In order to use Gaussian quadrature we must transform the semi-infinite range $[0,\infty)$ in equations (8-12) to [-1, 1]. We do this by dint of the following simple transformation equations:

$$x_d = \frac{s_x - 1}{1 + s_x}, \qquad y_d = \frac{1 - s_y}{s_y + 1}, \qquad x = \frac{t_x - 1}{1 + t_x}, \qquad y = \frac{1 - t_y}{t_y + 1} \tag{8-13}$$

and hence

$$\frac{dx_d}{ds_x} = \frac{1 - s_x}{(1 + s_x)^2} + \frac{1}{1 + s_x} \tag{8-14}$$

$$\frac{dy_d}{ds_y} = \frac{s_y - 1}{(s_y + 1)^2} - \frac{1}{s_y + 1}. \tag{8-15}$$

The integral equations then become

$$b_z G_{xz}(0, \frac{1 - t_y}{t_y + 1}, \xi, 0) - \int_1^1 B_z(s_y) G_{xz}(0, \frac{1 - t_y}{t_y + 1}, 0, \frac{1 - s_y}{s_y + 1}) \left[\frac{s_y - 1}{(s_y + 1)^2} - \frac{1}{s_y + 1} \right] ds_y$$
$$+ \int_{-1}^1 B_z(s_x) G_{xz}(0, \frac{1 - t_y}{t_y + 1}, \frac{s_x - 1}{1 + s_x}, 0) \left[\frac{1 - s_x}{(1 + s_x)^2} + \frac{1}{1 + s_x} \right] ds_x = 0, \quad -1 < t_y < 1 \tag{8-16a}$$

$$b_z G_{yz}(\frac{t_x - 1}{1 + t_x} 0, , \xi, 0) - \int_{-1}^1 B_z(s_y) G_{xz}(\frac{t_x - 1}{1 + t_x}, 0, 0, \frac{1 - s_y}{s_y + 1}) \left[\frac{s_y - 1}{(s_y + 1)^2} - \frac{1}{s_y + 1} \right] ds_y$$
$$+ \int_{-1}^1 B_z(s_x) G_{yz}(\frac{t_x - 1}{1 + t_x}, 0, \frac{s_x - 1}{1 + s_x}, 0) \left[\frac{1 - s_x}{(1 + s_x)^2} + \frac{1}{1 + s_x} \right] ds_x = 0, \quad -1 < t_x < 1. \tag{8-16b}$$

The next step is to establish the characteristic form of the solution. We expect that, as the observation point approaches the origin ($x/\xi << 1$) the state of stress will be singular in character, with the order of the singularity being given by a characteristic equation $\lambda = \pi / \phi$ (Hills *et al.*, 2004), and $\sigma_{ij} \sim x^{\lambda - 1}$, where ϕ is the notch internal angle. For a three quarter plane $\phi = 3\pi / 2$, so that $\lambda = 2/3$, whilst experience with the edge dislocation solution showed that $\sigma_{ij} \sim x^{-1}$ when $x/\xi >> 1$. The standard Gaussian numerical quadratures do not permit the near-field to be represented exactly, but approximately the correct behaviour can be achieved by choosing the following fundamental function:

$$w(s_j) = \sqrt{\frac{1 + s_j}{1 - s_j}} \qquad for\ j = x, y. \tag{8-17}$$

This form of solution was chosen to allow the dislocation density distribution to become singular at the apex ($s = 1$) and bounded in the far field ($s = -1$). It has been found from experience that by allowing the dislocation to possess a stronger singularity than required at the apex, the multiplier ϕ_z may be adjusted to weaken the singularity to the correct value. (A different quadrature with the correct end-point behaviour may be preferable but is not

necessary in these circumstances). The dislocation density may, therefore, be written as the product of this fundamental function and some unknown finite distribution ϕ_z.

$$B_z(s_j) = w(s_j)\phi_z(s_j), \qquad j = x, y. \tag{8-18}$$

The positions of the integration and collocation points are chosen as (Hills *et al.*, 1996)

$$s_X^I = s_Y^I = \cos\left(\pi \frac{2I-1}{2n+1}\right) \qquad for\ I = 1, ..., n \tag{8-19a}$$

$$t_X^K = t_Y^K = \cos\left(\pi \frac{2K}{2n+1}\right) \qquad for\ K = 1, ..., n \tag{8-19b}$$

with a weight function

$$W(s_J^I) = \frac{2\pi(1+s_J^I)}{2n+1} \qquad for\ J = X, Y\ and\ I = 1, ..., n.$$

The discretised integral equations then become

$$\begin{aligned} &b_z G_{xz}(0, \frac{1-t_Y^K}{t_Y^K+1}, \xi, 0) - \sum_{I=1}^{n} W(s_Y^I)\phi_z(s_Y^I) G_{xz}(0, \frac{1-t_Y^K}{t_Y^K+1}, 0, \frac{1-s_Y^I}{s_Y^I+1})\left[\frac{s_Y^I-1}{(s_Y^I+1)^2} - \frac{1}{s_Y^I+1}\right] \\ &+ \sum_{I=1}^{n} W(s_X^I)\phi_z(s_X^I) G_{xz}(0, \frac{1-t_Y^K}{t_Y^K+1}, \frac{s_X^I-1}{1+s_X^I}, 0)\left[\frac{1-s_X^I}{(1+s_X^I)^2} + \frac{1}{1+s_X^I}\right] = 0 \end{aligned} \tag{8-20a}$$

$$\begin{aligned} &b_z G_{yz}(\frac{t_X^K-1}{1+t_X^K}, 0, \xi, 0) - \sum_{I=1}^{n} W(s_Y^I)\phi_z(s_Y^I) G_{yz}(\frac{t_X^K-1}{1+t_X^K}, 0, 0, \frac{1-s_Y^I}{s_Y^I+1})\left[\frac{s_Y^I-1}{(s_Y^I+1)^2} - \frac{1}{s_Y^I+1}\right] \\ &+ \sum_{I=1}^{n} W(s_X^I)\phi_z(s_X^I) G_{yz}(\frac{t_X^K-1}{1+t_X^K}, 0, \frac{s_X^I-1}{1+s_X^I}, 0)\left[\frac{1-s_X^I}{(1+s_X^I)^2} + \frac{1}{1+s_X^I}\right] = 0. \end{aligned} \tag{8-20b}$$

These represent a system of $2n$ simultaneous equations for $2n$ unknown $\phi_z(s_X^I)$ and $\phi_z(s_Y^I)$. When these values are determined, the stresses $\sigma_{iz}(x, y)$ at an arbitrary point in the three-quarter plane due to the object screw dislocation, b_z, located at $(\xi, 0)$, can be determined.

8.3 Results

Our particular interest is the effect of the free surface boundaries on the state of stress. σ_{yz}, induced by the screw dislocation, along the line $y=0$ for $x>0$. The σ_{yz} stress is given by the superposition of the three stress components $\bar{\sigma}_{yz}+\tilde{\sigma}^{1}_{yz}+\tilde{\sigma}^{2}_{yz}$, with the appropriate dislocation densities found from the above analysis. The stress distribution is plotted in Figure 8-2. It clearly shows the Cauchy singularity due to the dislocation and the perturbation on this due to the 'free surface' dislocation distributions which we determine. The dominant Cauchy term may be separated out by writing

$$\sigma_{yz}(x,0)=\frac{\mu b_z}{2\pi}\left(F_{yz}(x,\xi)+G_{yz}(x,0,\xi,0)\right) \tag{8-21}$$

where

$$G_{yz}(x,0,\xi,0)=\frac{1}{x-\xi}, \qquad y=0,\ x>0 \tag{8-22}$$

is the Cauchy term, and the function $F_{yz}(x,\xi)$, represents the free boundary effect. In order to emphasize the universal nature of the solution, normalised coordinates are used in the subsequent equation by denoting x/ξ by $\hat{x}$. A series representation of the solution, of the following form was employed

$$\begin{aligned} F_{yz}(\hat{x}) &= \frac{1}{\hat{x}^{1-\lambda}+\hat{x}}\sum_{m=0}^{3} C_m\left(\frac{\hat{x}}{1+\hat{x}}\right)^m \\ &= \frac{1}{\hat{x}^{1-\lambda}+\hat{x}}\left[C_0+C_1\left(\frac{\hat{x}}{1+\hat{x}}\right)+C_2\left(\frac{\hat{x}}{1+\hat{x}}\right)^2+C_3\left(\frac{\hat{x}}{1+\hat{x}}\right)^3\right]. \end{aligned} \tag{8-23}$$

The constants C_0, C_1, C_2, C_3 were collocated with the numerically obtained solution, which is plotted in Figure 8-3. As noted earlier, the gradients at the end of the interval ($0\le\hat{x}<\infty$)

have a characteristic value, and these are explicitly given in terms of the coefficients in the series representation in the following way

$$As\ \ \hat{x} \to 0 \qquad F_{yz}(\hat{x}) = \frac{1}{\hat{x}^{1-\lambda}} C_0 \tag{8-24}$$

$$As\ \ \hat{x} \to \infty \qquad F_{yz}(\hat{x}) = \frac{1}{\hat{x}} \sum_{m=0}^{3} C_m . \tag{8-25}$$

The far-field solution has this form because the geometric stress intensity due to the comer will be swamped at large distances by the effect of the dislocation's Cauchy singularity. The collocated solution, finally, is

$$F_{yz}(\hat{x}) = \frac{1}{\hat{x}^{1/3} + \hat{x}} \left[-0.9106 + 0.46\left(\frac{\hat{x}}{1+\hat{x}}\right) - 2.055\left(\frac{\hat{x}}{1+\hat{x}}\right)^2 + 1.545\left(\frac{\hat{x}}{1+\hat{x}}\right)^3 \right], \tag{8-26}$$

and, thus the asymptotes are

$$F_{yz}(\hat{x}) = -0.9106\hat{x}^{1/3} \qquad \hat{x} << 1 \tag{8-27}$$

$$F_{yz}(\hat{x}) = -0.9606\hat{x}^{-1} \qquad \hat{x} >> 1 \tag{8-28}$$

For numerical convergence of the quadrature, it was found that $n = 500$ was necessary.

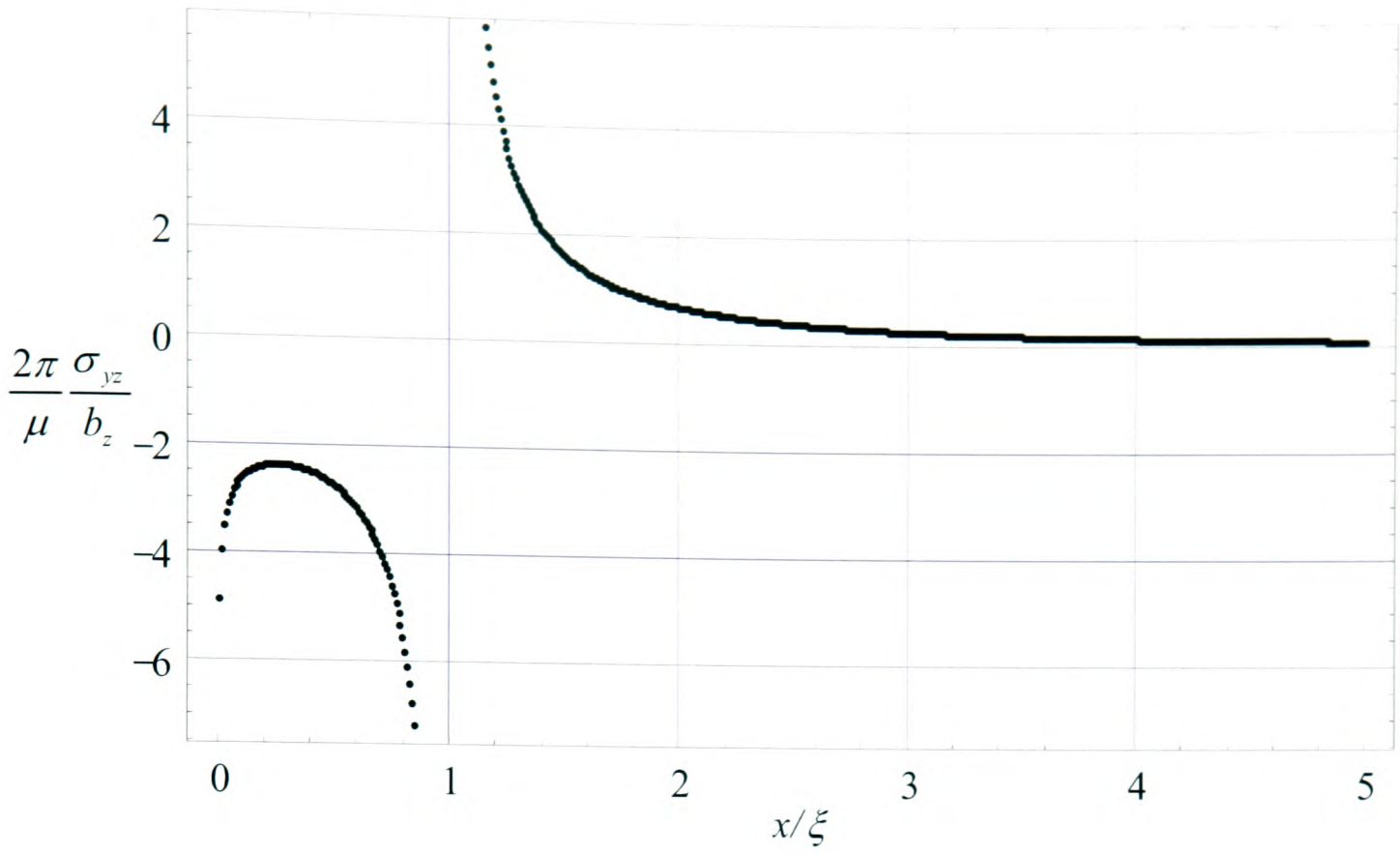

Figure 8-2: Linear plot of the dimensionless stress $\frac{2\pi}{\mu}\frac{\sigma_{yz}}{b_z}$ against normalised distance $\hat{x} = x/\xi$.

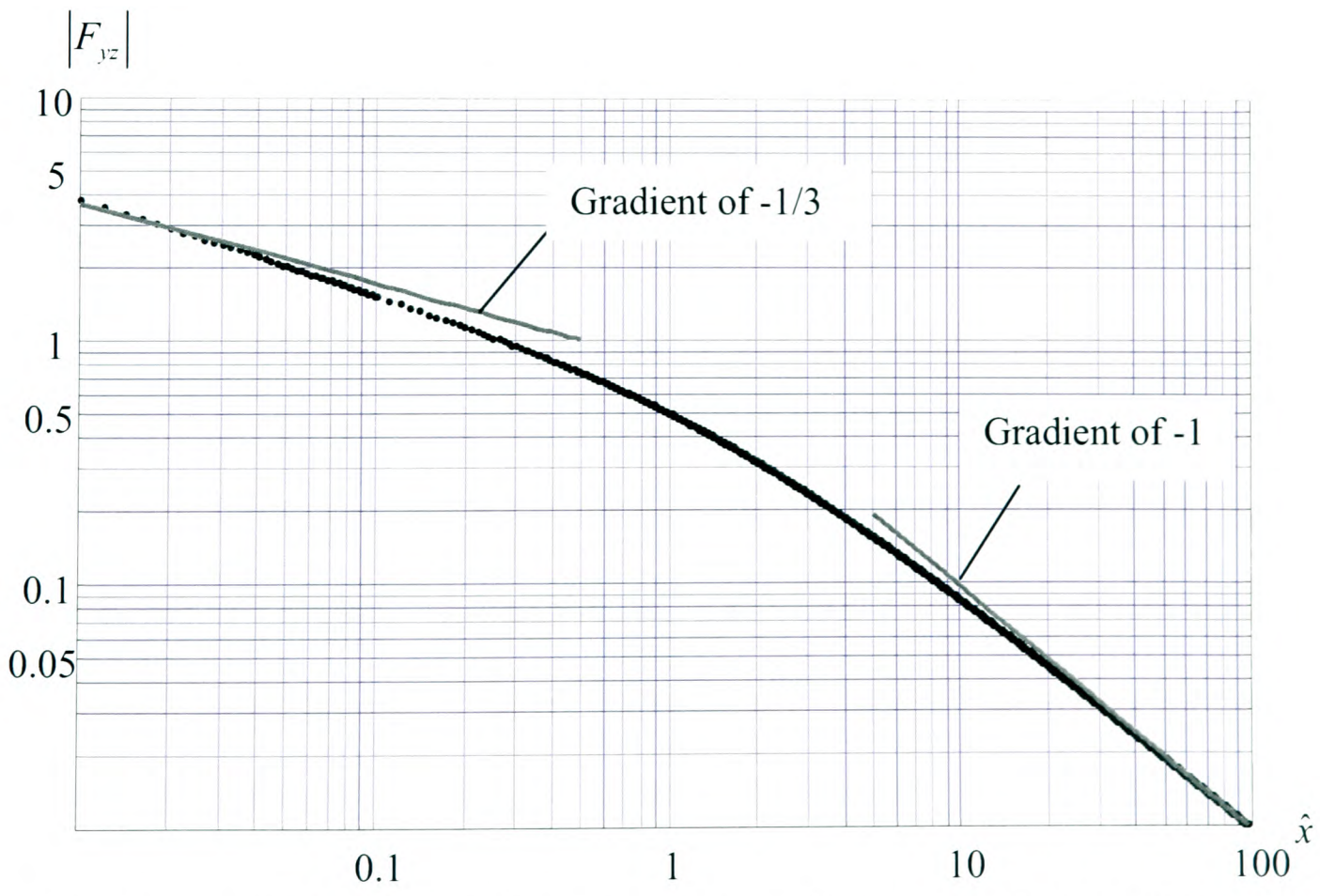

Figure 8-3: Log-log plot of the numerical result of the influence function $F_{yz}(\hat{x})$ (black points) with the asymptotes (grey line).

Chapter 9

The State of Stress Induced by Ring Dislocations in a Semi-Infinite Stepped Shaft

9.1 Introduction

This chapter is concerned with the state of stress induced by a set of ring-dislocations present in the axi-symmetric solid shown in Figure 9-1(a). The solid does not have an obvious description, but may be thought of as a stepped shaft, which is infinite in length in the axial direction, and where the larger diameter is also infinite, but the smaller one is of finite radius, R. In some respects it is the axi-symmetric equivalent of the three-quarter plane. The motivation for wanting to study this problem is that we wish, ultimately, to be able to describe in some detail torsion between complete contacts, and the plane $z = 0$ will become the interface between the two bodies. In the spirit of the equivalent plane problem (Churchman and Hills, 2006) the solution will be found by assuming that the two bodies are initially adhered, and deploying dislocations along the interface to represent the effects of slip and, if appropriate, separation.

The starting point for the formulation is the set of solutions for dislocations in an infinite space. A cylindrical axis set is used, and the three orthogonal Burgers components of

the dislocation lie in the r, θ, z directions. Of these, only the last is a true Volterra dislocation, in the sense of having a constant Burgers vector around the loop (a ring), whilst the others belong to the generalised Somigliana class, and hence the state of stress induced might be expected to be path-cut dependent. However, it turns out that this property is not observed for the screw dislocation. A solution for the screw dislocation in an infinite space (and also a half-space) was given by Barber *et al.* (Sackfield *et al.*, 2002), whilst that for an edge dislocation has a long history, and the first solution for a prismatic (z-direction Burgers vector) dislocation was given by Korsunsky (Korsunsky, 1996). The enigmatic radial dislocation has also featured in the literature, but with insufficient regard paid to the effect of path-cut, and this has recently been resolved by Paynter *et al.* (Paynter, Hills and Korsunsky, 2007), which we take as the starting point here.

The basic technique to be employed is to place the object dislocation being studied, here at $(\xi,0)$, in an infinite space, and then to clear the surfaces ($r=R$, $z\geq 0$) and ($r\geq R$, $z=0$) of tractions by distributing arrays of dislocations along them, Figure 9-1(b). The screw dislocation problem (with Burgers vector b_θ, Figure 9-2(a)) is naturally uncoupled from the edge dislocation pair (with Burgers vector components b_r, b_z, Figure 9-2(b)), and may be treated separately. It should be noted that, when we address the case of a dislocation having a radial Burgers vector we shall restrict our attention to the case when the path cut is made along the anti-disk $r\geq\xi$, $z=0$ as it is this solution which is relevant to studies of torsion, when slip nucleates at the edge and migrates inwards.

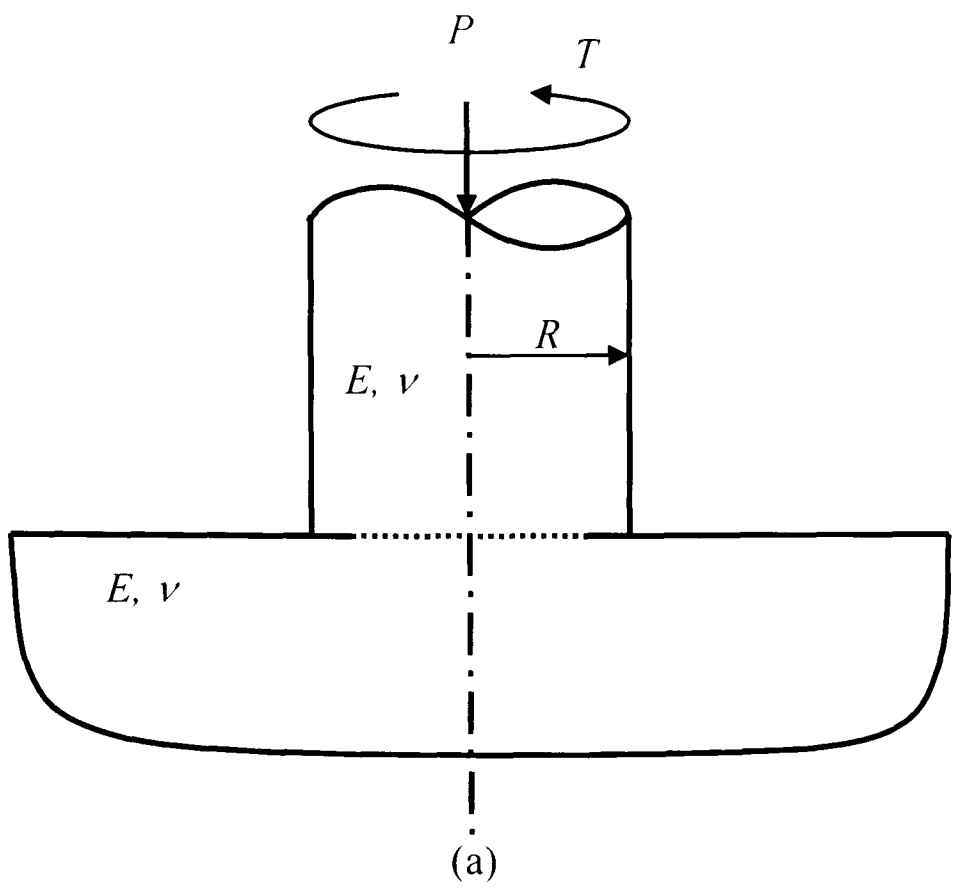

Figure 9-1: (a) Cylinder block bonded to an elastically similar half-space with an interface crack. (b) A set of ring-dislocations with components b_r, b_z and b_θ at the position $r = \xi$.

9.2 Formulation: Screw Dislocation

The screw dislocation problem will be treated first because it is the simpler of the two. As stated above, the state of stress induced at a general point (r, z) in an infinite space, by a screw dislocation, having Burgers vector b_θ, located at (r_d, z_d) is known for this problem (Paynter, Hills and Korsunsky, 2007), and is quoted here without proof:

$$\sigma_{i\theta}(r,z,r_d,z_d) = \frac{\mu}{2} b_\theta(r_d,z_d) G_{i\theta}(r,z,r_d,z_d), \quad i = r,z \tag{9-1}$$

where μ is the modulus of rigidity, and $G_{i\theta}(r,z,r_d,z_d)$ are stress kernel functions given at the end of the Appendix C(equations C-16, 17).

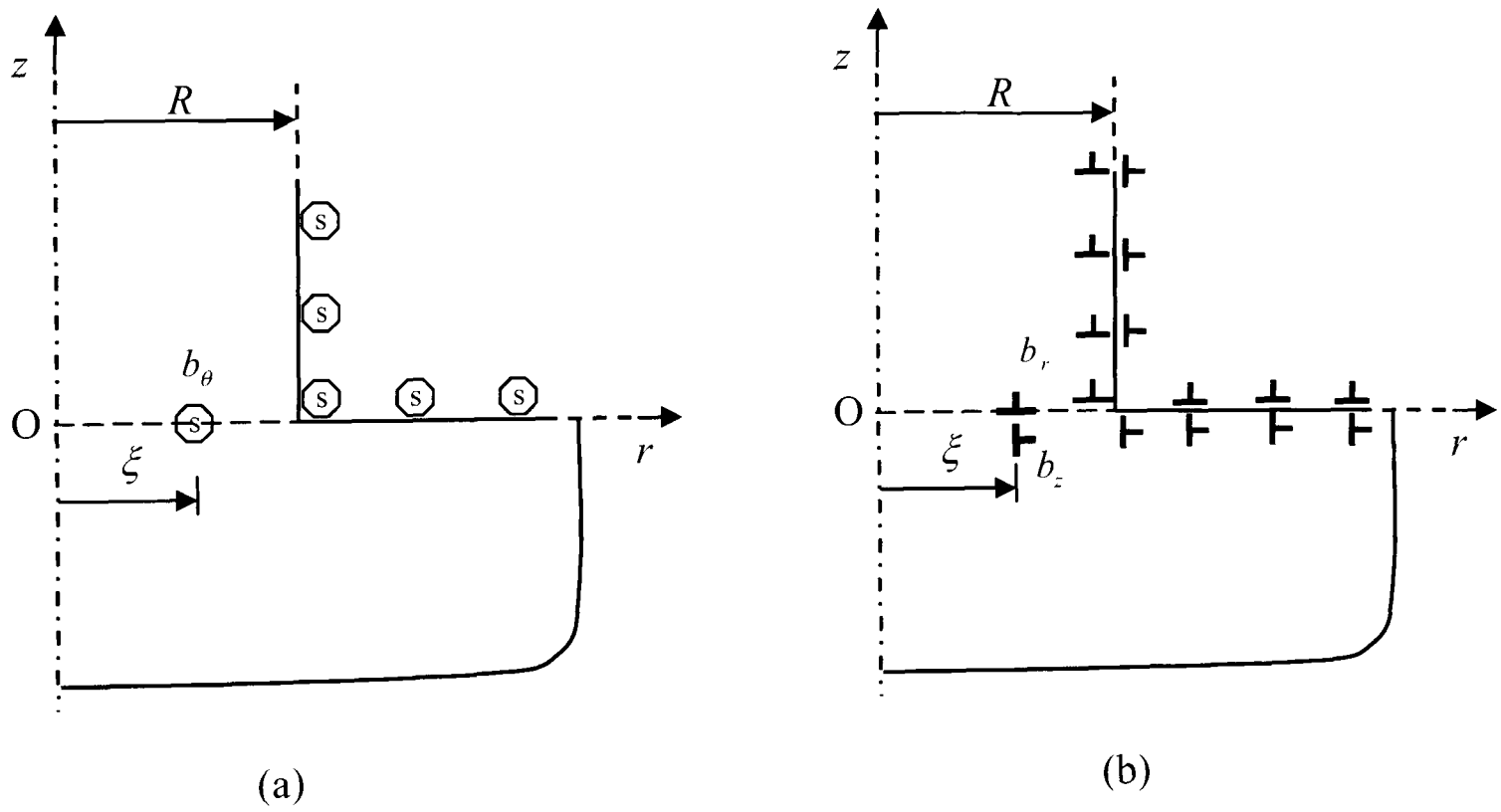

Figure 9-2: The dislocation in an axis-symmetric problem. (a) Screw dislocation (b) Edge dislocation

In order to find the state of stress in the domain under consideration, Figure 9-2(a), we shall need to deploy distributions of dislocations along the anti-disk $z=0$, $r \geq R$ and the semi-infinite cylinder $r=R$, $z \geq 0$ to ensure that these surfaces are traction-free, i.e. to achieve the conditions

$$\sigma_{z\theta}(r,0)=0 \qquad z=0, R \leq r \leq \infty, \tag{9-2a}$$

$$\sigma_{r\theta}(R,z)=0 \qquad r=R, 0 \leq z \leq \infty. \tag{9-2b}$$

First, we need to consider the influence of an individual object screw dislocation, the one whose effect we ultimately require, located at (ξ, 0), and assumed present in an infinite space. We shall confine ourselves to determining the traction arising on the disk containing the dislocation, and hence

$$\bar{\sigma}_{z\theta}(r,0)=\frac{\mu b_\theta(\xi,0)}{2} G_{z\theta}(r,0,\xi,0). \tag{9-3}$$

This dislocation will induce non-zero-tractions on what will become the free surfaces, and these will be cancelled using dislocation arrays on those surfaces. The effects of those cancelling dislocations are now written down. First, those present on the anti-disk $z=0$, $r \geq R$, induce a shear stress $\tilde{\sigma}_{z\theta}(r,0)$ given by

$$\tilde{\sigma}_{z\theta}(r,0)=\int_R^\infty \frac{\mu B_\theta(r_d)}{2} G_{z\theta}(r,0,r_d,0)dr_d, \tag{9-4}$$

where

$$B_\theta(r_d)=\frac{db_\theta}{dr_d} \tag{9-5}$$

is the dislocation density, and secondly those present along the semi-infinite cylinder $r=R$, $z \geq 0$, induce a shear stress $\tilde{\sigma}_{z\theta}(r,0)$ given by

$$\tilde{\sigma}_{z\theta}(r,0)=\int_0^\infty \frac{\mu B_\theta(z_d)}{2} G_{z\theta}(r,0,R,z_d)dz_d, \tag{9-6}$$

where

$$B_\theta(z_d) = \frac{db_\theta}{dz_d}. \tag{9-7}$$

We need, now, also to find the values of those tractions induced on what should be the free surfaces, so that they can be set to zero. Note that there are three contributions for each surface - one from the object dislocation itself, and one each from the array of dislocations present on the surface in question and one from the other surface. The combined contributions, together with the boundary conditions (equation 9-2) give the following pair of coupled simultaneous Cauchy singular integral equations, with generalised kernels

$$\begin{aligned} &b_\theta(\xi,0)G_{z\theta}(r,0,\xi,0) + \int_R^\infty B_\theta(r_d)G_{z\theta}(r,0,r_d,0)dr_d \\ &+ \int_0^\infty B_\theta(z_d)G_{z\theta}(r,0,R,z_d)dz_d = 0, \qquad z = 0, R \le r < \infty, \end{aligned} \tag{9-8a}$$

$$\begin{aligned} &b_\theta(\xi,0)G_{r\theta}(R,z,\xi,0) + \int_R^\infty B_\theta(r_d)G_{r\theta}(R,z,r_d,0)dr_d \\ &+ \int_0^\infty B_\theta(z_d)G_{r\theta}(R,z,R,z_d)dz_d = 0, \qquad r = R, 0 \le z < \infty, \end{aligned} \tag{9-8b}$$

which must be solved for the two unknown dislocation densities, $B_\theta(r_d)$, $B_\theta(z_d)$. In order to prepare the equations for solution two steps are needed to put them in standard form. First, the intervals of integration and imposition are normalised by dint of the substitutions $\hat{\xi} = \xi / R$, $\hat{r} = r / R$, $\hat{r}_d = r_d / R$, $\hat{z}_d = z_d / R$, and then the ranges are rendered finite by the substitutions

$$\hat{r}_d = \log[\frac{2e}{1-s_r}], \hat{z}_d = \log[\frac{2}{1-s_z}], \hat{r} = \log[\frac{2e}{1-t_r}], \hat{z} = \log[\frac{2}{1-t_z}], \tag{9-9}$$

giving

$$\frac{d\hat{r}_d}{ds_r} = \frac{1}{1-s_r}, \tag{9-10}$$

$$\frac{d\hat{z}_d}{ds_z} = \frac{1}{1-s_z}. \tag{9-11}$$

Hence the integral equations become

$$b_\theta(\hat{\xi},0)G_{z\theta}(\hat{r},0,\hat{\xi},0)+\int_{-1}B_\theta(s_r)G_{z\theta}(\hat{r},0,\hat{r}_d,0)\frac{1}{1-s_r}ds_r$$
$$+\int_{-1}B_\theta(s_z)G_{z\theta}(\hat{r},0,1,\hat{z}_d)\frac{1}{1-s_z}ds_z=0,\qquad -1<t_r<1 \tag{9-12a}$$

$$b_\theta(\hat{\xi},0)G_{r\theta}(1,\hat{z},\hat{\xi},0)+\int_{-1}B_\theta(s_r)G_{r\theta}(1,\hat{z},\hat{r}_d,0)\frac{1}{1-s_r}ds_r$$
$$+\int_{-1}B_\theta(s_z)G_{r\theta}(1,\hat{z},1,\hat{z}_d)\frac{1}{1-s_z}ds_z=0,-1<t_z<1. \tag{9-12b}$$

The next step is to establish the characteristic form of the solution. We expect that, as the observation point approaches the edge of the cylinder ($s/R<<1$, $s=R-r$) on $z=0$, the state of stress will be singular in character, with the order of the singularity being given by a characteristic equation (Duo, Korsunsky and Hills, 2005), i.e. $\sigma_{ij}\approx s^{\lambda-1}$, where $\lambda\equiv 2/3$. The standard Gaussian numerical quadratures do not permit the near-field to be represented exactly, but approximately the correct behaviour can be achieved by choosing the following fundamental function:

$$w(s_j)=\sqrt{\frac{1-s_j}{1+s_j}}\qquad for\qquad j=r,z, \tag{9-13}$$

so that the dislocation densities may be written as

$$B_\theta(s_j)=w(s_j)\phi_\theta(s_j),\qquad j=r,z. \tag{9-14}$$

The positions of the integration and collocation points are given by (Hills *et al.*, 1996)

$$s_{ri}=s_{zi}=\cos(\pi\frac{2i}{2n+1})\qquad for\qquad i=1,...,n \tag{9-15a}$$

$$t_{rk}=t_{zk}=\cos(\pi\frac{2k-1}{2n+1})\qquad for\qquad k=1,...,n \tag{9-15b}$$

with a weight function

$$W(s_{ji})=\frac{2\pi(1-s_{ji})}{2n+1}\qquad for\qquad j=r,z\qquad and\qquad i=1,..,n. \tag{9-16}$$

Finally, the discretised integral equations become

$$b_\theta(\hat{\xi},0)G_{z\theta}(\hat{r}(t_{rk}),0,\hat{\xi},0)+\sum_{i=1}^{n}W(s_{ri})\phi_\theta(s_{ri})G_{z\theta}(\hat{r}(t_{rk}),0,\hat{r}_d(s_{ri}),0)\frac{1}{1-s_{ri}}$$
$$+\sum_{i=1}^{n}W(s_{zi})\phi_\theta(s_{zi})G_{z\theta}(\hat{r}(t_{rk}),0,1,\hat{z}_d(s_{zi}))\frac{1}{1-s_{zi}}=0, \qquad (9\text{-}17a)$$

$$b_\theta(\hat{\xi},0)G_{r\theta}(\hat{r}(t_{rk}),0,\hat{\xi},0)+\sum_{i=1}^{n}W(s_{ri})\phi_\theta(s_{ri})G_{r\theta}(1,\hat{z}(t_{rk}),\hat{r}_d(s_{ri}),0)\frac{1}{1-s_{ri}}$$
$$+\sum_{i=1}^{n}W(s_{zi})\phi_\theta(s_{zi})G_{r\theta}(1,\hat{z}(t_{rk}),1,\hat{z}_d(s_{zi}))\frac{1}{1-s_{zi}}=0. \qquad (9\text{-}17b)$$

These represent a system of $2n$ simultaneous equations for $2n$ unknown $\phi_\theta(s_{ri})$ and $\phi_\theta(s_{zi})$. When these values have been determined, the stresses $\sigma_{i\theta}(\hat{r},\hat{z})$ at an arbitrary point can readily be found.

9.3 Formulation: Edge Dislocations

The formulation for the edge dislocation problem follows generally the same principles, but there are additional complications: the main ones are that there is coupling, so that each Burgers component of the object dislocation induces both components of traction along the plane $z=0$, and that dislocation distributions having both components of Burgers vector are needed to annul the two traction components arising on the 'free' surfaces. Lastly, as has been discussed, great care is needed when choosing the path cuts forming the dislocations with radial Burgers vectors. The object dislocation solution is here formed by installing shear slip on the anti-disk $r\geq\xi$, $z=0$, and similarly the dislocations on the surface $z=0$, $r\geq R$ must be formed also by shear slip exterior to their position, whilst those on the cylindrical surface $r=R$, $z\geq 0$ must be formed by imposing an opening displacement along a cylindrical surface (Paynter, Hills and Korsunsky, 2007).

The state of stress induced in an axi-symmetric infinite space, at a general point (r, z), by an edge dislocation, having Burgers vector b_k^s located at (r_d, z_d) is

$$\sigma_{rjk}^s(r,z,r_d,z_d) = \frac{2\mu}{\kappa+1} b_k^s(r_d,z_d) G_{rjk}^s(r,z,r_d,z_d), \qquad j,k = r,z \qquad s = o,c, \tag{9-18}$$

where κ is Kolosov's constant, $G_{kij}^s(r,z,r_d,z_d)$ are stress kernels functions given in Appendix C, and o, c mean outward, cylindrical path cuts respectively.

In order to satisfy the free surface conditions, Figure 9-2(b), we shall need to deploy distributions of edge dislocations along the anti-disk $z = 0$, $r \geq R$ and the semi-infinite cylinder $r = R$, $z \geq 0$ as before, to achieve the following boundary conditions

$$\sigma_{zz}(r,0) = 0, \quad \sigma_{rz}(r,0) = 0 \qquad R \leq r < \infty, \qquad z = 0, \tag{9-19a}$$

$$\sigma_{rr}(R,z) = 0, \quad \sigma_{rz}(R,z) = 0 \quad 0 \leq z < \infty, \qquad r = R. \tag{9-19b}$$

Also as before, we will first write down the tractions induced by the object dislocation, located at (ξ , 0), and having Burgers components b_r^o , b_z^o

$$\overline{\sigma}_{zz}^r(r,0) = \frac{2\mu}{\kappa+1} b_r^o(\xi,0) G_{rzz}^o(r,0,\xi,0), \quad \overline{\sigma}_{zz}^z(r,0) = \frac{2\mu}{\kappa+1} b_z(\xi,0) G_{zzz}(r,0,\xi,0), \tag{9-20}$$

$$\overline{\sigma}_{rz}^r(r,0) = \frac{2\mu}{\kappa+1} b_r^o(\xi,0) G_{rrz}^o(r,0,\xi,0), \quad \overline{\sigma}_{rz}^z(r,0) = \frac{2\mu}{\kappa+1} b_z(\xi,0) G_{zrz}(r,0,\xi,0). \tag{9-21}$$

We need, now, to superpose the effects of two further arrays to establish the free surfaces. The first of these, on the anti-disk $z = 0$, $r > R$, induces stresses $\tilde{\sigma}_{zz}^r(r,0)$, $\tilde{\sigma}_{rz}^r(r,0)$ given by

$$\tilde{\sigma}_{zz}^r(r,0) = \int_R^\infty \frac{2\mu}{\kappa+1} [B_r^o(r_d) G_{rzz}^o(r,0,r_d,0) + B_z(r_d) G_{zzz}(r,0,r_d,0)] dr_d, \tag{9-22}$$

$$\tilde{\sigma}_{rz}^r(r,0) = \int_R^\infty \frac{2\mu}{\kappa+1} [B_r^o(r_d) G_{rrz}^o(r,0,r_d,0) + B_z(r_d) G_{zrz}(r,0,r_d,0)] dr_d, \tag{9-23}$$

where

$$B_r^o(r_d) = \frac{db_r^o}{dr_d}, \quad B_z(r_d) = \frac{db_z}{dr_d} \tag{9-24}$$

are the dislocation densities. The second array, on the cylindrical surface $r = R$, $z > 0$, induces stresses $\tilde{\sigma}^{\infty}_{zz}(r,0)$, $\tilde{\sigma}^{\infty}_{rz}(r,0)$ given by

$$\tilde{\sigma}^{\infty}_{zz}(r,0) = \int_0^{\infty} \frac{2\mu}{\kappa+1}[B^c_r(z_d)G^c_{rzz}(r,0,R,z_d) + B_z(z_d)G_{zzz}(r,0,R,z_d)]dz_d, \tag{9-25}$$

$$\tilde{\sigma}^{\infty}_{rz}(r,0) = \int_0^{\infty} \frac{2\mu}{\kappa+1}[B^c_r(z_d)G^c_{rrz}(r,0,R,z_d) + B_z(z_d)G_{zrz}(r,0,R,z_d)]dz_d, \tag{9-26}$$

where

$$B^c_r(z_d) = \frac{db^c_r}{dz_d},\ B_z(z_d) = \frac{db_z}{dz_d}. \tag{9-27}$$

The interaction between the object dislocation and the two arrays must now be found, and tractions cleared from the free surfaces. This requirement is expressed by the following set of four coupled Cauchy singular integral equations with generalised kernels

$$\begin{aligned} &b^o_r(\xi,0)G^o_{rzz}(r,0,\xi,0) + \int_R^{\infty}[B^o_r(r_d)G^o_{rzz}(r,0,r_d,0) + B_z(r_d)G_{zzz}(r,0,r_d,0)]dr_d \\ &+ \int_0^{\infty}[B^c_r(z_d)G^c_{rzz}(r,0,R,z_d) + B_z(z_d)G_{zzz}(r,0,R,z_d)]dz_d = 0, \qquad R < r < \infty, z = 0 \end{aligned} \tag{9-28a}$$

$$\begin{aligned} &b^o_r(\xi,0)G^o_{rrz}(r,0,\xi,0) + \int_R^{\infty}[B^o_r(r_d)G^o_{rrz}(r,0,r_d,0) + B_z(r_d)G_{zrz}(r,0,r_d,0)]dr_d \\ &+ \int_0^{\infty}[B^c_r(z_d)G^c_{rrz}(r,0,R,z_d) + B_z(z_d)G_{zrz}(r,0,R,z_d)]dz_d = 0, \qquad R < r < \infty, z = 0, \end{aligned} \tag{9-28b}$$

$$\begin{aligned} &b^o_r(\xi,0)G^o_{rrr}(R,z,\xi,0) + \int_R^{\infty}[B^o_r(r_d)G^o_{rrr}(R,z,r_d,0) + B_z(r_d)G_{zrr}(R,z,r_d,0)]dr_d \\ &+ \int_0^{\infty}[B^c_r(z_d)G^c_{rrr}(R,z,R,z_d) + B_z(z_d)G_{zrr}(R,z,R,z_d)]dz_d = 0, \qquad 0 < z < \infty, r = R, \end{aligned} \tag{9-29a}$$

$$\begin{aligned} &b^o_r(\xi,0)G^o_{rrz}(R,z,\xi,0) + \int_R^{\infty}[B^o_r(r_d)G^o_{rrz}(R,z,r_d,0) + B_z(r_d)G_{zrz}(R,z,r_d,0)]dr_d \\ &+ \int_0^{\infty}[B^c_r(z_d)G^c_{rrz}(R,z,R,z_d) + B_z(z_d)G_{zrz}(R,z,R,z_d)]dz_d = 0.0 < z < \infty, r = R. \end{aligned} \tag{9-29b}$$

Precisely the same normalisation scheme is used here as was done for the screw dislocation and the integral equations then become

$$b_r^o(\hat{\xi},0)G_{rzz}^o(\hat{r},0,\hat{\xi},0)+\int_{-1}\frac{1}{1-s_r}\begin{bmatrix}B_r^o(s_r)G_{rzz}^o(\hat{r},0,\hat{r}_d,0)\\+B_z(s_r)G_{zzz}(\hat{r},0,\hat{r}_d,0)\end{bmatrix}ds_r$$
$$+\int_{-1}\frac{1}{1-s_z}\begin{bmatrix}B_r^c(s_z)G_{rzz}^c(\hat{r},0,1,\hat{z}_d)\\+B_z(s_z)G_{zzz}(\hat{r},0,1,\hat{z}_d)\end{bmatrix}ds_z=0,\quad -1<t_r<1 \tag{9-30a}$$

$$b_r^o(\hat{\xi},0)G_{rrz}^o(\hat{r},0,\hat{\xi},0)+\int_{-1}\frac{1}{1-s_r}\begin{bmatrix}B_r^o(s_r)G_{rrz}^o(\hat{r},0,\hat{r}_d,0)\\+B_z(s_r)G_{zrz}(\hat{r},0,\hat{r}_d,0)\end{bmatrix}ds_r$$
$$+\int_{-1}\frac{1}{1-s_z}\begin{bmatrix}B_r^c(s_z)G_{rrz}^c(\hat{r},0,1,\hat{z}_d)\\+B_z(s_z)G_{zrz}(\hat{r},0,1,\hat{z}_d)\end{bmatrix}ds_z=0,\quad -1<t_r<1, \tag{9-30b}$$

$$b_r^o(\hat{\xi},0)G_{rrr}^o(1,\hat{z},\hat{\xi},0)+\int_{-1}\frac{1}{1-s_r}\begin{bmatrix}B_r^o(s_r)G_{rrr}^o(1,\hat{z},\hat{r}_d,0)\\+B_z(s_r)G_{zrr}(1,\hat{z},\hat{r}_d,0)\end{bmatrix}ds_r$$
$$+\int_{-1}\frac{1}{1-s_z}\begin{bmatrix}B_r^c(s_z)G_{rrr}^c(1,\hat{z},1,\hat{z}_d)\\+B_z(s_z)G_{zrr}(1,\hat{z},1,\hat{z}_d)\end{bmatrix}ds_z=0,\quad -1<t_z<1 \tag{9-31a}$$

$$b_r^o(\hat{\xi},0)G_{rrz}^o(1,\hat{z},\hat{\xi},0)+\int_{-1}\frac{1}{1-u_r}\begin{bmatrix}B_r^o(s_r)G_{rrz}^o(1,\hat{z},\hat{r}_d,0)\\+B_z(s_r)G_{zrz}(1,\hat{z},\hat{r}_d,0)\end{bmatrix}ds_r$$
$$+\int_{-1}\frac{1}{1-s_z}\begin{bmatrix}B_r^c(s_z)G_{rrz}^c(1,\hat{z},1,\hat{z}_d)\\+B_z(s_z)G_{zrz}(1,\hat{z},1,\hat{z}_d)\end{bmatrix}ds_z=0,\quad 1<t_z<1. \tag{9-31b}$$

We expect that, as the observation point approaches the edge of the cylinder ($s/R<<1$) the state of stress will be singular in character, with the order of the singularity being given by a characteristic equation (Williams, 1952), i.e. $\sigma_{ij}\approx s^{\lambda-1}$, where $\lambda=0.5445$, the eigenvalue for symmetric loading. The standard Gaussian numerical quadratures do not permit the near-field to be represented exactly, but approximately the correct behaviour can be achieved by choosing the following fundamental function:

$$w(s_j)=\sqrt{\frac{1-s_j}{1+s_j}}\qquad for\qquad j=r,z, \tag{9-32}$$

so that the dislocation density may be written as

$$B_i(s_j)=w(s_j)\phi_i(s_j),\qquad i,j=r,z.. \tag{9-33}$$

The integration and collocation points are given by equations (9-15).

The discretised integral equations can now be written down. A system of $4n$ simultaneous equations for $4n$ unknowns $\phi_r(s_{r_1})$ $\phi_r(s_{r_2})$ $\phi_z(s_{z_1})$ and $\phi_z(s_{z_2})$ are obtained. When these values are found, the stresses $\sigma_{ij}(\hat{r},\hat{z})$ at an arbitrary point due to the object dislocation, b_r^o, located at $(\hat{\xi}, 0)$ can be determined.

9.4 Results

The primary output from this paper is a representation of the tractions induced along the disk $0 \le r \le R$, $z = 0$ by dislocations present on that disk. Care is needed in displaying the output meaningfully, and in a rigorous form suitable for subsequent numerical processing. The output will be displayed in one of three forms, depending on the position of the object dislocation, and the position of the observation point. When neither is near an end of the interval, the best way to form the solution is as a superposition of the infinite space solution and a corrective term for the presence of the free surface. Thus

$$\sigma_{z\theta}(r,0) = \frac{\mu b_\theta(\xi,0)}{2}\left[G_{z\theta}(r,0,\xi,0) + H_{z\theta}(r,0,\xi,0)\right]$$

$$\sigma_{iz}(r,0) = \frac{2\mu}{\kappa+1} b_k(\xi,0)\left[G^s_{kiz}(r,0,\xi,0) + H^s_{kiz}(r,0,\xi,0)\right] \qquad i,k = r,z$$

where, in each case, the first function on the right hand side is the infinite space influence function already defined (see Appendix C) and is Cauchy singular in nature, whilst the second term is a bounded correction for the free surface effects. Figure 9-3 displays the five corrective functions needed. This approach is satisfactory in general, and it should be noted that, in each case, provided $\xi > 0$, if $r \to 0$, the shear tractions always vanish, but additional care needs to be taken in the following cases (§9.4.1, §9.4.2)

(a)

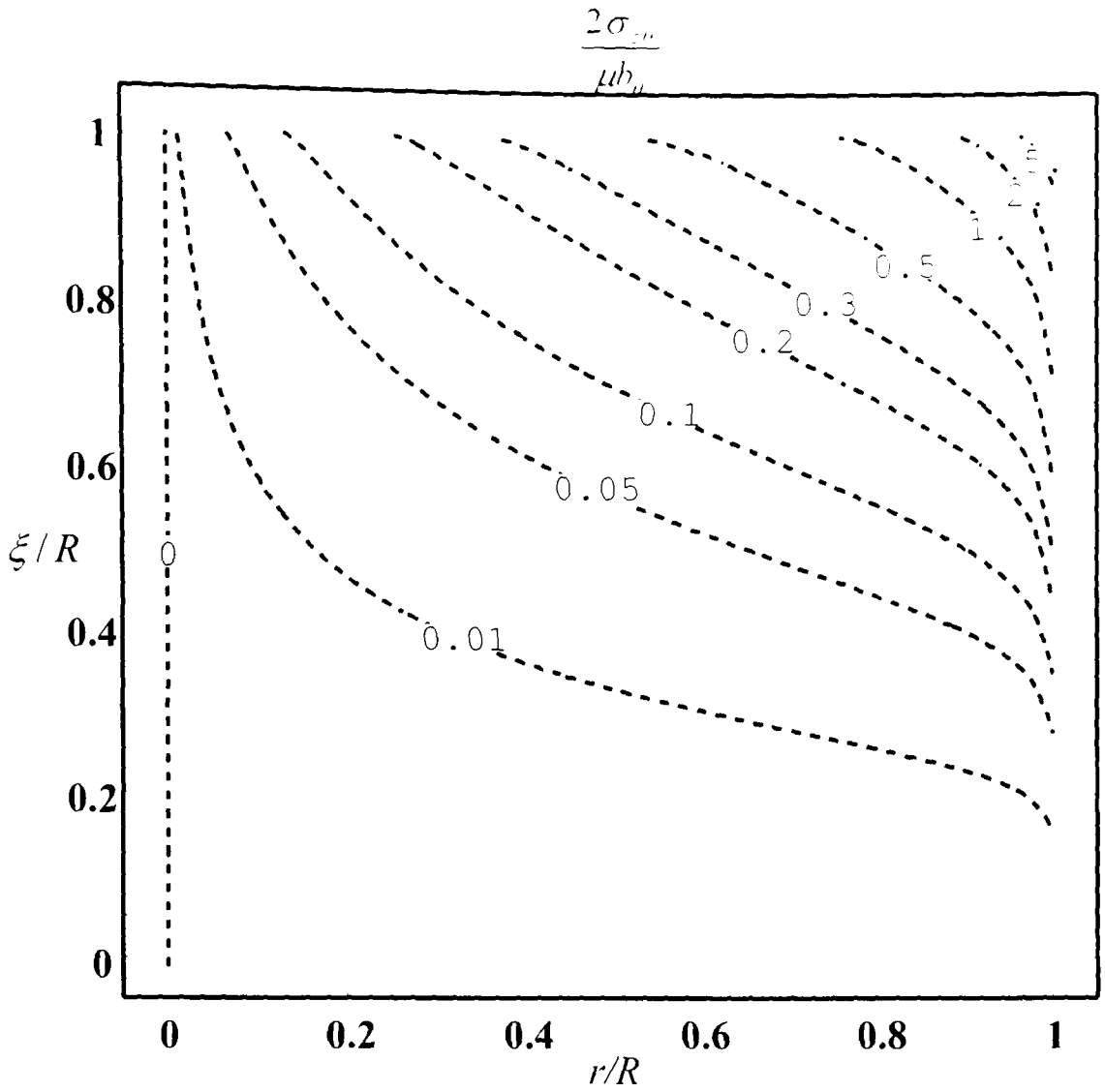
$\frac{2\sigma_{zz}}{\mu b_z}$
1
0.8
0.6
0.4
0.2
0
ξ / R
0
0.01
0.05
0.1
0.2
0.3
0.5
1
0
0.2
0.4
0.6
0.8
1
r/R

(b)

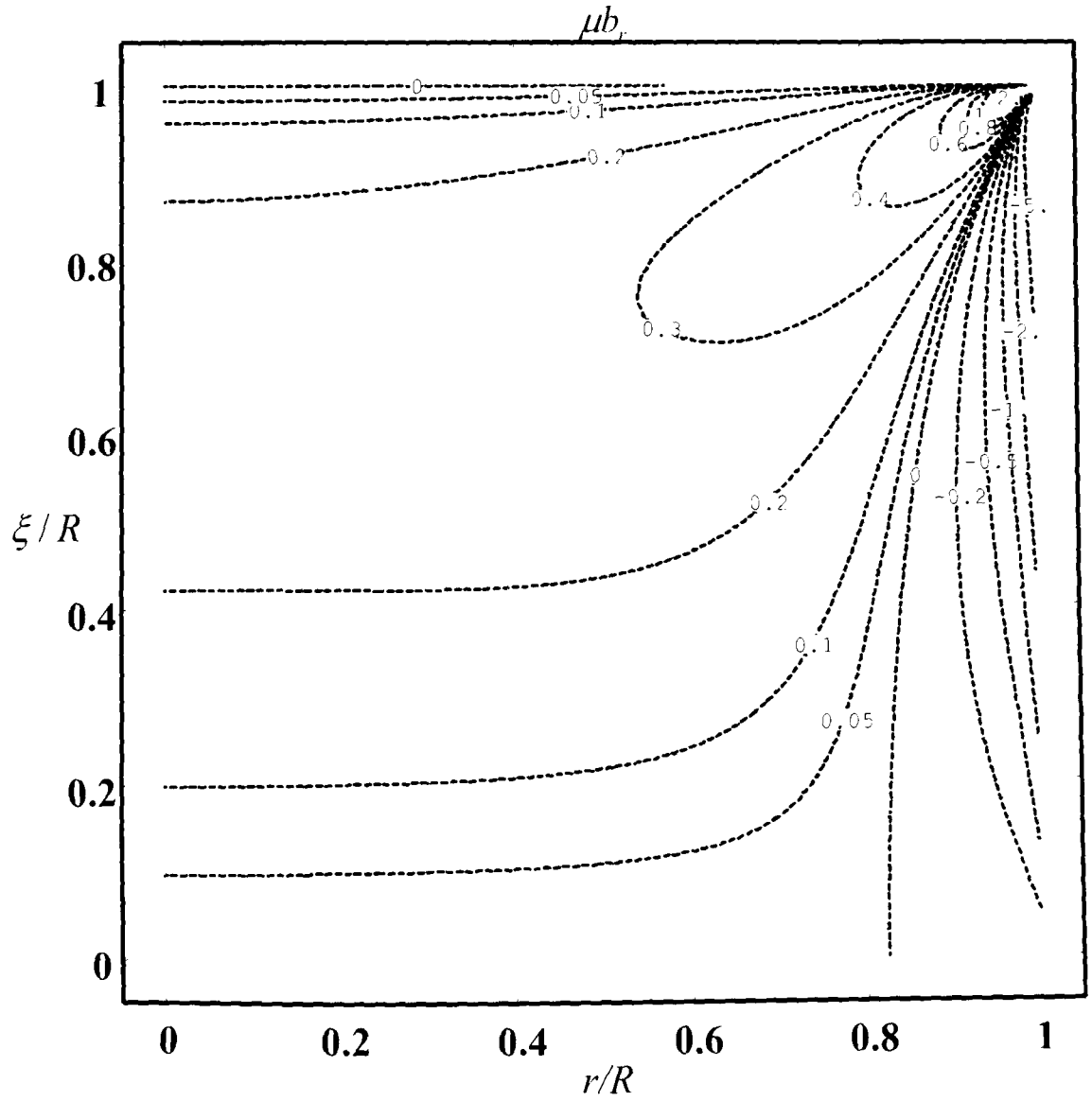
$\frac{2\sigma_{rr}}{\mu b_z}$
1
0.8
0.6
0.4
0.2
0
ξ / R
0
0.05
0.1
0.2
0.3
0.4
0.6
0.8
1
2
-0.2
-0.4
-1
-2
-5
0
0.2
0.4
0.6
0.8
1
r/R

(c)

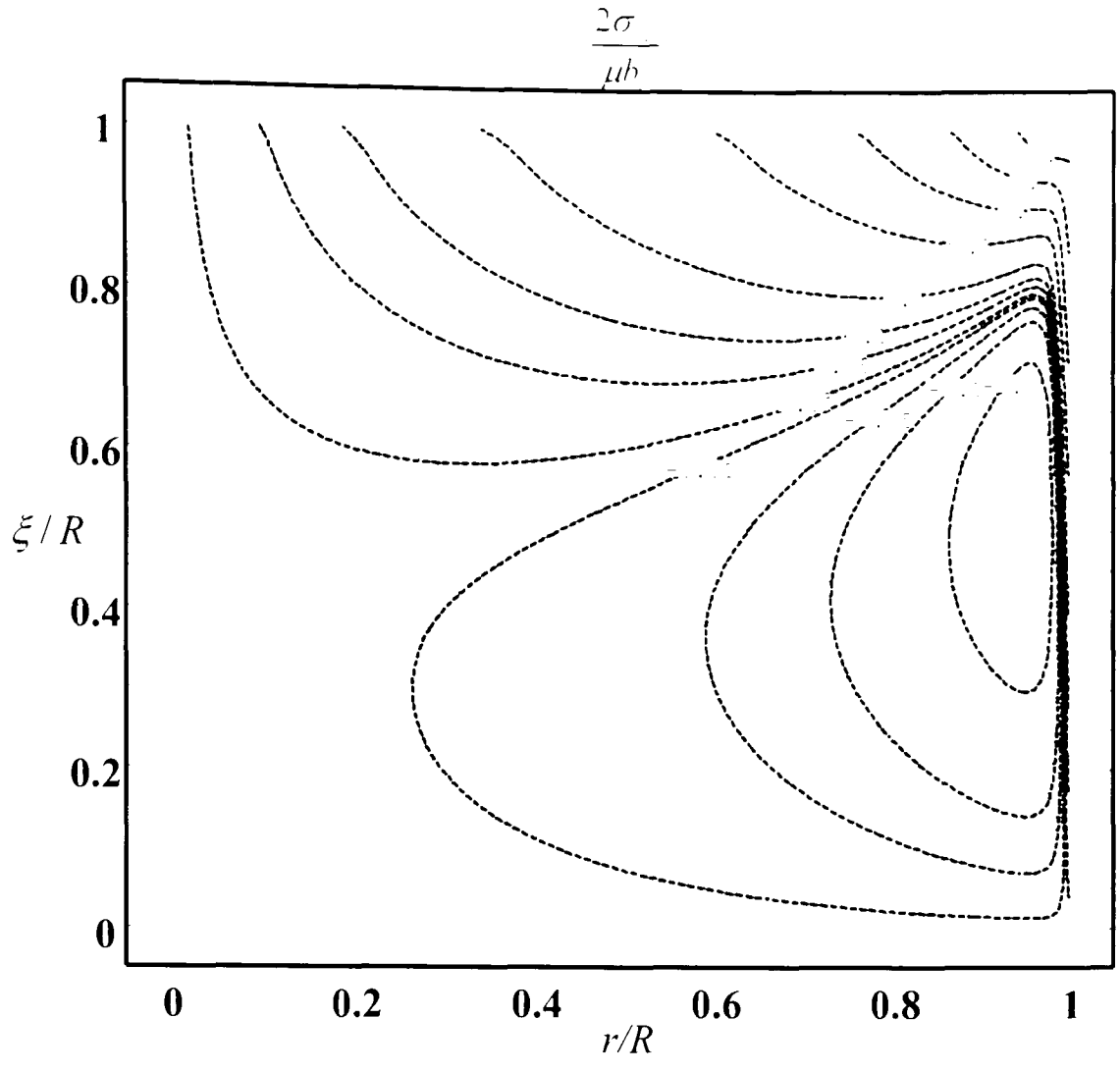
$\frac{2\sigma}{\mu b}$
1
0.8
0.6
ξ / R
0.4
0.2
0
0
0.2
0.4
0.6
0.8
1
r/R

(d)

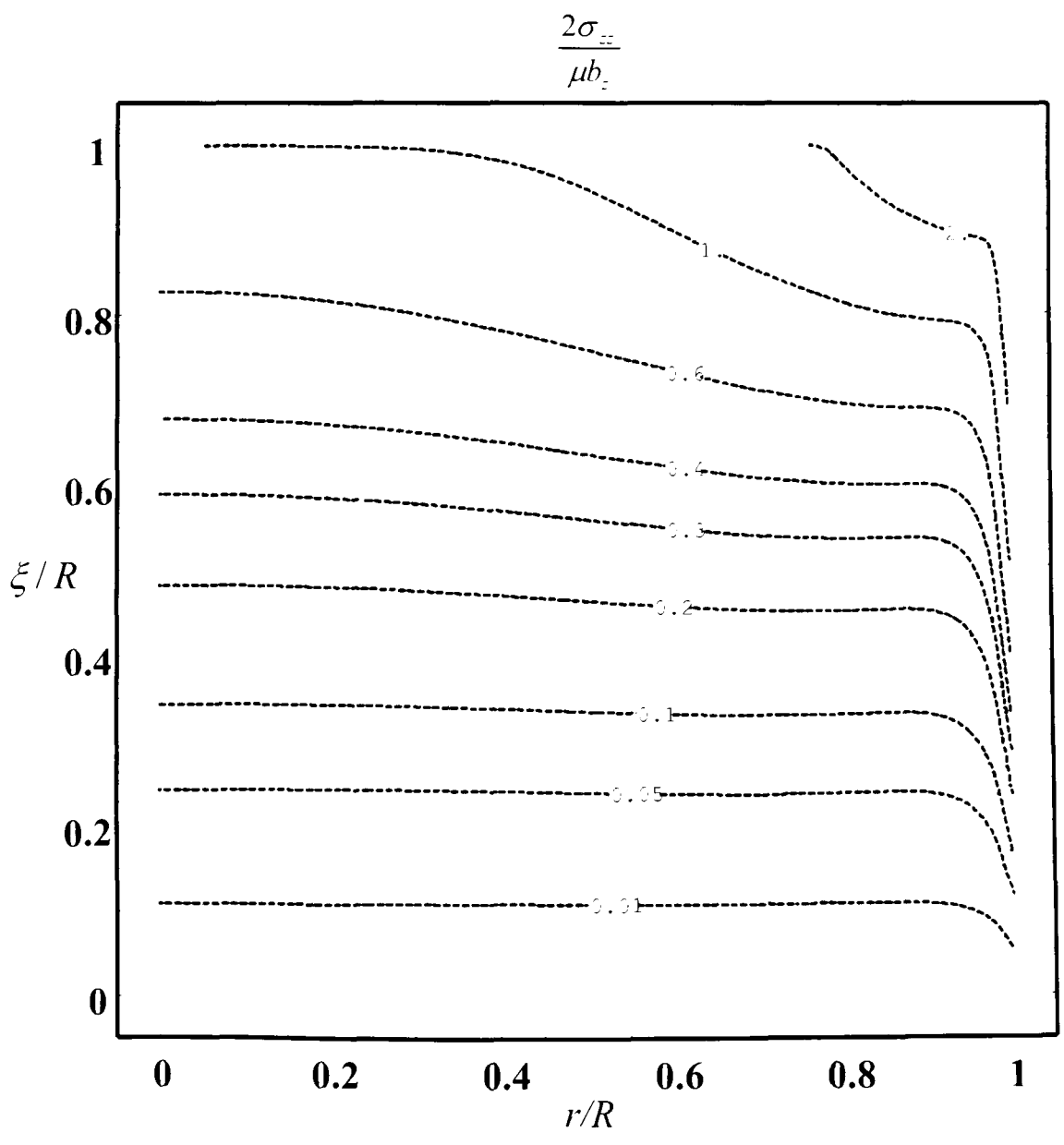
$\frac{2\sigma_{zz}}{\mu b_z}$
1
0.8
0.6
ξ / R
0.4
0.2
0
0
0.2
0.4
0.6
0.8
1
r/R

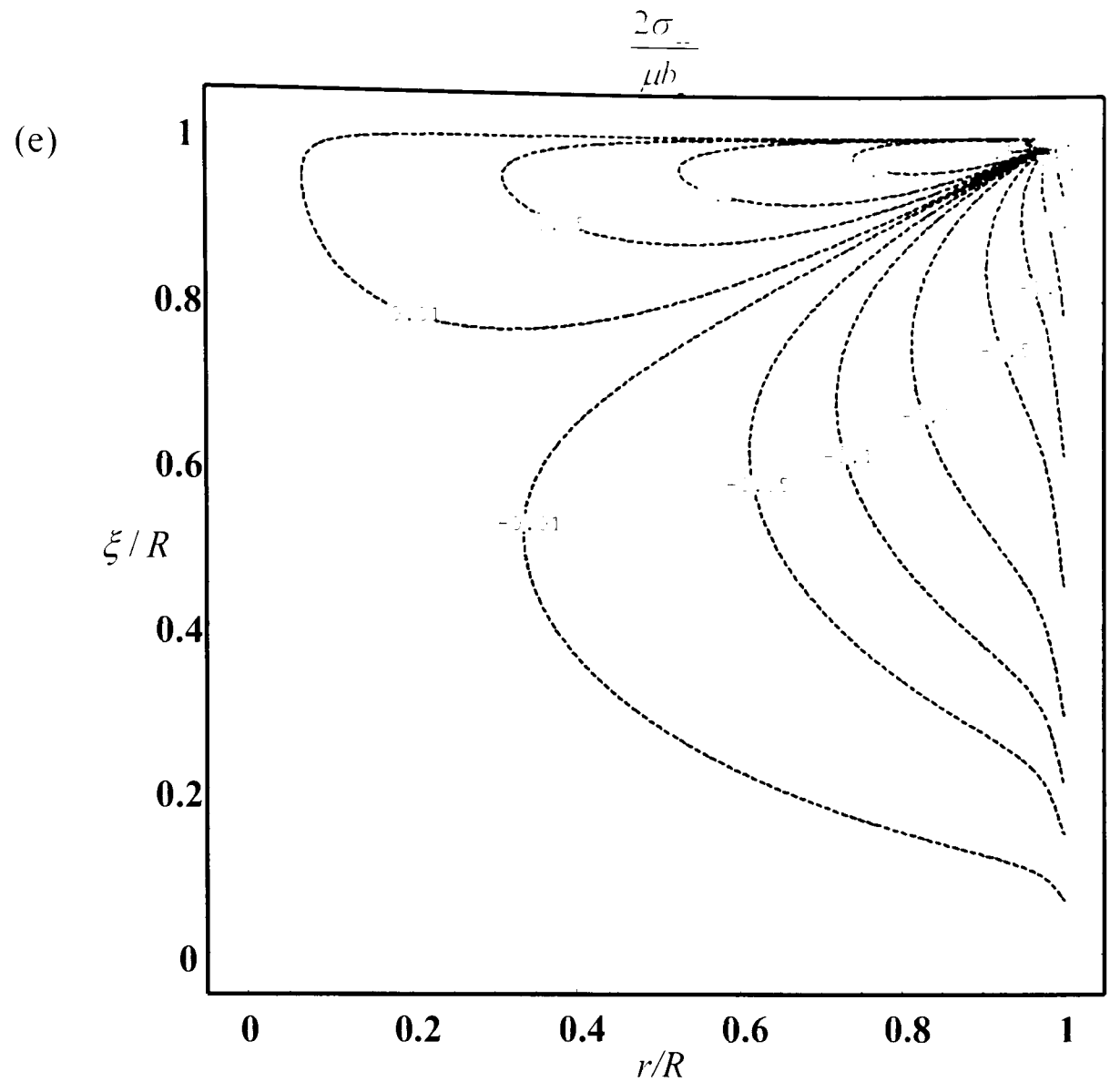

Figure 9-3: Corrective terms to the infinite space solutions to account for the presence of the free surfaces.

(a) $\sigma_{z\theta}$ component of stresses induced by screw dislocation b_θ.

(b) σ_{zz} component of stresses induced by edge dislocation b_r.

(c) σ_{rz} component of stresses induced by edge dislocation b_r.

(d) σ_{zz} component of stresses induced by edge dislocation b_z.

(e) σ_{rz} component of stresses induced by edge dislocation b_z.

9.4.1 Observation point approaches corner ($r \to R$, $\xi \to R$ not approaching unity)

Here the local state of stress is given by the plane strain Williams solution (Williams, 1952) for the edge dislocation, and the corresponding notch eigensolution (Duo, Korsunsky and Hills, 2005) for the screw dislocation case. We may then write

$$\sigma_{z\theta}(s,0) = \frac{\mu b_\theta(\xi,0)}{2} f_{z\theta}^{\theta}(\xi) s^{-1/3} \tag{9-34}$$

$$\sigma_{zz}(s,0) = \frac{2\mu}{\kappa+1}\left[b_r(\xi,0) f_{zz}^{r}(\xi) s^{-0.4555} + b_z(\xi,0) f_{zz}^{z}(\xi) s^{-0.4555}\right] \tag{9-35}$$

$$\sigma_{rz}(s,0) = \frac{2\mu}{\kappa+1} 0.543\left[b_r(\xi,0) f_{zz}^{r}(\xi) s^{-0.4555} + b_z(\xi,0) f_{zz}^{z}(\xi) s^{-0.4555}\right] \tag{9-36}$$

We have carefully collocated the functions f_{ij}^{k} and they are given by

$$f_{z\theta}^{\theta}(\xi) = -87.98 + \frac{87.98}{1-\xi/R} - 87.46\frac{\xi}{R} - 94.77(\frac{\xi}{R})^2 + 36.22(\frac{\xi}{R})^3 - 116.77(\frac{\xi}{R})^4 \tag{9-37}$$

$$f_{zz}^{r}(\xi) = -0.038 - \frac{0.038}{1-\xi/R} + 0.209(\frac{\xi}{R}) + 0.195(\frac{\xi}{R})^2 - 0.078(\frac{\xi}{R})^3 \tag{9-38}$$

$$f_{zz}^{z}(\xi) = -0.052 + \frac{0.052}{1-\xi/R} - 0.073(\frac{\xi}{R}) + 0.373(\frac{\xi}{R})^2 - 0.097(\frac{\xi}{R})^3 \tag{9-39}$$

The factor of 0.543 is the stress ratio revealed by Williams' eigenvectors.

9.4.2 Observation point and object dislocation approach corner

$(r/R, \xi/R \to 1)$

This case is of some practical interest and, potentially, difficulties arise because of the interaction between the Cauchy singularity and the geometric effect of the internal sharp

corner. However, this problem may be averted by noting that, providing $r \neq \xi$, the corresponding problem for a three-quarter plane geometry may be recovered: either the plane strain problem for the edge dislocation (Churchman and Hills, 2006) or the antiplane strain problem for the screw dislocation (Qiu, Churchman and Hills, 2007). These have the interesting feature that the solution no longer depends on the radius of the smaller cylindrical part of the domain (R), and the only remaining length dimension in the problem is the distance from the object dislocation to the corner (s). These plane/antiplane solutions, which are included here for completeness, may therefore be employed without modification.

$$\sigma_{z\theta}(s,0) = \frac{\mu}{2} b_\theta \left(\frac{1}{\pi(R-\xi)} F_{z\theta}(s, R-\xi) + G_{z\theta}(R-s, 0, \xi, 0) \right) \tag{9-40}$$

$$\sigma_{rz}(s,0) = \frac{2\mu}{(\kappa+1)} \left[\begin{array}{l} b_r^o \left(\dfrac{1}{\pi(R-\xi)} F_{rrz}(s, R-\xi) + G_{rrz}^o(R-s, 0, \xi, 0) \right) \\ + b_z \left(\dfrac{1}{\pi(R-\xi)} F_{zrz}(s, R-\xi) + G_{zrz}(R-s, 0, \xi, 0) \right) \end{array} \right] \tag{9-41}$$

$$\sigma_{zz}(s,0) = \frac{2\mu}{(\kappa+1)} \left[\begin{array}{l} b_r^o \left(\dfrac{1}{\pi(R-\xi)} F_{rzz}(s, R-\xi) + G_{rzz}^o(R-s, 0, \xi, 0) \right) \\ + b_z \left(\dfrac{1}{\pi(R-\xi)} F_{zzz}(s, R-\xi) + G_{zzz}(R-s, 0, \xi, 0) \right) \end{array} \right] \tag{9-42}$$

where

$$F_{z\theta}(s, R-\xi) = \frac{1}{2\left[\left(\dfrac{s}{R-\xi} \right)^{1/3} + \left(\dfrac{s}{R-\xi} \right) \right]} \left[\begin{array}{l} 0.9106 - 0.46 \left(\dfrac{s}{R-\xi+s} \right) \\ + 2.055 \left(\dfrac{s}{R-\xi+s} \right)^2 - 1.545 \left(\dfrac{s}{R-\xi+s} \right)^3 \end{array} \right] \tag{9-43}$$

$$\begin{aligned} F_{rrz}(s, R-\xi) &= F_{zzz}(s, R-\xi) \\ &= \frac{1}{\left(\dfrac{s}{R-\xi} \right)^{0.4555} + \left(\dfrac{s}{R-\xi} \right)} \left[\begin{array}{l} 0.3650 + 0.1416 \left(\dfrac{s}{R-\xi+s} \right) \\ + 3.942 \left(\dfrac{s}{R-\xi+s} \right)^2 - 3.450 \left(\dfrac{s}{R-\xi+s} \right)^3 \end{array} \right] \end{aligned} \tag{9-44}$$

$$F_{rzz}(s,R-\xi)=\frac{1}{\left(\frac{s}{R-\xi}\right)^{0.4555}+\left(\frac{s}{R-\xi}\right)^{1.45}}\left[\begin{array}{l}-0.8416+3.602\ \frac{s}{R-\xi+s}\\ -3.146\left(\frac{s}{R-\xi+s}\right)^{2}+0.6288\left(\frac{s}{R-\xi+s}\right)^{3}\end{array}\right] \tag{9-45}$$

$$F_{zrz}(s,R-\xi)=\frac{1}{\left(\frac{s}{R-\xi}\right)^{0.4555}+\left(\frac{s}{R-\xi}\right)^{1.45}}\left[\begin{array}{l}-0.2726-1.016\left(\frac{s}{R-\xi+s}\right)\\ +2.333\left(\frac{s}{R-\xi+s}\right)^{2}-0.3687\left(\frac{s}{R-\xi+s}\right)^{3}\end{array}\right] \tag{9-46}$$

Figure 9-4 displays results for sample cases to show continuity between the asymptotic forms just described and the general axi-symmetric solution. This has been done by focusing on the region $0.9 \le r/R \le 1$, $0.9 \le \xi/R \le 1$. In each plot the solid line represents the plane/antiplane solution whereas the dotted line is the true axi-symmetric solution. The asymptotic form given in section 9.4.1 should be used when the observation point is extremely close to the corner.

(a)

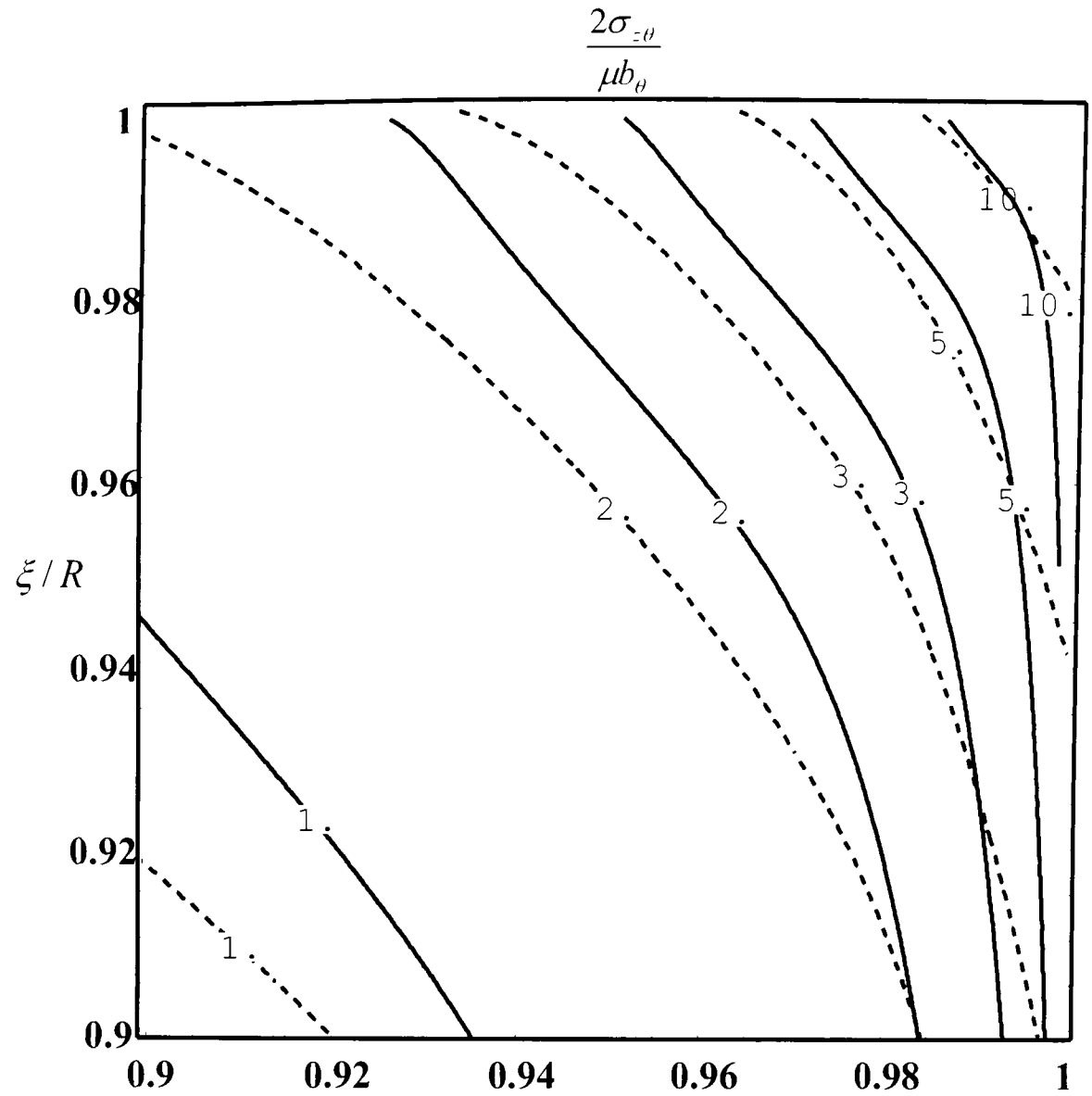
$\frac{2\sigma_{z\theta}}{\mu b_\theta}$
1
0.98
0.96
0.94
0.92
0.9
ξ / R
0.9
0.92
0.94
0.96
0.98
1
r/R
10.
10.
5.
5.
3.
3.
2.
2.
1.
1.

(b)

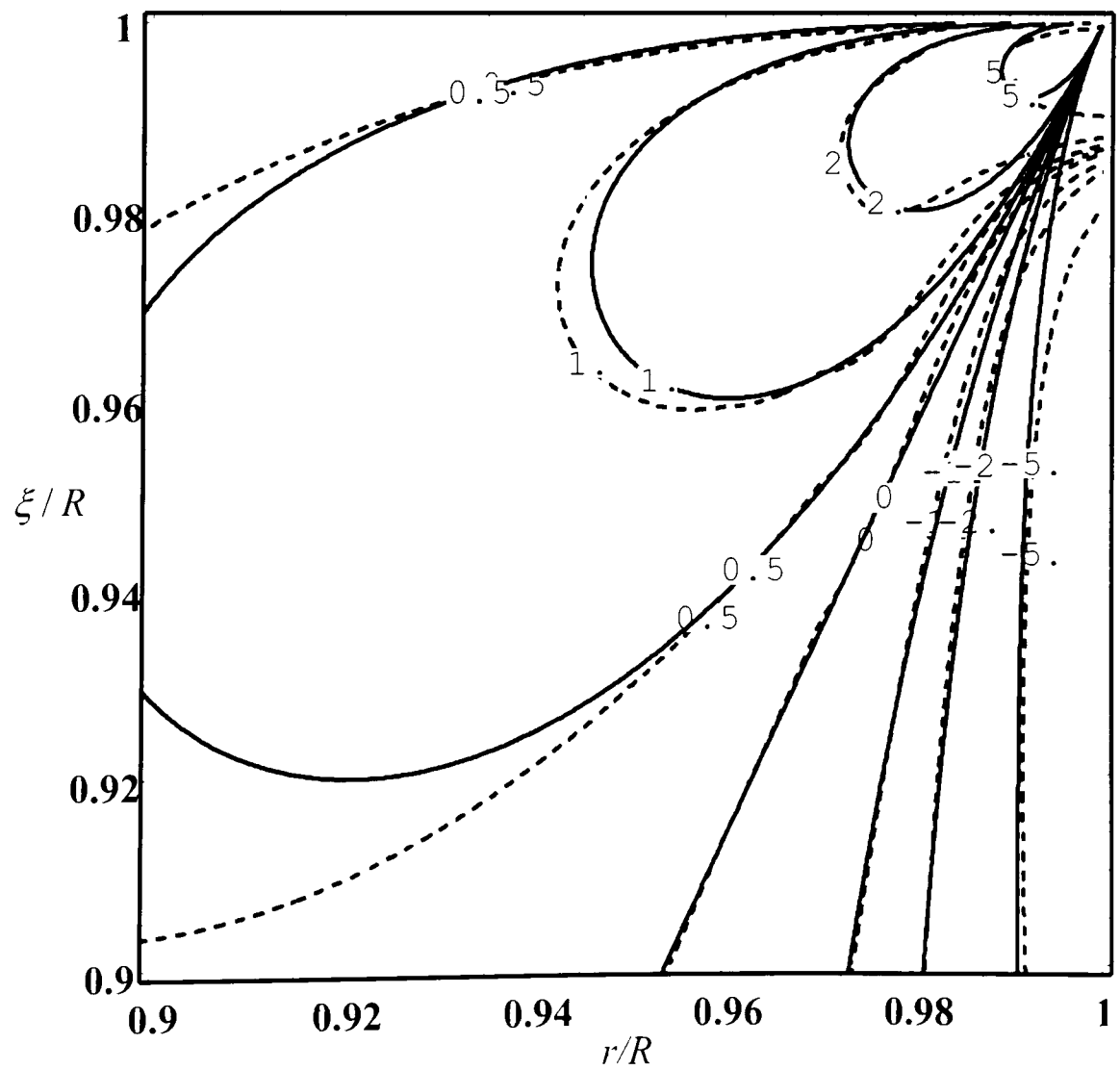
$\frac{2\sigma_{rr}}{\mu b_r}$
1
0.98
0.96
0.94
0.92
0.9
ξ / R
0.9
0.92
0.94
0.96
0.98
1
r/R
0.5
0.5
0.5
0.5
1.
1.
2.
2.
5.
5.
-2
-5.
-5.

(c)

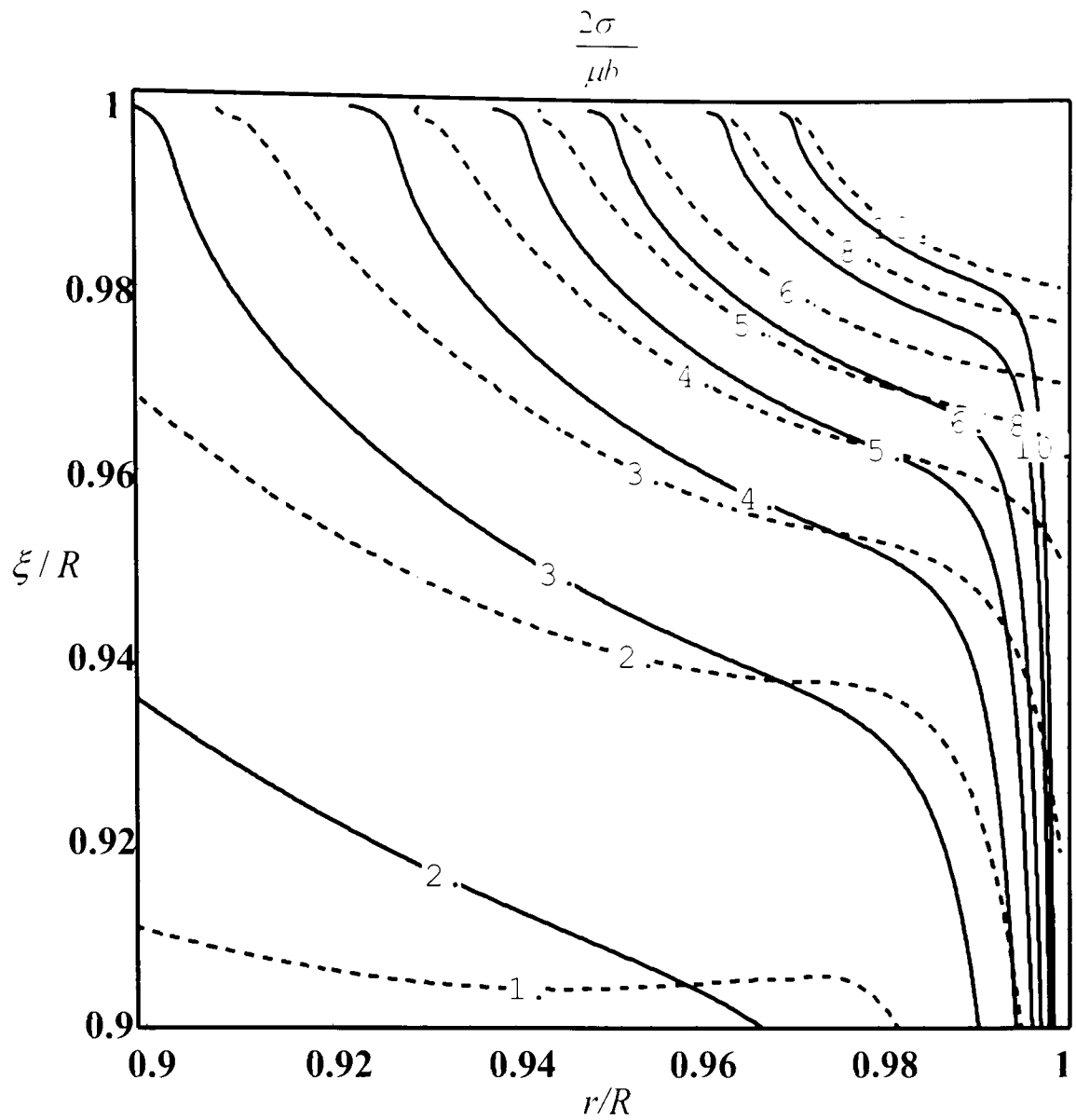
$\frac{2\sigma}{\mu b}$
1
0.98
0.96
0.94
0.92
0.9
ξ / R
0.9
0.92
0.94
0.96
0.98
1
r/R
1
2
3
4
5
6
8
10

(d)

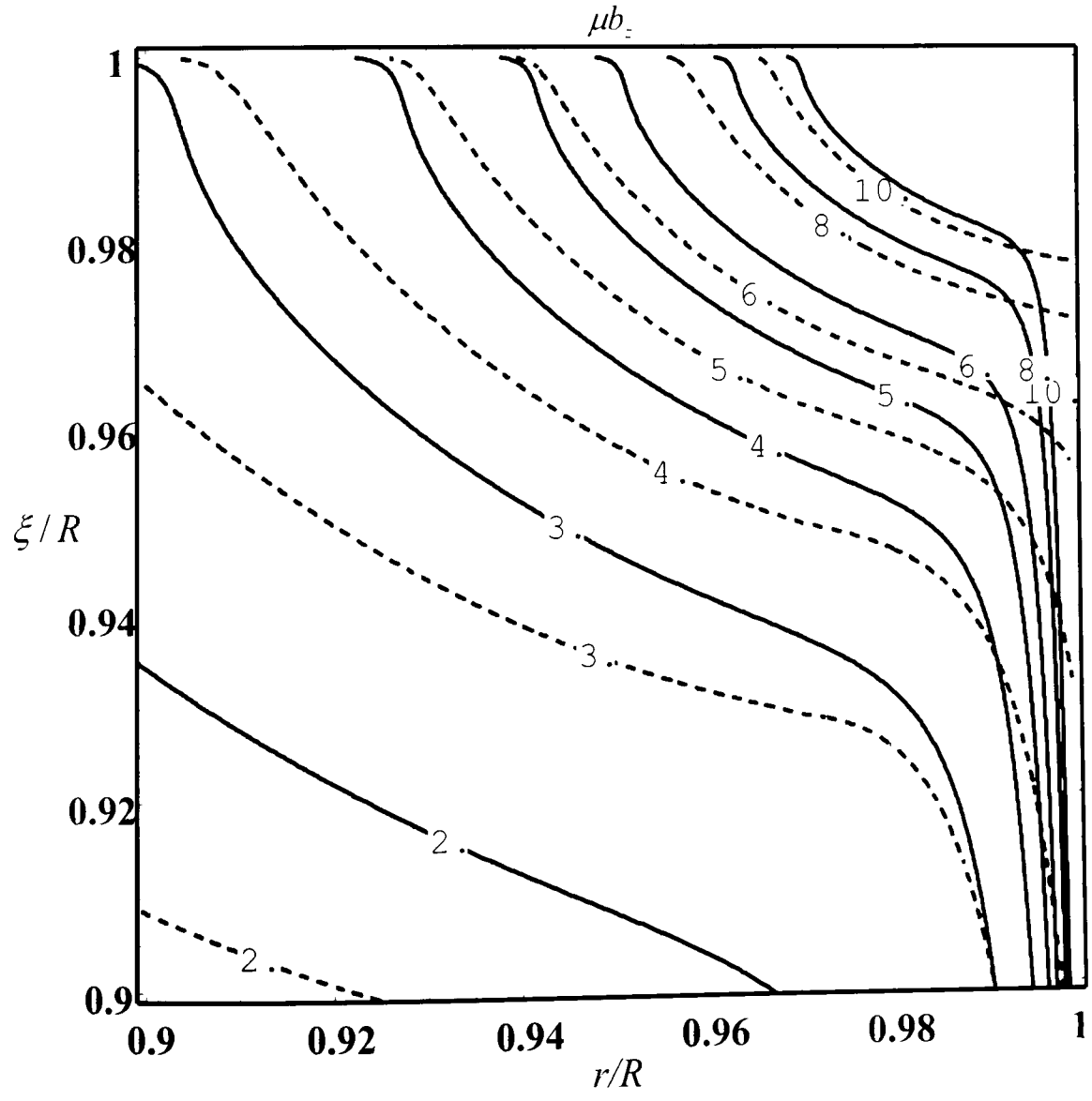
$\frac{2\sigma_{zz}}{\mu b_z}$
1
0.98
0.96
0.94
0.92
0.9
ξ / R
0.9
0.92
0.94
0.96
0.98
1
r/R
2
3
4
5
6
8
10

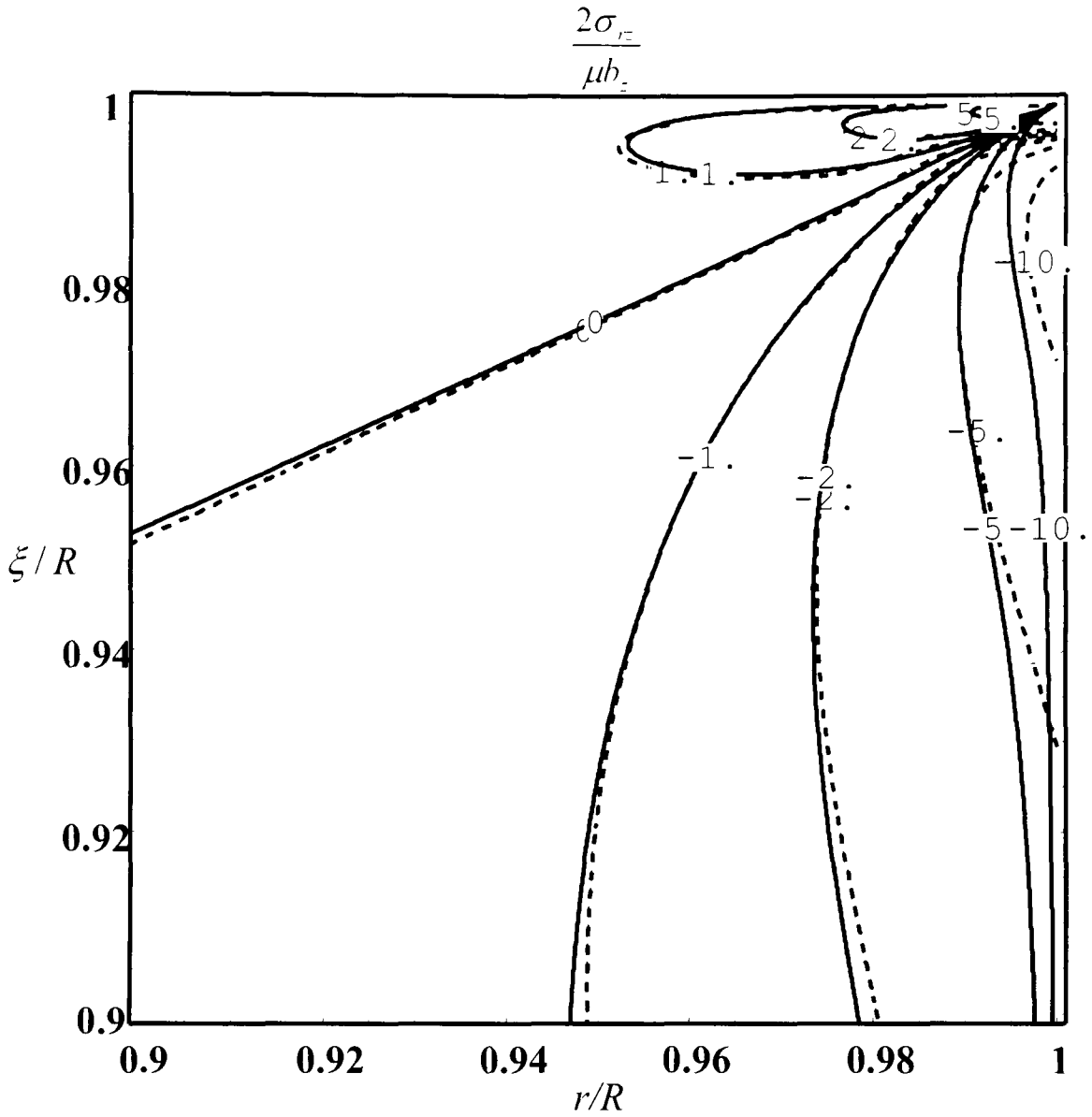

Figure 9-4: Asymptotic plane/antiplane approximation when object dislocation and observation points both approach the corner. Solid line represents the plane/antiplane solution whereas the dotted line is the true axi-symmetric solution.

(a) $\sigma_{z\theta}$ component of stresses induced by screw dislocation b_θ.

(b) σ_{zz} component of stresses induced by edge dislocation b_r.

(c) σ_{rz} component of stresses induced by edge dislocation b_r.

(d) σ_{zz} component of stresses induced by edge dislocation b_z.

(e) σ_{rz} component of stresses induced by edge dislocation b_z.

Chapter 10

Torsional Contact of an Elastic Flat-Ended Cylinder

10.1 Introduction

Complete contacts are hard to analyse analytically, because traditional half-space idealisations of the contacting bodies may not be used [1], and closed-form elasticity formulations for other domains are usually intractable. It is therefore necessary to fall back on purely numerical approaches such as the finite element method or boundary element method. However, it is usually very difficult to obtain sufficient detail, particularly around the contact edges and in the presence of friction, for the precise evolution of the contact stress field, together with the stick/slip zone regime, to be defined. Also, it should be stated that, in incomplete contacts it is perfectly feasible to separate the contact problem from the load paths and functioning of the remainder of the structure, but in complete contacts this is not so, i.e. the contact stress field will depend, to some extent, on the geometry and precise nature of the applied loads, significantly away from the contacting interface. However, a good way both to add detail to a numerical solution and to add generality to the applicability of the results is to

[1] In many textbooks complete contact problems are often solved by assuming that the body defining the size of the contact is rigid. This is a legitimate procedure, of course, but it has a very major effect on the stick-slip pattern at the contact edge, because of the elastic mismatch. This remains true even when the half-space is incompressible.

use a formulation appropriate to a semi-infinite wedge, which may be used to represent the corner of the body which defines the size of the contact, whilst the contacting body is represented by a half-space. Fundamental solutions in which the very near-edge state of stress is evaluated have been known for some time; if the contact is locally adhered the Williams solution (Williams, 1952) is appropriate, whilst if the contact is locally slipping the Gdoutos & Theocaris (Gdoutos and Theocaris, 1975) and Comninou (Comninou, 1976) solutions apply. These would seem, *prima facie*, to describe the local solution completely, but in fact there are many additional properties of the contact which stem from the asymptotes but become apparent only when they are embedded in an example problem (Karuppanan *et al.*, 2008). One very significant example is that of an elastic punch having square sides which, when pressed onto an elastically similar half-plane and dragged along against friction, lifts its trailing edge of contact and separates locally if the coefficient of friction, f, exceeds $1/\pi$. In the problems we have addressed to date the contacts have been plane, and the frictional shearing traction has always acted perpendicular to the line defining the contact edge. Here, we take a further step by looking at an example problem in which the shearing traction may have a component parallel with the contact edge. This is very important because it introduces many additional features, of a generic kind, into the problem. A plane/antiplane sliding contact was considered as a vehicle for studying the phenomenon, but this was abandoned because of the inability of most finite element packages to analyze problems of this kind and, instead, an axi-symmetric torsion problem was studied.

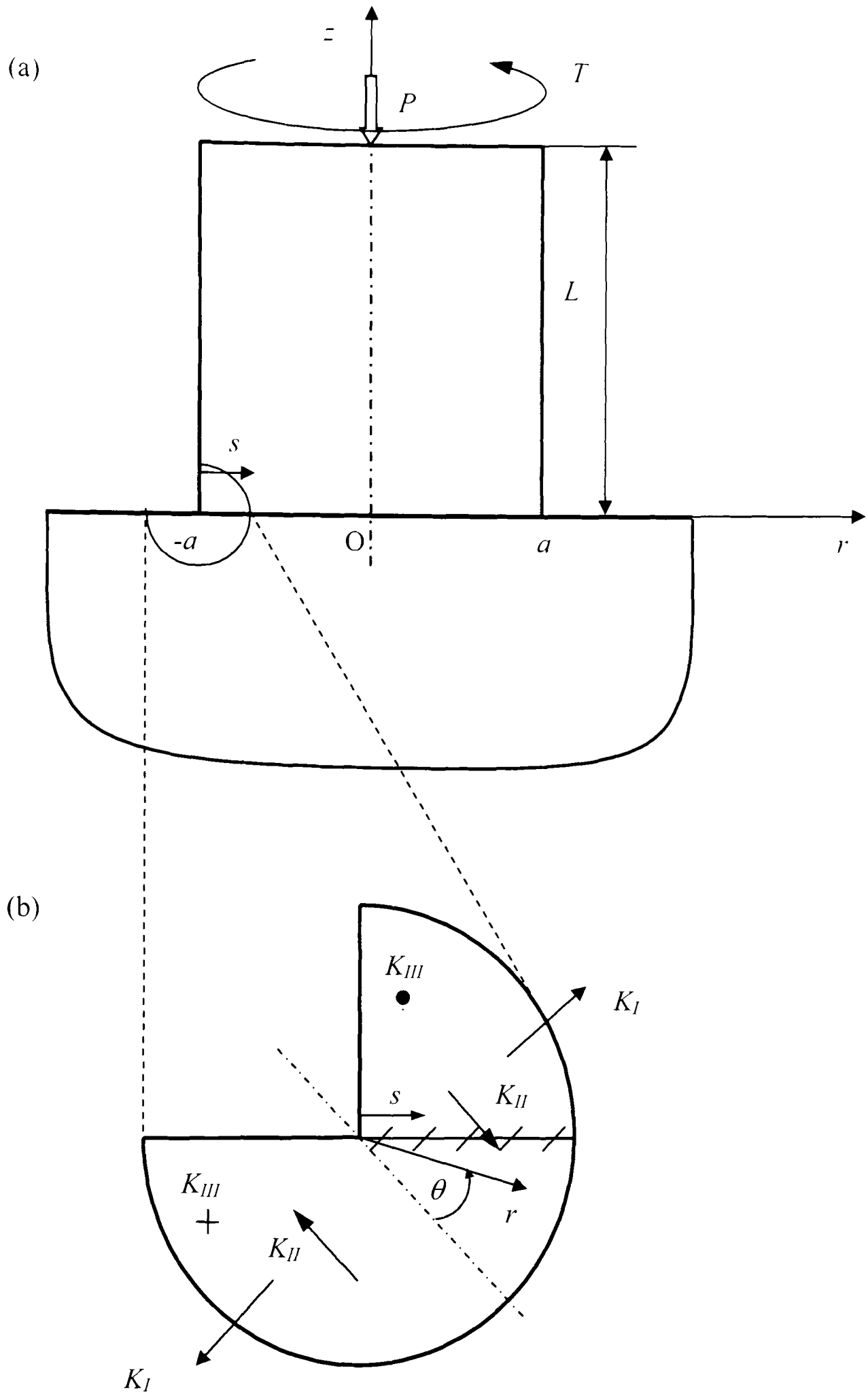

Figure 10-1: (a) A cylinder pressed into a half-space under the normal load P and subject to a torque T. (b) A close up view of the contact edge

The problem we chose to analyze is depicted in Figure 10-1(a). It consists of a half-space, into which is pressed an elastically similar cylinder of radius a, and assumed to be very long ($L >> a$). The interfacial coefficient of friction is f, and the normal load pressing the two bodies into contact is P. Some elements of the solution may be found from either a finite element analysis or, as here, using a dislocation array to develop both the loaded state and correct interfacial conditions, whilst a detailed study of the edge of the contact disk may be conducted using asymptotic analysis: in doing this, the standard plane asymptotic form is inserted on a $\theta = 0$ constant plane, Figure 10-1(a, b), and this is appropriate for characterising the state of stress induced by a normal load alone. When a torque is applied a θ direction displacement is induced, and hence the anti-plane asymptotic forms are excited. The first step in understanding the details of the problem is therefore to look at the conditions for adhesion. This is not easy to achieve using a finite element analysis because the contact tractions all become infinite at the contact edge, and hence, working out the ratio of shear to direct traction is hampered.

10.2 Full Stick Case

Figure 10-1 (b) shows a close up view of the contact edge. The cylinder is assumed to be stuck to the half-space right up to the edge of the contact, so that, local to the contact corner, the two bodies may be considered as a monolithic wedge of total included angle $3\pi/2$ radians. The local state of stress may be analysed using the Williams procedure; although the symmetric and anti-symmetric solutions naturally uncouple along the bisector line, we shall, here, focus on the traction components of stress arising along the trace line of the interface. The symbols K_I, K_{II}, K_{III} are the conventionally defined multipliers on the eigensolutions, using the stresses present along the wedge bisector, whilst those with a superscript ^{0} relate to

the adhered tractions along the interface. Details of the Williams solution are given in the original paper (Williams, 1952), amplified in Barber (Barber, 2002), and in the form used here were introduced in (Churchman and Hills, 2006a). Thus, the contact pressure, $p^0(s)$, radial shearing traction, $q_r^0(s)$ and circumferential shearing stress, $q_\theta^0(s)$ are given by

$$p^0(s) = K_I^0 s^{\lambda_I - 1} + K_{II}^0 s^{\lambda_{II} - 1}, \tag{10-1}$$

$$q_r^0(s) = K_I^0 s^{\lambda_I - 1} g_{r\theta}^I + K_{II}^0 s^{\lambda_{II} - 1} g_{r\theta}^{II}, \tag{10-2}$$

$$q_\theta^0(s) = K_{III}^0 s^{\lambda_{III} - 1}, \tag{10-3}$$

where s is measured inward from the edge, and the eigenvectors and eigenvalues are

$$\lambda_I = 0.5445, \quad \lambda_{II} = 0.9085, \quad \lambda_{III} = 1/3, \tag{10-4}$$

$$g_{r\theta}^I = 0.543, \quad g_{r\theta}^{II} = -0.219, \tag{10-5}$$

$$K_I^0 = 0.7304 K_I, \qquad K_{II}^0 = -1.087 K_{II}, \qquad K_{III}^0 = 0.866 K_{III}. \tag{10-6}$$

The anti-plane solution is, of course, uncoupled from the two in-plane solutions. The values of the stress intensity factors were found from an analysis of the cylinder/half-space monolith using the definitions (in the coordinate set of Figure 10-1(b))

$$K_I = \sigma_{rr} r^{1-\lambda_I} \quad Lt\ r \to 0, \qquad \theta = 0, \tag{10-7}$$

$$K_{II} = \sigma_{r\theta} r^{1-\lambda_{II}} \quad Lt\ r \to 0, \qquad \theta = 0, \tag{10-8}$$

$$K_{III} = \sigma_{rz} r^{1-\lambda_{III}} \quad Lt\ r \to 0, \qquad \theta = 0. \tag{10-9}$$

This could have been done by using a commercial finite element analysis package, but here an alternative approach, giving quicker convergence, was adopted. The state of stress induced in the body by the normal load, P, and torque, T, maybe found by employing an array of ring dislocations, within the shaft part of the component. The state of stress induced by ring climb and twist dislocations in this domain has been found (Paynter, Hills and Korsunsky, 2007). Initially, as complete adhesion is assumed, it is necessary only to ensure that, remote from the interface ($z >> a$), a uniform direct strain (ε_{zz}) is present, together with a linearly varying

shear strain ($\varepsilon_{r\theta} \sim r$). For brevity, details of the calculation are omitted, but the contact pressure and shearing traction distributions ($p^{(1)}(s) \equiv \sigma_{zz}(s,0)$, $q^{(1)}(s) \equiv \sigma_{rz}(s,0)$, $s = a - r$), are included in Figure 10-2. By exploiting the definitions of the stress intensity factors just given, the following results were found

$$\begin{bmatrix} K_I^0 a^{1-\lambda_I} \\ K_{II}^0 a^{1-\lambda_{II}} \\ K_{III}^0 a^{1-\lambda_{III}} \end{bmatrix} = \begin{bmatrix} -0.07773 & 0 \\ -0.08897 & 0 \\ 0 & 0.2517 \end{bmatrix} \begin{bmatrix} \frac{P}{a^2} \\ \frac{T}{a^3} \end{bmatrix}. \tag{10-10}$$

It is noted that the normal load excites both in-plane eigensolutions, but that the mode I solution is more strongly singular. Consequently, as an observation point moves near to the contact edge, the mode I solution dominates the other two and assuming, for the time being, that the controlling point is the extreme contact edge, it is clear that the ratio of shear to direct traction is given by (Churchman and Hills, 2006a)

$$\frac{q}{p} = \frac{K_I^0 s^{1-\lambda_I} g_{r\theta}^I}{K_I^0 s^{1-\lambda_I}} = g_{r\theta}^I = 0.543. \tag{10-11}$$

It follows that, as with the complete plane problem, adhesion will be maintained to the contact edge, on applying the normal contact force, providing that $f > 0.543$. If this inequality does not hold, when the normal load is applied, a region of radial slip exists around the contact periphery. Its width increases with decreasing coefficient of friction, but is independent of the applied normal load.

As with the complete plane problem, adhesion will be maintained to the contact edge, on applying the normal contact force, providing only that $f > 0.543$, and this boundary is shown prominently in Figure 10-3(a) as point A. If this inequality does not hold, when the normal load is applied, a region of radial slip exists around the contact periphery. Its width increases with decreasing coefficient of friction, but is independent of the applied normal load.

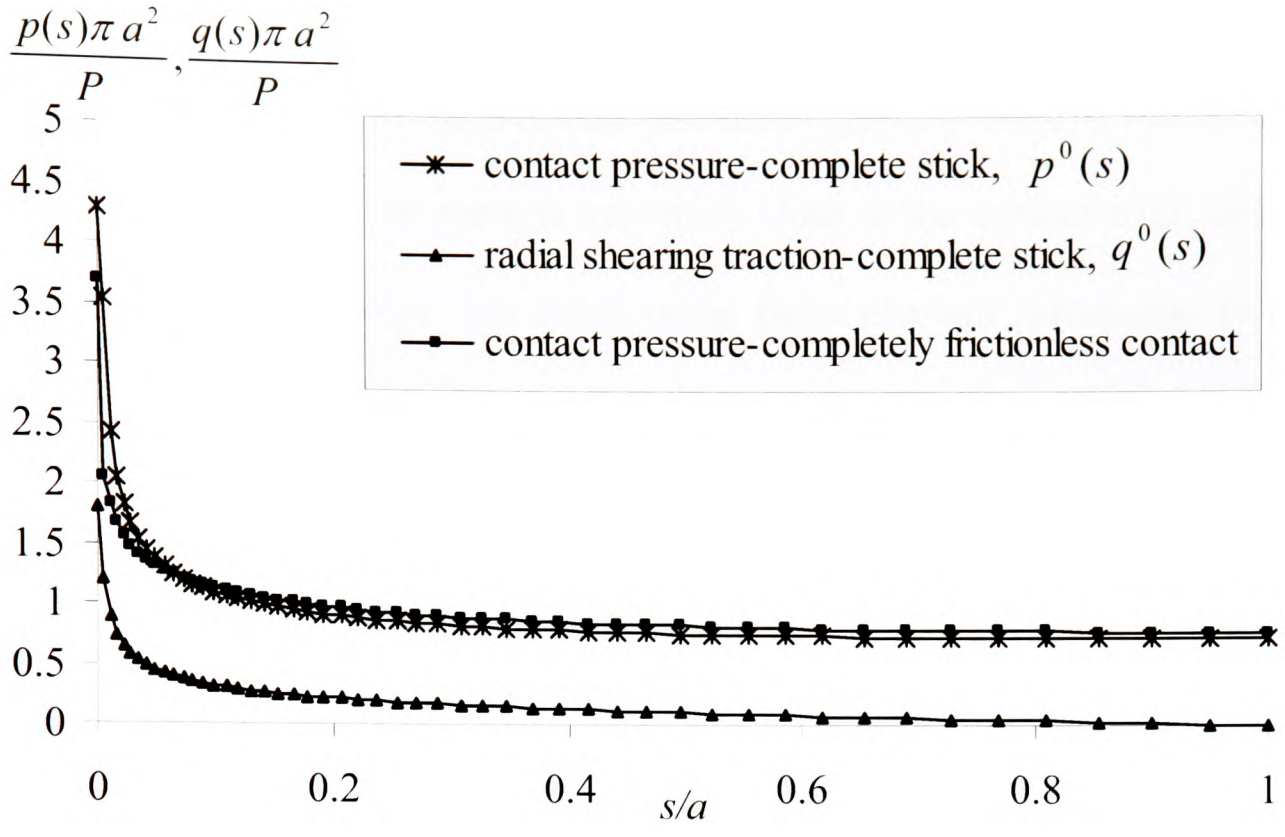

Figure 10-2: Contact pressure and radial shearing traction under complete stick and spinning condition.

If the coefficient of friction exceeds 0.543 the application of a normal load alone causes stick over the entire punch face. Both the symmetric (mode I) and antisymmetric (mode II) eigensolutions are excited, but the ratio between them is fixed (as implied by equation 10-10 and the traction ratio q_r / p decreases monotonically with s. It should be noted that the three eigenvalues lie in the order $0 < \lambda_I < \lambda_{III} < \lambda_{II} < 1$. Therefore when a torque is applied and the anti-plane eigensolution is also excited, an internal turning point in the ratio q/p may appear, where

$$q^2(s) = q_r^2(s) + q_\theta^2(s). \tag{10-12}$$

This indicates that limiting friction will be encountered at an internal point first. The turning point is, in fact, located very close to the edge, so that the tractions are properly described by the asymptotes, and the ratio *T/Pa* at which there is incipient slip is easily found by locating

the turning point, and setting the traction ratio to the coefficient of friction, f. The results of this calculation are summarised in Figure 10-3(a) which gives the torque at which slip starts (line A B), and the position of the point of first slip, Figure 10-3(b). It will be noted that, in practice, the point at which slip starts is extremely close to the contact edge, and it would be very difficult indeed to resolve this detail using finite element calculation results without using the asymptotes, as a ratio between two large numbers is being sought at a position where it is very difficult to achieve convergence. It is interesting to note that, for coefficients of friction above 0.6, the range of normalised torque where partial slip occurs is narrow, so that there is quite an abrupt transition from complete adhesion to spinning.

(a)

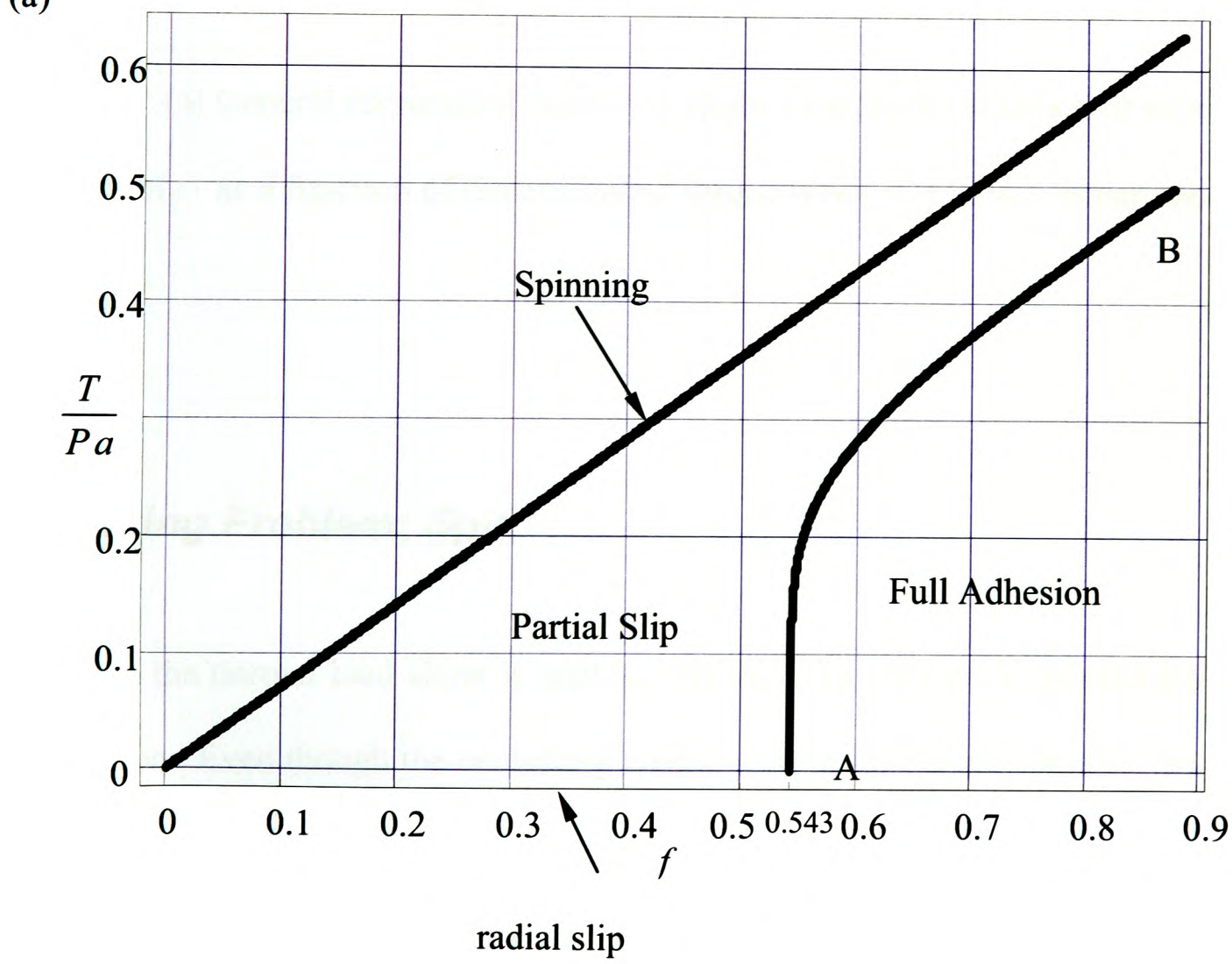

(b)

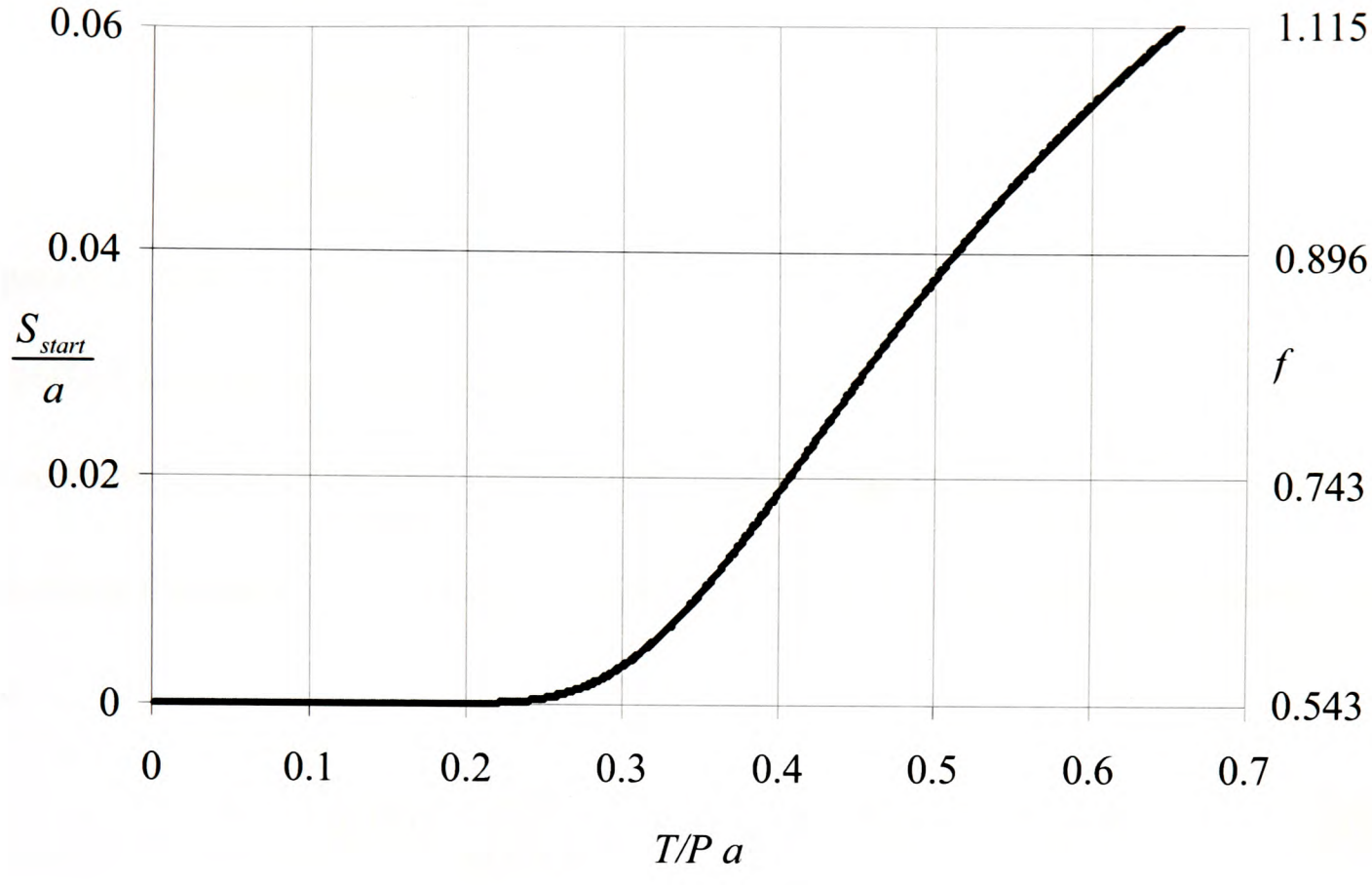

Figure 10-3: (a) General response of contact to applied torque (b) Location of maximum of ratio $q(s)/p(s)$ as a function of dimensionless torque when $f > 0.543$, under condition of full stick.

10.3 Limiting Problem: Spin

When the normal load alone is applied, the shearing traction is directed purely in the radial direction. Even though the contacting components are elastically similar, the shear and direct traction distributions are coupled because the domains representing the two bodies are very different. The next stage in the development of the solution is to determine what happens under conditions of 'spin', when the applied torque is sufficient to permit a rigid-body rotation of the shaft with respect to the half-space, and this, too, permits a sweeping

simplification, viz. that the shearing traction is now directed in a purely circumferential direction (i.e. perpendicular to the initial direction), and with a magnitude given by

$$q_\theta(r) = fp(r) \quad (r \le a). \tag{10-13}$$

It should be noted that coupling occurs only between the radial component of shearing traction and the contact pressure so that, when the contact is spinning, the pressure is the same as that present under a normal load alone, but when the coefficient of friction vanishes, i.e. there is perfect lubrication. The contact pressure distribution present may be found from the adhered solution, $p_o(r)$ already found, by deploying an array of radial glide dislocations, with path puts along the plane $z = 0$, along that plane, i.e. by finding the dislocation density, $B_r(r)$ such that

$$q_o(r) + \frac{2\mu}{\pi(\kappa+1)} \int_0^a G_{rr}(r,\rho) B_r(\rho) d\rho = q_r(r) = 0, \tag{10-14}$$

where G_{rr} is defined by

$$\frac{2\mu}{\pi(\kappa+1)} b_r(\rho) G_{rr}(r,\rho) = \sigma_{rz}(r), \tag{10-15}$$

and is given explicitly in (Qiu, Paynter, Dini and Hills, 2008). When once this has been done the modified contact pressure can be found from

$$p_o(r) + \frac{2\mu}{\pi(\kappa+1)} \int_0^a G_{rz}(r,\rho) B_r(\rho) d\rho = p(r), \tag{10-16}$$

where G_{rz} is defined by

$$\frac{2\mu}{\pi(\kappa+1)} b_r(\rho) G_{rz}(r,\rho) = \sigma_{zz}(r), \tag{10-17}$$

and again is given explicitly in (Qiu, Paynter, Dini and Hills, 2008). Lastly, the torque supported when friction is present is found from

$$T = 2\pi \int_0^a r^2 p(r) dr, \tag{10-18}$$

and this gives the immediate result

$$\frac{T}{f P a} = 0.712059. \tag{10-19}$$

The contact pressure distribution is included in Figure 10-2, and equation 10-19 provides the gradient of the limit state line in Figure 10-3(a).

Just as the Williams' solution can describe the stress distribution at the extreme contact edge under conditions of adhesion, so the Gdoutos and Theocaris (Gdoutos and Theocaris, 1975) and Comninou (Comninou, 1976) solution can describe the condition there when slip is present. In this section on spin, we will quote the relevant asymptotic form. As the radial shearing traction vanishes, we need to look at the characteristic equation which corresponds to $f_r = q_r / p = 0$. The contact pressure varies as $p(s) \sim s^{\lambda_s - 1}$ where λ_s is given by the smallest solution of

$$\nabla(\lambda_s) = \cos \lambda_s \pi (\sin^2(\frac{\lambda_s \pi}{2}) - \lambda_s^{\,2}) + \frac{1}{2}\sin^2(\lambda_s \pi) = 0. \tag{10-20}$$

The root is given by $\lambda_s = 0.774$.

10.4 Initial Slip

In this section we return to the transient problem, where initially a normal load alone has been applied, and we investigate the influence of applying a monotonically increasing torque. Two cases can be distinguished; first, when the coefficient of friction is high ($f > g^I_{r\theta}$) we know that slip starts at an interior point, and migrates both inwards and outwards as the torque is increased. On the other hand, at low coefficients of friction ($f < g^I_{r\theta}$) there is an initial slip annulus, attached to the outside of the contact disk, and the stick-slip boundary migrates inwards as the torque is increased. In the following paragraphs we will develop the

family of equations which have to be satisfied in order to track out the behaviour of the contact, and which is, in the form written, common to both regimes.

At any general point in time, when the current torque supported is T, the tractions present q_r, q_θ, p are given by

$$q_r(s,T) = q_r^0(s,T) + \frac{2\mu}{\pi(\kappa+1)} \int_{slip} B_r(\xi,T) G_{rrz}(s,\xi) d\xi \tag{10-21}$$

$$q_\theta(s,T) = q_\theta^0(s,T) + \frac{\mu}{2\pi} \int_{slip} B_\theta(\xi,T) G_{\theta z}(s,\xi) d\xi \tag{10-22}$$

$$p(s,T) = p^0(s,T) + \frac{2\mu}{\pi(\kappa+1)} \int_{slip} B_r(\xi,T) G_{rzz}(s,\xi) d\xi \tag{10-23}$$

where p^0, q_i^0 are the tractions implied by the bilateral adhered solution, μ is the modulus of rigidity, κ Kolsov's constant, $G_{rrz}(s,\xi)$ $G_{\theta z}(s,\xi)$ $G_{rzz}(s,\xi)$ are ring dislocations stress influence functions, and the integrals are evaluated over the slipping region. Also $B_r(\xi,T)$ is the edge dislocation density, $B_\theta(\xi,T)$ is the screw dislocation density and

$$B_r(\xi,T) = \frac{du_r(\xi,T)}{d\xi}, \quad B_\theta(\xi,T) = \frac{du_\theta(\xi,T)}{d\xi}. \tag{10-24}$$

Within the slip region we have

$$[q_r(s,T)]^2 + [q_\theta(s,T)]^2 = f^2 p^2(s,T), \ \ s \in slip\,region \tag{10-25}$$

$$P = \int_0^a 2\pi r\, p(a-r,T) dr \tag{10-26}$$

$$T = \int_0^a 2\pi r^2\, q_\theta(a-r,T) dr \tag{10-27}$$

and the slip displacements are

$$u_r(s,T) = \int_c^s B_r(\xi,T) d\xi, \ \ 0 < s < c \tag{10-28}$$

$$u_\theta(s,T) = \int_c^s B_\theta(\xi,T) d\xi, \ \ 0 < s < c, \tag{10-29}$$

where c is the distance from the contact edge to the edge of the stick disk. Also, within the slipping region the frictional orthogonality principle must be satisfied, which may be imposed by requiring

$$\frac{\dfrac{du_r(s,T)}{dT}}{\dfrac{du_\theta(s,T)}{dT}} = \frac{q_r(s,T)}{q_\theta(s,T)}, \qquad \frac{du_i}{dT} = \frac{du_i}{dt}\frac{dt}{dT}. \tag{10-30}$$

and t represents time. Strictly speaking these are time-derivatives but as $T \propto t$, we can replace t by T.

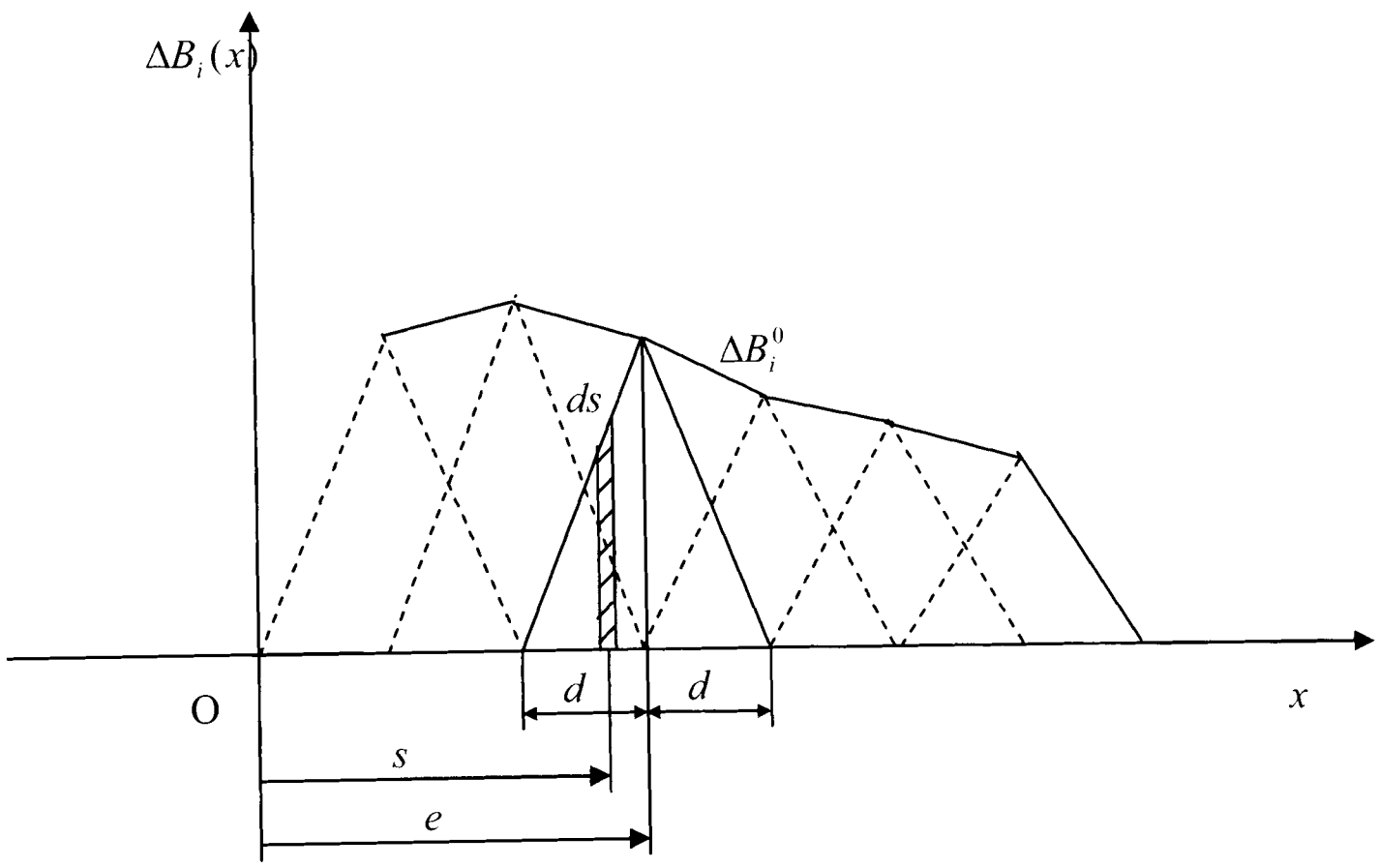

Figure 10-4: Triangle element of dislocations in a three-quarter plane

This is a formidably difficult set of equations to solve, with coupling implied by the orthogonality requirement, and also by the effect of radial shearing tractions on the contact pressure. No attempt was made to solve the equations in the form just stated, and two simplifications were made: first, it is clear from Figure 10-2 that the contact pressure does not

change very much as the solution evolves. It was therefore decided that the pressure distribution would be held constant at that present under a normal load, fully adhered. Secondly, it was decided not to attempt to solve the singular integral equations directly, but to replace the unknown dislocation densities by piecewise linear representations, in a manner analogous to that originally employed by Benthall and Johnson (Benthall and Johnson, 1968), and more recently adopted for skew-sliding problems (Qiu, Hills, Nowell and Dini, 2008, Qiu, Hills and Dini, 2008). It is still necessary to solve the problem incrementally, of course, because it is important, for orthogonality, for the increments of slip direction to be in proportion to the total shearing tractions present.

Figure 10-4 displays the general form of the two dislocation densities, $B_r(\xi,T)$, $B_\theta(\xi,T)$ to be found. Because we need to ensure that it is the change of displacement which is orthogonal to the shearing traction direction, this figure may be thought of as displaying not the total dislocation density, but the change in density corresponding to a general torque increment. A typical element is shown, in the form of a triangle centred at the position e, of half-width d, and of altitude ΔB_i^o. It follows that the total change ve slip displacement induced by the element is given by $u_i = \Delta B_i^o d$, and that the corresponding shearing tractions along the surface may be found by evaluating the following integrals

$$\begin{aligned}\Delta B_i(\xi) &= \Delta B_i^o\left(1-\frac{\xi-e}{d}\right) \quad e<\xi<e+d \\ &= \Delta B_i^o\left(1+\frac{\xi-e}{d}\right) \quad e-d<\xi<e\end{aligned} \tag{10-31}$$

$$\Delta\sigma_{rrz}(x,e,d) = \int_{e-d}^{e+d}\Delta B_r(\xi)G_{rrz}(x,\xi)d\xi \tag{10-32}$$

$$\Delta\sigma_{\theta z}(x,e,d) = \int_{e-d}^{e+d}\Delta B_\theta(\xi)G_{\theta z}(x,\xi)d\xi\,. \tag{10-33}$$

When once this has been done and 'look up' a table formed, the problem can be formulated and solved. It is now much easier to determine the strengths of the elements within the slip zone, by evaluating the traction from

$$q_r(s,T+\Delta T) = q_r(s,T) + \sum_{i=1}^{n-1} \Delta B_{ri}(s,T)\sigma_{ri}(s,e_i,d_i) \tag{10-34}$$

$$q_\theta(s,T+\Delta T) = q_\theta(s,T) + \sum_{i=1}^{n-1} \Delta B_{\theta i}(s,T)\sigma_{\theta i}(s,e_i,d_i) \tag{10-35}$$

and ensuring that the orthogonality requirement

$$\frac{\int_{c_1} \Delta B_r(\xi,T_j)d\xi}{\int_{c_1} \Delta B_\theta(\xi,T_j)d\xi} = \frac{q_r(s,T_j)}{q_\theta(s,T_j)}, \quad c_0 < s < c_1, \tag{10-36}$$

is satisfied at all points within the slip region.

In practice, we increase the applied torque until the first point slips (see 10-2). A small increment of torque is then applied, giving rise to a solitary element within the slip region. We solve for the dislocation densities at this point, and this information is stored. The torque is increased again. We re-solve for the increment in dislocation densities, ensuring that (a) the traction is pulled down to the precise slipping condition (equation 10-25) and (b) that the orthogonality requirement is satisfied (equations 10-30 or 10-36). The process is repeated until the required torque is reached.

10.5 Results

The results of the partial slip transient calculations are shown in Figures 10-5—10-9. First, for the example case when the coefficient of friction is 0.6 ($f > g^I_{r\theta}$) the point of initial slip is close to the edge ($s/a \cong 0.002$, at a torque ($T/fPa \cong 0.4714$), and the initial slip direction ϕ, measured relative to a radial line is at about 40°, Figure 10-5. As the torque is

increased beyond this value the slip annulus spreads both inwards (rapidly), and outwards, rather more slowly, Figure 10-6. The calculation was stopped at $T \quad fPa \cong 0.52$ only because, at this torque, the slip annulus is 10% of the contact disk radius, and this was chosen arbitrarily. The arrows in Figure 10-6 show graphically the slip direction at various torque levels and for various values of torque, and show how, qualitatively, the slip direction is gradually moving round towards a circumferential direction. More detailed information is provided in Figures 10-5.

For the case $f = 0.45$ ($f < g'_{r\theta}$), there is an initial radial annular slip region attached to the contact disk edge, and of approximate width $s/a \cong 0.08$, Figure 10-7. Further slip starts, of course, as soon as any torque is applied, and the growing width of the slip annulus is clear in Figure 10-7. Calculations were stopped at a *T/fPa* value of 0.4 again solely because this corresponds to a slip annulus which is 10% of the contact radius. The arrows in Figure 10-7 also display the gradual rotation of the local slip direction, which is rather more pronounced, here, than in the case of a confined slip region. More detailed information is provided in Figures 10-8.

Lastly, as a partial check on the solutions developed, and also to investigate what happens when the coefficient of friction is near to the critical value ($f \sim g'_{r\theta}$), three cases were examined in detail, viz. for coefficients of friction of 0.53 (slip band present on normal loading only), 0.56 (initially, stick everywhere), and 0.543 itself. Figure 10-9 displays the position of the inner stick slip boundary for these three cases. As expected, when $f < g'_{r\theta}$ the stick slip boundary starts to move inwards from an infinitesimal torque, whereas when $f > g'_{r\theta}$ slip does not start until $T/fPa \cong 0.4$. However, as the torque is increased further, the stick-slip transition radius implied by the two solutions gradually converge, as might intuitively be expected.

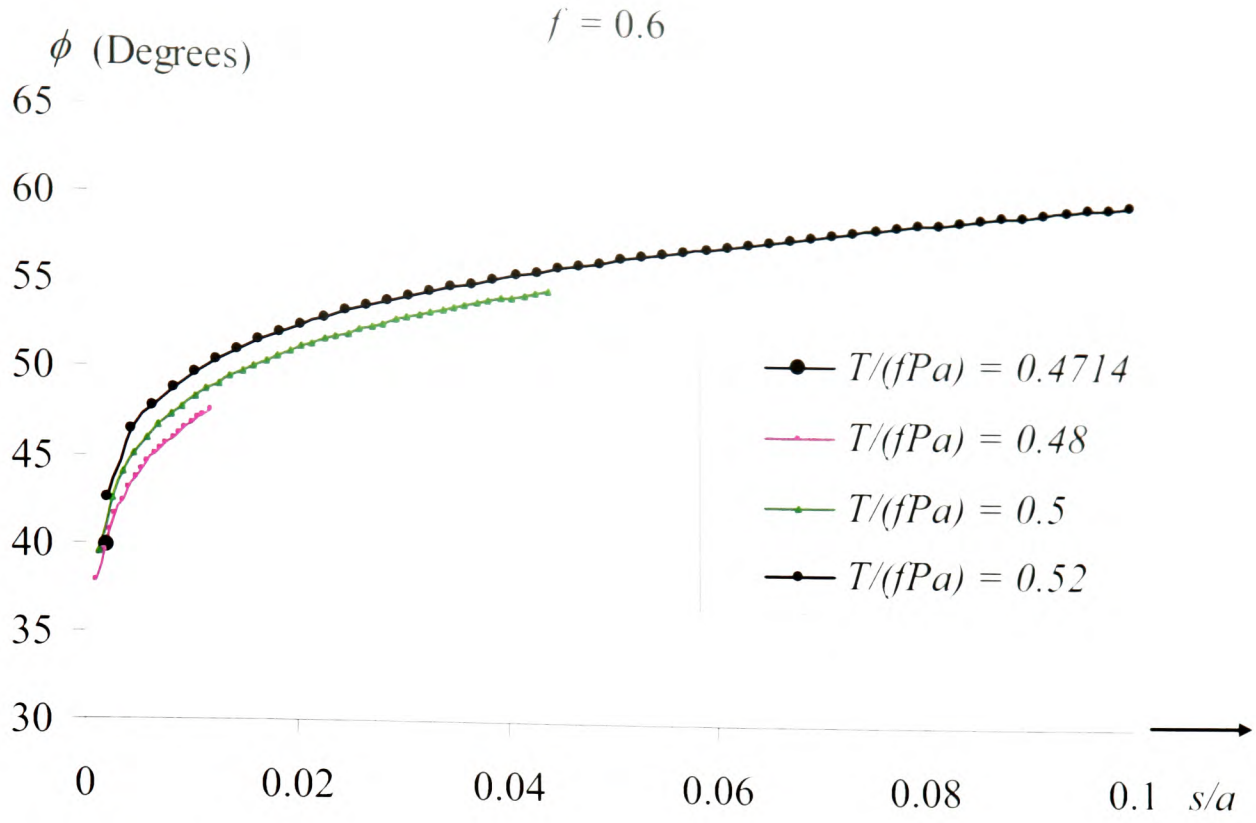

Figure 10-5: Local slip angles under different torsions for the case $f = 0.6$

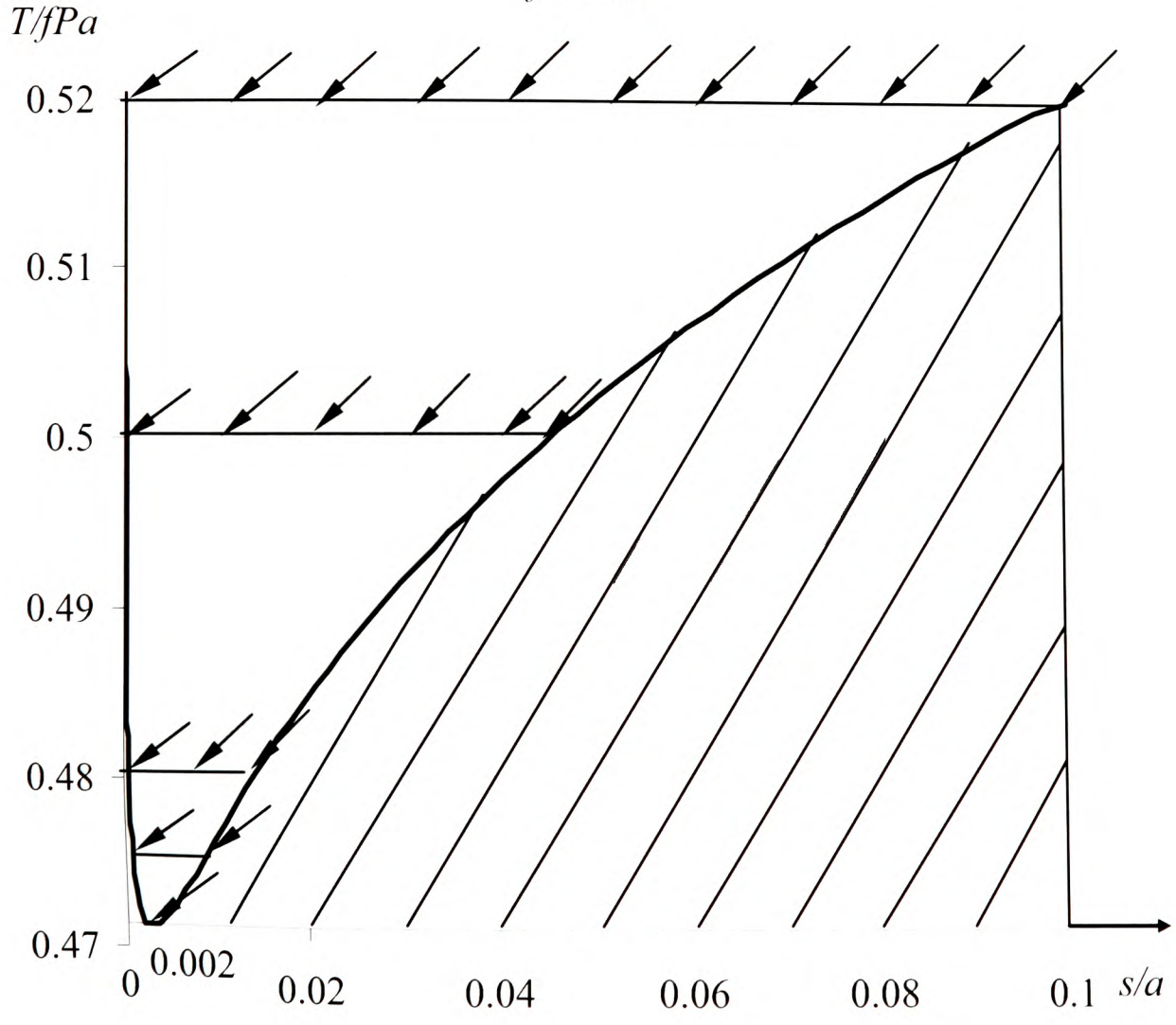

Figure 10-6: Slip region under different degrees of torsional load for the case $f = 0.6$

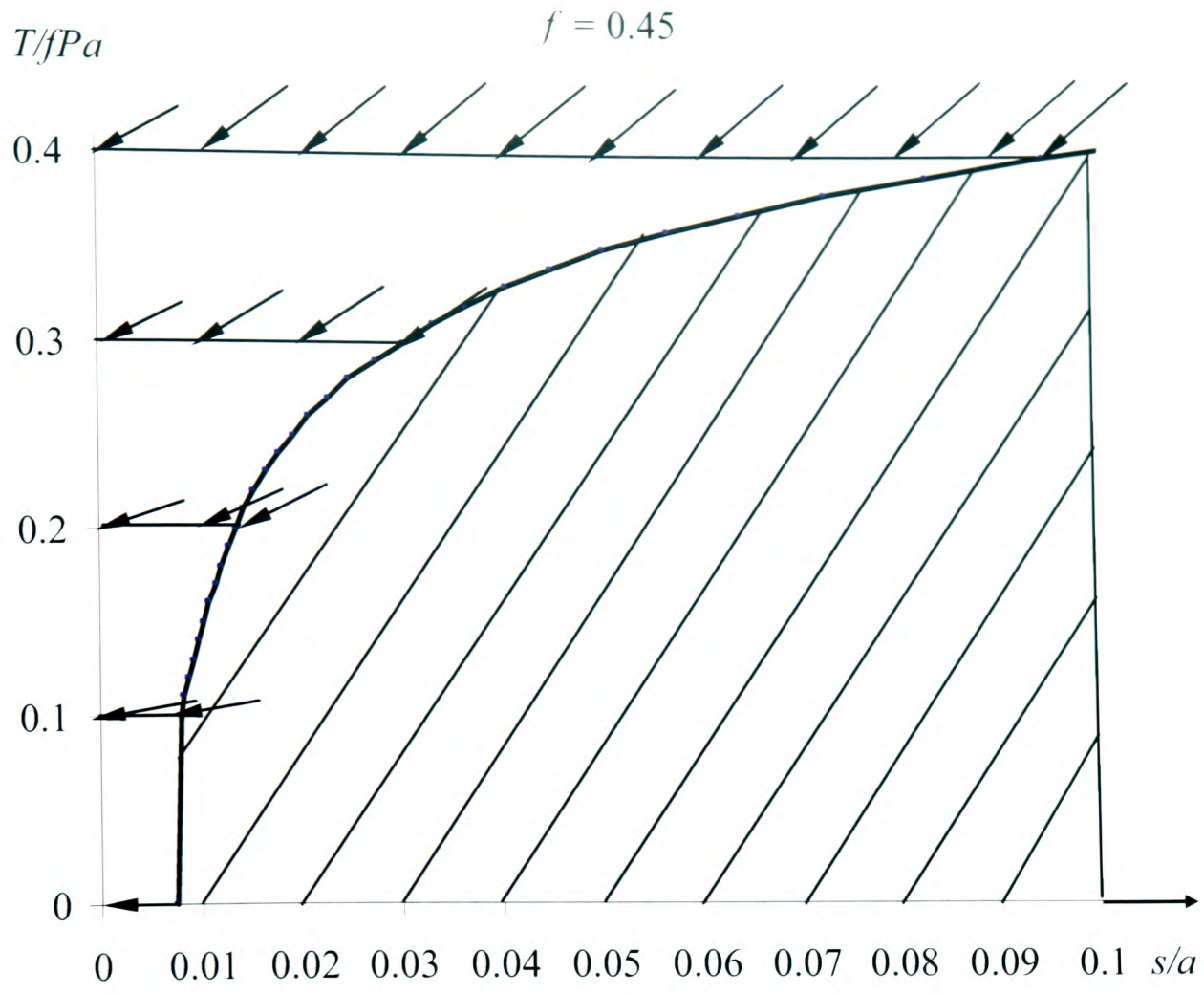

Figure 10-7: Slip region under different degrees of torsional load for the case $f = 0.45$

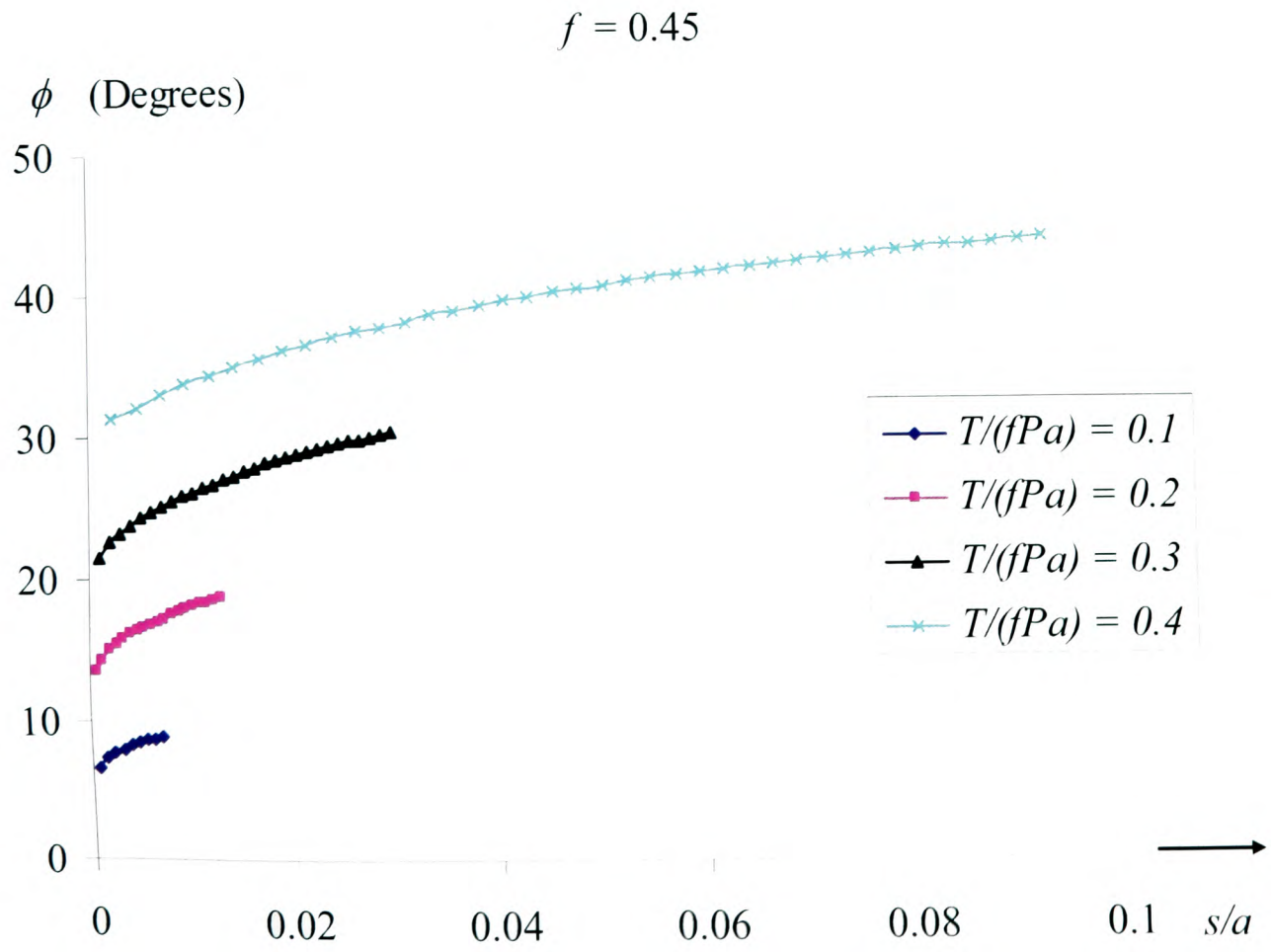

Figure 10-8: Local slip angles under different torsions for the case $f = 0.45$

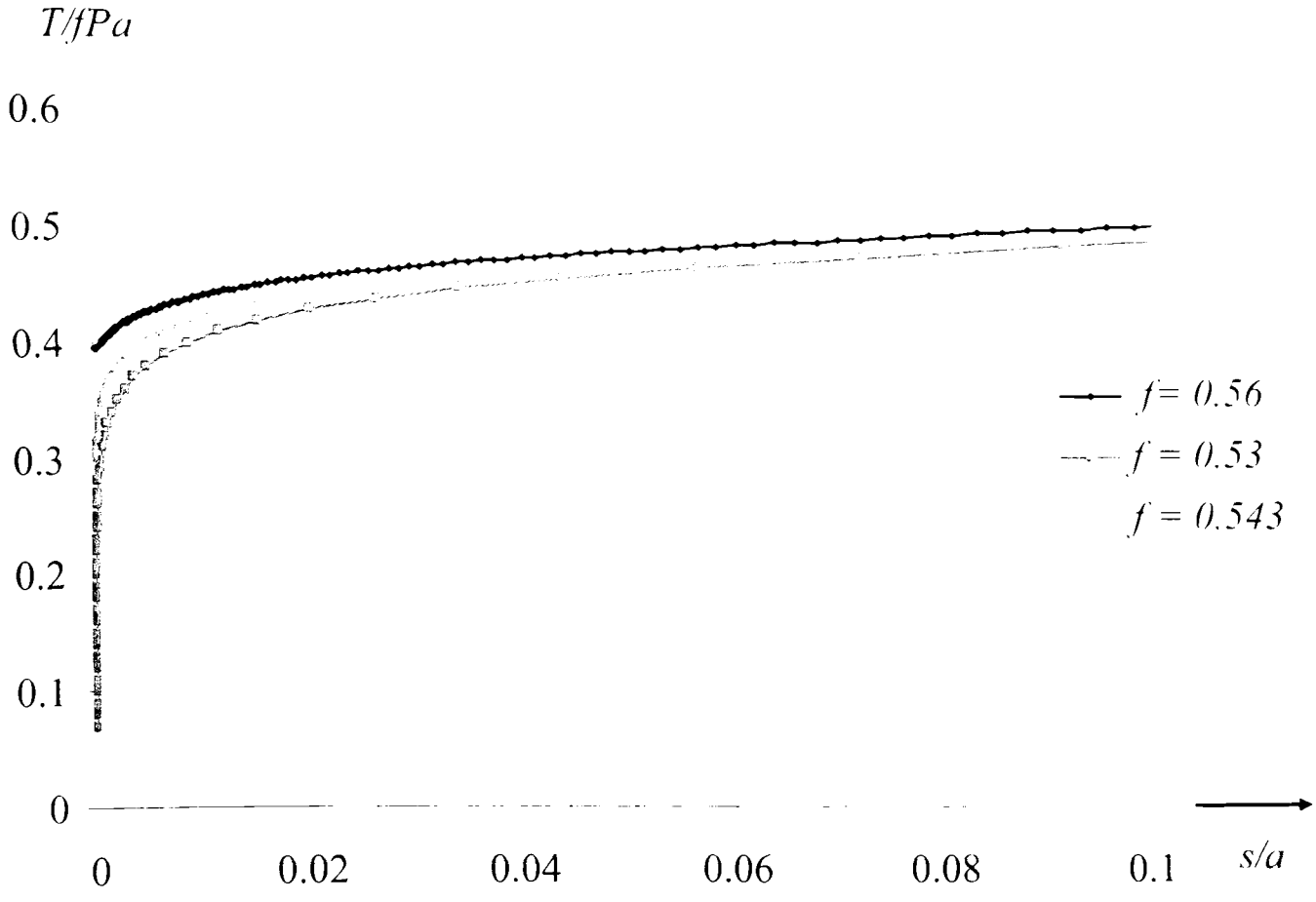

Figure 10-9: Local slip angles under different torsions for the three cases $f = 0.53$, $f = 0.543$, $f = 0.56$.

10.6 Conclusion

The object was to investigate a complete, slipping contact problem when the shear traction had components both perpendicular to and parallel to the boundary. Although a torsional problem was chosen as a vehicle, because almost all attention is focused on the contact edge, where the asymptotic solutions control fully what is going on, the general characteristics found apply to any contact having this form. The analysis shows that for moderately high coefficients of friction (> 0.543) slip starts just in from the contact edge whereas at lower coefficients of friction slip is present at the contact edge on applying a normal force alone. A method for tracking out the evolving slip problem whilst maintaining

orthogonality was developed and successfully implemented. The process developed is of general, as the results derived fit within the 'complete' asymptotic forms. the good result discussed maybe applied to any complete contact suffering plane and anti-plane edge slip.

Chapter 11

Conclusions and Future Work

11.1 Conclusions

The state of stress in a complete contact is very important and at present is the focus of research. It is because the state of stress often directly determines not only the life of a component with contacting surfaces, but also the normal running and service life of the device. Slip and edge effects in complete contacts were considered and their effects on the state of stresses along the contact interface were discussed in this dissertation. According to the class of contact being studied, this dissertation can be divided into four parts.

When a remote compressive load is applied to a plate containing a sharp notch closure will occur at the root. In order to solve this problem, first, the general problem of an anticrack, present in a simple domain and subject to general remote loading was considered. The problem is solved using distributed line forces, acting as strain nuclei, along the line of the anticrack and strong parallels are drawn with the use of distributed dislocations in the solution of conventional cracks. Then, both dislocations and point forces are used as strain nuclei to achieve mixed boundary value conditions. The influence function for a pair of forces applied to the faces on a semi-infinite notch is found and finally used to find the true closure length

and interfacial contact pressure. The contact pressure between the notch faces is very large at the root, but falls smoothly to zero in a square root bound fashion at the point of separation. The relationship between the bounded stress intensity factor K_I^B (which characterises the contact edge solution) and the generalised stress intensity factor, K_I which relates to the crack root, is found. Thus, the power order singularity has been replaced by a logarithmic one.

When a sharp indenter is pressed into an elastic half-space, there will be implied side contact, according to linear elasticity theory, if $\phi < \pi/2$. As an example, the problem of a plane punch sliding along a compressible half-plane has been treated in full. This provides a vehicle for comparison with a different form of the solution to problems of this class, using a semi-infinite asymptote. The asymptotic form has also been derived explicitly, and applied to the trapezium shaped indenter. The important feature of the application of the asymptotic form is that it is necessary to solve the initial contact problem only under conditions of front-face contact, which is very much easier to do, and then to abstract the generalised stress intensity factor characterising the solution at the contact edge. When once this has been found the collocation of the asymptotic form into the edge of the simplified contact solution is extremely straightforward, and very accurate. The procedure as a whole is important because it demonstrates, quantitatively, that in many problems of the class considered the power order singularity present at a contact edge is, in fact, replaced by a logarithmic singularity, which is in close juxtaposition to a power-order bounded contact pressure. Thus, in many practical problems, even without plasticity, the contact edge pressure distribution may be ameliorated from its singular form.

The convection effect for frictional sliding contact between elastically similar bodies has been explored for the simplest possible configuration - skew sliding of a Hertzian contact.

This has permitted a very straightforward analysis of an effect known to be present in more complex geometries, for example, a sliding sphere, under similar conditions. Later the similar method was used to analyse the convection effect for frictional sliding complete and almost complete contacts, for the case when the punch is rigid. First, the skew sliding of a square-ended punch on an elastic half-space has been studied. For practical engineering materials the effect is very small, but the analysis is important because the magnitude of mismatch between local slip and sliding direction is revealed. It is usually assumed that macroscopic frictional orthogonality and a pointwise application of the same principle are completely consistent. It is shown that this is not precisely correct, and that this is manifested in several ways. If the contacting half-plane is incompressible, there is no convection effect whatsoever, and the classical assumptions apply without modification. Secondly, it is shown that, even if the half-plane is incompressible, the presence of any degree of local edge rounding does introduce convection effects, and that these become progressively greater as the edge radii become more important in describing a bigger fraction of the contact profile. This effect is also accurately represented by a semi-infinite punch when the edge radius is small.

Lastly, a circular cylinder pressed into and twisted on an elastic half plane under the actions of normal load and torsion was considered. First, an accurate representation of the state of stress induced in a three-quarter plane by a screw dislocation has been found and a simple representation, giving the appropriate characteristics at various points along a projection line from the free surface, collocated. Subsequently a technique was found to find the state of stress induced by the family of circular ring dislocations present in a semi-infinite stepped shaft problem. The dislocations are assumed to be present on a plane continuous with the free surface of the step. Particular care has been taken in abstracting the characteristic forms of the solution for all positions of the dislocation and observation point, and the state of stress induced successfully found. The state of stress induced by a screw dislocation and ring

dislocations were used as stress kernel functions to analyse the torsion problem. Torsional contact between a semi-infinite elastic rod with square ends and an elastically similar half-space were solved using the ring dislocations' influence functions just described.

11.2 Future Work

When a punch is pressed into a block of half-plane, if the coefficient of friction between the two bodies is big enough, they will stick together. If they have similar material properties, it can be simplified to be a sharp notch under the actions of external loads. When a sharp notch is under the action of external loads, 'overlap' will occurs at the contact corner. The solution of a pair of forces applying normally on the sharp notch has been found using dislocation and line force distribution along the mixed boundary condition line. The contact pressure and closure length have been achieved using pair of forces influence functions but only for elastically similar material pairs. If the punch and the half-plane have different material properties, it still worth considering what will happen at the contact edge and what is the contact pressure distribution and how long the contact length is. If the coefficient of friction between the punch and the half-plane is small, partial slip or full sliding will happen at the contact region. The contact pressure at the closure part and the closure length for these two cases should be studied in the future.

A rigid trapezium punch is pressed into and sliding on an elastic half-plane has been studied in the thesis. The trapezium punch has a sharp edge at the corner. What will happen when the trapezium punch has a radius rounded corner is an interesting topic to study in the future.

A cylinder is pressed into and twisted on a half-plane under the action of pressure and torque has been considered and the local slip angels at the slip region have been given in

detail in this thesis. The cylinder and half-plane were assumed to have same material properties. In the future, we could consider what will happen when the cylinder and half-plane are different material.

References:

Adams, G.G. and Nosonovsky, M., 2000, Contact Modelling-Forces, *Tribology International*, **33**, 431-442.

Adams, G.G., 1979, A Rigid Punch Bonded to a Half Plane, *ASME Journal of Applied Mechanics*, **46**, 844-848.

Adams, G.G., Barber, J.R., Ciavarella, M., and Rice, J.R., 2005, A Paradox in Sliding Contact Problems With Friction, *ASME Journal of Applied Mechanics*, **72**, 450-452

Atkinson, C., 1973, Some Ribbon-Like Inclusion Problems, *International Journal of Engineering Science*, **11**, 243-266.

Barber, J.R. and Ciavarella, M., 2000, Contact Mechanics, *International Journal of Solids and Structure*, **37**, 29-43.

Barber, J.R. 2002, *Elasticity*, Kluwer, Dordrecht 2nd edition.

Bentall R.H. and Johnson K.L., 1968, An elastic strip in plane rolling contact. *International Journal of Solids and Structures*, **10**, 637-63.

Bhushan, B., 1996, Contact Mechanics of Rough Surfaces in Tribology: Single Asperity Contact, *Applied Mechanics Reviews*, **49**, 275-298.

Bhushan, B., 1998, Contact Mechanics of Rough Surfaces in Tribology: Multiple Asperity Contact, *Tribology Letters*, **4**, 1-35.

Bogy, D.B., 1971, Two edge-bonded elastic wedges of different materials and wedge angles under surface tractions, *ASME Journal of Applied Mechanics*, 377-386.

Brussat, T.R., and Westmann, R.A., 1975, A Westergaard-Type Stress Function For Line Inclusion Problems, *International Journal of Solids and Structure*, **11**, 665-677.

Burgel, B., Perry, A.J., and Schneider, W.R., 1970, On the theory of fiber strengthening, *J. Mech. Phys. Solids*, **18**, 101-114.

Cattaneo C., 1938, Sul contatto di due corpi elastici: distribuzione locale degli sforzi. Rendiconti dell' Accademia nazionale dei lincei, 27 Ser, **6**, 342.

Chang, C. S., and Conway, H.D., 1968, Bond stresses in fiber reinforced composites subjected to uniform tension, *Journal of Composite Materials*, **2**, 168-185.

Chu, W.W.L., and Conway, H.D., 1970, Bond stresses in composite with overlapping fibers, *International Journal of Mechanical Sciences*, **12**, 761-774.

Churchman, C.M. and Hills, D.A., 2006a, General results for complete contacts subject to oscillatory shear, *Journal of The Mechanics and Physics of Solids*, **54**, 1186-1205

Churchman, C.M. and Hills, D.A., 2006b, The edge dislocation in a three-quarter plane. Part II: Application to an edge crack, *European Journal of Mechanics A/Solids*, **25**,389-396.

Churchman, C.M. and Hills, D.A., 2006c, Slip zone length at the edge of a complete contact, *International Journal of Solids and Structures*, **43**, 2037-2049.

Churchman, C.M., Dini, D. and Hills, D.A., 2006, Closure at the root of a sharp notch, *International Journal of Mechanical Sciences*, **48**, 1063-1071.

Churchman, C.M., Korsunsky, A.M., and Hills, D.A., 2006, The edge dislocation in a three-quarter plane. Part I: Influence functions, *European Journal of Mechanics A/Solids*, **25**, 42-50.

Churchman, C.M., Mugadu, A. and Hills, D.A., 2003, Asymptotic results for slipping complete frictional contacts, *European Journal of Mechanics A/Solids*, **22**, 793-800.

Ciavarella, M., 1998, The generalized Cattaneo partial slip plane contact problem. I—Theory, II—Examples, *International Journal of Solids and Structure*, **35**, 2349-2378.

Ciavarella, M., Hills, D.A. and Monno, G., 1998, The influence of rounded edges on indentation by a flat punch, *Proceedings of the Institution of Mechanical Engineers, Part C: Journal of Mechanical Engineering Science*, **212**, 319-328.

Collins, J.A. and Tovey, F.M., 1972, Fretting fatigue mechanisms and the effect of direction of fretting motion on fatigue strength, *Journal of Materials, JMSLA*, **7**,460-464.

Comninou, M. and Dundurs, J., 1982, An educational elasticity problem with friction – Part II: Unloading for strong friction and reloading, *ASME Journal of Applied Mechanics*, **49**, 47-51.

Comninou, M., 1976, Stress singularity at a sharp edge in contact problems with friction, *Journal of Applied Mechanics and Physics*, **27**, 493-499.

Conway, H.D., and Chang, C.I., 1971, The effective elastic constants and bond stresses for a fiber-reinforced elastic sheet, *Fibre Science and Technology*, **3**, 249-260.

Conway, H.D., Chu, W.W., and Chang, C.I., 1970, Effect of bond stresses of partial bond failure of overlapping fibres in a composite material, *Fibre Science and Technology*, **2**, 289-297.

Cooper, D.H., 1969, Hertzian contact-stress deformation coefficients, *ASME Journal of Applied Mechanics*, **36**, 296-303.

Dini, D., Churchman, C., Rajasekaran, R. and Hills, D.A., 2004, A correlation of the process zone properties in complete, incomplete and almost complete fretting contacts, *International Journal of Mechanical Science*, **46**, 491-508.

Dundurs, J., 1968, Analogy between Concentrated Force and Edge Dislocations, *Journal of Applied Physics*, **39**, 4152-4156.

Dundurs, J., 1975, Properties of elastic bodies in contact, *Mechanics of Contact between Deformable Bodies* (ed. A. D. de Pater and J. J. Kalker), Delft University Press.

Dundurs, J., and Markenscoff, X., 1989, A Green's Function Formulation of Anticracks and Their Interaction With Load-Induced Singularities, *ASME Journal of Applied Mechanics*, **56**, 550-555.

Duo, P., Korsunsky, A.M., and Hills, D.A., 2005, The application of asymptotic analysis for modes I and III semi-infinite wedge solutions to a circumferentially notched shaft, *The Journal of Strain Analysis for Engineering Design*, **40**, 255-262.

Erdogan, F., and Gupta, G.D., 1972, Stresses near a flat inclusion in bonded dissimilar materials, *International Journal of Solids and Structure*, **8**, 533-547.

Fenner,A.J., Wright, K.H.R. and Mann, J.Y., 1956, Fretting corrosion and its influence on fretting failure, *Proceedings. International Conference on Fatigue of Metals*. Institute for Mechanical Engineers, 386-393.

Gdoutos, E.E., and Theocaris, P.S., 1975, Stress concentrations at the apex of a plane indenter acting on an elastic half plane, *ASME Journal of Applied Mechanics*, 688-692.

Gladwell, G.M.L., 1976, On some unbonded contact problems in plane elasticity theory, *ASME Journal of Applied Mechanics*, **43**, 263-267.

Gladwell, G.M.L., 1980, *Contact Problems in the Classical Theory of Elasticity*, Sijtoff and Noordhoff, Maryland. USA.

Goodman, L.E., 1962, Contact stress analysis of normally loaded rough spheres, *ASME Journal of Applied Mechanics*, **29**, 515-522.

Greenwood, J.A., 1985, Formulas for moderately elliptical Hertzian contacts,*ASME J.Tribol.*, **107**, 501-504.

Hertz, H., 1882, On the contact of elastic solids, *J. Teine Angew. Math.*, **92**, 156-171

Hills, D.A., Nowell, D., and Sackfield, A., 1993, *Mechanics of Elastic Contacts*, Butterworth-Heinemann Ltd, Oxford.

Hills, D.A. and Nowell, D., 1994, *Mechanics of Fretting Fatigue*, Kluwer, Dordrecht.

Hills, D.A., Kelly, P.A., Dai, D.N. and Korsunsky, A.M., 1996, *Solution of Crack Problems - The Distributed Dislocation Technique*, Kluwer Academic, Dordrecht.

Hills, D.A., Dini, D., Magadu, A. and Korsunsky, A.M., 2004, A review of asymptotic procedures in stress analysis: known solutions and their applications, *The Journal of Strain Analysis for Engineering Design*, **39**, 553-568.

Hills, D.A., Sackfield, A., and Churchman, C.M., 2006, Discussion: "A Paradox in Sliding Contact Problems With Friction" (Adams, G.G., Barber, J.R., Ciavarella, M., and Rice, J.R., 2005,Journal of Applied Mechanics, 72, 450-452), ASME Journal of Applied Mechanics, **73**, 884-886.

Jäger, J., 1997, Half-planes without coupling under contact loading, Arch. *Applied Mechanics*, **67**, 247-259.

Johnson, K.L., 1985, *Contact Mechanics*, Cambridge University Press, Cambridge

Kalker, J.J., 1990, *Three-Dimensional Elastic Bodies in Rolling Contact*, Kluwer, Dordrecht.

Karuppanan, S., Churchman, C.M., Hills, D.A. and Giner, E., 2007, Sliding frictional contact between a square block and an elastically similar half-plane, *European Journal of Mechanics A/Solids*, in press.

Keer, L.M., Dundurs, J., and Tsai, K.C., 1972, Problems involving receding contact between a layer and a half-space, *ASME Journal of Applied Mechanics*, **39**, 1115-1120.

Khadem, R. and O'Conner, J.J., 1969, Adhesive or frictionless compression of an elastic rectangle between two identical elastic half-spaces, *International Journal of Engineering Science*, **7**, 153-168.

Kikuchi and Oden, 1988, *Contact problems in elasticity : a study of variational inequalities and finite element methods*, Philadelphia: SIAM.

Kim H.-K, Hills D.A. and Nowell D. 2000, Partial slip between contacting cylinders under transverse and axial shear. *International Journal of Mechanical Sciences*, **42**:199-212.

Korsunsky, A.M., 1996, The somigliana ring dislocation revisited. 1. Papkovich potential solutions for dislocations in an infinite space, *Journal of Elasticity*, 44, 97-114.

Markenscoff, X., Ni, L., and Dundurs, J., 1994, The Interface Anticrack and Green's Functions for Interacting Anticracks and Cracks/Anticracks, *ASME Journal of Applied Mechanics*, **61**, 797-802.

Mellin : Barber, J.R., 1992, Elasticity, Kluwer Academic Press, Dordrecht.

Mindlin, R.D., Deresiewicz, H., 1953, Elastic spheres in contact under varying oblique forces, *ASME Journal of Applied Mechanics*, **75**, 327-344.

Mugadu, A. and Hills, D.A., 2002, A generalised stress intensity approach to characterising the process zone in complete fretting contacts, *International Journal of Solids and Structures*, **39**, 1327-1335.

Mugadu, A. and Hills, D.A., 2003, The evolution of the process zone when a complete contact is subject to cyclically varying load, *International Journal of Solids and Structures*, **40**, 4417-4435.

Mugadu, A., Hills, D.A. and Limmer, L., 2002, An asymptotic approach to crack initiation in fretting fatigue of complete contacts, *Journal of the Mechanics and Physics of Solids*, **50**, 531-547.

Mugadu, A., Hills, D.A. and Nowell, D., 2002, Modification of fretting-fatigue testing apparatus based upon an analysis of contact stresses at complete and nearly complete contacts, *Wear*, **252**, 475-483.

Mugadu, A., Hills, D.A., Barber, J.R. and Sackfield, A., 2004, The application of asymptotic solutions to characterising the process zone in almost complete frictional contacts, *International Journal of Solids and Structures*, **41**, 385-397.

Munisamy RL. A study of dry frictional contacts. DPhil Thesis, Oxford University, 1994.

Muskhelishvili, N.I., 1953a, *Some Basic Problems of the Mathematical Theory of Elasticity*, Noordhoff, Groningen.

Muskhelishvili, N.I., 1953b, *Singular Integral Equations, Boundary Problems of Function Theory and Their Application to Mathematical Physics*, Noordhoff, Groningen.

Navarro, C., Mugadu, A., Hills, D.A. and Dominguez, J., 2003, The influence of underlying tension on partial slip in complete and nearly complete contacts, *International Journal of Mechanical Science*, **45**, 77-773.

Nowell, D., and Hills, D.A., 1987, Open Cracks At or Near Free Edges, *Journal of Strain Analysis*, **22**, 177-185.

Paynter, R.J.H., Hills, D.A. and Korsunsky, A.M., 2007, The effect of path cut on Somigliana ring dislocation elastic fields, *International Journal of Solids and Structures*, **44**, 6653-6677.

Porter, M.I. and Hills, D.A., 2002, Note on the complete contact between a flat rigid punch and an elastic layer attached to a dissimilar substrate, *International Journal of Mechanical Science*, **44**, 509-530.

Qiu, H., Churchman, C.M., and Hills, D.A., 2008, The screw dislocation in a three-quarter plane, *European Journal of Mechanics A/Solids*, **27**, 730-736.

Qiu H., Dini D. and Hills D.A., 2007, The influence function for self-equilibrating forces on a semi-infinite wedge, *The Journal of Strain Analysis for Engineering Design*, **42**, 351-360

Qiu, H., Hills, D.A. and Dini, D., 2008, An investigation of convection effects in complete and almost complete contact problems, *European Journal of Mechanics A/Solids*, under review

Qiu H., Hills, D.A., Nowell, D., and Dini, D., 2008, Skew sliding of an elastic cylinder: An investigation of convection in contact, *International Journal of Mechanical Science*, **50**, 293-298.

Qiu, H. , Paynter, J.H. R., Dini, D. and Hills, D.A., 2008, The state of stress induced by ring dislocations in a semi-infinite stepped shaft, *European Journal of Mechanics - A/Solids*, **27**, 269-284

Sackfield, A., Barber, J.R., Hills, D.A. and Truman, C.E., 2002, A shrink-fit shaft subject to *torsion, European Journal of Mechanics*, **21**, 73-84.

Sackfield, A., Mugadu, A., Barber, J.R. and Hills, D.A., 2003, The application of asymptotic solutions to characterising the process zone in almost complete frictionless contacts, *Journal of Mechanics and Physics of Solids*, **51**, 1333-1346.

Spence, D.A., 1971, An eigenvalue problem for elastic contact with finite friction, *Proc. Camb. Phil. Soc.*, **73**, 249-268.

Spence, D.A., 1975, The Hertz contact problem with finite friction, *Journal of Elasticity*, **5**, 297-319.

Sundelius, B., 1981, An axisymmetric contact problem with given region of adhesion, *IMA Journal of Applied Mathematics*, **27**, 455-475.

Timoshenko, S.P., and Goodier, J.N., 1970, *Theory of Elasticity*, 3rd ed., McGraw-Hill, New York.

Wang, Z.Y., Zhang, H.T., and Chou, Y.T., 1985, Characteristics of the Elastic Field of a Rigid Line Inhomogeneity, *ASME Journal of Applied Mechanics*, **52**,818-822.

Weertman, J., 1996, Dislocation Based Fracture Mechanics, World Scientific Press, Singapore.

Williams, M.L., 1952, Stress singularities resulting from various boundary conditions in angular plates in extension, *ASME Journal of Applied Mechanics*, **19**, 526-528.

Wright, T. and O'Connor, J.J., 1972, The influence of fretting and geometric stress concentrations on the fatigue strength of clamped joints, *Proceedings, The Institution of Mechanical Engineers*, **186**, 827-835

Appendix A: General Solution for a Line Force in a Half-Plane

The stresses and displacements at the point (x, y) due to a line force P_x acting at the point (c, d) in the x-direction in a half plane are

$$\sigma_{xx} = \frac{P_x}{2\pi(\kappa+1)} S_{xxx}$$

$$S_{xxx} = \{\frac{(-\kappa+1)x_1}{r_1^2} - \frac{4x_1^3}{r_1^4} + \frac{1}{r_2^2}[-2(\kappa-1)c + (\kappa-1)x_2] + \frac{-4\kappa x_2^3 + 4\kappa c x_2^2 + 20c x_2^2 - 24c^2 x_2}{r_2^4} + \frac{32c^2 x_2^3 - 32c x_2^4}{r_2^6}\} \quad \text{(A-1)}$$

$$\sigma_{yy} = \frac{P_x}{2\pi(\kappa+1)} S_{xyy}$$

$$S_{xyy} = \{\frac{(\kappa-5)x_1}{r_1^2} + \frac{4x_1^3}{r_1^4} + \frac{-5\kappa x_2 + x_2 + 2\kappa c + 6c}{r_2^2} + \frac{4\kappa x_2^3 - 4\kappa c x_2^2 - 36c x_2^2 + 24c^2 x_2}{r_2^4} + \frac{-32c^2 x_2^3 + 32c x_2^4}{r_2^6}\} \quad \text{(A-2)}$$

$$\sigma_{xy} = \frac{P_x}{2\pi(\kappa+1)} S_{xxy}$$

$$S_{xxy} = (y-d)\{\frac{1-\kappa}{r_1^2} - \frac{4x_1^2}{r_1^4} + \frac{\kappa-1}{r_2^2} + \frac{-4\kappa x_2^2 + 12c x_2 + 4\kappa c x_2 - 8c^2}{r_2^4} + \frac{-32c x_2^3 + 32c^2 x_2^2}{r_2^6}\} \quad \text{(A-3)}$$

$$u_x = \frac{P_x}{2\mu 2\pi(\kappa+1)} D_{xx}$$

$$D_{xx} = \{-2\kappa \log r_1 + \frac{2x_1^2}{r_1^2} - (\kappa^2+1)\log r_2 + \frac{(2\kappa x_2^2 - 4c x_2 + 4c^2)}{r_2^2} + \frac{8c x_2^2}{r_2^4}(x_2 - c)\} \quad \text{(A-4)}$$

$$u_y = \frac{P_x}{2\mu 2\pi(\kappa+1)} D_{xy}$$

$$D_{xy} = \{(y-d)[\frac{2x_1}{r_1^2} + \frac{2\kappa x_2 - 4\kappa c}{r_2^2} - \frac{8c x_2}{r_2 4}(c - x_2)] - (\kappa^2-1)\theta_2\} \quad \text{(A-5)}$$

and those due to a line force P_y acting at the point (c, d) in the y-direction in a half plane are

$$\sigma_{xx} = \frac{P_y}{2\pi(\kappa+1)} S_{xxx}$$

$$S_{xxx} = (y-d)\{\frac{\kappa-1}{r_1^2} - \frac{4x_1^2}{r_1^4} - \frac{\kappa-1}{r_2^2} + \frac{-4\kappa x_2^2 - 4cx_2 + 4\kappa cx_2 + 8c^2}{r_2^4} + \frac{32cx_2^3 - 32c^2x_2^2}{r_2^6}\} \quad \text{(A-6)}$$

$$\sigma_{yy} = \frac{P_y}{2\pi(\kappa+1)} S_{yyy}$$

$$S_{yyy} = (y-d)\{\frac{-\kappa-3}{r_1^2} + \frac{4x_1^2}{r_1^4} + \frac{-3\kappa-1}{r_2^2} + \frac{4\kappa x_2^2 - 4\kappa cx_2 + 20cx_2 - 8c^2}{r_2^4} + \frac{32c^2x_2^2 - 32cx_2^3}{r_2^6}\} \quad \text{(A-7)}$$

$$\sigma_{xy} = \frac{P_y}{2\pi(\kappa+1)} S_{xxy}$$

$$S_{xxy} = \{\frac{-(\kappa+3)x_1}{r_1^2} + \frac{4x_1^3}{r_1^4} + \frac{-3\kappa x_2 - x_2 + 2\kappa c - 2c}{r_2^2} + \frac{4\kappa x_2^3 - 4\kappa cx_2^2 + 28cx_2^2 - 24c^2x_2}{r_2^4} + \frac{32c^2x_2^3 - 32cx_2^4}{r_2^6}\} \quad ; \quad \text{(A-8)}$$

$$u_x = \frac{P_y}{2\mu 2\pi(\kappa+1)} D_{yx}$$

$$D_{yx} = \{(y-d)[\frac{2x_1}{r_1^2} - \frac{2\kappa x_2 - 4\kappa c}{r_2^2} + \frac{8cx_2}{r_2 4}(c-x_2)] + (\kappa^2-1)\theta_2\} \quad \text{(A-9)}$$

$$u_y = \frac{P_y}{2\mu 2\pi(\kappa+1)} D_{yy}$$

$$D_{yy} = \{-2\kappa \log r_1 - \frac{2x_1^2}{r_1^2} - (\kappa^2+1)\log r_2 + \frac{(-2\kappa x_2^2 - 4cx_2 + 4c^2)}{r_2^2} + \frac{8cx_2^2}{r_2^4}(x_2-c)\} \quad \text{(A-10)}$$

where

$$x_1 = x - c$$

$$x_2 = x + c$$

$$r_1 = \sqrt{x_1^2 + (y-d)^2}$$

$$r_2 = \sqrt{x_2^2 + (y-d)^2}$$

$$\theta_2 = \arcsin(\frac{y-d}{r_2})$$

Appendix B: Finite Punch Problem

B.1 First Integral I_1

Make the substitutions

$$t=\frac{u-\alpha_0}{u+\alpha_0},\qquad s=\frac{y-\alpha_0}{y+\alpha_0},\qquad \alpha_0=\frac{1+c_0}{1-c_0}. \tag{B-1}$$

Then

$$t=(-1,-c_0)\rightarrow u=(0,1), \tag{B-2.1}$$

$$1-t=\frac{2\alpha_0}{u+\alpha_0},\quad 1+t=\frac{2u}{u+\alpha_0},\quad \frac{dt}{du}=\frac{2\alpha_0}{(u+\alpha_0)^2}, \tag{B-2.2}$$

$$t-s=\frac{2\alpha_0(u-y)}{(u+\alpha_0)(y+\alpha_0)},\qquad w(t)=\frac{2\alpha_0^{1-\lambda}u^{\lambda}}{u+\alpha_0}, \tag{B-2.3}$$

so that

$$\int_{-1}^{-c_0}\frac{dt}{w(t)(t-s)}=\frac{y+\alpha_0}{2\alpha_0^{1-\lambda}}\int_0^1\frac{u^{-\lambda}du}{u-y}. \tag{B-3}$$

This integral is hypergeometric and must be evaluated both in its regular and CPV form.

B.1.1. The Regular Solution, $y>1$.

First, the general '2F1' hypergeometric function is defined as

$$F(a,b;c;z)=\frac{\Gamma(c)}{\Gamma(b)\Gamma(c-b)}\int_0^1\frac{t^{b-1}(1-t)^{c-b-1}}{(1-zt)^a}dt,\ |z|<1,\quad \mathrm{Re}(c)>\mathrm{Re}(b) \tag{B-4}$$

and it is noted that if $c=a+b$ then the function is divergent (and this will certainly be the case here) at z=1.

Then

$$\int_0 \frac{u^{-\lambda} du}{u - y} = -\frac{1}{y} \int_0 \frac{u^{-\lambda} du}{1 - u/y}. \tag{B-5}$$

Thus the hypergeometric parameters are

$$a = 1, \quad b = 1 - \lambda, \qquad c = 2 - \lambda, \qquad z = 1/y, \tag{B-6}$$

and it is noted that $c = a + b$. Now

$$\frac{\Gamma(c)}{\Gamma(b)\Gamma(c-b)} = \frac{\Gamma(2-\lambda)}{\Gamma(1-\lambda)\Gamma(1)} = 1 - \lambda. \tag{B-7}$$

Thus

$$\int_0 \frac{u^{-\lambda} du}{u - y} = \frac{1}{1-\lambda} F(1,\ 1-\lambda;\ 2-\lambda;\ \frac{1}{y}), y > 1. \tag{B-8}$$

Hence

$$\int_1^{c_0} \frac{dt}{w(t)(t-s)} = -\frac{y + \alpha_0}{2\alpha_0^{1-\lambda} y(1-\lambda)} F(1,\ 1-\lambda;\ 2-\lambda;\ \frac{1}{y}), \qquad y > 1. \tag{B-9}$$

Note that $y = 1$ corresponds to $s = -c_0$, i.e. the sharp 'buried' corner at $x = -b$, where singular behaviour in the pressure is anticipated at this point.

B.1.2. The CPV Solution of I_1 when $y < 1$

Now the CPV integral

$$\int_0^{\infty} \frac{u^{-\lambda} du}{1 - u/y} = y^{1-\lambda} \int_0^{\infty} \frac{x^{-\lambda} dx}{1 - x} = -\frac{\pi y^{1-\lambda}}{\tan \pi\lambda}. \tag{B-10}$$

Now

$$\int_0^{\infty} \frac{u^{-\lambda} du}{1 - u/y} = \int_0 \frac{u^{-\lambda} du}{1 - u/y} + \int_{\infty} \frac{u^{-\lambda} du}{1 - u/y} \tag{B-11}$$

and only the first integral on the RHS is CPV as $y < 1$ is:

$$\int_0 \frac{u^{-\lambda} du}{1 - u/y} = -\frac{\pi y^{1-\lambda}}{\tan \pi\lambda} - \int_{\infty} \frac{u^{-\lambda} du}{1 - u/y}, \qquad y < 1. \tag{B-12}$$

In the RHS integral make the substitution $u \to 1/u$ to get

$$\int_0^y \frac{u^{-\lambda}du}{1-u/y} = -y\int_0^1 \frac{u^{\lambda-1}du}{1-uy}. \tag{B-13}$$

Thus

$$\int_0^y \frac{u^{-\lambda}du}{1-u/y} = -\frac{\pi y^{1-\lambda}}{\tan\pi\lambda} + y\int_0^1 \frac{u^{\lambda-1}du}{1-uy}, \qquad y<1. \tag{B-14}$$

Now the RHS integral is a regular hypergeometric function with

$$a=1, \quad b=\lambda, \quad c=1+\lambda, \tag{B-15}$$

$$\frac{\Gamma(c)}{\Gamma(b)\Gamma(c-b)} = \frac{\Gamma(1+\lambda)}{\Gamma(\lambda)\Gamma(1)} = \lambda, \tag{B-16}$$

$$\int_0^1 \frac{u^{\lambda-1}du}{1-uy} = \frac{1}{\lambda}F(1,\ \lambda;\ 1+\lambda;\ y). \tag{B-17}$$

Thus

$$\int_0^y \frac{u^{-\lambda}du}{1-u/y} = -\frac{\pi y^{1-\lambda}}{\tan\pi\lambda} + \frac{y}{\lambda}F(1,\ \lambda;\ 1+\lambda;\ y), \qquad y<1 \tag{B-18}$$

$$I_1 = \begin{cases} J_1 = \dfrac{\pi}{w(s)\tan\pi\lambda} - \dfrac{\alpha_0^{\lambda}}{\lambda(1-s)}F(1,\ \lambda;\ 1+\lambda;\ \alpha_0\dfrac{1+s}{1-s}), & -1<s<-c_0, \\ J_2 = -\dfrac{\alpha_0^{\lambda-1}}{(1-\lambda)(1+s)}F(1,\ 1-\lambda;\ 2-\lambda;\ \dfrac{1}{\alpha_0}\dfrac{1-s}{1+s}), & -c_0<s<1, \end{cases} \tag{B-19}$$

where

$$\alpha_0 = \frac{1+c_0}{1-c_0}, \qquad c_0 = \frac{b+d}{a}. \tag{B-20}$$

B.2. Second Integral I_2

$$I_2 = \begin{cases} K_1 = \dfrac{\pi}{w(s)\tan\pi\lambda} + \dfrac{\alpha_1^{1-\lambda}}{(1-\lambda)(1+s)} F(1,\ 1-\lambda;\ 2-\lambda;\ \alpha_1 \dfrac{1-s}{1+s}), & c_1 < s < 1, \\ K_2 = -\dfrac{\alpha_1^{\ 1}}{\lambda(1-s)} F(1,\ \lambda;\ 1+\lambda;\ \dfrac{1}{\alpha_1}\dfrac{1+s}{1-s}), & -1 < s < c_1, \end{cases} \tag{B-21}$$

where now

$$\alpha_1 = \frac{1+c_1}{1-c_1}, \qquad c_1 = \frac{b-d}{a}. \tag{B-22}$$

So

$$c_1 < s < 1 \text{ corresponds to } b < x < a+d \tag{B-23}$$

whilst

$$c-1 < s < c_1 \text{ corresponds to } -a+d < x < b\,. \tag{B-24}$$

Note that K_1 and K_2 have been written for the two versions of I_2.

Appendix C: Stress Kernels Functions

The basic function is

$$J_{\mu,\nu,\lambda}(a,r,z)=\int J_{\mu}(a\xi)J_{\nu}(r\xi)e^{-z\xi}\xi^{\lambda}d\xi$$

when $|\mu-\nu|>\lambda$ the angle of the path cut matters so we have included the angle as an argument otherwise it has been omitted.

Axial

$$G_{zzz}(r,z,r_d,z_d)=-r_d\left[J_{1,0;1}(r_d,r,z-z_d)+(z-z_d)J_{1,0;2}(r_d,r,z-z_d)\right] \tag{C-1}$$

$$G_{zrz}(r,z,r_d,z_d)=-r_d(z-z_d)J_{1,1;2}(r_d,r,z-z_d) \tag{C-2}$$

$$G_{zrr}(r,z,r_d,z_d)=-r_d\left[\begin{array}{l}J_{1,0;1}(r_d,r,z-z_d)-(z-z_d)J_{1,0;2}(r_d,r,z-z_d)\\+\dfrac{(z-z_d)}{r}J_{1,1;1}(r_d,r,z-z_d)-\dfrac{(\kappa-1)}{2r}J_{1,1;0}(r_d,r,z-z_d)\end{array}\right] \tag{C-3}$$

Outer Radial

$$G^{o}_{rzz}(r,z,r_d,z_d)=-r_d(z-z_d)J_{0,0;2}(r_d,r,z-z_d) \tag{C-4}$$

$$G^{0}_{rrz}(r,z,r_d,z_d)=-r_d\left[J_{0,1;1}(r_d,r,z-z_d)+(z-z_d)J_{0,1;2}(r_d,r,z-z_d)\right] \tag{C-5}$$

$$G^{o}_{rrr}(r,z,r_d,z_d)=-r_d\left[\begin{array}{l}2J_{0,0;1}(r_d,r,z-z_d)-(z-z_d)J_{0,0;2}(r_d,r,z-z_d)\\+\dfrac{(z-z_d)}{r}J_{0,1;1}(r_d,r,z-z_d)-\dfrac{(\kappa-1)}{2r}J_{0,1;0}(r_d,r,z-z_d,0)\end{array}\right] \tag{C-6}$$

Inner Radial

$$G^{i}_{rzz}(r,z,r_d,z_d)=r_d(z-z_d)J_{2,0;2}(r_d,r,z-z_d) \tag{C-7}$$

$$G^{i}_{rrz}(r,z,r_d,z_d)=r_d\left[-J_{2,1;1}(r_d,r,z-z_d)+(z-z_d)J_{2,1;2}(r_d,r,z-z_d)\right] \tag{C-8}$$

$$G^{i}_{rrr}(r,z,r_d,z_d)=r_d\left[\begin{array}{l}2J_{2,0;1}(r_d,r,z-z_d,\dfrac{\pi}{2})-(z-z_d)J_{2,0;2}(r_d,r,z-z_d)\\+\dfrac{(z-z_d)}{r}J_{2,1;1}(r_d,r,z-z_d)-\dfrac{(\kappa-1)}{2r}J_{2,1;0}(r_d,r,z-z_d,\dfrac{\pi}{2})\end{array}\right] \tag{C-9}$$

Distributed force (Kelvin) with a $\pi/2$ cut

$$G^{k}_{zz}(r,z,r_d,z_d)=\frac{r_d}{\kappa+1}\left[-\frac{\kappa+1}{2}J_{1,0,0}(r_d,r,z-z_d,\frac{\pi}{2})-(z-z_d)J_{1,0,0}(r_d,r,z-z_d)\right] \quad \text{(C-10)}$$

$$G^{k}_{rz}(r,z,r_d,z_d)=\frac{r_d}{\kappa+1}\left[-\frac{\kappa-1}{2}J_{1,1,0}(r_d,r,z-z_d)-(z-z_d)J_{1,1,1}(r_d,r,z-z_d)\right] \quad \text{(C-11)}$$

$$G^{k}_{rr}(r,z,r_d,z_d)=\frac{r_d}{\kappa+1}\left[\begin{array}{l}\frac{\kappa-3}{2}J_{1,0,0}(r_d,r,z-z_d,\frac{\pi}{2})+(z-z_d)J_{1,0,1}(r_d,r,z-z_d)\\-\frac{(z-z_d)}{r}J_{1,1,0}(r_d,r,z-z_d)\end{array}\right] \quad \text{(C-12)}$$

Cylinder cut Radial

$$G^{c}_{rzz}(r,z,r_d,z_d)=\frac{\kappa-1}{\kappa+1}G^{i}_{rzz}(r,z,r_d,z_d)+\frac{2}{\kappa+1}G^{o}_{rzz}(r,z,r_d,z_d)-\frac{(3-\kappa)}{r_d}G^{\kappa}_{zz}(r,z,r_d,z_d) \quad \text{(C-13)}$$

$$G^{c}_{rrz}(r,z,r_d,z_d)=\frac{\kappa-1}{\kappa+1}G^{i}_{rrz}(r,z,r_d,z_d)+\frac{2}{\kappa+1}G^{o}_{rrz}(r,z,r_d,z_d)-\frac{(3-\kappa)}{r_d}G^{\kappa}_{rz}(r,z,r_d,z_d) \quad \text{(C-14)}$$

$$G^{c}_{rrr}(r,z,r_d,z_d)=\frac{\kappa-1}{\kappa+1}G^{i}_{rrr}(r,z,r_d,z_d)+\frac{2}{\kappa+1}G^{o}_{rrr}(r,z,r_d,z_d)-\frac{(3-\kappa)}{r_d}G^{\kappa}_{rr}(r,z,r_d,z_d) \quad \text{(C-15)}$$

Screw

$$G_{r\theta}(r,z,r_d,z_d)=r_d\left[J_{2,0,1}(r_d,r,z-z_d,0)-\frac{2}{r}J_{2,1,0}(r_d,r,z-z_d,0)\right] \quad \text{(C-16)}$$

$$G_{z\theta}(r,z,r_d,z_d)=-r_d J_{2,1,1}(r_d,r,z-z_d) \quad \text{(C-17)}$$

Appendix D

Expressions for the surface displacements in terms of the traction elements are:

$$\frac{\partial u_x}{\partial x}(i) = -\frac{1}{\pi E^*}\left\{ \sum_{j=-n+1}^{n-1} q_{xj}\left((i-j+1)\ln(\frac{i-j+1}{i-j})^2 + (i-j-1)\ln(\frac{i-j-1}{i-j})^2 \right) \right.$$
$$\left. + f\cos\varphi\sin(\lambda\pi)\left[2^{\lambda-1}c^{\lambda}\left[\frac{2csF[1-\lambda,1,2-\lambda,\frac{cn}{i-ci+n}]}{[(c-1)i-n](\lambda-1)} + \frac{2-2c-(c-1)(i+n-1)\log(\frac{i+n-1}{i+n})^2}{1-c} \right] - \right.\right.$$
$$\left.\left. 2^{-\lambda}c^{\lambda-1}\left[\frac{cn\left(((c-1)i+n)(1+\lambda) + cn\lambda F[1+\lambda,1,2+\lambda,\frac{cn}{ic-i+n}] \right)}{(ic-i+n)^2\lambda(1+\lambda)} + \frac{2-2c+(c-1)(1+i-n)\log(\frac{i+1-n}{i-n})^2}{1-c} \right] \right] \right\}$$
$$-\frac{1-2\nu}{E^{**}}p(i)$$

$$\frac{\partial u_z}{\partial x}(i) = -\frac{1}{\pi E^{**}}\left\{ \sum_{j=-n+1}^{n-1} q_{zj}\left((i-j+1)\ln(\frac{i-j+1}{i-j})^2 + (i-j-1)\ln(\frac{i-j-1}{i-j})^2 \right) \right.$$
$$\left. + f\sin\varphi\sin(\lambda\pi)\left[2^{\lambda-1}c^{-\lambda}\left[\frac{2csF[1-\lambda,1,2-\lambda,\frac{cn}{i-ci+n}]}{[(c-1)i-n](\lambda-1)} + \frac{2-2c-(c-1)(i+n-1)\log(\frac{i+n-1}{i+n})^2}{1-c} \right] - \right.\right.$$
$$\left.\left. 2^{-\lambda}c^{\lambda-1}\left[\frac{cn\left(((c-1)i+n)(1+\lambda) + cn\lambda F[1+\lambda,1,2+\lambda,\frac{cn}{ic-i+n}] \right)}{(ic-i+n)^2\lambda(1+\lambda)} + \frac{2-2c+(c-1)(1+i-n)\log(\frac{i+1-n}{i-n})^2}{1-c} \right] \right] \right\}$$

where E^* is the plane strain stiffness $= E/(1-\nu^2)$, E^{**} is the antiplane stiffness $= E/(1+\nu)$ (which is, of course, twice the modulus of rigidity), and a third form of the material stiffness. $E^{**}/(1-2\nu)$, appears in relation to the effect of normal pressure.